Utilization of yeast pheromones and hydrophobin-based surface engineering for novel whole-cell sensor applications

DISSERTATION

zur Erlangung des akademischen Grades
Doctor rerum naturalium
(Dr. rer. nat.)

vorgelegt der
Fakultät Mathematik und Naturwissenschaften
der Technischen Universität Dresden

von

Stefan Hennig

geboren am 07.06.1990 in Großröhrsdorf

Tag der Einreichung: 3. November 2016
Tag der Disputation: 3. April 2017

Gutachter:
Prof. Dr. Gerhard Rödel, Technische Universität Dresden
Prof. Dr. Tilo Pompe, Universität Leipzig

“Science knows no country,

because knowledge belongs to humanity,

and is the torch that illuminates the world.”

Louis Pasteur

List of Publications

Peer-reviewed scientific articles

Hennig S, Clemens A, Rödel G, Ostermann K. A yeast pheromone-based inter-species communication system. *Appl Microbiol Biotechnol* **2015**, 99(3):1299-1308.

Ostermaier F, Scharfenberg L, Schneider K, Hennig S, Ostermann K, Posseckardt J, Rödel G, Mertig M. From 2D to 1D functionalization: Steps towards a carbon nanotube based biomembrane sensor for curvature sensitive proteins. *Phys Status Solidi A* **2015**, 212(6):1389-1394.

Hennig S, Rödel G, Ostermann K. Artificial cell-cell communication as an emerging tool in synthetic biology applications. *J Biol Eng* **2015**, 9:13.

Hennig S, Rödel G, Ostermann K. Hydrophobin-based surface engineering for sensitive and robust quantification of yeast pheromones. *Sensors (Basel)* **2016**, 16(5).

Patents

Hennig S, Clemens A, Rödel G, Ostermann K. Verfahren und Kit zur *in vivo* Detektion von Primärsignalen mittels Interspezies-Kommunikation. **May 2013**, DE102013209312B3 (granted).

Hennig S, Rödel G, Ostermann K. System und Verfahren zur Detektion von Primärsignalen an mittels selbstassemblierenden Proteinen funktionalisierten Oberflächen. **September 2015**, DE102015218513.3 (submitted).

Conference contributions

Hennig S, Rödel G, Ostermann K. Hydrophobin-based surface functionalization for sensitive and robust quantification of a yeast pheromone. *Biosensors*, **May 2016**, Gothenburg (Sweden), *poster presentation*.

Table of Contents

List of Tables

List of Figures

List of Abbreviations

A. adeninivorans	*Arxula adeninivorans*
AFM	Atomic force microscopy
APS	Ammonium persulfate
ATPS	Aqueous two-phase system
BSA	Bovine serum albumin
C. cinerea	*Coprinopsis cinerea*
CDK	Cyclin-dependent kinase
CNT	Carbon nanotube
ddH_2O	Double-distilled water
DIC	Differential interference contrast
E. coli	*Escherichia coli*
EDC	Endocrine disrupting compound
EDTA	Ethylene diamine tetraacetic acid
EGFP	Enhanced green fluorescent protein
EGTA	Ethylene glycol tetraacetic acid
ELISA	Enzyme-linked immunosorbent assay
EMM	Edinburgh minimal medium
ER	Endoplasmic reticulum
FET	Field-effect transistor
FSC	Forward Scatter
GDP	Guanosine diphosphate
GFP	Green fluorescent protein
GOx	Glucose oxidase
GPCR	G-protein coupled receptor
GRAS	Generally recognized as safe
GST	Glutathione S-transferase
GTP	Guanosine triphosphate
HA	Hemagglutinin
HPLC	High-performance liquid chromatography

HRP	Horseradish peroxidase
IgG	Immunoglobulin G
IPTG	Isopropyl-β-D-thiogalactoside
kDa	Kilodalton
LB	Luria Broth
MAPK	Mitogen-activated protein kinase
MAPKK	Mitogen-activated protein kinase kinase
MAPKKK	Mitogen-activated protein kinase kinase kinase
MBP	Maltose binding protein
MOPS	3-(N-morpholino)propanesulfonic acid
MWCO	Molecular weight cut-off
N. crassa	*Neurospora crassa*
OD_{600}	Optical density at 600 nm wavelength
ORF	Open reading frame
PBS	Phosphate-buffered saline
PBS-T	Phosphate-buffered saline with 0.01 % (v/v) Tween® 20
PCR	Polymerase chain reaction
PEG	Polyethylene glycol
PRE	Pheromone response element
PVDF	Polyvinylidene fluoride
QCM	Quartz crystal microbalance
rpm	Rounds per minute
S. cerevisiae	*Saccharomyces cerevisiae*
S. commune	*Schizophyllum commune*
S. pombe	*Schizosaccharomyces pombe*
SDS	Sodium dodecyl sulfate
SDS-PAGE	Sodium dodecyl sulfate polyacrylamide gel electrophoresis
SPR	Surface plasmon resonance
T. reesei	*Trichoderma reesei*
TEMED	N,N,N′,N′-Tetramethylethane-1,2-diamine
TFA	Trifluoroacetic acid
TREC	Topography and recognition imaging
tRFP	Turbo red fluorescent protein
Tris	Tris(hydroxymethyl)aminomethane

1 Introduction

1.1 Biosensors

1.1.1 General considerations

Biosensors are self-contained, integrated analytical devices that combine biological sensing components with cognate transducer elements to generate a signal correlating to the concentration of a target analyte [1-9]. Therefore, biosensors couple biological material with microelectronic systems to facilitate rapid and accurate detection of a target analyte in complex sample matrices, taking use of the inherent specificity of biomolecules.

Most commonly, biosensors utilize immobilized enzymes as biological sensing elements, exploiting their tremendous sensitivity and substrate specificity to specifically detect a substrate or a specific inhibitor of the respective enzyme as an analyte of choice [7]. However, antibodies, cofactors, nucleic acids as well as isolated cellular organelles, intact microorganisms or even tissues of plants or animals could be utilized as biological compounds in biosensor applications [2, 3, 6, 7]. Typically, the immobilized biological compound and the transducer element are in close proximity, allowing for the detection of the biological response to the target analyte by the respective transducer element to generate a measurable output signal corresponding to the analyte concentration. The transducer elements employed in biosensor applications are highly diverse, including *e.g.* electrochemical, optical, acoustic, mechanical, calorimetric, magnetic or piezoelectric measurements to detect the response of the biological compound [2, 6, 7, 10, 11]. In addition, nanomaterials such as nanoparticles, carbon nanotubes (CNTs) and quantum dots have been integrated into biosensor devices since they are extremely stable, provide a high surface-to-volume ratio and are ideal candidates for the development of miniaturized, portable biosensors [6, 8, 9, 12].

Classical analytical chemistry techniques, including atomic absorption spectroscopy, mass spectrometry or chromatography methods, are highly sensitive and provide

very accurate results, but are not suitable for routine and on-site analysis due to their complexity and associated costs. In addition, these techniques are often very time-consuming, require trained operators and their size as well as their power requirements limit the use of these methods to highly equipped laboratories [2, 13]. Therefore, these techniques are not suitable to develop portable sensors for real-time detection of target analytes in remote areas. Hence, the development of biosensors aims for compact, field-deployable and easy-to-use devices for non-trained operators, allowing for the rapid on-site detection of a target analyte in various sample matrices [2, 8].

In fact, biosensors represent an emerging branch in sensor technologies, estimated to cover a world market of about US$ 17 billion in 2018 [8]. Currently, glucose biosensors for healthcare applications (*i.e.* blood glucose monitoring for diabetes patients) dominate the world market, covering about 85 % of the current biosensor market value [8]. However, novel approaches are emerging rapidly, focusing on a plethora of different analytes. For example, biosensors harbor great potential for environmental monitoring, including the detection of heavy metals, organic pollutants, pesticides and endocrine disrupting compounds (EDCs) in aqueous systems, monitoring of bioremediation processes and toxicity evaluation in soil and water [6, 8, 9]. Likewise, biosensors are applicable in food industry, monitoring fermentation processes as well as the nutrient content and putative contamination of food products with pathogens or pesticides. Additionally, biosensors are important tools for personalized medicine and healthcare, allowing for the detection of disease biomarkers and monitoring of the nutrient status of individuals. In particular, mass-produced and inexpensive biosensor devices harbor great potential for the development of easy-to-use, portable point-of-care diagnostics for convenient home analysis. Furthermore, biosensors are of great interest for drug discovery and homeland security, *e.g.* allowing for the detection of explosives as well as chemical and biological warfare agents [6, 8, 9, 14].

1.1.2 Immunosensors

The application of a specific recognition event between the target analyte and the biological compound is among the most commonly employed principles in biosensor

devices, taking use of the inherent specificity of biological components. Traditionally, immunosensors almost exclusively relied on specific antibodies to allow for the detection of cognate antigens. However, antibodies can only be raised for a limited palette of analytes since antibodies against toxic, non-immunogenic or very small compounds such as heavy metals cannot be produced [15, 16]. Furthermore, production and purification of antibodies are time-consuming as well as expensive processes, and antibodies are comparatively unstable in adverse conditions such as elevated temperatures or upon long-term storage. Therefore, numerous antibody substitutes have been successfully applied in immunosensors, including antibody fragments [12, 17, 18], aptamers (short DNA or RNA oligonucleotides that fold into a unique three-dimensional conformation [15, 16]), peptides [19, 20] and engineered phages [21-24]. Additionally, “plastic antibodies” are an emerging class of antibody substitutes for the development of novel immunosensors [8, 9]. “Plastic antibodies” represent small polymer particles upon molecular imprinting, *i.e.* they are synthesized *via* polymerization of functional monomers around the target analyte and subsequent analyte extraction from the polymerized particle, resulting in polymer particles that carry highly specific binding pockets for the analyte of choice [25, 26].

The recognition event between the target analyte and the biological compound has to be detected specifically and with high sensitivity by the use of appropriate transducer elements [1-9]. Almost without exclusion, the biological recognition element is immobilized at the surface of the respective transducer to ensure intimate contact. Several modes of action for immunosensors can be envisaged, relying *e.g.* on the immobilization of the recognition element to facilitate adsorption of the analyte (or desorption of a labeled analyte mimic triggered by the presence of the target analyte). Likewise, an analyte (mimic) can be immobilized at the surface, allowing for attachment of the biological recognition element and subsequent competitive detachment triggered by the target analyte. Evidently, immobilization of the biological recognition element (or an analyte mimic) in an active and accessible manner is to be seen as a key issue for the development of immunosensor devices [27-30]. Numerous methods for the immobilization of these compounds have been developed. The majority of them is focusing on regioselective modification of the biological compound to introduce unique functional groups that subsequently react with specific functional groups exposed at the surface. Currently employed techniques such as click chemistry or thiol maleimide coupling provide high yields

and specificity, but rely on the *in vitro* modification of the biological compound and the presence of specific functional groups at the transducer surface to facilitate immobilization [19, 27-30].

A variety of transducer elements are employed to enable immunosensor read-out. For example, the biological recognition element could be detected by field-effect transistors (FETs) or impedance spectroscopy, relying on the attachment or detachment of charged molecules at the functionalized transducer surface [31, 32]. Likewise, optical transducer elements such as surface plasmon resonance (SPR) instruments could be utilized, detecting a change in the refractive index upon adsorption or desorption of molecules at the functionalized surface [33, 34]. In addition, technologies based on evanescent field excitation (*e.g.* using fluorescently labeled antibodies attaching to the surface of an optical waveguide [35]) or surface-enhanced Raman scattering [36] are promising candidates for application in immunosensors. Furthermore, piezoelectric transducers such as quartz crystal microbalances (QCM) [37, 38] and surface acoustic wave devices [39, 40] or surface-stress based transducers like microcantilevers [41] harbor great potential to detect the biological recognition event. As stated above, nanomaterials can be used to enhance the performance of immunosensors and to pave the way for biosensor miniaturization. For example, gold nanoparticles exhibit superior properties for fluorophore quenching, allowing for facile detection of the attachment or detachment of fluorescently labeled biological recognition elements or analyte mimics to the nanoparticle surface [42]. Similarly, quantum dots (semi-conductor nanoparticles with size-dependent light emission properties) can be utilized to detect adsorption or desorption of fluorescently labeled molecules [43].

1.1.3 Whole-cell biosensors

1.1.3.1 General considerations

Whole-cell sensors are an emerging branch in the field of biosensors, relying on the use of viable cells as the biological recognition element coupled to an appropriate transducer element in order to gain qualitative and quantitative information on the

presence of a target analyte [1-5, 11, 13]. The majority of currently available whole-cell sensors are transcription-based sensors, taking use of the analyte-induced or analyte-repressed expression of a reporter gene encoding *e.g.* fluorescent proteins, luciferases or β-galactosidases (section 1.1.3.3). Accumulation of reporter proteins can easily be detected by the use of an appropriate transducer element to create the read-out signal. Whilst the majority of currently developed whole-cell sensors rely on prokaryotic sensor cells, promising results were also obtained upon employing yeast and fungi (section 1.1.3.2), unicellular algae [44-49], viable ciliates [50] and nematodes [51] as well as mammalian cells [52].

Whole-cell sensors show a variety of advantages and disadvantages in comparison to other types of biosensors relying on the use of immobilized enzymes or antibodies as biological compounds (Table 1). A key feature of whole-cell sensors is their inherent ability to assess the biological relevance of certain analytes, given that the living organisms only respond to the bioavailable fraction of the sample [1-5, 53-62]. Likewise, biosensors utilizing intact cells allow for the detection of global parameters such as the toxicity or genotoxicity of an environmental sample as a result of multiple sample components and their mutual interactions. Therefore, whole-cell sensors are highly valuable tools for risk assessment and monitoring of bioremediation processes. In addition, the use of intact cells obviates the need for expensive, tedious and time-consuming purification of enzymes or antibodies and provides an opportunity for prolonged shelf-life since enzymes are more stable in their natural surroundings than upon purification and storage under *in vitro* conditions [1-5, 53-62]. As co-factors and co-enzymes are often present in the intact cells, the use of whole-cell sensors overcomes the need for their addition. Moreover, intact cells can be mass-produced in a facile and cost-effective manner compared to purified enzymes and antibodies [1-5, 53-62] (Table 1).

However, whole-cell sensors often suffer from low sensitivity and specificity as well as long response times compared to enzyme- or antibody-based biosensors, in part resulting from the cellular envelop displaying an additional diffusion barrier for the target analyte [1-5, 53-62] (Table 1). In particular, transcription-based whole-cell sensors relying on the analyte-induced expression of reporter genes are inherently slow and non-specific sample matrix effects such as cytotoxicity might affect the whole-cell biosensor in undesired ways, requiring the implementation of viability

controls to increase the sensor robustness and reliability [3, 11, 13, 55, 58]. Whole-cell sensors for the detection of a specific target analyte almost exclusively rely on the use of genetically engineered sensor cells, potentially limiting their application in field-deployable devices due to legal regulations and ethical concerns regarding the risk of environmental release of genetically modified organisms [11, 13, 53, 55].

Table 1. Advantages and disadvantages of whole-cell biosensors.

Advantage/disadvantage	References
Advantages	
Assessment of global parameters (toxicity, genotoxicity and bioavailability)	[1-5, 53-62]
No need for expensive, tedious and time-consuming purification of enzymes and antibodies	[1-5, 53-62]
Enhanced tolerance against adverse conditions compared to isolated enzymes	[1-5, 53-62]
Increased stability and activity of enzymes in their authentic environment, no need for co-factor addition	[3, 4, 10, 53]
Cost-effective and rapid mass-production	[1-5, 53-62]
Facile manipulation and engineering compared to purified enzymes	[1-5, 53-62]
Utilization of long metabolic chains (multi-step enzymatic cascades) existing in intact cells	[1-5, 54]
Long shelf-life compared to purified enzymes	[3, 7, 52, 54]
Amenable to multiplexing (simultaneous detection of multiple analytes upon utilization of different reporter genes)	[13]
Disadvantages	
Low specificity and sensitivity compared to enzyme-based biosensors	[1-5, 53-62]
Slow response of transcription-based whole-cell sensors	[1-5, 53-62]
Cellular envelop displays additional diffusion barrier	[1-5, 53-62]
Non-specific sample matrix effects on cell viability or metabolism	[3, 11, 55]
Legal regulations and ethical issues regarding the use of genetically modified organisms	[1-5, 53-62]

Whole-cell sensors harbor tremendous potential for application in a wide variety of disciplines, in particular focusing on environmental monitoring, bioprocess control and healthcare applications. They have been utilized to detect environmental pollutants such as heavy metal ions, EDCs, xenobiotics and pesticides in soil and water [1-5, 53-62], representing efficient tools to monitor wastewater treatment and bioremediation. Likewise, whole-cell sensors are valuable tools to detect explosives or warfare agents [11, 57] as well as nutrient availability in bioreactors [11, 54, 57] and are suitable for high-throughput drug screening and doping tests [55, 57].

1.1.3.2 Yeast-based whole-cell sensors

The vast majority of currently developed whole-cell sensors utilize prokaryotic cells as the biological recognition element [52, 53, 57]. However, yeast and fungi such as the budding yeast *Saccharomyces cerevisiae* (*S. cerevisiae*) harbor several advantages compared to bacteria, making them highly attractive hosts for application in whole-cell sensors. Yeast cells are highly robust, showing enhanced tolerance against adverse conditions such as extreme pH values or high osmolarity compared to bacteria [53, 57, 62]. Therefore, yeast-based whole-cell sensors can be applied in a wide variety of sample matrices and have prolonged shelf-lives as well as in-use lives. In addition, yeast cells can be lyophilized for extended storage with far higher survival rates than bacteria [52, 53, 57] and serve as suitable hosts for the expression of intracellular and membrane-embedded receptors from higher eukaryotes, thereby broadening the range of analytes to be detected [57, 62]. Importantly, the cellular response of prokaryotic and eukaryotic cells towards certain analytes varies greatly, depending on the mode of action of the analyte. Therefore, bacteria-based biosensors show limited applicability for toxicity evaluation, risk assessment and drug screening, whereas the results obtained with eukaryotic yeast cells are more relevant for higher eukaryotes [52, 53, 57]. It should be noted that some analytes such as certain EDCs require activation in the liver of mammals to become biologically active, preventing their detection by yeast sensor cells [63]. However, yeast cells are far more robust than mammalian cells, require less sophisticated growth conditions and storage and produce reliable results significantly faster than mammalian sensor cells [53, 57, 62].

Similar to *Escherichia coli* (*E. coli*) as the model prokaryotic host for whole-cell sensor applications, yeast cells grow rapidly on numerous substrates, enabling fast mass-production of the sensor cells [53, 57, 62]. In addition, a plethora of information on the yeast genome, proteome and metabolome is available and mature protocols for genetic engineering as well as suitable expression vectors for *S. cerevisiae* exist [52, 53, 57]. Importantly, *S. cerevisiae* is approved by the U.S. Food and Drug Administration and harbors the GRAS status (Generally recognized as safe) [64], implying that yeast cells do not exert any adverse effect on the human health. This might serve to improve public acceptance for the utilization in commercial whole-cell sensors.

Consequently, *S. cerevisiae* has been employed in numerous whole-cell sensor applications, facilitating the detection of heavy metal ions [65-72] or DNA damaging agents [65, 73-79]. Upon heterologous expression of mammalian G-protein coupled receptors (GPCRs) or hormone receptors (*e.g.* estrogen receptors or androgen receptors), yeast cells could be engineered to respond to the respective ligands to detect the presence of authentic hormones and signaling molecules [80-83], EDCs [63, 67, 84-92], olfactory ligands [93-95], saturated medium-chain fatty acids [96] or explosives [95, 97]. In addition, yeast-based whole-cell sensors have been used to detect glucose [98, 99], antibiotics [100], disinfectants [101], organic pollutants [102, 103], toxins [104, 105], bacterial antigens [106] and oxidative stress inducing agents [78, 107]. Due to the high robustness of yeast cells, these analytes could be detected in a wide variety of sample matrices, including wastewater and creek water [71, 72, 86, 88], beverages [99], sediments [102] as well as milk and fermented milk products [105, 108].

Although the majority of the yeast-based whole-cell sensors developed so far focused on the use of wild-type or genetically engineered *S. cerevisiae* cells, several other yeast and fungal species have been successfully employed. Among them, *Arxula adeninivorans* (*A. adeninivorans*) is of great interest since it is able to withstand high temperatures and salinity, allowing for the detection of EDCs and hazardous compounds in extreme environments [109-113]. In addition, the fission yeast *Schizosaccharomyces pombe* (*S. pombe*) has been engineered to sense EDCs [92, 114, 115], and *Aureobasidium pullulans* as well as the basidiomycetes *Armillaria mellea* and *Mycena citricolor* were utilized to assess the general toxicity of

environmental samples [116, 117]. Further approaches included *Aspergillus niger* and *Hansenula polymorpha* for heavy metal detection [68, 118], *Candida tropicalis* [119] as well as the white rot fungus *Phanerochaete chrysosporium* [120] or the slime mould *Physarum polycephalum* [121].

1.1.3.3 Reporter proteins in whole-cell sensor applications

As stated above, the majority of the so far developed whole-cell sensors are transcription-based, *i.e.* they rely on analyte-induced or analyte-repressed expression of a reporter gene by placing an analyte-responsive promoter element upstream of the respective reporter gene, ultimately creating the measurable output signal. The corresponding reporter protein should be easily detectable even in small quantities – preferably without the addition of exogenous substrates – and should be compatible with a wide variety of transducer elements to generate the whole-cell sensor read-out [54, 60]. Most commonly, fluorescent proteins, luciferases or β-galactosidases are employed as reporter proteins for whole-cell biosensors [2, 4, 13, 54, 57, 59-62], and alternative reporter genes such as carotenoid-metabolizing enzymes, chloramphenicol acetyltransferases, aequorin or uroporphyrinogen III methyltransferases only represent niche applications [2, 54, 61].

Fluorescent proteins such as the green fluorescent protein (GFP) are most commonly used as reporter proteins in whole-cell sensor applications. Favorably, light emission by fluorescent proteins does not require the addition of substrates or co-factors nor cell lysis prior to measurements, resulting in autonomous systems that are amenable to near real-time analysis [2, 54, 56]. In addition, a huge palette of fluorescent proteins with unique excitation and emission properties is available, allowing for multiplexing (*i.e.* the detection of multiple analytes by a single sensor cell as the perception of each analyte is coupled to the expression of a different fluorescent protein to generate the read-out signal) [2, 13, 54, 56, 122]. However, fluorescent proteins require posttranslational maturation steps for light emission, resulting in a delay between translation and fluorescence [2, 5, 54, 60]. Furthermore, the use of fluorescent proteins might be restricted by the requirements of suitable transducer elements, considering that light excitation and appropriate optical filters (to separate the excitation light and the emitted fluorescent light) are necessary, resulting in

complex transducer elements that are often not suitable for the development of portable devices [2]. Additionally, several strains and species exhibit considerable background fluorescence [2, 54], limiting the applicability of fluorescent proteins for whole-cell sensor applications.

Luciferases are considered as bioluminescent proteins since they catalyze redox reactions that are accompanied by the emission of photons. Two types of luciferases are commonly employed in whole-cell sensors: firefly luciferases (Luc) and bacterial luciferases (Lux) [54]. In comparison to fluorescent proteins, the use of luciferases in whole-cell biosensors obviates the need for excitation light and optical filters, therefore providing an opportunity for the development of cost-effective, miniaturized devices [55, 57]. In addition, the use of luciferases harbors the potential to enhance the sensitivity of whole-cell sensors compared to fluorescent proteins since luciferases catalyze enzymatic reactions instead of relying on (fluorescent) protein accumulation exclusively. Moreover, endogenous luminescence is rarely found in nature, eliminating background activity of the sensor cells [1, 3, 7, 54, 55, 57]. However, the use of luminescent proteins in whole-cell sensor applications relies on the addition of the luciferase substrate, preventing their use in real-time applications [2, 54-57]. However, this limitation could be overcome by the expression of the entire bacterial *lux* operon in the host cells, encoding the luciferase as well as the enzymes catalyzing the substrate synthesis to form autonomous systems [2, 54, 55, 57]. Nevertheless, the oxidation catalyzed by luciferases crucially depends on the presence of molecular oxygen, limiting their applicability to aerobic systems [2, 54, 55]. This might be particularly challenging if the sensor cells are immobilized at the surface of the optical transducer by entrapment into biocompatible polymers, limiting the diffusion of oxygen to the sensor cells [55].

The β-galactosidase (LacZ) from *E. coli*, catalyzing the hydrolysis of β-galactosides, represents the third most commonly employed reporter protein for whole-cell sensor applications [54, 57]. Numerous substrates for β-galactosidase are available, providing the opportunity to utilize optical read-out strategies (colorimetric, fluorimetric and luminescent) or electrochemical transducers [54, 56]. Thus, the use of β-galactosidase provides large flexibility regarding the transducer element whereas fluorescent protein and luciferases are restricted to optical transducers. In addition, the reaction catalyzed by β-galactosidases is independent on the presence

of oxygen, allowing for application in anaerobic environments [54]. However, all read-out strategies relying on β-galactosidases crucially depend on the addition of appropriate substrates, preventing real-time measurements and increasing the costs of a single measurement [54, 57]. In yeast-based whole-cell sensors utilizing β-galactosidases, cell lysis is typically required to ensure substrate accessibility, further limiting the applicability and increasing the time demand for the measurement [75, 76, 79, 80, 91, 101, 115, 123, 124]. Although a chromogenic LacZ substrate not requiring cell lysis was recently reported, assessment of the β-galactosidase activity using this substrate required 24 – 48 h incubation of the sensor cells in the presence of the substrate, indicating poor diffusion through the cell wall [104].

Most commonly, reporter proteins accumulate in the cytoplasm of the sensor cells, possibly complicating the read-out strategy due to light scattering and absorption by intact sensor cells and/or due to the necessity to disrupt the cells prior to the measurement. Therefore, low sensor cell densities have to be maintained to limit the detrimental influence of light scattering and absorption [116, 125]. In contrast, several previous studies took use of secreted reporter proteins to overcome these limitations. For example, secreted phytase and tannase enzymes have been used to create the read-out signal of *A. adeninivorans* whole-cell sensors [110-113], whereas secreted α-galactosidases [126] and secreted luciferases [127, 128] have been exploited in *S. cerevisiae* based whole-cell sensors. Although the use of secreted reporter proteins obviates the need for cell disruption and might serve to limit light scattering issues (*e.g.* by transport of the secreted enzyme in a fluid stream resulting in spatial separation of the sensor cells and the transducer element, section 1.4), the use of extracellular enzymes might be limited by non-specific sample matrix effects. If non-specific enzyme inhibitors such as heavy metal ions are present in the environmental sample, the use of secreted enzymes in whole-cell sensor applications might not be feasible. Considering the shortcomings of currently available reporter proteins, Jarque *et al.* recently highlighted that the “validation and establishment of new reporter genes could contribute to both increased sensitivity and broadened applicability of yeast biosensors” [62]. Development of a novel whole-cell biosensor read-out possibility represents of the major aims of this study (section 1.4).

1.2 Hydrophobins

Hydrophobins represent a class of unique, low molecular weight proteins (typically about 100 amino acids) secreted by filamentous fungi [129-135]. The first hydrophobin was found in *Schizophyllum commune* (*S. commune*) in 1991 [136], and several hundred hydrophobins from diverse fungal species have been identified since that time. Except for eight conserved cysteine residues forming four intramolecular disulfide bonds, fungal hydrophobins share very limited sequence similarity. However, all hydrophobins show an amphipathic structure, allowing for self-assembly into protein monolayers at hydrophilic-hydrophobic interfaces [129-135].

According to the cysteine spacing pattern and the hydropathy plots, hydrophobins have been traditionally grouped into two classes (class I and class II), although recent studies revealed that several intermediate hydrophobins may exist [137-140]. Class I hydrophobins are present in both ascomycetes and basidiomycetes, whereas class II hydrophobins have been found exclusively in ascomycetes so far [130, 134, 135, 141, 142]. In numerous species, both class I and class II hydrophobins are encoded in the genome, suggesting that they may have distinct, non-overlapping functions [130, 143]. In general, class II hydrophobins seem to be more conserved in amino acid composition as well as the length of the flexible loop domains spacing the four disulfide bonds, whereas class I hydrophobins are more diverse in amino acid sequence, loop length and conformational flexibility [131]. Remarkably, the differences between class I and class II hydrophobins are also reflected by the features of the monolayers formed upon self-assembly at an interface. While class I hydrophobins self-assemble into highly robust monolayers characterized by a mosaic pattern of rodlets, the monolayers formed by class II hydrophobins are less robust and show hexagonal, honeycomb-like packing [131, 132].

1.2.1 Structure and self-assembly of hydrophobins

In contrast to the low degree of sequence similarity between hydrophobins, these proteins share a conserved three-dimensional structure [129-135]. Since class I hydrophobin EAS (also termed Bli-7 and Ccg-2 [144, 145]) from *Neurospora crassa*

(*N. crassa*) was employed in this study, description of the protein structure and self-assembly process will focus on this particular hydrophobin.

Structure determination revealed that the EAS hydrophobin consists of an irregular four-stranded β-barrel core structure with a diameter of 2.7 nm [146]. Four disulfide bonds stabilize the core structure, rendering the hydrophobin structure very compact and rigid. Two disordered loop regions are identified in the solution structure of the EAS hydrophobin: an extremely hydrophobic loop between the third and fourth cysteine residue (that is dispensable for self-assembly at the air-water interface [147] but strongly localizes to the interface region to expose the hydrophobic amino acid residues to the air [148]) and a second loop spacing the seventh and the eighth cysteine residue (that harbors sequence elements with crucial importance for hydrophobin self-assembly [149]). Importantly, the hydrophobin structure revealed a striking spatial separation of charged and uncharged residues as the majority of the charged residues point towards a single surface spot of the protein whereas the opposite face of the protein (hydrophobic patch) is essentially uncharged [146]. The resulting amphipathic structure of the hydrophobin is crucial for its surface activity and self-assembly at hydrophilic-hydrophobic interfaces.

Hydrophobins seem to share a common hydrophobin fold, given that the three-dimensional structures of the class I hydrophobins MPG1 (from *Magnaporthe grisea*) and DewA (from *Aspergillus nidulans*) as well as the class II hydrophobins HFBI and HFBII from *Trichoderma reesei* (*T. reesei*) and NC2 from *N. crassa* are essentially similar to the structure of EAS [150-155]. These studies also suggested that the disulfide bonds are crucial to stabilize the hydrophobin fold to keep the hydrophobic amino acid residues exposed at the protein surface (which might otherwise be buried in the interior of the protein). However, some of the previously characterized hydrophobins differ from the common hydrophobin structure. For example, the hydrophobins SC3 from *S. commune* and POH2 from *Pleurotus ostreatus* are glycosylated [156-158]. Additionally, large hydrophobins consisting of multiple hydrophobin domains (such as the pentahydrophobin CPPH1 encompassing five hydrophobin domains), were found in *Claviceps sp.* and *Aspergillus sp.* [139, 159, 160].

In the presence of a hydrophilic-hydrophobic interface, class I hydrophobins such as EAS self-assemble into highly robust monolayers characterized by a mosaic pattern

of rodlets [129-135]. The formation of rodlets is achieved by head-to-tail stacking of EAS monomers along the rodlet axis, allowing for infinite extension of the rodlets that are consequently several hundred nanometers in length but only a few nanometers in width [146, 147]. In the dissolved state of the EAS hydrophobin, regular secondary structure elements are almost absent – except for the core structure stabilized by the disulfide bonds – and the hydrophobin monomers are largely unstructured in solution [161, 162]. In contrast, upon self-assembly at a hydrophilic-hydrophobic interface, a high content of β-sheets is observed in the EAS monomers. In fact, EAS monomers self-assemble into rodlets *via* β-sheet stacking, closely resembling the aggregation of amyloids. As the rodlets also interact with amyloid-specific dyes such as Congo Red [161] and Thioflavin T [131], class I hydrophobins are considered as functional amyloids of filamentous fungi.

Close examination revealed that self-assembly of the EAS hydrophobin at interfaces proceeds *via* two steps [148, 163, 164]. First, due to their amphipathic structure, individual monomers of the EAS hydrophobin accumulate at the air-water interface. Due to a high content of hydrophobic amino acid residues, the flexible loop between the third and fourth cysteine residue interacts with the interface, thereby unlocking the loop between the seventh and the eighth cysteine residue [149, 165]. Subsequently, this loop undergoes conformational changes, exposing the amyloidogenic region of the hydrophobin to allow for interaction with adjacent EAS monomers *via* β-sheet stacking, thereby forming the cross-β core of the EAS rodlets. Rodlet formation by monomer stacking and lateral packing of the rodlets occur simultaneously, resulting in the formation of densely packed, defect-free hydrophobin monolayers [131].

Although all hydrophobins share the unique hydrophobin fold, the self-assembly mechanisms between individual members of this protein family differ dramatically. For example, self-assembly of the class I hydrophobins SC3 (from *S. commune*) and ABH1 (from *Agaricus bisporus*) seems to proceed *via* intermediate stages. The SC3 hydrophobin first self-assembles into a helical state (protein structure rich in α-helices) that is converted into β-sheet state 1 (amorphous protein layer enriched in β-sheets) and β-sheet state 2 (rodlet layer) consecutively [166]. Upon self-assembly at a hydrophobic solid support, self-assembly of SC3 is locked in the helical state unless treatment with hot detergents is applied, thereby accelerating the conversion

into the final β-sheet 2 state. Likewise, schizophyllan and other glycans promote amyloid formation by SC3 [167, 168]. Self-assembly of ABH1 at a hydrophobic solid support also proceeds *via* intermediate states, although additional treatment was not required to yield rodlet layers [169]. Curiously, self-assembly of the class I hydrophobin Vmh2 from *Pleurotus ostreatus* does not depend on the presence of a hydrophilic-hydrophobic interface but is induced by Ca^{2+} or high temperatures [170, 171].

In contrast to the rodlets characteristic for class I hydrophobin monolayers, class II hydrophobins self-assemble into polycrystalline monolayers that do not resemble amyloid formation. Analysis of the monolayers formed by the class II hydrophobins HFBI, HFBII and HFBIII from *T. reesei* revealed that these monolayers consist of two-dimensional crystalline domains laterally packed to form a polycrystalline protein layer [172-174]. Individual crystalline domains are characterized by a hexagonal packing of hydrophobin monomers into honeycomb-like structures [175-177]. Interestingly, interfacial layers of HFBII undergo phase transition, resulting in layer solidification [178, 179]. Although comparable monolayer morphologies were observed for the *N. crassa* hydrophobin NC2 [155, 163], self-assembly of class II hydrophobins also does not follow a common route. Cerato-ulmin (class II hydrophobin from the Dutch elm disease pathogen *Ophiostoma novo-ulmi*) self-assembles into monolayers *via* a “progressive pearl necklace collapse mechanism” that is not consistent with the monolayer topography observed for *T. reesei* hydrophobins [180].

Remarkably, class I hydrophobin monolayers are extremely robust. EAS monolayers are not disturbed upon alkali or acid treatment and also withstand treatment with organic solvents [163, 164]. Consequently, very harsh conditions are required to dissociate EAS monolayers, and only treatment with 100 % trifluoroacetic acid (TFA) or 100 % formic acid have been reported to result in disturbance of the hydrophobin monolayers [163, 181]. In contrast, class II hydrophobin layers are less resistant against adverse conditions and dissociate upon ethanol or detergent treatment or by applying pressure [129-135].

1.2.2 Functions of hydrophobins *in vivo*

Due to their unique properties, hydrophobins have been reported to fulfill a variety of functions in their authentic hosts [129-131, 134, 135, 142, 182-187]. Self-assembly of hydrophobins at the surface of fungal structures or at the air-water interface is of crucial importance for fungal development and life style. Interestingly, hydrophobins are often encoded by multiple genes. Several fungal species encode ten or more hydrophobins in their genome (*e.g. Trichoderma harzianum* [188] and several *Aspergillus sp.* [139]), and extremely high copy numbers resulting from gene duplication events exist in *Bjerkandera adusta* (27 genes), *Coprinopsis cinerea* (*C. cinerea*, 34 genes) and *Trametes versicolor* (40 genes) [189-191]. However, hydrophobins might be functionally redundant, at least in certain aspects [192].

Self-assembly of hydrophobins at the air-water interface dramatically lowers the surface tension. In fact, the class I hydrophobin SC3 from *S. commune* represents the most surface-active protein currently known [193-195]. Reduction of the surface tension of aqueous media is an obligatory prerequisite for the formation of aerial structures, allowing fungal structures to breach the interface [195-198]. Therefore, the development of aerial structures crucially depends on the secretion of hydrophobins by the submerged mycelium. Likewise, hydrophobins self-assemble at the surface of aerial structures, conferring a hydrophobic coating to spores and aerial hyphae. Numerous studies revealed that fungal species lacking hydrophobins expose hydrophilic aerial structures that are easily wettable [196, 199-211]. Water-repellant coatings are particularly important for conidia (fungal spores), facilitating their dispersal in the air [205, 208, 210]. This might also be the predominant function of the *N. crassa* EAS hydrophobin [212]. Likewise, hydrophobins cover air channels in fungal fruiting bodies and lichens, preventing air channel collapse and water entry to allow for efficient gas exchange [198, 213-215].

Fungal hydrophobins also play an important role in pathogenic fungi. As hydrophobins self-assemble at any hydrophilic-hydrophobic interface, they are also capable of covering the surface of host organisms, mediating attachment of the pathogenic fungus to its host [201, 207, 211, 216, 217] or to insects that act as disease vectors by mediating spore dispersal [218]. In addition, fungal hydrophobins serve to recruit hydrolytic enzymes for host penetration to the surface of the pathogen [219, 220], and several mutants lacking certain hydrophobin genes have

been reported to be impaired in virulence, host penetration, symptom development and disease spreading [206, 207, 211, 221-223]. Furthermore, hydrophobin layers covering airborne spores of *Aspergillus fumigatus* prevent immune recognition by shielding immunogenic cell wall components and platelet-activating compounds, thereby decreasing the extent of host defense mechanisms [224-228].

Moreover, fungal hydrophobins have been reported to protect their hosts against desiccation [218, 229] and to influence several fungal properties such as cell wall composition [209, 230], microconidial chain formation [231], biofilm formation [232], pigmentation [223] and cell dispersal [211]. Likewise, hydrophobins have been reported to play an important role in mycorrhiza formation [233] and root colonization [234-236] by filamentous fungi present in soil.

Recently, the bacterial hydrophobin BslA (from *Bacillus subtilis*) was reported to share several functions with fungal hydrophobins, including surface tension reduction and formation of water-repellent coatings of aerial structures [237-239]. However, bacterial hydrophobins are very different from their fungal counterparts regarding amino acid sequence and three-dimensional structure, suggesting that both protein classes evolved independently. Surface-active proteins and peptides were also found in Streptomycetes [240] and *Ustilago maydis* [241-243], highlighting the importance of these functions for life style and development of the respective host.

1.2.3 Applications of hydrophobins

Owing to the unique properties of hydrophobins in terms of surface-activity, self-assembly and monolayer stability, these proteins harbor tremendous potential for application in a wide variety of disciplines. Numerous applications for authentic and recombinant hydrophobins have been proposed previously [129-131, 133, 135, 141, 244, 245]. Hydrophobins self-assemble into robust monolayers at any hydrophilic-hydrophobic interface, allowing for the functionalization of solid supports with hydrophobin layers in controlled orientation and density [246]. This may be advantageous as the resulting surfaces are biocompatible [247-253] and show enhanced lubrication properties [254, 255] as well as very low friction at the nanoscale [256].

Hydrophobin layers can be used to functionalize a variety of solid substrates to mediate the immobilization of proteins, peptides and low molecular weight compounds that adsorb to hydrophobin layers. Likewise, recombinant fusion proteins encompassing the desired functional domain and a hydrophobin domain as a surface anchor can be employed. Based on these approaches, hydrophobins have been utilized for surface patterning [257-261] and for the immobilization of peptides [248-251, 262-265], enzymes [266-274], fluorescent proteins [275, 276], carbohydrate-binding proteins [277-279], antibodies [280-282] and DNA [283].

Hydrophobins could also be employed for the functionalization of electrodes with electroactive co-factors (such as ubiquinone [284] or copper-based redox centers [193]) and enzymes [285-287] to implement novel biosensors. Due to its inherent affinity to glucose, the class I hydrophobin Vmh2 could be utilized to develop novel glucose biosensors based on hydrophobin-modified gold nanoparticles [288, 289]. Likewise, biosensors for xenobiotics [273] and thrombin protease activity [275] have been developed based on hydrophobin-functionalized surfaces. Furthermore, Soikkeli *et al.* recently demonstrated that recombinant hydrophobins could be used to functionalize a graphene-modified FET device to display tailored recognition elements at the functionalized surface, yielding a novel biosensor for specific peptides and antibodies [265].

Hydrophobins do not exert immunogenic or cytotoxic effects on mammalian cells [224, 248-253, 282, 290-294]. Therefore, they offer the possibility for utilization in tissue engineering and healthcare applications. For example, hydrophobins have been used to display ligands for specific cellular receptors at a functionalized surface, allowing for specific attachment of cells carrying the cognate receptor [248, 249, 263]. Likewise, scaffold materials commonly used in medical implants could be functionalized with hydrophobins to improve their biocompatibility and to enhance cell adhesion [264, 282, 295]. In addition, hydrophobins have been shown to reduce the proliferation of melanoma tumor cells in mice, potentially providing a novel possibility for cancer treatment [290].

Due to their extremely high surface-activity, hydrophobins also proved to be powerful tools for the stabilization of emulsions and foams [296-300]. Hence, hydrophobins might also be useful for the food industry, serving to stabilize food foams [301], to produce air-based fat mimics [300] or to design the properties of ice cream [302].

Likewise, hydrophobins have been shown to be powerful co-emulsifiers, providing a possibility for application in laundry processes [303]. However, the extremely high surface activity of hydrophobins might also be a disadvantage in certain fields. By stabilizing carbon dioxide bubbles, hydrophobins present in carbonated beverages (resulting from the use of raw materials infected with filamentous fungi) cause spontaneous and vigorous overfoaming immediately upon opening (gushing), resulting in economic losses [304-308].

Owing to their superior surface-to-volume ratio as well as their chemical and thermal stability, nanomaterials such as nanoparticles and CNTs harbor great potential for application in several fields. However, these materials often suffer from low solubility and aggregation in aqueous media, dramatically limiting their applicability [8, 9]. Hydrophobins have been employed previously to solubilize and functionalize nanomaterials such as nanoparticles [289, 309-313], CNTs [294, 314-316], individual graphene layers [317] and quantum dots [318] in aqueous media, yielding suspensions of monodisperse nanomaterials with enhanced long-term stability. In this regard, hydrophobins have also been used to synthesize monodisperse drug nanoparticles for oral administration, particularly beneficial for highly insoluble drugs or vitamins, showing increased drug bioavailability without affecting drug release from the nanoparticles [292, 319-322].

In addition, hydrophobins have been used as fusion partners for recombinant proteins upon expression in plants [293, 323-328] and fungi [329]. Targeting the recombinant fusion protein to the endoplasmic reticulum (ER) resulted in the formation of membrane-enveloped protein bodies in the cytosol, allowing for facile protein purification with high recovery and purity. Additional applications of hydrophobins include the functionalization of textile materials for water-repellency [330], the use as etch resists in silicon wet etching processes [331], controlled biomineralization [332, 333], enhancement of enzyme activity [334] as well as the stabilization of peptides and luciferases [335, 336].

1.3 The pheromone system of *S. cerevisiae*

The life cycle of the yeast *S. cerevisiae* – a unicellular ascomycete – includes haploid and diploid phases [337]. Two haploid cells are able to mate to form a diploid cell that – upon starvation for nitrogen and growth on a poor carbon source – undergoes meiosis and sporulation to give rise to four haploid ascospores. Like all ascomycetes, *S. cerevisiae* carries a bipolar mating locus, *i.e.* one of two alternative alleles is present at the single mating locus [338]. Haploid *S. cerevisiae* cells exist in one of two opposite mating types termed **a** and α, according to the allele present in the mating locus, whereas **a**/α diploid cells carry both alleles. The majority of the commonly used haploid laboratory strains of *S. cerevisiae* are heterothallic, *i.e.* they cannot switch between the two mating types [337]. However, homothallic strains also exist, frequently switching between the mating types to allow for self-diploidization and formation of ascospores in nutrient limited conditions [337, 339, 340].

The allele present at the mating locus determines the cellular identity: haploid cells carrying the *MAT**a*** allele and the *MATα* allele are regarded as **a**-type cells and α-type cells, respectively. The presence of both alleles in a single cell serves as an intracellular signal for diploidy [337]. Both the *MAT**a*** and the *MATα* allele control the expression of a variety of cell-type specific genes to confer the respective phenotype [337, 340]. According to the α1-α2 hypothesis first proposed by Strathern *et al.* [341], the *MATα* locus encodes the α1 homeodomain transcriptional activator interacting with Mcm1p and Ste12p to positively regulate the expression of α-specific genes such as *STE3*, *MFα1* and *MFα2* [338, 340-343]. In addition, the *MATα* locus encodes the α2 transcriptional repressor suppressing the expression of **a**-specific genes (*e.g. STE2*, *STE6*, *MFA1*, *MFA2*) by forming a complex with Mcm1p, Tup1p and Ssn6p. Similarly, the *MAT**a*** locus encodes two proteins (**a**1 and **a**2), but the molecular function of the **a**2 protein remains elusive. Apparently, the **a**1 homeodomain transcription factor does not fulfill a specific function in **a**-type haploid cells and the cellular identity of **a**-type cells is determined by a lack of the *MATα* allele, *i.e.* these cells do not stimulate the expression of α-specific genes nor repress the expression of **a**-specific genes. The mating type **a** is therefore considered as the default mating type of haploid *S. cerevisiae* cells [338, 340-343].

In contrast, diploid cells carrying *MAT**a*** and *MATα* information suppress the expression of haploid-specific genes including *STE4*, *STE18*, *GPA1*, *STE12* and *RME1* [338, 340-343]. In diploid cells, the presence of the α2 transcriptional repressor inhibits the expression of **a**-specific genes, similar to its function in α-type haploid cells. In addition, a novel complex of **a**1 and α2 is formed, acting as a repressor of haploid-specific genes by interaction with Tup1p and Ssn6p. The **a**1-α2 complex also represses the expression of the α1 transcription factor, thereby suppressing the expression of α-specific genes. Thus, at least three transcription factors encoded by the mating locus (**a**1, α1 and α2) contribute to determine cell-type identity in yeast.

1.3.1 Pheromone synthesis and maturation

Haploid cells of *S. cerevisiae* communicate by mating pheromones as a prerequisite for the initiation of the mating process and the formation of diploid zygotes. To this end, **a**-type cells secrete the **a**-factor pheromone in their surroundings, whereas α-type cells release the α-factor pheromone [344, 345]. In addition, both cell types carry membrane-embedded pheromone receptors for the pheromone released by cells of the other mating type, *i.e.* **a**-type cells expose the receptor for the α-factor (Ste2p) whereas α-type cells harbor the **a**-factor receptor (Ste3p). Perception of the pheromone of the respective other mating type triggers an intracellular signaling cascade ultimately resulting in plasmogamy and karyogamy, giving rise to a diploid zygote (section 1.3.2).

The mating pheromones of *S. cerevisiae* are short peptide hormones, and each of the pheromones is encoded by two respective genes: *MFA1* and *MFA2* encode **a**-factor pheromone precursors, whereas *MFα1* and *MFα2* encode the precursors of the α-factor pheromone [344, 345]. However, both mating pheromones differ considerably in amino acid sequence, posttranslational modification as well as synthesis and secretion. The α-factor represents an unmodified peptide pheromone comprised of 13 amino acids whereas the **a**-factor pheromone is composed of twelve amino acids with the C-terminal cysteine residue being posttranslationally carboxymethylated and S-farnesylated [344, 345]. The **a**-factor pheromone is synthesized from the Mfa1p or Mfa2p precursors by several consecutive processing

and modification steps carried out in the cytoplasm, and the mature pheromone is actively transported across the plasma membrane by the Ste6p transporter [344-346]. As this study focuses on the α-factor pheromone for artificial cell-cell communication and as a novel whole-cell biosensor read-out strategy (section 1.4), processing and maturation of the α-factor pheromone are described in more detail.

The α-factor pheromone precursor Mfα1p carries an N-terminal signal sequence, three N-linked glycosylation sites as well as four identical copies of the mature α-factor pheromone sequence separated by short spacer peptides [347, 348] (Figure 1). The Mfα2p precursor shows extensive structural similarity, but harbors only two repeats of the mature pheromone, one of them with a slightly different amino acid sequence [348]. Importantly, both precursors are imported into the ER and further processed within the Golgi network, ultimately resulting in secretion of the mature α-factor pheromone by the secretory pathway of yeast cells. Pheromone precursor processing upon trafficking through the secretory pathway is schematically illustrated for the Mfα1p precursor in Figure 1, but is carried out essentially similar for the Mfα2p precursor.

Upon co-translational import of the pheromone precursor into the ER, the N-terminal hydrophobic signal sequence is cleaved off immediately by the signal peptidase [349]. Subsequently, the Mfα1p precursor is modified at all three N-linked glycosylation sites by core oligosaccharide moieties [349-351]. Glycosylation of the precursor mediates efficient pheromone processing and secretion, preventing precursor accumulation in yeast [350]. Upon further trafficking through the secretory pathway, the precursor enters the Golgi apparatus (Figure 1).

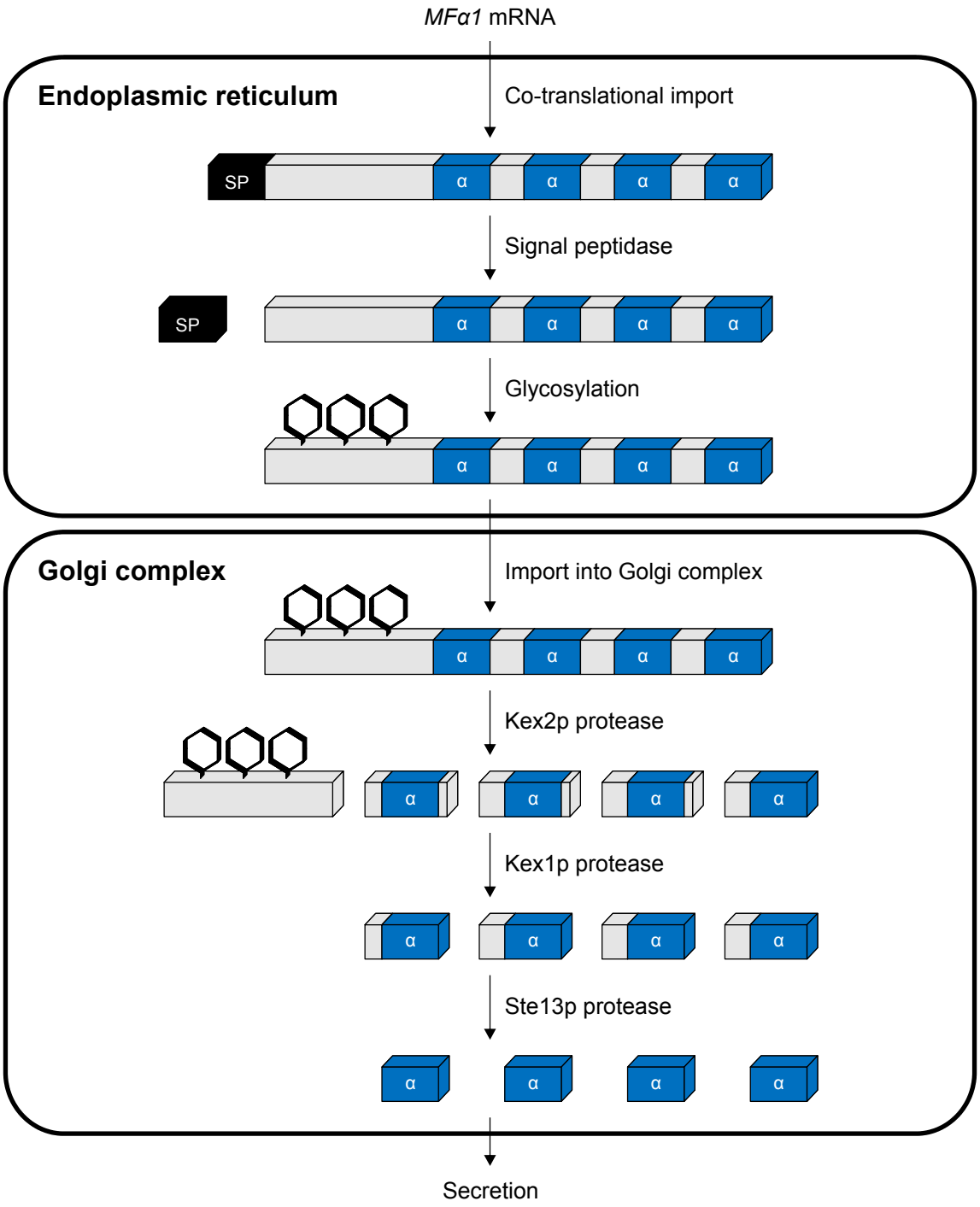

Figure 1. Schematic illustration of α-factor pheromone precursor processing upon trafficking through the secretory pathway. Processing of the pheromone precursor is exemplified for the Mfα1p precursor, but is carried out essentially similar for the Mfα2p precursor. Detailed information on the pheromone maturation process are given in the text. Modified from [344, 345].

After trimming of the attached sugar chains [349], the precursor undergoes three sequential proteolytic processing steps to release mature α-factor pheromones. First, the Mfα1p precursor is cleaved by Kex2p protease, a type I membrane protein

localized to late Golgi compartments [352, 353]. Kex2p cleaves the pheromone precursor at conserved moieties consisting of two consecutive basic amino acid residues [352]. Subsequently, the termini of the α-factor pheromone are processed by the action of respective peptidases. C-terminal pheromone maturation is carried out by Kex1p peptidase, removing the two basic amino acid residues that served as a recognition signal for Kex2p cleavage [354]. In contrast, Ste13p peptidase removes dipeptide moieties at the N-terminus of the α-factor [355], giving rise to the fully mature pheromone that is finally packed in secretory vesicles and secreted into the cellular environment (Figure 1).

1.3.2 Pheromone response of *S. cerevisiae*

Cellular response to the mating pheromone released by cells of the opposite mating type is mediated by a network of intracellular signaling cascades, ultimately preparing the pheromone-responding cell for fusion with a cognate mating partner [337]. Yeast pheromone response is coupled to cell cycle arrest in G1 phase to synchronize the cell cycle of the putative mating partners. In addition, mating pheromones stimulate the formation of mating projections (also termed shmoo tips) along the pheromone gradient, *i.e.* polarized growth of the pheromone-responding cell towards the pheromone source. Polarized growth is crucial for non-motile yeast cells to enable contact and fusion of the mating partners. Furthermore, perception of the pheromone stimulates the expression of more than 200 genes involved in mating [356, 357].

The yeast pheromone response represents one of the most studied signaling cascades, and several excellent reviews have covered this area in detail [342, 345, 358-364]. The intracellular signal transduction cascade in response to the yeast pheromone is schematically illustrated in Figure 2, exemplified for the response of **a**-type cells to the α-factor pheromone. However, the pheromone response pathway is essentially identical in α-type cells, except for the pheromone receptor (the **a**-factor is perceived by the Ste3p receptor).

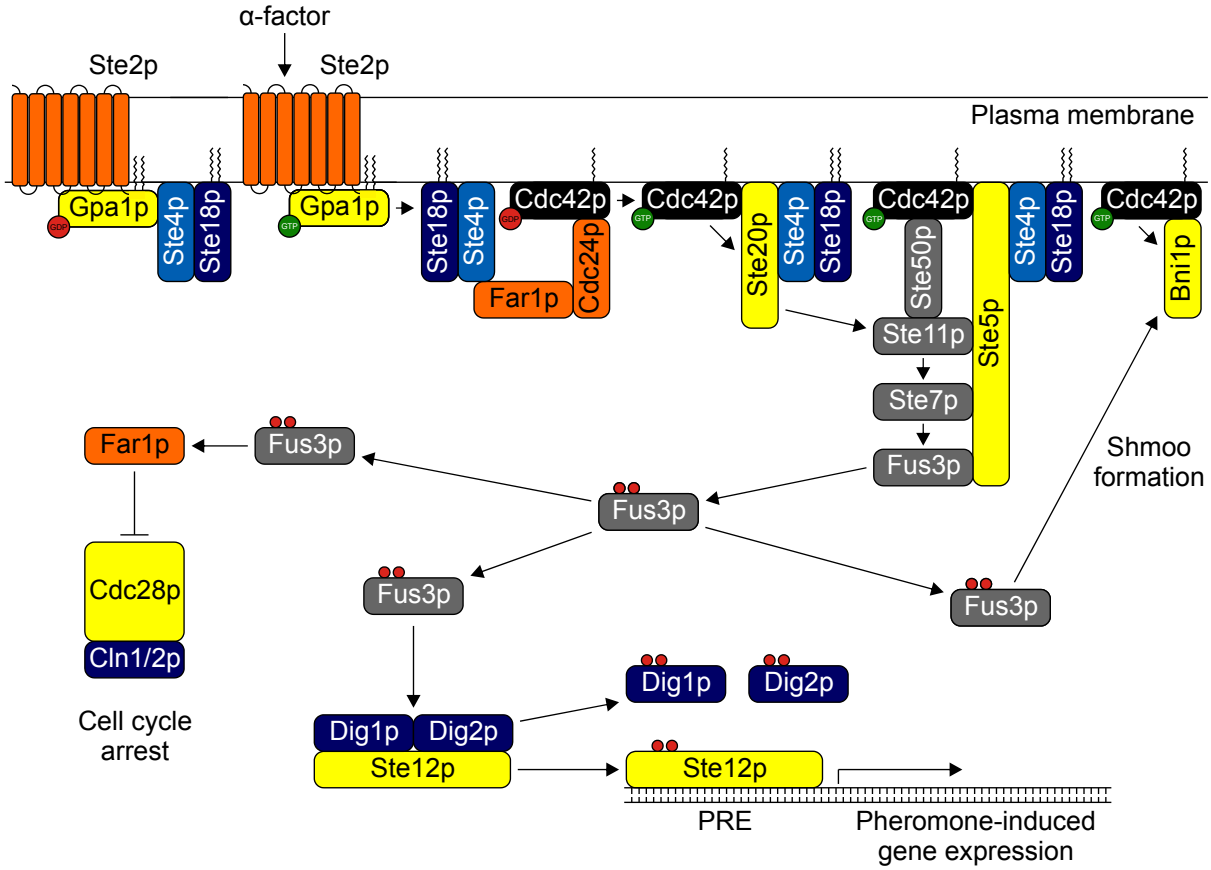

Figure 2. Schematic illustration of the intracellular signaling pathway mediating pheromone response in *S. cerevisiae*. Key factors of the signal transduction cascade of **a**-type cells responding to the α-factor mating pheromone are depicted. The signaling cascade in α-type cells responding to the **a**-factor is essentially similar, except for the pheromone receptor. For clarity, several proteins and interactions were omitted. Small red spheres indicate phosphorylation. Detailed information on the proteins and their mutual interactions can be found in the text. Modified from [358].

The initial steps of the yeast pheromone response involve perception of the mating pheromone by a cognate receptor and G-protein signaling [342, 345, 358-364]. The Ste2p GPCR embedded in the plasma membrane is responsible for the detection of the α-factor pheromone. It is composed of seven transmembrane domains, an extracellular N-terminus and an intracellular C-terminal domain involved in signal adaptation, receptor desensitization and endocytosis of the pheromone-receptor complex. The Ste2p receptor interacts with the trimeric G-protein consisting of Gpa1p (Gα subunit), Ste4p (Gβ subunit) and Ste18p (Gγ subunit). Both Gpa1p and Ste18p are posttranslationally modified with lipid moieties to mediate membrane attachment. In the absence of the pheromone, Gpa1p is bound to guanosine diphosphate (GDP) and interacts with the Ste4p-Ste18p Gβγ dimer (inactive form). Activation of the

pheromone receptor by the α-factor results in exchange of GDP with guanosine triphosphate (GTP), causing dissociation of Gpa1p from the Ste4p-Ste18p dimer. As a consequence, the released Gβγ dimer triggers subsequent signaling events. Although the activated Gpa1p also exerts several positive functions during the pheromone response, its prime function is to repress Gβγ dimer signaling in the absence of the pheromone. The free Gβγ dimer has several intracellular effectors: the Far1p/Cdc24p complex, the Ste20p kinase as well as the Ste5p scaffold protein (Figure 2). Interestingly, all of these effectors interact with the Gβ subunit, indicating that the major function of the Ste18p Gγ subunit is to keep the Gβγ dimer in close proximity to the plasma membrane [342, 345, 358-364].

The Far1p/Cdc24p complex translocates from the nucleus to the plasma membrane upon pheromone perception, interacting with the Ste4p Gβ subunit. Cdc24p represents the sole activator of Cdc42p (the main regulator of cell polarization in yeast) that is tethered to the plasma membrane by a covalently attached lipid anchor. Cdc24p activates Cdc42p by mediating exchange of GDP with GTP. One of the major functions of activated Cdc42p during the yeast pheromone response is the interaction with the Ste20p kinase. Combined action of the Gβγ dimer and activated Cdc42p result in membrane recruitment and activation of Ste20p kinase [342, 345, 358-364] (Figure 2).

The activated Ste20p kinase transmits the signal by phosphorylation of the Ste11p mitogen-activated protein kinase kinase kinase (MAPKKK), aided by the action of the Ste50p protein. The Ste11p MAPKKK subsequently activates the Ste7p mitogen-activated protein kinase kinase (MAPKK) *via* phosphorylation, which in turn phosphorylates the Fus3p mitogen-activated protein kinase (MAPK). Efficiency of MAPK signaling is strongly enhanced by the Ste5p scaffold protein arranging the corresponding protein kinases for optimal interaction [342, 345, 358-364]. In addition, the Ste5p scaffold protein recruits the MAPK signaling module to the plasma membrane *via* its interaction with Cdc42p and the Gβγ dimer (Figure 2). Furthermore, Ste5p has an important role in isolating the pheromone response pathway from other cellular signaling cascades relying on the same kinases (*e.g.* Ste11p and Ste7p are also involved in the filamentous growth pathway and osmolarity sensing [360, 362]). Upon dual phosphorylation by Ste7p MAPKK, the Fus3p MAPK dissociates from the Ste5p scaffold to interact with numerous downstream targets [342, 345, 358-364].

As a result of Fus3p-induced phosphorylation, Far1p inhibits the action of the Cdc28p cyclin-dependent kinase (CDK) that forms a complex with the G1 cyclins Cln1p/Cln2p to mediate cell cycle progression through the G1 phase (Figure 2). Therefore, Far1p-induced suppression of CDK activity results in cell cycle arrest in G1 phase, one of the hallmark features of the yeast pheromone response. In addition, Far1p is also involved in shmoo formation and the pheromone-dependent downregulation of a specific set of genes [342, 345, 358-364].

In addition, Fus3p targets the Ste12p/Dig1p/Dig2p complex. The Ste12p transcription factor is of crucial importance for pheromone-induced expression of mating-related genes, whereas Dig1p and Dig2p serve to suppress Ste12p activity in the absence of the pheromone signal. Upon phosphorylation of all three proteins by Fus3p, the complex dissociates to release active Ste12p, subsequently binding to the pheromone response element (PRE) in the upstream regulatory region of pheromone-induced genes to activate their expression (Figure 2). Ste12p is essential for the pheromone-induced expression of more than 200 genes [356, 357], indicating that numerous Ste12p target sites exist in the yeast genome. Importantly, Ste12p is part of a positive feedback circuit, stimulating its own expression to reinforce the signal [342, 345, 358-364].

During the yeast pheromone response, mating projections (*i.e.* polarized growth towards the potential mating partner) are formed. To this end, the Fus3p MAPK activates the formin Bni1p that is involved in actin polarization and cell-cell fusion [358]. By interaction with Cdc42p, Bni1p is recruited to the plasma membrane, mediating assembly of actin filaments to ensure vesicle delivery to the nascent shmoo tip (Figure 2). The pheromone gradient results in local activation of the pheromone receptor, thereby causing localized high activities of Cdc42p and Fus3p as well as localized Bni1p recruitment and activation, ensuring that the mating projection is aligned to the pheromone gradient. Ultimately, both mating partners undergo plasmogamy and karyogamy to complete the mating process [342, 345, 358-364].

Several negative feedback mechanisms exist to mediate signal adaptation in the presence of a continued pheromone stimulus [342, 345, 358-364]. These negative feedback mechanisms involve pheromone receptor desensitization and endocytosis, enhanced GTP hydrolysis by Gpa1p (to attenuate Gβγ dimer signaling), the

activation of several phosphatases to limit the activity of the MAPK signaling module as well as the degradation of the α-factor in the extracellular space by the Bar1p protease. Bar1p represents a secreted protease that cleaves the α-factor between the sixth and the seventh amino acid residue [365]. Additionally, Bar1p activity is important to shape the extracellular pheromone gradient as well as to promote recovery from the pheromone-induced cell cycle arrest in cells that did not undergo successful mating [366-372].

1.3.3 Applications of yeast pheromones in synthetic biology and whole-cell sensors

The entire yeast pheromone system, including pheromone secretion and maturation as well as cellular pheromone response, is well characterized. Therefore, yeast pheromones could be employed to implement artificial cell-cell communication modes between specifically engineered sender and receiver cell populations. Ultimately, synthetic cell-cell communication modules can be adopted into synthetic biology and biosensor applications, yielding artificial communication modes to control the behavior of individual subpopulations in cellular consortia [373-377].

For example, Regot *et al.* developed a yeast-based consortium for the calculation of Boolean functions [378]. Implementation of complex logic gates within a single cell is not feasible, given the increased risk of circuit cross-talk and the high metabolic burden as well as the low genetic stability associated with an increasing number of genetic elements transformed into a single host cell [373-377]. In the consortium approach, multiple yeast subpopulations were utilized, each engineered to calculate a specific function. The subpopulations were wired by the α-factor pheromone to achieve artificial cell-cell communication [378]. The consortium approach allowed for the implementation of highly complex circuits such as multiplexers and 1-bit adders with carry. Mathematical modelling of the design revealed that further tuning of the consortium performance might be feasible, focusing on modifications of the cell density or utilization of pheromone receptor variants with reduced ligand affinity [379]. Employing multiple, spatially confined yeast consortia, Macia *et al.* recently reported cell-based devices able to compute complex logic functions with up to six inputs, further pushing the limits of cellular logics [380]. In addition, artificial cell-cell

communication based on the yeast α-factor pheromone has been utilized to generate synthetic flip-flop memory devices as basic elements for information storage in biological systems [381, 382].

Synthetic cell-cell communication based on yeast pheromones could also be applied to implement artificial social behavior or quorum-sensing circuits. By employing **a**-type cells engineered to secrete the α-factor pheromone (*i.e.* secreting and sensing the same ligand), Youk and Lim engineered a yeast-based system to model social behavior [383]. By the additional use of "sense-only" cells, self-communication (asocial behavior) and neighbor-communication (social behavior) could be distinguished and the extent of both communication modes could be tuned by modulating the cell density as well as the expression levels of *MFα1*, *BAR1* and *STE2* [383]. In addition, Williams *et al.* developed an artificial quorum-sensing circuit relying on the secretion and perception of the α-factor pheromone by a single type of engineered cells [384]. In this design, the pheromone response was coupled to the expression of *MFα1*, essentially implementing a positive feedback loop. With increasing cell density, the pheromone concentration in the extracellular environment similarly increased. Upon passing a defined threshold value, a population-wide pheromone response was induced, strikingly resembling bacterial quorum-sensing systems [384].

Furthermore, the yeast α-factor pheromone has been exploited to achieve signal amplification in whole-cell sensors and to implement autonomous sensor-actor systems [385]. Yeast sensor cells were engineered to respond to a certain environmental cue by secreting high amounts of the α-factor pheromone, and a population of actor cells was engineered to couple the response to the secreted pheromone with the expression of a fluorescent protein, yielding the whole-cell biosensor read-out. Due to the inherent signal amplification in this design, the sensor-actor system proved to be more sensitive than a whole-cell sensor relying on a single population of engineered sensor-cells. In addition, amplifier cells (responding to the α-factor by *MFα1* expression) could be utilized to further reinforce the read-out signal of the whole-cell sensor [385]. Upon immobilization of sensor cells and actor cells in adjacent compartments, this strategy could be applied to create artificial patterns, taking use of the diffusion of the peptide pheromone across the compartment boundary [386].

1.4 Aim of this study

In this study, a novel technique to create the read-out signal of whole-cell sensors, based on the yeast α-factor mating pheromone, should be developed. In this design, engineered sensor cells respond to a defined environmental signal by secreting high amounts of the α-factor pheromone, similar to the engineered sensor cells in sensor-actor systems [385]. However, the extracellular pheromone should be quantified directly in this study, without the need for engineered actor cells, to generate the whole-cell sensor read-out.

Evidently, this design depends on the availability of a highly sensitive method for α-factor pheromone quantification. Therefore, a novel immunoassay – based on the enzyme-linked immunosorbent assay (ELISA) concept – for the detection and quantification of the yeast pheromone should be developed. This assay relies on surface functionalization with the recombinant class I hydrophobin EAS and a derivative carrying the α-factor pheromone (EAS-α, Figure 3). Upon self-assembly of the recombinant hydrophobins, the α-factor pheromone should be exposed at a transducer surface, using the hydrophobin domain as a surface anchor to immobilize the yeast pheromone in defined orientation and density. Due to the exposed yeast pheromone, hydrophobin-functionalized surfaces would allow for attachment of pheromone-specific antibodies.

Connecting the pheromone-secreting sensor cells with the functionalized surfaces *via* a fluid stream should result in pheromone transport from the sensor cells to the hydrophobin-functionalized surface. Excess of the α-factor pheromone in close vicinity of the functionalized surface should trigger a competition between the soluble pheromone (resulting from secretion by engineered sensor cells) and the immobilized α-factor (*via* EAS-α hydrophobin), ultimately resulting in competitive detachment of the antibodies from the functionalized surface. By the use of appropriate transducer elements, antibody detachment could be detected and quantified, providing the read-out signal of the whole-cell sensor (Figure 3).

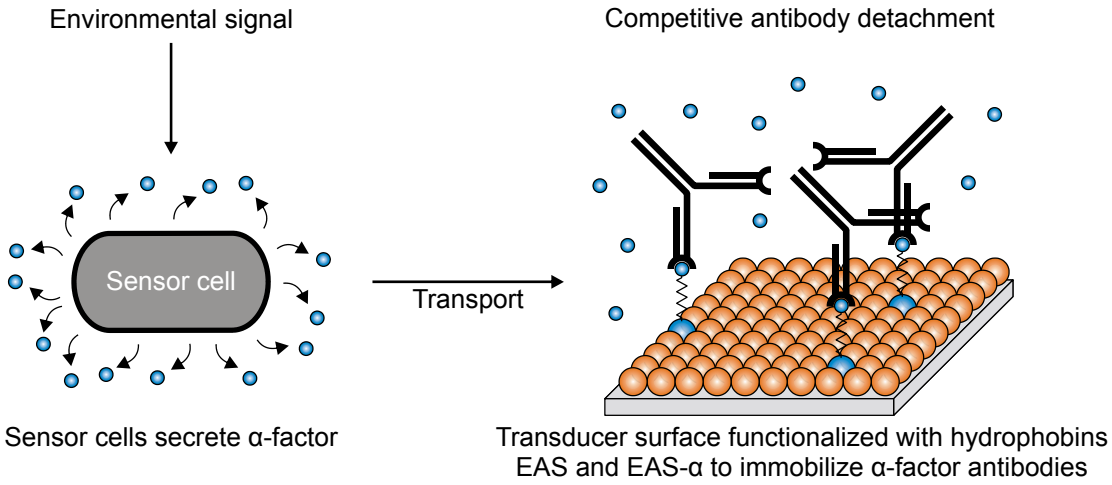

Figure 3. Schematic illustration of a novel whole-cell biosensor utilizing the α-factor pheromone to generate the sensor read-out. This approach encompasses a population of engineered sensor cells responding to an environmental cue by modulating the synthesis and secretion of the α-factor pheromone (small blue spheres). Owing to its low molecular weight, the α-factor pheromone is used as a highly mobile signal molecule that can be transported in a fluid stream. A novel hydrophobin-based immunoassay is employed to quantify the α-factor pheromone, relying on the functionalization of an appropriate transducer element with the recombinant hydrophobins EAS (orange) and EAS-α (blue). EAS-α represents a derivative of the EAS hydrophobin engineered to expose the α-factor at the functionalized surface, allowing for the specific immobilization of α-factor antibodies (black Y-shaped structures) at the surface. Soluble α-factor, resulting from α-factor secretion by the sensor cells, in the vicinity of the functionalized surface should trigger a competition between the pheromone in solution and the pheromone immobilized at the surface (*via* EAS-α), ultimately causing antibody displacement from the functionalized surface that should be detected by the transducer element, resulting in a measurable read-out signal of the whole-cell sensor.

In comparison to previously established read-out strategies for whole-cell sensors (section 1.1.3.3), this approach might provide some unique advantages. Commonly employed reporter proteins such as fluorescent proteins or luciferases depend on the use of optical transducers, limiting the flexibility regarding the transducer element. In addition, low sensor cell densities have to be maintained to avoid detrimental light scattering effects [116, 125]. In contrast, whole-cell sensors utilizing the α-factor pheromone to create the read-out signal would serve to overcome these limitations.

Since the read-out signal is based on a secreted peptide pheromone, neither cell lysis nor substrate addition are required for this type of whole-cell sensors. The pheromone might be transported in a fluid stream, providing an opportunity for spatial

separation of sensor cells and the functionalized transducer surface, allowing for high sensor cell densities to be utilized. Moreover, the proposed whole-cell sensor read-out would benefit from inherent signal amplification since the α-factor is synthesized as part of a large precursor molecule that gives rise to four identical copies of the α-factor pheromone upon maturation (Figure 1). Additionally, the hydrophobin-based immunoassays should be compatible with numerous transducer elements commonly employed in immunosensors (section 1.1.2), providing an opportunity to develop miniaturized devices for portable, field-deployable whole-cell biosensors (section 4.5.1).

This study aimed at the development of hydrophobin-based immunoassays for the quantification of the α-factor pheromone as a prerequisite for the establishment of novel whole-cell sensors relying on the secreted mating pheromone. Therefore, the recombinant hydrophobins should be purified upon expression in a heterologous host and utilized for surface engineering, allowing for the development of novel immunoassays. These immunoassays should be applied to study the pheromone secretion of wild-type and engineered yeast strains, including proof-of-concept sensor cells modulating the pheromone secretion in response to an exogenous signal. Furthermore, an artificial cell-cell communication mode – based on *S. pombe* cells engineered to secrete the α-factor pheromone of *S. cerevisiae* – should be established, providing an opportunity to implement novel control elements in yeast-based cellular consortia. In addition, the engineered *S. pombe* cells should be interfaced with the hydrophobin-based immunoassays, allowing for the development of whole-cell sensors relying on diverse yeast species.

2 Materials and Methods

2.1 Laboratory equipment

Table 2. Special laboratory equipment used in this study.

Description	Specification	Manufacturer
Cell disruptor	Mixer Mill MM 200	RETSCH GmbH (Germany)
Centrifugal evaporator	Concentrator 5301	Eppendorf AG (Germany)
Desiccator	Nalgene™ Transparent Polycarbonate Classic Design Desiccator	Thermo Fisher Scientific (Germany)
Electroporation system	Gene Pulser II	Bio-Rad Laboratories GmbH (Germany)
Flow cytometer	CyFlow® SL	Partec GmbH (Germany)
Fluorescence microscope	Axio Observer.Z1	Carl Zeiss Microscopy GmbH (Germany)
High performance liquid chromatography system	Agilent 1200 series	Agilent Technologies GmbH (Germany)
Horizontal gel electrophoresis device	PerfectBlue™ Gel System Mini M/Midi S	Peqlab Biotechnologie GmbH (Germany)
Microplate reader	infinite M200	Tecan Group Ltd. (Switzerland)
Rotating wheel	Stuart® Rotator SB3	Bibby Scientific Ltd. (UK)
Semi-dry electro-transfer system	PerfectBlue™ Semi-Dry Electro Blotter Sedec™ M	Peqlab Biotechnologie GmbH (Germany)
Thermocycler	Mastercycler ep gradient S	Eppendorf AG (Germany)

Table 2 (continued).

Description	Specification	Manufacturer
Ultrasonic homogenizer	Sonopuls GM 2070 and UW 2070	BANDELIN electronic GmbH & Co. KG (Germany)
UV Transilluminator	AlphaImager HP Imaging System	Biozym Scientific GmbH (Germany)
UV/Vis Spectro-photometer	Nanodrop ND-1000	Peqlab Biotechnologie GmbH (Germany)
UV/Vis Spectro-photometer	UltroSpec 3000	Pharmacia Biotech (Germany)
Vertical gel electro-phoresis device	PerfectBlue™ Twin ExW S Vertical Gel System	Peqlab Biotechnologie GmbH (Germany)
Water contact angle measurement device	Drop Shape Analysis System DSA10	Kruess GmbH (Germany)

2.2 Laboratory materials

2.2.1 Chemicals

All chemicals were received in analytical grade or higher purity. Unless listed in Table 3, all chemicals were purchased from Sigma-Aldrich Co. LLC (Germany), Merck KGaA (Germany), AppliChem GmbH (Germany), Carl Roth GmbH + Co. KG (Germany) or VWR International GmbH (Germany).

Table 3. Special laboratory chemicals used in this study.

Chemical	Supplier
Acetic acid	Fisher Scientific GmbH (Germany)
Agar	Formedium™ (UK)
Agarose	Biozym Scientific GmbH (Germany)
Bromophenol blue	SERVA Electrophoresis GmbH (Germany)
cOmplete EDTA-free Protease Inhibitor Cocktail Tablets	Roche Diagnostics GmbH (Germany)
His·Bind® Resin	Novagen (Germany)
Hydrogen peroxide 50 % (w/v), stabilized	Acros Organics (USA)
Isopropyl-β-D-thiogalactoside	Calbiochem (USA)
KODAK GBX developer and replenisher	Eastman Kodak Company (USA)
KODAK GBX fixer and replenisher	Eastman Kodak Company (USA)
Molybdic trioxide	ICN Biomedicals Inc. (USA)
Peptone	Formedium™ (UK)
RedSafe™ Nucleic Acid Staining Solution	iNtRON Biotechnology (Korea)
Sheath Fluid	Partec GmbH (Germany)
Yeast extract powder	Formedium™ (UK)
Yeast Nitrogen Base without amino acids and without ammonium sulphate	Formedium™ (UK)

2.2.2 Consumables

Table 4. Laboratory consumables used in this study.

Description	Specification	Supplier
96-well Polystyrene Microplates	Flat bottom (No. 473-800)	Dr. Ilona Schubert Laborfachhandel (Germany)
Autoradiography films	Amersham Hyperfilm™ ECL	GE Healthcare GmbH (Germany)
Blotting filter paper	Rotilabo®-blotting paper, 0.36 mm	Carl Roth GmbH + Co. KG (Germany)
Columns for protein purification	Protino® Columns, 35 mL	MACHEREY-NAGEL GmbH & Co. KG (Germany)
Dialysis membrane	Millipore V-series membrane, 0.025 µm pore size	Millipore (Germany)
Dialysis tubes	Spectra/Por® 1 Dialysis Membrane, 6 – 8 kDa MWCO	Spectrum Laboratories Inc. (USA)
Electroporation cuvettes	Signature™ Disposable Electroporation Cuvettes, 2 mm gap distance	VWR International GmbH (Germany)
Glass beads	0.25 – 0.5 mm diameter	Carl Roth GmbH + Co. KG (Germany)
Micro inserts for vials (HPLC)	Micro insert, strongly tapered	MACHEREY-NAGEL GmbH & Co. KG (Germany)
Polyvinylidene fluoride (PVDF) membrane	Immobilon®-P, 0.45 µm pore size	Millipore (Germany)
Screw caps for vials (HPLC)	Screw caps N 9 blue	MACHEREY-NAGEL GmbH & Co. KG (Germany)
Spectrophotometer cuvettes	Rotilabo®-single use cells (Polystyrene)	Carl Roth GmbH + Co. KG (Germany)

Table 4 (continued).

Description	Specification	Supplier
Sterile filters (HPLC)	CHROMAFIL® AO-45/3, Polyamide, 0.45 µm pore size	MACHEREY-NAGEL GmbH & Co. KG (Germany)
Sterile filters for syringes	Rotilabo®-syringe filters, PES, 0.22 µm pore size	Carl Roth GmbH + Co. KG (Germany)
Syringes	BD 1 mL/10 mL/50 mL syringe with Luer-Lok™ tip	BD Diagnostics (USA)
Ultrafiltration column	Vivaspin 20, 5000 Da MWCO, PES	Sartorius AG (Germany)
Vials (HPLC)	2 mL Standard Opening (8 mm) Screw Top Vials	Agilent Technologies GmbH (Germany)

2.2.3 Molecular weight standards

Table 5. Molecular weight standards used in this study.

Molecular weight standard	Supplier
Agarose gel electrophoresis	
GeneRuler 100 bp DNA Ladder	Thermo Fisher Scientific (Germany)
GeneRuler 1 kb DNA Ladder	Thermo Fisher Scientific (Germany)
SDS-PAGE and Tricine SDS-PAGE	
PageRuler Plus Prestained Protein Ladder	Thermo Fisher Scientific (Germany)
Spectra Multicolor Low Range Protein Ladder	Thermo Fisher Scientific (Germany)

2.2.4 Enzymes

Table 6. Commercial enzymes used in this study.

Enzyme	Supplier
Enzymes for molecular cloning	
*Bam*HI-HF® restriction endonuclease	New England Biolabs GmbH (Germany)
*Hin*dIII-HF® restriction endonuclease	New England Biolabs GmbH (Germany)
*Nhe*I-HF® restriction endonuclease	New England Biolabs GmbH (Germany)
Phusion® High-Fidelity DNA Polymerase	New England Biolabs GmbH (Germany)
*Spe*I-HF® restriction endonuclease	New England Biolabs GmbH (Germany)
*Sph*I-HF® restriction endonuclease	New England Biolabs GmbH (Germany)
T4 DNA Ligase	New England Biolabs GmbH (Germany)
Taq DNA Polymerase	New England Biolabs GmbH (Germany)
*Xho*I restriction endonuclease	New England Biolabs GmbH (Germany)
*Xma*I restriction endonuclease	New England Biolabs GmbH (Germany)
Enzymes used for purification of proteins from E. coli	
Benzonase® Nuclease	Merck KGaA (Germany)
DNase I	AppliChem GmbH (Germany)
Lysozyme	Carl Roth GmbH + Co. KG (Germany)
RNase A	AppliChem GmbH (Germany)
Further enzymes	
Proteinase K	Carl Roth GmbH + Co. KG (Germany)
Zymolyase	Seikagaku Biobusiness (Japan)

2.2.5 Antibodies

Table 7 summarizes commercial antibodies used in this study. Antibodies were diluted in 5 % (w/v) nonfat milk powder in TBS-T and 0.5 % (w/v) bovine serum albumin (BSA) in PBS-T for application in Western analyses and ELISA measurements, respectively.

Table 7. Antibodies used in this study and their final concentrations for application in Western analyses and ELISA measurements.

Antibody	Western analyses	ELISA	Supplier
Primary antibodies			
Anti-α-factor (polyclonal, from rabbit)	2.0 µg/mL	0.4 µg/mL	Peninsula Laboratories Inc. (USA)
Anti-GFP (monoclonal, from mouse)	0.4 µg/mL	---	Roche Diagnostics GmbH (Germany)
Anti-HA (monoclonal, from mouse)	0.4 µg/mL	0.08 µg/mL	Roche Diagnostics GmbH (Germany)
Anti-$(His)_6$ (monoclonal, from mouse)	0.2 µg/mL	0.1 µg/mL	Roche Diagnostics GmbH (Germany)
Anti-tRFP (polyclonal, from rabbit)	0.2 µg/mL	---	Evrogen Joint Stock Company (Russia)
Secondary antibodies			
ECL™ Anti-Mouse IgG, Horseradish Peroxidase-linked whole antibody (from sheep)	1:5,000	1:10,000	GE Healthcare GmbH (Germany)
ECL™ Anti-Rabbit IgG, Horseradish Peroxidase-linked whole antibody (from donkey)	1:5,000	1:10,000	GE Healthcare GmbH (Germany)

2.2.6 Synthetic peptides

Table 8. Synthetic peptides used in this study.

Synthetic peptide	Primary sequence	Concentration	Supplier
α-factor mating pheromone	WHWLQLKPGQPMY	10 mM in 0.1 M sodium acetate (pH 5.2)	Zymo Research Corp. (USA)
HA peptide	YPYDVPDYA	1 mM in ddH_2O	GenScript Inc. (USA)

2.2.7 DNA oligonucleotides

DNA oligonucleotides were synthesized by biomers.net GmbH (Germany). Oligonucleotides were dissolved in ddH_2O yielding a final concentration of 100 pmol/µL and stored at -20 °C. DNA oligonucleotides used for DNA sequencing exclusively are given in section 2.5.9.

Table 9. DNA oligonucleotides used in this study.

Cleavage sites for restriction endonucleases are underlined. DNA sequences complementary to the template sequence are indicated by capital letters.

Oligonucleotide	Sequence (5' → 3')	Cleavage site(s)
3HA_*Spe*I_*Hin*dIII_for	aatataaagcttactagtTACCCATACGATGTT-CCTGACTATG	*Hin*dIII, *Spe*I
EAS_*Bam*HI_rev	tatattggatccGGCAACGCAGTTGGCAGC	*Bam*HI
EAS_*Nhe*I_for	ggagtagctagcATCGGCCCCAACACCTGC	*Nhe*I
EAS_STOP_*Bam*HI_rev	tagattggatccTTAGGCAACGCAGTTGGCAGC	*Bam*HI
EAS-α-KR_*Xho*I_rev	tatattctcgagttaacgtttATACATCGGCTG-GCCCGG	*Xho*I
EAS-HA_*Xho*I_rev	tgtaccctcgagttaCGCATAGTCAGGAACATC-GTATGG	*Xho*I

Table 9 (continued).

Oligonucleotide	Sequence (5' → 3')	Cleavage site(s)
KEX1_*Xho*I_for	aaggtactcgagATGTTTTACAATAGGTGGCT-CGGA	*Xho*I
KEX1_*Xma*I_rev	aatatacccgggTTAAAAATCAGTCATCTCAAA-AGATTCATC	*Xma*I
map2/MFα1_3HA_ *Nhe*I_rev	cgcgcggctagcGCTCTCAAATTTGGCAGTAA-TATTG	*Nhe*I
map2/MFα1_ *Bam*HI_rev	tattgtggatccTTAGCTCTCAAATTTGGCAGT-AATATT	*Bam*HI
map2/MFα1_*Xho*I_ for	ataatactcgagATGAAGATCACCGCTGTCAT-TG	*Xho*I
MCS_$(GGGGS)_3$_ *Spe*I_rev	tatattactagtgctgccgccgccgccgctgcc-gccgccgccgctgccgccgccgccggatccCGA-CCCATTTGCTG	*Spe*I, *Bam*HI
MCS_*Spe*I_α_*Xho*I_ rev	tatattctcgagttaatacatcggctggcccgg-tttcagctgcagccaatgccaactagtaagctt-GTCGACGGAGCTCG	*Xho*I, *Spe*I, *Hin*dIII
MFα1_*Bam*HI_for	ataataggatccATGAGATTTCCTTCAATTTTT-ACTGCAGTT	*Bam*HI
MFα1_*Bam*HI_rev	atatatggatccTTAGTACATTGGTTGGCCGG-GTTTTAA	*Bam*HI
MFα1_*Xho*I_for	acttatctcgagATGAGATTTCCTTCAATTTTT-ACTGCAGTTTTATT	*Xho*I
MFα1-3HA_*Nhe*I_ rev	ataattgctagcGTACATTGGTTGGCCGGGTT-TTAACT	*Nhe*I
MFα1-KR_ *Bam*HI_ rev	ataattggatccttatcttttGTACATTGGTTG-GCCGGGTTTTAACT	*Bam*HI
MFα1-KR_*Xho*I_rev	ataattctcgagttatcttttGTACATTGGTTG-GCCGGGTTTTAACT	*Xho*I
pET28b_*Sph*I_for	AATGGTGCATGCAAGGAGATGG	*Sph*I
STE13_*Bam*HI_rev	aatctaggatccTTATAAATGCAAAACTTCAGT-GTTGTCAA	*Bam*HI

Table 9 (continued).

Oligonucleotide	Sequence (5' → 3')	Cleavage site(s)
STE13_*Xho*I_for	aatatactcgagATGTCTGCTTCAACTCATTC-GCA	*Xho*I

2.2.8 Plasmids

All plasmids used in this study are listed in Table 10. Plasmids applied for heterologous expression in *E. coli* were derivatives of the pET23b and pET28b expression vectors (Novagen, Germany). Vectors used for the expression of heterologous genes in *S. cerevisiae* were derived from p426GPD [387] whereas *S. pombe* expression vectors were derivatives of pJR1-3XL and pJR1-3XU [388].

Table 10. Plasmids used in this study including relevant features.

Vector	Relevant features	Reference
Vectors for E. coli		
pET23b-HA-EGFP	pBR322 origin, *amp*^{R}, T7 promoter, T7 terminator, *HA-EGFP*	A. Clemens, Institute of Genetics, Technische Universität Dresden
pET28b	pBR322 origin, *kan*^{R}, *lacI*, T7 promoter, T7 terminator	Novagen (Germany)
pET28b-EAS	T7 promoter, *EAS*	This study
pET28b-EAS-α	T7 promoter, *EAS-α*	This study
pET28b-EAS-α-KR	T7 promoter, *EAS-α-KR*	This study
pET28b-EAS-HA	T7 promoter, *EAS-HA*	This study

Table 10 (continued).

Vector	Relevant features	Reference
Vectors for S. cerevisiae		
p426GPD	*ColE1* origin, *amp*^{R}, 2µ origin, *URA3*, *GPD* promoter, *CYC1* terminator	[387]
p426GPD-MFα1	*GPD* promoter, *MFα1*	This study
p426GPD-MFα1-KR	*GPD* promoter, *MFα1-KR*	This study
Vectors for S. pombe		
pJR1-3XL	f1 origin, *amp*^{R}, *ars1*, *LEU2*, *nmt1* promoter, *nmt1* terminator	[388]
pJR1-3XU	f1 origin, *amp*^{R}, *ars1*, *ura4*$^+$, *nmt1* promoter, *nmt1* terminator	[388]
pJR1-3XU-KEX1	*nmt1* promoter, *KEX1*	This study
pJR1-3XU-STE13	*nmt1* promoter, *STE13*	This study
pJR1-map2/MFα1	*nmt1* promoter, chimeric gene *map2/MFα1*	This study
pJR1-map2/MFα1-3HA	*nmt1* promoter, chimeric gene *map2/MFα1-3HA*	This study
pJR1-MFα1	*nmt1* promoter, *MFα1*	This study
pJR1-MFα1-3HA	*nmt1* promoter, *MFα1-3HA*	This study
pJR1-MFα1-KR	*nmt1* promoter, *MFα1-KR*	This study

2.3 Microorganisms

2.3.1 *Escherichia coli* (*E. coli*) strains

Table 11. *E. coli* strains used in this study.

Strain	Genotype	Reference
BL21 (DE3) pLysS	F$^-$ *ompT hsdS*$_B$($r_B^-m_B^-$) *gal dcm* (DE3) pLysS (Cam^R)	Novagen (Germany)
SHuffle® T7 Express *lysY*	MiniF *lysY* (Cam^R)/ *Δ(ara-leu)7697 araD139 fhuA2 lacZ::T7 gene1 Δ(phoA)PvuII phoR ahpC* galE (or U) galK λatt::pNEB3-r1-cDsbC ($Spec^R$, lacIq) ΔtrxB rpsL150(Str^R) Δgor Δ(malF)3*	New England Biolabs GmbH (Germany)
Top10F`	*F'[lacI^q Tn10(tet^R)] mcrA Δ(mrr-hsdRMS-mcrBC) φ80lacZΔM15 ΔlacX74 deoR nupG recA1 araD139 Δ(ara-leu)7697 galU galK rpsL(Str^R) endA1 λ$^-$*	Invitrogen GmbH (Germany)

2.3.2 Yeast strains

Table 12. Yeast strains used in this study.

Strain	Genotype	Reference
Saccharomyces cerevisiae (S. cerevisiae)		
BY4741	*MAT**a** his3Δ1 leu2Δ0 met15Δ0 ura3Δ0*	EUROSCARF (Germany)
BY4741 *Δbar1*	*MAT**a** his3Δ1 leu2Δ0 met15Δ0 ura3Δ0 YIL015w::kanMX4*	EUROSCARF (Germany)
BY4741 *Δbar1 FIG1-tRFP*	*MAT**a** his3Δ1 leu2Δ0 met15Δ0 ura3Δ0 YIL015w::kanMX4 YBR166c::FIG1-tRFP*	Dr. A. Groß, Institute of Genetics, Technische Universität Dresden

Table 12 (continued).

Strain	Genotype	Reference
BY4742	*MATα his3Δ1 leu2Δ0 lys2Δ0 ura3Δ0*	EUROSCARF (Germany)
BY4742 *Δkex1*	*MATα his3Δ1 leu2Δ0 lys2Δ0 ura3Δ0 YGL203c::kanMX4*	EUROSCARF (Germany)
BY4742 *Δste13*	*MATα his3Δ1 leu2Δ0 lys2Δ0 ura3Δ0 YOR219c::kanMX4*	EUROSCARF (Germany)
Schizosaccharomyces pombe (S. pombe)		
HE620	h^{+S} *leu1-32 ura4-D18*	[389]

2.4 Cultivation of microorganisms

2.4.1 Cultivation of *E. coli*

E. coli was grown in Luria Broth (LB) medium at 30 °C or 37 °C under constant rotation (180 rpm). If selection for transformed cells had to be applied, ampicillin (100 µg/mL), kanamycin (60 µg/mL) and/or chloramphenicol (34 µg/mL) were added. Antibiotics were dissolved in ddH_2O (ampicillin and kanamycin) or 70 % (v/v) ethanol (chloramphenicol), passed through a sterile filter and stored at -20 °C.

LB medium (pH 7.4):
- 10 g/L Peptone
- 5 g/L Yeast extract
- 5 g/L NaCl
- 15 g/L Agar for solid LB medium

2.4.2 Cultivation of *S. cerevisiae*

S. cerevisiae was cultivated using either rich medium (YPD medium) or minimal medium (SD medium) at 30 °C under constant rotation (180 rpm). SD medium was employed to select for plasmid-carrying yeast cells. Different supplements were added to SD medium according to the auxotrophies of the respective yeast strain.

YPD medium:	20 g/L Peptone
	10 g/L Yeast extract
	20 g/L Glucose
	15 g/L Agar for solid YPD medium
SD medium:	1.9 g/L Yeast Nitrogen Base
	5 g/L $(NH_4)_2SO_4$
	20 g/L Glucose
	20 g/L Agar for solid SD medium
Supplements:	80 mg/L L-Leucine
	20 mg/L L-Methionine
	60 mg/L L-Histidine
	30 mg/L Uracil
	30 mg/L L-Tyrosine

2.4.3 Cultivation of *S. pombe*

S. pombe HE620 was grown in rich medium (YES medium) or Edinburgh minimal medium (EMM) [390] at 30 °C under constant shaking (180 rpm). If required, supplements were added to EMM to complement the auxotrophies of the respective *S. pombe* strain.

YES medium (pH 6.5):	5 g/L Yeast extract
	30 g/L Glucose
	0.1 % (v/v) Solution A3a
	0.1 % (v/v) Solution A3b
	100 mg/L L-Leucine
	50 mg/L L-Proline
	50 mg/L L-Lysine
	100 mg/L Uracil
	20 g/L Agar for solid YES medium
Solution A3a:	1 g/L Calcium-D(+)-pantothenic acid
	10 g/L Myo-inositol
	10 g/L Nicotinic acid
Solution A3b:	10 mg/L Biotin
	50.0 % (v/v) Ethanol
EMM (pH 5.5):	5 g/L NH_4Cl
	2.2 g/L Na_2HPO_4
	20 g/L Glucose
	5.0 % (v/v) Salt stock solution
	0.1 % (v/v) Solution A3a
	0.1 % (v/v) Solution A3b
	0.01 % (v/v) Mineral stock solution
	20 g/L Agar for solid EMM
Salt stock solution (pH 5.5):	60 g/L Potassium hydrogen phthalate
	21 g/L $MgCl_2 \cdot 6\ H_2O$
	0.8 g/L Na_2SO_4
	20 g/L KCl
	0.39 g/L $CaCl_2 \cdot 2\ H_2O$

Mineral stock solution:	5.0 g/L Boric acid
	4.48 g/L $MnSO_4 \cdot H_2O$
	4.0 g/L $ZnSO_4 \cdot 7\ H_2O$
	1.2 g/L $FeCl_3$
	356 mg/L MoO_3
	1.0 g/L KI
	400 mg/L $CuSO_4 \cdot 5\ H_2O$
	10.0 g/L Citric acid
Supplements:	250 mg/L L-Leucine
	100 mg/L Uracil

2.5 Molecular cloning techniques

2.5.1 Isolation of chromosomal DNA from *S. cerevisiae*

About 10 mL of YPD medium were inoculated with cells of the respective *S. cerevisiae* strain and grown for 14 – 16 h at 30 °C. About 6 mL of the cell suspension were harvested (3,500 × g, 5 min, 4 °C), washed once with ddH_2O and harvested again under identical conditions. Subsequently, cells were resuspended in 500 µL yeast lysis buffer, glass beads (diameter 0.25 – 0.5 mm) were added and the cells were disintegrated mechanically by using a cell disruptor (30 Hz, 5 min). Glass beads were allowed to sediment, the supernatant was transferred to a new vial and mixed with 275 µL 7 M ammonium acetate (pH 7.0) prior to incubation for 5 min at 65 °C. After chilling the solution for 5 min on ice, 500 µL chloroform were added, mixed thoroughly for 1 min and centrifuged at 13,000 × g for 5 min. The upper (aqueous) phase was carefully withdrawn, mixed with 1 mL 2-propanol and incubated for 30 min at -20 °C. Precipitated DNA was pelleted by centrifugation (13,000 × g, 15 min, 4 °C), washed three times with 70 % (v/v) ethanol and dried in a centrifugal evaporator. Eventually, DNA was dissolved in 50 µL ddH_2O and stored at -20 °C.

Yeast lysis buffer (pH 8.0):	100 mM Tris/HCl
	50 mM EDTA
	1.0 % (w/v) SDS

2.5.2 Polymerase chain reaction (PCR)

Targeted amplification of DNA fragments for molecular cloning purposes was achieved by PCR employing the Phusion® High-Fidelity DNA polymerase, owing to its proof-reading activity. Diagnostic PCR was carried out using the *Taq* DNA polymerase. The composition of PCR mixtures is detailed in Table 13.

Table 13. Composition of PCR mixtures for different DNA polymerases.

Component	**Phusion® High-Fidelity DNA polymerase**	***Taq* DNA polymerase**
Reaction buffer	1 × Phusion® HF Buffer	1 × GoldStar PCR Buffer
$MgCl_2$	1.5 mM (1)	1.5 mM
Forward Primer	0.4 pM	0.4 pM
Reverse Primer	0.4 pM	0.4 pM
dNTPs	0.2 mM	0.2 mM
DNA template	1-10 ng	1-10 ng
DNA polymerase	0.02 U/µL	0.025 U/µL

(1) 1 × Phusion® HF Buffer already contained 1.5 mM $MgCl_2$.

10 × GoldStar PCR Buffer (pH 8.8):	750 mM Tris/HCl
	200 mM $(NH_4)_2SO_4$
	0.1 % (v/v) Tween® 20

Standard PCR amplification featured ten cycles with lower primer annealing temperature and 25 subsequent cycles with elevated primer annealing temperature. The standard PCR temperature profile is indicated in Table 14.

Table 14. Temperature profile for standard PCR.

Cycle step	Temperature	Time	Cycles
Initial denaturation	98/94 °C (1)	3:00/5:00 min (2)	1
Denaturation	98/94 °C (1)	0:30 min	
Primer annealing	T_{A1} (3)	0:30 min	10
Primer extension	72 °C	$t_{extension}$ (4)	
Denaturation	98/94 °C (1)	0:30 min	
Primer annealing	T_{A2} (3)	0:30 min	25
Primer extension	72 °C	$t_{extension}$ (4)	
Final extension	72 °C	3:00/5:00 min (2)	1

(1) Temperature during the denaturation step was adjusted to 98 °C and 94 °C for reactions using Phusion® High-Fidelity DNA polymerase and *Taq* DNA polymerase, respectively.

(2) Time interval for initial denaturation and final extension was set to 3:00 min and 5:00 min for reactions using Phusion® High-Fidelity DNA polymerase and *Taq* DNA polymerase, respectively.

(3) Temperatures during primer annealing steps were calculated by considering the melting temperature of the specifically hybridizing sequence (T_{A1}) and the full nucleotide sequence (T_{A2}) of the oligonucleotides used. Oligonucleotide melting temperatures were determined by Vector NTI software.

(4) Extension time $t_{extension}$ was calculated by considering the speed of each DNA polymerase (3 kb/min for Phusion® High-Fidelity DNA polymerase, 1 kb/min for *Taq* DNA polymerase) and the length of the DNA fragment to be amplified.

2.5.3 Restriction of DNA

About 1 – 2 µg of purified DNA were mixed with 20 U of the respective restriction endonuclease and incubated for at least 1 h at 37 °C. Commercial reaction buffers purchased from New England Biolabs GmbH (Germany) were chosen according to the specific activity of the restriction endonuclease(s). If required, 0.1 mg/mL BSA was added.

2.5.4 Agarose gel electrophoresis

DNA fragments were separated by the use of agarose gel electrophoresis. Respective gels were prepared by dissolving 1.0 – 1.5 % (w/v) agarose in TAE buffer by heating in a microwave oven. Agarose solutions were cooled down prior to adding 1 × RedSafe™ Nucleic Acid Staining Solution. Upon solidification, agarose gels were placed into horizontal gel electrophoresis systems and loaded with DNA samples premixed with DNA loading buffer. About 500 ng of an appropriate molecular weight size standard were also loaded. DNA fragments were separated by applying a constant voltage of 90 – 130 V and visualized by illumination at 365 nm in a UV Transilluminator.

TAE buffer (pH 8.3):	40 mM Tris/HCl
	20 mM Acetic acid
	1 mM EDTA
6 × DNA loading buffer (pH 8.0):	0.2 % (w/v) Bromophenol blue
	100 mM EDTA
	30.0 % (v/v) Glycerol

2.5.5 Extraction of DNA fragments from agarose gels

For molecular cloning purposes, DNA fragments were excised from agarose gels by the use of a sterile scalpel. DNA was purified from agarose gel fragments using the Zymoclean™ Gel DNA Recovery Kit system (Zymo Research Corp., USA) according to the manufacturer`s instruction.

2.5.6 DNA ligation

The concentration of DNA fragments was determined by measuring the UV absorption at 280 nm using a Nanodrop ND-1000 UV/Vis spectrophotometer prior to setting up DNA ligation reactions. The DNA fragments were mixed in equimolar ratio and DNA ligation buffer as well as T4 DNA ligase were added. DNA ligation was carried out at ambient temperature for 2 h or at 16 °C for at least 14 h. To remove

excess salts prior to electroporation, about 5 µL of the DNA ligation reaction were placed on a Millipore V-series dialysis membrane and dialyzed for at least 15 min against ddH_2O.

2.5.7 Transformation of *E. coli via* electroporation

2.5.7.1 Preparation of electrocompetent cells

E. coli cells were grown in 15 mL LB medium at 37 °C for 14 – 16 h to stationary phase and 400 mL fresh LB medium were inoculated with 8 mL of this cell suspension. The main culture was incubated at 37 °C until cells reached mid-log phase (OD_{600} = 0.4 – 0.6). The cell suspension was chilled on ice for 15 min and cells were harvested by centrifugation (3,500 × g, 10 min, 4 °C). *E. coli* cells were washed twice with cold, sterile ddH_2O and twice with cold, sterile 10 % (v/v) glycerol. Each washing step was followed by centrifugation under aforementioned conditions. Finally, the cells were resuspended in 2 mL cold, sterile 10 % (v/v) glycerol and 50 µL aliquots were stored at -80 °C until use.

2.5.7.2 Electroporation

E. coli cells were transformed with plasmid DNA by employing the electroporation technique. Aliquots of electrocompetent cells were thawed on ice and mixed with about 100 ng of purified plasmid DNA. Alternatively, 3 µL of a DNA ligation reaction were added. The resulting suspension was filled in chilled electroporation cuvettes and electroporation was carried out using appropriate parameters (2.5 kV, 25 µF, 200 Ω). Cells were immediately resuspended in 1 mL SOC medium, incubated for 1 h at 37 °C under constant shaking (400 rpm) and finally plated on LB medium containing the respective antibiotic(s) for selection of transformed cells. LB plates were incubated for at least 14 h at 37 °C.

SOC medium:	20 g/L Peptone
	5 g/L Yeast extract
	10.0 mM NaCl
	2.5 mM KCl
	20.0 mM Glucose
	10.0 mM $MgCl_2 \cdot 6\ H_2O$
	10.0 mM $MgSO_4 \cdot 7\ H_2O$

2.5.8 Isolation of plasmid DNA from *E. coli*

A single colony of transformed *E. coli* cells was used to inoculate 10 mL LB medium containing the respective antibiotic(s) and cells were grown for at least 14 h at 37 °C. Plasmid DNA was isolated by the use of the ZR Plasmid Miniprep™-Classic kit system (Zymo Research Corp., USA) according to the manufacturer`s instruction.

2.5.9 DNA sequencing

DNA sequencing was carried out by Eurofins Genomics GmbH (Germany). DNA oligonucleotides used exclusively for sequencing purposes were provided by Eurofins Genomics GmbH (Germany) or purchased from biomers.net GmbH (Germany).

Table 15. DNA oligonucleotides used for DNA sequencing.

DNA oligonucleotide	Sequence (5' → 3')
CYCtermrev	GCGTGAATGTAAGCGTGAC
GPD promfor	CGGTAGGTATTGATTGTAATTCTG
KEX1 Seq	CGTTTGCTATGGAGAAGAAACTGA
nmt1 for	AGGAATCCTGGCATATCATC
nmt1 rev	TGCAGCTTGAATGGGCTTCC
STE13 Seq1	GACGTAAAAGTGTATGATATACCATCATCTC
STE13-Seq2	TCTGGCTTTGGGGGGATG

Table 15 (continued).

DNA oligonucleotide	Sequence (5' → 3')
T7	TAATACGACTCACTATAGGG
T7term	CTAGTTATTGCTCAGCGGT

2.5.10 DNA synthesis

The Open Reading Frame (ORF) encoding the synthetic *map2/MFα1* gene comprising parts of *S. pombe map2* and *S. cerevisiae MFα1* was synthesized by ATG:biosynthetics GmbH (Germany).

2.5.11 Yeast transformation

Transformations of *S. cerevisiae* and *S. pombe* were carried out by the lithium acetate/single-stranded carrier DNA/polyethylene glycol (PEG) method according to Gietz and Woods [391]. Briefly, yeast cells were grown at 30 °C to stationary phase in 10 mL YPD or YES medium. About 2 mL of the cell suspension were taken and cells were harvested by centrifugation (3,500 × g, 5 min, 4 °C). Cells were washed once with cold, sterile ddH_2O and once with cold, sterile 100 mM lithium acetate. Each washing step was followed by centrifugation under aforementioned conditions. The cell pellet was covered with 240 µL cold, sterile 50 % (w/v) PEG 3350, and 36 µL 1 M lithium acetate, 25 µL 10 mg/mL single-stranded carrier DNA and about 2 µg plasmid DNA (dissolved in 50 µL ddH_2O) were added sequentially. The cells were resuspended in the transformation mixture and incubated at 30 °C for 30 min prior to a heat shock treatment (42 °C, 20 min). Finally, cells were harvested under aforementioned conditions, resuspended in 100 µL cold, sterile ddH_2O and spread on minimal medium plates containing the respective supplements to select for plasmid-carrying cells. Minimal medium plates were incubated at 30 °C for three to seven days.

2.6 Western Blot analysis

2.6.1 Preparation of yeast cell lysates

Total cell lysates of yeast cells were prepared for Western analyses. Therefore, the cells were suspended in phosphate-buffered saline (PBS) containing protease inhibitors and were disintegrated mechanically by the use of glass beads (0.25 – 0.5 mm diameter) using a cell disruptor (30 Hz, 5 min). Subsequently, glass beads and intact cells were removed by centrifugation (3,500 × g, 5 min, 4 °C) to obtain cellular lysates. Total protein concentrations were determined by the use of the Bio-RAD DC™ Protein Assay (Bio-Rad Laboratories GmbH, Germany) according to the manufacturer`s instruction. Eventually, cell lysates were subjected to electrophoretic separation (section 2.6.2) and immunological analysis (sections 2.6.5 and 2.6.6).

PBS (pH 7.4)	2.68 mM KCl
	1.47 mM KH_2PO_4
	7.82 mM $Na_2HPO_4 \cdot 12\ H_2O$
	137 mM NaCl

2.6.2 Sodium dodecyl sulfate polyacrylamide gel electrophoresis (SDS-PAGE)

SDS-PAGE was carried out to separate proteins under denaturing conditions following the principle of discontinuous electrophoresis [392]. A vertical gel electrophoresis cassette was assembled by employing spacers (0.8 mm thickness) and respective glass plates. The separating gel was prepared according to Table 16 and carefully poured into the cassette. The gel was covered with 1 mL 2-propanol and allowed to polymerize for at least 45 min at ambient temperature. Upon withdrawal of 2-propanol, the stacking gel (Table 16) was poured on top of the separating gel. A suitable comb was inserted and the gel was allowed to polymerize overnight at room temperature under moist conditions.

Table 16. Composition of separating and stacking gels for SDS-PAGE.

Component	Separating gel 15 % (w/v) Polyacrylamide	Stacking gel 5 % (w/v) Polyacrylamide
30 % (w/v) Acrylamide: bis-acrylamide (37.5 : 1)	5.0 mL	1.7 mL
Separating gel buffer (1.5 M Tris/HCl, pH 8.8)	2.5 mL	---
Stacking gel buffer (1.0 M Tris/HCl, pH 6.8)	---	1.25 mL
10 % (w/v) SDS	100 µL	100 µL
10 % (w/v) Ammonium persulfate (APS)	100 µL	100 µL
N,N,N′,N′-Tetramethyl-ethane-1,2-diamine (TEMED)	4 µL	10 µL
ddH_2O	2.3 mL	6.8 mL

Protein samples were mixed with 6 × Protein loading buffer prior to adding dithiothreitol to a final concentration of 100 mM. The samples were incubated for 5 min at 95 °C and subsequently loaded on the gel. The electrophoresis chamber was filled with running buffer and the proteins were separated by applying a maximum voltage of 120 V while limiting the current to 30 mA per gel.

6 × Protein loading buffer (pH 6.8):
- 300 mM Tris/HCl
- 12.0 % (w/v) SDS
- 0.6 % (w/v) Bromophenol blue
- 26.3 % (v/v) Glycerol

Running buffer:
- 24.9 mM Tris
- 191.8 mM Glycine
- 0.1 % (w/v) SDS

2.6.3 Tricine SDS-PAGE

Due to the comparatively low molecular weight of recombinant hydrophobins, a modified SDS-PAGE version (Tricine SDS-PAGE [393]) was carried out for the electrophoretic separation of these proteins. The composition of the separating gel and stacking gel for Tricine SDS-PAGE is detailed in Table 17. Protein samples containing the recombinant hydrophobins were prepared according to the standard SDS-PAGE protocol (section 2.6.2). The electrophoretic device was filled with Tricine running buffer and the proteins were separated by applying an electric field with a maximum voltage of 150 V and a maximum current of 60 mA per gel. The electrophoresis was carried out in a cold room to prevent heating up of the device.

Table 17. Composition of separating and stacking gels for Tricine SDS-PAGE.

Component	**Separating gel** 18 % (w/v) Polyacrylamide	**Stacking gel** 2.5 % (w/v) Polyacrylamide
40 % (w/v) Acrylamide: bis-acrylamide (19 : 1)	4.5 mL	---
40 % (w/v) Acrylamide: bis-acrylamide (29 : 1)	---	1.3 mL
Tricine gel buffer	2.5 mL	2.5 mL
10 % (w/v) APS	40 µL	40 µL
TEMED	15 µL	40 µL
ddH_2O	3.0 mL	6.2 mL

Tricine gel buffer (pH 8.45):	3.0 M Tris/HCl 0.4 % (w/v) SDS
Tricine running buffer (pH 8.3):	100 mM Tris/HCl 100 mM Tricine 0.1 % (w/v) SDS

2.6.4 Colloidal Coomassie staining

Upon electrophoretic separation, proteins could be visualized in the gel matrix by colloidal Coomassie staining [394]. Therefore, electrophoresis cassettes were disassembled and the separating gels were washed in ddH_2O for 1 min. Subsequently, the proteins were fixed in the polyacrylamide matrix by incubating the separating gels for 30 min in colloidal Coomassie fixer. Upon separation *via* Tricine SDS-PAGE, 5 % (v/v) glutaraldehyde was used to fix the proteins in the gel matrix. The separating gels were washed three times for 5 min using ddH_2O and finally transferred into the colloidal Coomassie staining solution to visualize proteins. The gels were allowed to stain for at least 24 h at ambient temperature.

Colloidal Coomassie fixer:	40 % (v/v) Ethanol
	10 % (v/v) Acetic acid
Colloidal Coomassie staining solution:	0.8 g/L Coomassie brilliant blue G-250
	80 g/L Ammonium sulfate
	0.82 % (v/v) Phosphoric acid
	20 % (v/v) Methanol

2.6.5 Transfer of proteins to PVDF membranes

Upon electrophoretic separation, proteins could be transferred to PVDF membranes *via* the semi-dry Western Blot method. To this end, the electrophoresis cassettes were disassembled and the separating gels were equilibrated in transfer buffer for at least 15 min. Separating gels derived from Tricine SDS-PAGE were incubated in transfer buffer for at least 30 min. The PVDF membrane was activated by incubation for 1 min in methanol and subsequently stored in transfer buffer. Likewise, six sheets of blotting filter paper were soaked with transfer buffer prior to assembling the Western Blot. Three sheets of the blotting filter paper, the activated PVDF membrane, the separating gel and another three sheets of the blotting filter paper were sequentially stacked on the anode of a semi-dry Western Blotting device. The transfer of the proteins was carried out by applying an electric field with a maximum voltage of 25 V and a current of 1.5 mA/cm^2 (considering the area of the separating

gel). The transfer was stopped after 45 min (Tricine SDS-PAGE) or 1 h (SDS-PAGE) and the PVDF membranes were allowed to dry.

Transfer buffer:	24.9 mM Tris
	191.8 mM Glycine
	0.01 % (w/v) SDS
	20.0 % (v/v) Methanol

2.6.6 Immunological detection

Upon electrotransfer of proteins to PVDF membranes, specific proteins could be detected immunologically. Therefore, the PVDF membrane was activated by incubation in methanol for 1 min, washed twice with TBS-T for 5 min and residual protein binding sites of the membrane were blocked by treatment with 5 % (w/v) nonfat milk powder (dissolved in TBS-T) for 1 h at ambient temperature. Subsequently, the blocking solution was discarded and the membrane was incubated with the primary antibody (Table 7) for 1 h at room temperature. Non-specifically bound antibodies were removed by three washing steps in TBS-T (3 × 10 min) prior to applying the secondary antibody solution (Table 7). After 30 min, the secondary antibody solution was withdrawn and the membrane was washed again with TBS-T (3 × 10 min). Finally, bound antibodies were visualized by the use of Amersham™ ECL™ Prime Western Blotting Detection Reagent (GE Healthcare GmbH, Germany) according to the manufacturer`s instruction and exposure of autoradiography films.

TBS-T (pH 7.6):	20 mM Tris/HCl
	137 mM NaCl
	0.1 % (v/v) Tween® 20

2.7 Expression and purification of recombinant proteins

2.7.1 Heterologous expression of recombinant proteins

2.7.1.1 Heterologous expression of recombinant hydrophobins

Cells of the *E. coli* strain T7 SHuffle® T7 Express *lysY* were transformed with plasmids encoding recombinant hydrophobins. A single colony of transformants was used to inoculate 15 mL LB medium and grown to stationary phase at 30 °C. About 400 mL of LB medium buffered with 50 mM 3-(N-morpholino)propanesulfonic acid (MOPS) were inoculated with 8 mL of the cell suspension and incubated at 30 °C. When the cells reached mid-log phase (corresponding to OD_{600} = 0.4 – 0.6), isopropyl-β-D-thiogalactoside (IPTG) was added to a final concentration of 0.4 mM to induce the expression of the recombinant hydrophobins. The cells were incubated at 30 °C for further 4 h. Subsequently, the culture was chilled on ice for 15 min and cells were harvested by centrifugation (15,000 × g, 10 min, 4 °C). Cells were washed once with cold 50 mM Tris/HCl (pH 7.5) and harvested again under similar conditions. Finally, the cells were stored at -20 °C until use for protein purification.

2.7.1.2 Heterologous expression of HA-EGFP

Cells of *E. coli* BL21 (DE3) pLysS were transformed with pET23b-HA-EGFP. About 15 mL LB medium were inoculated with a single colony of transformed cells and incubated at 30 °C until cells reached stationary phase. 8 mL of this suspension were used to inoculate 400 mL LB medium and cells were grown at 30 °C until mid-log phase (corresponding to OD_{600} = 0.4 – 0.6) was reached. Expression of the *HA-EGFP* gene was induced by adding IPTG to a final concentration of 0.5 mM. After further incubation for 4 h at 30 °C, the cell suspension was chilled on ice for 15 min and cells were harvested (3,500 × g, 10 min, 4 °C). Cells were washed once with PBS, harvested under similar conditions and finally stored at -20 °C until use.

2.7.2 Purification of recombinant proteins by Ni^{2+} affinity chromatography

2.7.2.1 Extraction of recombinant hydrophobins from inclusion bodies

Extraction of hydrophobins from inclusion bodies was carried out essentially as described previously [246]. Briefly, *E. coli* cells from the main culture expressing recombinant hydrophobins (section 2.7.1.1) were thawed on ice and resuspended in 30 mL cold 50 mM Tris/HCl (pH 7.5) containing protease inhibitors. Cells were disrupted by ten sonication steps (1 min, 90 % cycles, 70 % power) in a Sonopuls GM2070 ultrasonic homogenizer. Subsequently, lysozyme (2 mg/mL), DNase I (0.1 mg/mL), RNase A (0.1 mg/mL) and Benzonase (8 U/mL) were added and the suspension was incubated at 37 °C for 20 min. After chilling the suspension on ice for 15 min, insoluble compounds of the cell lysate (including the recombinant hydrophobins in inclusion bodies) were harvested by centrifugation (20,000 × g, 10 min, 4 °C) and washed twice with cold 50 mM Tris/HCl (pH 7.5). Each washing step was followed by centrifugation under similar conditions.

Hydrophobins were extracted from inclusion bodies by treatment with lysis buffer. Therefore, the pelleted insoluble lysate fraction was resuspended in 15 mL lysis buffer and incubated for 30 min at ambient temperature followed by centrifugation under aforementioned conditions. Urea treatment resulted in solubilization of the recombinant hydrophobins that were consequently present in the supernatant upon centrifugation. Hydrophobin extraction was carried out three times, the latter two extraction steps were performed at 37 °C. The fractions of all three extraction steps were pooled, sonicated once under the aforementioned conditions to reduce sample viscosity (owing to residual genomic DNA) and finally used for protein purification.

Lysis buffer (pH 8.0):	50 mM KH_2PO_4
	50 mM Na_2HPO_4
	10 mM Tris/HCl
	8 M Urea

2.7.2.2 Purification of recombinant hydrophobins

Recombinant hydrophobins were purified by Ni^{2+} affinity chromatography essentially as described previously [146, 246], utilizing the His·Bind® Resin sepharose matrix. The sepharose matrix was poured into a Protino® Column and covered with a filter frit to avoid matrix disturbance during the protein purification process. Next, the column matrix was washed three times with ddH_2O prior to adding 15 mL 1 M nickel sulfate to load the column with Ni^{2+} ions. The column was washed again three times with ddH_2O and at least seven times with lysis buffer. Solubilized hydrophobins (section 2.7.2.1) were loaded and allowed to run through the column twice. The column was washed sequentially with 100 mL lysis buffer, 100 mL wash buffer A and 100 mL wash buffer B to remove non-specifically bound proteins. Recombinant hydrophobins were eluted from the column by adding 25 mL elution buffer in five consecutive steps. The fractions corresponding to the third, fourth and fifth elution step, containing the recombinant hydrophobin in sufficient quantity and purity, were pooled and concentrated by ultrafiltration. Therefore, Vivaspin 20 ultrafiltration columns with a molecular weight cut-off (MWCO) of 5,000 Da were utilized to reduce the volume of the pooled eluate fractions to about 3 – 5 mL.

Wash buffer A (pH 6.3):	50 mM KH_2PO_4
	50 mM Na_2HPO_4
	10 mM Tris/HCl
	8 M Urea
	20 mM Imidazole
Wash buffer B (pH 5.9):	50 mM KH_2PO_4
	50 mM Na_2HPO_4
	10 mM Tris/HCl
	8 M Urea
	40 mM Imidazole

Elution buffer (pH 4.5):	50 mM KH_2PO_4
	50 mM Na_2HPO_4
	10 mM Tris/HCl
	8 M Urea
	250 mM Imidazole

2.7.2.3 Purification of HA-EGFP

E. coli cells derived from the main culture expressing the *HA-EGFP* gene (section 2.7.1.2) were thawed on ice, resuspended in 30 mL buffer B and disrupted by six sonication steps (1 min, 90 % cycles, 70 % power) using a Sonopuls GM2070 ultrasonic homogenizer. Subsequently, lysozyme (2 mg/mL), DNase I (0.1 mg/mL), RNase A (0.1 mg/mL) and Benzonase (8 U/mL) were added and the suspension was incubated for 30 min at 37 °C. After chilling the suspension on ice for 15 min, insoluble compounds of the cell lysate were removed by centrifugation (15,000 × g, 30 min, 4 °C). Recombinant HA-EGFP was found in the soluble lysate fraction and could be purified by Ni^{2+} affinity chromatography. Briefly, His·Bind® Resin was poured into a Protino® column, covered with a filter frit and washed three times with ddH_2O. The column was loaded with Ni^{2+} ions by adding 15 mL 1 M nickel sulfate prior to washing the column three times with ddH_2O and at least seven times with buffer B. Next, the cell extract containing the recombinant HA-EGFP was allowed to flow through the column twice. The column was washed twice with buffer B, twice with buffer W1 and twice with buffer W2 subsequently to remove non-specifically bound proteins. Finally, recombinant HA-EGFP was eluted from the column by adding 15 mL buffer E. The entire Ni^{2+} affinity purification procedure was performed at 4 °C to avoid protein degradation.

Buffer B (pH 7.9):	20 mM Tris/HCl
	500 mM NaCl
	0.2 % (v/v) Triton X-100
	5 mM Imidazole

Buffer W1 (pH 7.9):	20 mM Tris/HCl 500 mM NaCl 0.2 % (v/v) Triton X-100 20 mM Imidazole
Buffer W2 (pH 7.9):	20 mM Tris/HCl 500 mM NaCl 0.2 % (v/v) Triton X-100 40 mM Imidazole
Buffer E (pH 7.9):	20 mM Tris/HCl 500 mM NaCl 0.2 % (v/v) Triton X-100 1 M Imidazole

2.7.3 Dialysis of purified proteins

For dialysis of purified proteins, Spectra/Por® 1 Dialysis tubes (6,000 – 8,000 Da MWCO) were used. Dialysis tubes were cut into pieces of about 30 cm length and boiled in buffer D and 1 mM EDTA (pH 8.0) for 10 min each. Each boiling step was followed by excessive rinsing of the dialysis tubes with water. Finally, dialysis tubes were stored in 1 mM EDTA (pH 8.0) at 4 °C until use.

Purified protein fractions were filled into dialysis tubes and the tubes were tightly sealed. Recombinant hydrophobins were dialyzed twice for at least 24 h against 1 L redox-refolding buffer [146] at 4 °C, whereas purified HA-EGFP was dialyzed once for at least 24 h against 5 L PBS at 4 °C. Finally, insoluble protein aggregates were removed by centrifugation (3,500 × g, 5 min, 4 °C).

Buffer D:	2.0 % (w/v) Sodium carbonate 1 mM EDTA
Redox-refolding buffer (pH 5.4):	10 mM Glutathione reduced 1 mM Glutathione oxidized

2.7.4 Quantification of purified proteins

The concentration of purified proteins was determined by a modified Bradford assay [395]. Therefore, 60 µL of the protein solution or appropriate dilutions (in the respective dialysis buffer) were filled into the cavities of a 96-well microplate. BSA was used for assay calibration by diluting a BSA stock solution (New England Biolabs GmbH, Germany) in the dialysis buffer of the respective purified protein, and 60 µL of the resulting solutions (corresponding to 0 – 5.5 µg BSA) were similarly filled into the cavities of 96-well microplates. Next, 140 µL of Bradford`s reagent were added to each well and the microplate was incubated for 5 min at ambient temperature in the dark. Finally, absorbance measurements at 595 nm wavelength were carried out in a microplate reader. Linear calibration plots obtained from the BSA standards were used to evaluate the concentration of the recombinant proteins.

Bradford`s reagent:	100 mg/L Coomassie brilliant blue G-250
	8.5 % (v/v) Phosphoric acid
	4.75 % (v/v) Ethanol

2.8 Hydrophobin-based surface functionalization

2.8.1 Functionalization of polystyrene surfaces with recombinant hydrophobins

Purified hydrophobins were diluted in the respective dialysis buffer to a final concentration of 2 µM and applied to hydrophobic polystyrene surfaces. About 100 µL of the hydrophobin solution were used for the functionalization of individual cavities of 96-well polystyrene microplates, whereas 500 µL of the hydrophobin solution were required to functionalize flat polystyrene supports. Both types of polystyrene substrates were incubated for 10 min at 80 °C to allow for hydrophobin self-assembly [251, 396, 397]. Subsequently, functionalized substrates were washed twice with ddH_2O and twice with PBS containing 0.01 % (v/v) Tween® 20 (PBS-T).

2.8.2 Water contact angle measurements

Flat polystyrene substrates were cut out of sterile Petri dishes and functionalized with recombinant hydrophobins (section 2.8.1). Additionally, some functionalized surfaces were treated with 2 % (w/v) SDS at 80 °C for 10 min in a water bath to analyze the stability of the hydrophobin layers. All functionalized supports were rinsed intensively with ddH_2O and stored overnight in a desiccator. Water droplets (2 µL ddH_2O) were placed on functionalized surfaces and contact angles were determined by the Drop Shape Analysis System and the accompanying software. Each substrate was measured at four to five different spots, and three independent substrates were measured for each type of surface functionalization.

2.8.3 Determination of the accessibility of tags fused to recombinant hydrophobins

To evaluate the accessibility of tags fused to the N- or C-terminal end of recombinant hydrophobins, individual cavities of 96-well polystyrene microplates were functionalized with the recombinant hydrophobins EAS and EAS-α (section 2.8.1) or subjected to control treatments with 2 µM BSA, 2 µM lysozyme or water. Residual protein binding sites of the polystyrene surfaces were blocked by treatment with 300 µL 1 % (w/v) BSA in PBS-T for 1 h at ambient temperature. Functionalized surfaces were washed twice with 300 µL PBS-T and treated with 100 µL $(His)_6$-tag antibody solution (0.1 µg/mL in 0.5 % (w/v) BSA in PBS-T, Table 7) or α-factor antibody solution (0.4 µg/mL in 0.5 % (w/v) BSA in PBS-T, Table 7) for 1 h at ambient temperature. Subsequently, functionalized surfaces were washed four times with 300 µL PBS-T and treated with 100 µL of the respective secondary antibody solution (1:10,000 in 0.5 % (w/v) BSA in PBS-T, Table 7) for 1 h at room temperature. Functionalized surfaces were washed four times with 300 µL PBS-T and twice with 300 µL 0.1 M sodium acetate (pH 5.2). Secondary antibodies present at the surface were quantified by the catalytic activity of the horseradish peroxidase (HRP) linked to the secondary antibodies. Therefore, 100 µL ELISA substrate solution were added and incubated for 10 min at ambient temperature. Finally, the reaction was stopped by adding 100 µL 2 M sulfuric acid and the colorimetric product of the HRP-catalyzed reaction was quantified by absorbance measurements at 450 nm wavelength in a

microplate reader. The antibody coverage was calculated by normalizing the data to the absorbance values obtained for surfaces consisting of EAS-α exclusively (100 % antibody coverage).

ELISA substrate solution:	0.1 M Sodium acetate (pH 5.2)
	0.1 mg/mL 3,3',5,5'-Tetramethylbenzidine
	0.01 % (w/v) Hydrogen peroxide

2.8.4 Determination of the pheromone activity of functionalized surfaces

To assess the pheromone activity of polystyrene surface functionalized with EAS-α, pheromone-responsive reporter cells of *S. cerevisiae* were employed. Therefore, 15 mL SD medium were inoculated with *S. cerevisiae* BY4741 *Δbar1 FIG1-tRFP* and incubated at 30 °C for at least 16 h. About 5 mL fresh SD medium were inoculated with the yeast cells at an initial cell density of approximately 5×10^6 cells/mL and the cell suspensions were filled into small polystyrene Petri dishes (55 mm diameter). Some of the Petri dishes were functionalized with the recombinant EAS-α hydrophobin (section 2.8.1) in advance. As a positive control, cells transferred to unmodified Petri dishes were treated with 1 µM synthetic α-factor. After 8 h of incubation at 30 °C, cells were fixed with ethanol (section 2.12.1) and the cellular morphology as well as fluorescence were analyzed by flow cytometry (section 2.12.3) and fluorescence microscopy (section 2.12.4).

2.9 Competitive ELISA

2.9.1 Optimization of the hydrophobin layer composition

The recombinant hydrophobins EAS and EAS-α were diluted in the respective dialysis buffer to a final concentration of 2 µM and the resulting hydrophobin solutions were mixed in several different ratios. Individual cavities of 96-well polystyrene microplates were functionalized with the resulting solutions containing both

recombinant hydrophobins. Residual protein binding sites of the cavities were blocked with BSA and functionalized surfaces were treated with the α-factor antibody, the secondary antibody and the ELISA substrate solution according to section 2.8.3. The antibody coverage was calculated as detailed in section 2.8.3.

2.9.2 Competitive ELISA calibration

Individual cavities of 96-well polystyrene microplates were functionalized with the recombinant hydrophobins EAS and EAS-α in different molar ratios (sections 2.8.1 and 2.9.1). Residual protein binding sites of the cavities were blocked with BSA and the functionalized surfaces were treated with the α-factor antibody as detailed in section 2.8.3. Functionalized surfaces were washed four times with 300 µL PBS-T prior to adding serial dilutions of the α-factor (0 – 100 µM of the synthetic α-factor pheromone diluted in 0.5 % (w/v) BSA in PBS-T). The 96-well plates were incubated for 1 h at 40 °C in a water bath to allow for competitive antibody detachment from the functionalized surfaces. Next, the functionalized surfaces were washed four times with 300 µL PBS-T and subsequent reaction steps (treatment with the secondary antibody and the ELISA substrate solution) were carried out as described in section 2.8.3. The antibody coverage was calculated by data normalization to the absorbance values obtained for surfaces not treated with the α-factor pheromone (100 % antibody coverage).

2.9.3 Evaluation of the competitive ELISA under varying conditions

The influence of changes in the sample matrix compositions or varying environmental conditions on the competitive ELISA behavior was analyzed by carrying out slightly modified competitive ELISA measurements. Therefore, individual cavities of 96-well polystyrene microplates were functionalized with recombinant hydrophobins (1.6 % EAS-α), residual protein binding sites were blocked with BSA and functionalized surfaces were treated with the α-factor antibody according to the competitive ELISA protocol (section 2.9.2). The functionalized surfaces were washed four times with 300 µL PBS-T and twice using the respective sample matrix buffer (Table 18). Functionalized surfaces were treated with 0 µM or 10 µM synthetic

α-factor dissolved in 0.5 % (w/v) BSA in the respective sample matrix buffer. Microplates were allowed to incubate for 1 h at room temperature (unless otherwise indicated). Functionalized surfaces were washed four times with the respective sample matrix buffer and twice with PBS-T prior to proceeding with the competitive ELISA protocol (secondary antibody treatment and ELISA substrate addition) as detailed in section 2.9.2. Data normalization was carried out as described previously (section 2.9.2) to calculate the antibody coverage.

Table 18. Composition of the sample matrix buffers used to analyze the behavior of the competitive ELISA under varying conditions.

Parameter		Sample matrix buffer
pH	pH 4.0 – 5.0	50 mM Sodium acetate, 100 mM NaCl, 0.01 % (v/v) Tween® 20
	pH 6.0 – 8.0	50 mM Na_2HPO_4/NaH_2PO_4, 100 mM NaCl, 0.01 % (v/v) Tween® 20
	pH 9.0 – 10.0	50 mM Tris/HCl, 100 mM NaCl, 0.01 % (v/v) Tween® 20
Ionic strength		50 mM Na_2HPO_4/NaH_2PO_4 (pH 7.5), 0.0 – 0.5 M NaCl, 0.01 % (v/v) Tween® 20
Detergent concentration		50 mM Na_2HPO_4/NaH_2PO_4 (pH 7.5), 100 mM NaCl, 0.0 – 1.0 % (v/v) Tween® 20
Temperature		50 mM Na_2HPO_4/NaH_2PO_4 (pH 7.5), 100 mM NaCl, 0.01 % (v/v) Tween® 20
Viscosity		50 mM Na_2HPO_4/NaH_2PO_4 (pH 7.5), 100 mM NaCl, 0.01 % (v/v) Tween® 20, 0 – 60 % (w/v) Sucrose

2.9.4 Reusability of functionalized surfaces

To analyze the reusability of functionalized surfaces, individual cavities of 96-well polystyrene microplates were functionalized with recombinant hydrophobins (1.6 % EAS-α) and competitive ELISA measurements were performed (section 2.9.2). Upon completion of the absorbance measurements, functionalized surfaces were washed three times with 300 µL PBS-T and treated with 300 µL ELISA stripping

buffer for 15 min at 55 °C in a water bath to denature the antibodies attached to the surface. Subsequently, functionalized surfaces were washed four times with 300 µL PBS-T and blocked overnight with 1 % (w/v) BSA in PBS-T at 4 °C. Competitive ELISA measurements were carried out the next day, repeatedly using the hydrophobin-functionalized surfaces. Hydrophobin-functionalized surfaces were reused up to five times.

ELISA stripping buffer (pH 7.0):	50 mM Tris/HCl
	1.0 % (w/v) SDS
	50 mM 2-Mercaptoethanol

2.10 Inverse ELISA

2.10.1 Inverse ELISA calibration

Serial dilutions of the synthetic α-factor pheromone, diluted in 0.5 % (w/v) BSA in PBS-T, were prepared and the α-factor antibody was added to a final concentration of 0.4 µg/mL. The resulting samples were incubated for 2 h at ambient temperature under constant rotation (30 rpm) using a rotating wheel. Meanwhile, individual wells of 96-well microplates were functionalized with the hydrophobins EAS and EAS-α in different molar ratios and residual protein binding sites were blocked with BSA according to the competitive ELISA protocol (section 2.9.2). Subsequently, the functionalized surfaces were washed twice with 300 µL PBS-T and 100 µL of the pre-incubated samples containing the α-factor pheromone and the antibody were added. The microplates were incubated for 2 h at 4 °C to allow for attachment of the α-factor antibodies to the hydrophobin-functionalized surfaces. Thereafter, the functionalized surfaces were washed four times using PBS-T prior to proceeding with the secondary antibody treatment and the ELISA substrate solution as detailed in section 2.8.3. The antibody coverage was calculated by data normalization to absorbance values obtained for surfaces treated with control samples lacking the pheromone, *i.e.* only containing the α-factor antibody (100 % antibody coverage).

2.10.2 Evaluation of the inverse ELISA under varying conditions

To investigate the behavior of the inverse ELISA under varying sample matrix conditions, the inverse ELISA protocol was slightly modified. In particular, the buffer used for the initial step (pre-incubation of the α-factor antibodies with the synthetic α-factor pheromone) was exchanged. Therefore, 100 nM α-factor diluted in 0.5 % (w/v) BSA in the respective sample matrix buffers (Table 18) were pre-incubated with the α-factor antibody and subsequently applied to hydrophobin-functionalized polystyrene surfaces. For control purposes, functionalized surfaces were also treated with samples lacking the pheromone. The remainder of the inverse ELISA protocol was carried out as described in section 2.10.1.

2.10.3 Determination of α-factor concentrations in yeast culture supernatants

Minimal medium was inoculated with wild-type or engineered yeast cells of different strains and species at an initial cell density of approximately 5×10^6 cells/mL (using appropriate precultures) and further incubated at 30 °C. To determine the concentration of the α-factor, a sample of the respective culture was taken at the indicated time points and cell-free culture supernatants were obtained by centrifugation (5,000 × g, 5 min, 20 °C). Subsequently, 90 µL of the supernatant were transferred to a new vial and ethylene glycol tetraacetic acid (EGTA) and Tris/HCl (pH 8.0) were added to final concentrations of 10 mM and 200 mM, respectively. The addition of EGTA as a calcium-chelating agent was mandatory to minimize precipitate formation when adjusting the pH of the supernatant by Tris/HCl addition. Protease inhibitors were added and the samples were stored at -20 °C until use. Finally, the α-factor antibody was added to a final concentration of 0.4 µg/mL and the resulting samples (100 µL) were used to carry out inverse ELISA measurements as described previously (section 2.10.1).

2.11 Evaluation of the heterologous expression of the yeast α-factor pheromone in *S. pombe*

2.11.1 Preparation of culture supernatants of engineered *S. pombe* cells

S. pombe HE620 was transformed with plasmids containing pheromone precursor genes to confer the synthesis and secretion of the *S. cerevisiae* α-factor pheromone. Likewise, the empty vector was transformed into *S. pombe* HE620 for control purposes. EMM was inoculated with the plasmid-carrying *S. pombe* cells adjusting an initial cell density of approximately 2×10^6 cells/mL and the cells were grown for 24 h at 30 °C to allow for accumulation of the α-factor pheromone in the culture supernatants. Finally, cell-free culture supernatants of the *S. pombe* cultures were obtained by centrifugation (10,000 × g, 10 min, 20 °C)

2.11.2 Transfer of pheromone-responsive *S. cerevisiae* reporter cells into cell-free culture supernatants

To assess the presence of the α-factor pheromone in cell-free culture supernatants of *S. pombe* cells (section 2.11.1), pheromone-responsive reporter cells of *S. cerevisiae* were utilized. EMM was inoculated with the reporter cells at an initial cell density of approximately 2×10^6 cells/mL and the reporter cells grown for 24 h at 30 °C. Subsequently, the reporter cells were transferred into the cell-free culture supernatants of *S. pombe* cells (section 2.11.1) at an initial cell density of approximately 2×10^6 cells/mL. Essential supplements required for growth of the *S. cerevisiae* reporter cells were added and the cell suspensions were incubated at 30 °C for up to 24 h.

2.12 Assessment of *S. cerevisiae* pheromone response

2.12.1 Ethanol-fixation and rehydration of yeast cells

Ethanol-fixation of yeast cells was carried out essentially as described previously [398]. Briefly, at least 2×10^6 yeast cells were harvested from respective cell suspensions by centrifugation (3,500 × g, 5 min, 4 °C), resuspended in 1 mL ddH_2O and harvested again under similar conditions. Subsequently, the cells were resuspended in 300 µL ddH_2O prior to slowly adding 700 µL ethanol (-20 °C) under constant shaking (1000 rpm). The cells were fixed at -20 °C for at least 12 h.

The cell size and the fluorescence of fixed cells were analyzed by flow cytometry (section 2.12.3) and fluorescence microscopy (section 2.12.4). To this end, fixed cells had to be rehydrated prior to analysis. Fixed cells were harvested under the aforementioned conditions, washed once with 1 mL PBS and harvested again under similar conditions. Finally, the cells were suspended in 1 mL PBS and incubated for at least 14 h at 4 °C under constant rotation (30 rpm).

2.12.2 Cell cycle analysis

Cell cycle analysis was carried out essentially as described previously [398, 399]. About 2×10^6 cells were harvested from respective cultures and fixed with ethanol (section 2.12.1). Ethanol-fixed cells were harvested (3,500 × g, 5 min, 4 °C), washed once in PI buffer and harvested again under similar conditions. Subsequently, the cells were resuspended in 500 µL PI buffer containing 0.2 mg/mL RNase A and incubated for 4 h at 37 °C. The cells were harvested again under aforementioned conditions and suspended in 500 µL PI buffer containing 1 mg/mL proteinase K. After further incubation for 20 min at 37 °C, the fixed cells were harvested again. Quantitative DNA staining was achieved by propidium iodide, a commonly used DNA intercalating dye. Therefore, the cells were finally resuspended in 500 µL PI buffer containing 0.2 µg/mL propidium iodide and incubated at 4 °C for at least 14 h under constant rotation (30 rpm) in dark vials. Cell cycle analysis was carried out by flow cytometry as detailed in the section 2.12.3.

PI buffer (pH 6.8):	200 mM Tris/HCl
	50 mM EDTA

2.12.3 Flow cytometry

Ethanol-fixed cells were rehydrated (section 2.12.1) or stained with propidium iodide (section 2.12.2) for cell cycle analysis. Cell suspensions were briefly sonicated (30 s, 50 % cycles, 70 % power) using a Sonopuls GM2070 ultrasonic homogenizer prior to flow cytometry to disperse cell aggregates resulting from ethanol-fixation. Subsequently, the cell suspensions were diluted in Sheath Fluid and flow cytometry was carried out using a CyFlow® SL and the accompanying software. The instrument was equipped with a solid state laser (50 mW) emitting light at a wavelength of 488 nm. Cell size distribution was determined by analyzing the Forward Scatter (FSC) signals recorded using a band pass filter (IBP 488 D) and appropriate channel settings (Table 19). Red fluorescence, resulting from the expression of a fluorescent protein or from propidium iodide staining (section 2.12.2), was quantitatively analyzed in the FL2 channel by the use of a band pass filter (IBP 590 DF 50) and appropriate channel settings (Table 19). At least 20,000 cells were analyzed for each sample using a constant sample speed of 2 µL/s.

Table 19. Channel settings for flow cytometry experiments using a CyFlow® SL instrument.

Channel	Gain	Lower limit (L-L)	Upper Limit (U-L)	Amplification
FSC	100	36	999.9	log4
FL2	560	10	999.9	log3

2.12.4 Fluorescence microscopy

Ethanol-fixed cells were rehydrated (section 2.12.1) and analyzed by fluorescence microscopy to assess the cellular morphology and the expression of reporter genes encoding fluorescent proteins. To this end, an Axio Observer.Z1 fluorescence microscope was used. Brightfield images were obtained by differential interference contrast (DIC) microscopy using a 63 × objective (LCI Plan-Neofluar 63 ×/1.30 Imm

Korr DIC M27) and white light illumination. Fluorescence images were obtained using the same objective and appropriate optical filters (BP 550/25 and BP 605/70 for excitation and emission, respectively). Images were captured using an AxioCam Mrm camera and further processed by the use of ZEN 2012 blue edition software.

2.13 Software and databases

Table 20. Software and databases used in this study.

Software/database	Application	Reference
Alpha Ease FC™ Software (4.0.1)	UV Transilluminator instrument control and data acquisition	Biozym Scientific GmbH (Germany)
Antibody Epitope Prediction	Prediction of putative epitopes	http://tools.immuneepitope.org/tools/bcell
AxioVision (4.8.2)	Fluorescence microscope control and data acquisition	Carl Zeiss Microscopy GmbH (Germany)
BioEdit Sequence Alignment Editor (7.0.9.0)	Alignments of DNA sequences	[400]
ChemStation for LC 3D systems (B.04.01 SP1)	HPLC instrument control, data acquisition and analysis	Agilent Technologies GmbH (Germany)
Drop Shape Analysis Software (1.51.0.26)	Water contact angle measurement device control and data acquisition	Kruess GmbH (Germany)
ExPASy Compute pI/Mw	Calculation of protein molecular weight and isoelectric point	http://web.expasy.org/compute_pi/
FloMax (2.52)	Flow cytometer instrument control and data acquisition	Partec GmbH (Germany)
HomoloGene	Search for homologous genes	http://www.ncbi.nlm.nih.gov/homologene

Table 20 (continued).

Software/database	Application	Reference
i-control™	Microplate reader instrument control and data acquisition	Tecan Group Ltd. (Switzerland)
PomBase	Nucleic acid and protein information for *S. pombe*	http://www.pombase.org/
PubMed	Literature research	http://www.ncbi.nlm.nih.gov/pubmed/
Saccharomyces Genome Database	Nucleic acid and protein information for *S. cerevisiae*	http://www.yeastgenome.org/
Vector NTI (3.1)	Calculation of melting temperatures of DNA oligonucleotides	InforMax Inc. (USA)
ZEN 2012 blue edition (1.1.2.0)	Processing of microscope images	Carl Zeiss Microscopy GmbH (Germany)

3 Results

This study aimed at the development of a novel immunoassay for the detection and quantification of the yeast α-factor pheromone, which in combination with genetically engineered sensor cells could allow for the creation of a whole-cell sensor read-out based on the secreted peptide pheromone (section 1.4). The desired immunoassay relied on the immobilization of the α-factor at the surface of a transducer, allowing for subsequent attachment of α-factor antibodies to the functionalized surface. The presence of additional pheromone in the vicinity of the engineered surface, resulting from the secretion of the α-factor by engineered sensor cells, was expected to cause competitive detachment of the antibodies. Antibody detachment might be detected by the use of appropriate transducer elements (section 1.4).

Evidently, immobilization of the α-factor at the transducer surface represented the most critical step: the pheromone has to be immobilized in a defined density while guaranteeing accessibility of the pheromone to cognate antibodies. Two recombinant hydrophobins, one of them engineered to expose the pheromone, were applied to obtain functionalized surfaces with these characteristics. The first section of this chapter (section 3.1) covers the design and purification of the recombinant hydrophobins as well as the characterization of hydrophobin-functionalized surfaces, while subsequent sections focus on the implementation and characterization of novel immunoassays for the α-factor pheromone (sections 3.2 and 3.3) as well as their application to study the pheromone secretion of wild-type and engineered yeast cells of *S. cerevisiae* (section 3.4) and *S. pombe* (section 3.5). Finally, the immunoassays were combined with engineered sensor cells to yield a proof-of-concept whole-cell biosensor (section 3.6.1). In addition, the versatility of the hydrophobin-based surface engineering for the development of immunoassays for a variety of analytes was investigated (section 3.6.2).

3.1 Functionalization of hydrophobic surfaces with recombinant hydrophobins

3.1.1 Cloning, expression and purification of recombinant hydrophobins

Recombinant hydrophobins were obtained by heterologous expression in *E. coli* and subsequent purification *via* Ni^{2+} affinity chromatography. To this end, the sequence of the class I hydrophobin EAS from *N. crassa*, lacking its N-terminal signal sequence, was cloned into the vector pET28b. Authentic hydrophobins are secreted into the extracellular environment and therefore possess an N-terminal hydrophobic signal sequence that mediates targeting to the ER [129-135]. As the signal peptide is cleaved off in the ER, it is dispensable for hydrophobin folding and trafficking of the mature hydrophobin through the secretory pathway. Thus, the DNA sequence encoding the signal sequence was omitted in the ORFs of the recombinant hydrophobins employed in this study. The respective sequence was inserted 3' of the sequence encoding the $(His)_6$-tag and a thrombin cleavage site, giving rise to pET28b-EAS. Additionally, the sequences encoding a highly flexible $(GGGGS)_3$ linker element as well as the *S. cerevisiae* α-factor were codon-optimized for the expression in *E. coli* [401] and inserted 3' of the sequence encoding the EAS hydrophobin, resulting in pET28b-EAS-α. Both recombinant hydrophobins are schematically illustrated in Figure 4 a, and the DNA and amino acid sequences corresponding to EAS and EAS-α are depicted in Appendix A.1 and A.2.

EAS and EAS-α were expressed in *E. coli* and subsequently purified by the use of their N-terminal $(His)_6$-tag. For this purpose, the expression vectors pET28b-EAS and pET28b-EAS-α were transformed into *E. coli* strain T7 SHuffle® *lysY* and expression of the recombinant hydrophobin genes was induced by addition of IPTG (section 2.7.1.1). This strain was selected as it promotes the intracellular formation of disulfide bonds, due to a deletion in thioredoxin reductase (*ΔtrxB*) and glutathione oxidoreductase (*Δgor*) [402]. The presence of four intramolecular disulfide bonds is a hallmark feature of all hydrophobins [129-135]. These intramolecular bonds are of crucial importance to stabilize the soluble state of hydrophobins by preventing their premature aggregation in the absence of a hydrophilic-hydrophobic interface [403, 404]. Upon cell lysis and centrifugation, both recombinant hydrophobins were

found in the pellet fraction (data not shown), most likely due to the formation of inclusion bodies in the *E. coli* host. However, the hydrophobins could be efficiently solubilized by application of 8 M urea and subsequently purified by Ni^{2+} affinity chromatography, taking use of the N-terminal $(His)_6$-tag (section 2.7.2). Purified hydrophobins were subjected to high-resolution Tricine SDS-PAGE to analyze protein purity and integrity (Figure 4 b).

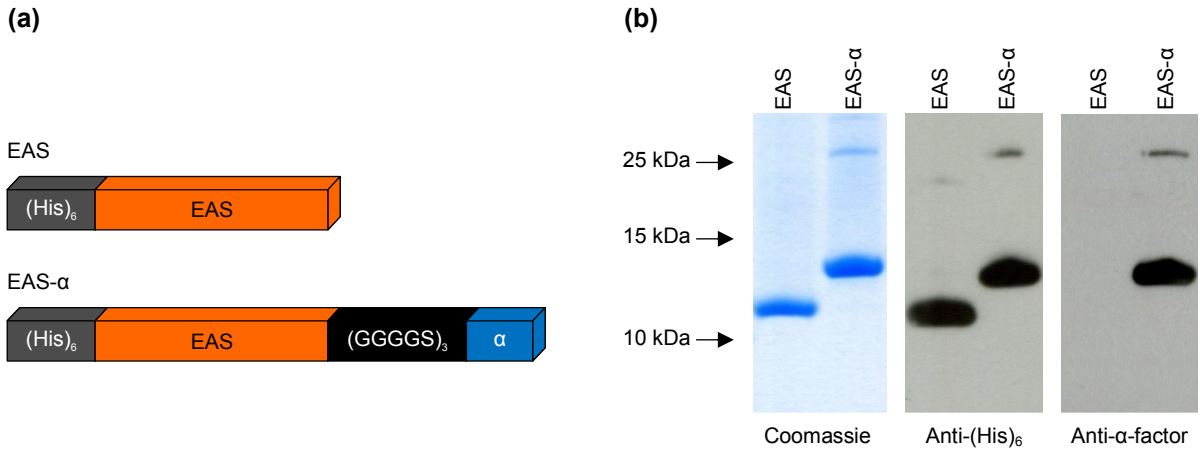

Figure 4. Design and purification of recombinant hydrophobins. (a) Schematic illustration of the recombinant hydrophobins EAS and EAS-α. Both proteins included an N-terminal $(His)_6$-tag and the sequence of the mature EAS hydrophobin. Additionally, EAS-α harbored a flexible $(GGGGS)_3$ linker element and the sequence of the yeast α-factor at its C-terminus. **(b)** Electrophoretic separation of the recombinant hydrophobins by Tricine SDS-PAGE. A fraction of the purified proteins, corresponding to 3 µg, was separated and proteins were visualized by colloidal Coomassie staining or transferred to PVDF membranes and probed with the indicated antibodies.

Upon electrophoretic separation and visualization by Coomassie staining, a predominant signal in accordance with the calculated molecular weight of both hydrophobins (10.4 kDa and 13.3 kDa for EAS and EAS-α, respectively [405]), was observed. Except for a faint signal, most likely representing dimers of the hydrophobins, additional bands were barely visible, indicating a high degree of purity and stability of recombinant hydrophobins (Figure 4 b). The presence of a single predominant protein representing intact hydrophobins is in line with the exceptionally high stability of hydrophobins [292, 406, 407]. Dimer formation, even upon separation in SDS-PAGE, was previously observed for numerous hydrophobins [159, 214, 215,

227, 232, 307, 408-411]. However, it should be noted that the mature EAS hydrophobin was reported to be monomeric in solution [161, 164]. Although an influence of the N- and C-terminal hydrophobin modification could not be excluded, dimer formation might also result from non-specific EAS aggregation as a consequence of incomplete disulfide bond formation upon expression in *E. coli*. Since solubility depends on proper formation of disulfide bonds [403, 404], impaired formation might cause protein aggregation. A previous study also suggested that non-specific protein aggregation, mediated by a flexible loop region of the EAS hydrophobin, occurred at lower temperatures [148]. Thus, storage of the purified proteins at 4 °C might have similarly contributed to the formation of dimers and aggregates.

Both proteins could be detected immunologically by the use of antibodies directed against the $(His)_6$-tag, whereas EAS-α was additionally detected by the use of α-factor antibodies (Figure 4 b). Immunological detection thus revealed that the antigenic properties of the α-factor were not affected by the fusion to the hydrophobin, allowing for specific binding of the antibody to the fusion protein. This was of crucial importance to attach α-factor antibodies to a functionalized surface and hence to establish an immunoassay. Taken together, these results indicated that both EAS and EAS-α were successfully cloned, expressed and purified as an important prerequisite for hydrophobin-based surface functionalization.

3.1.2 Characterization of functionalized polystyrene surfaces

3.1.2.1 Analysis of surface wettability

For the implementation of the α-factor immunoassay, it was mandatory to obtain surfaces functionalized with the recombinant hydrophobins. Due to their amphipathic structure, hydrophobins are known to reverse the wettability of solid substrates upon self-assembly [129-135]. Therefore, the surface activity and self-assembling properties of the purified proteins were evaluated by water contact angle measurements (section 2.8.2). Hydrophobins were allowed to self-assemble on hydrophobic polystyrene supports (section 2.8.1) and water contact angle

measurements were performed (Figure 5). Self-assembly of the recombinant hydrophobins was carried out at 80 °C since hydrophobin layers are more densely packed when self-assembled at elevated temperatures [251, 396, 397].

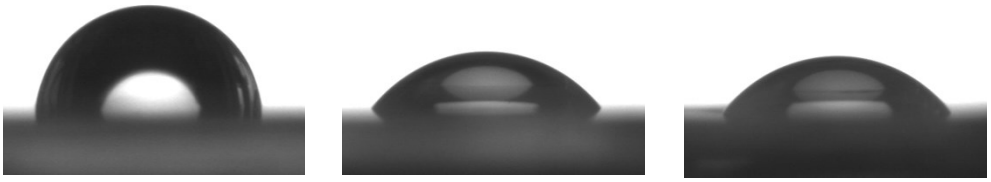

	Polystyrene	EAS/polystyrene	EAS-α/polystyrene
Surface functionalization	85.5° ± 2.3° n = 13	53.0° ± 5.0° n = 15	53.6° ± 5.5° n = 15
Hot SDS extraction	87.0° ± 1.4° n = 15	72.0° ± 3.4° n = 15	75.5° ± 3.2° n = 14

Figure 5. Water contact angle measurements of bare and hydrophobin-functionalized polystyrene surfaces. Polystyrene substrates were functionalized with the recombinant hydrophobins EAS or EAS-α and the hydrophobicity of the surfaces was assessed by water contact angle measurements (images and upper panel). In order to evaluate the stability of the hydrophobin layers, some of the functionalized surfaces were treated with 2 % (w/v) SDS at 80 °C for 10 min prior to contact angle measurement (lower panel). Mean values and standard deviation are given.

Unmodified polystyrene proved to be hydrophobic, showing a water contact angle of 85.5 ± 2.3°, whereas functionalization of the polystyrene surfaces with recombinant hydrophobins clearly increased the wettability of the surfaces (Figure 5). The water contact angles of surfaces functionalized with EAS and EAS-α (53.0 ± 5.0° and 53.6 ± 5.5°, respectively) were similar to the values reported previously for EASΔ15, a derivative of EAS lacking 15 amino acids in a flexible loop region (56.0 ± 10.9° [164]). However, it should be noted that there are large differences in the water contact angles reported for EAS monolayers on hydrophobic substrates, given that the values differ between 16.6° [294], 69.2° [155] and 73.7° [147]. In summary, water contact angle measurements unambiguously demonstrated that EAS and EAS-α were able to self-assemble at hydrophobic polystyrene and to reverse its wettability.

In contrast, polystyrene surfaces functionalized with BSA only showed a slight decrease in water contact angle (76.1 ± 4.0°, data not shown).

It was found that 2 µM of both hydrophobins were sufficient to functionalize the polystyrene substrates (data not shown). Higher concentrations of the hydrophobins did not result in further reduction of the contact angle, indicating that the binding sites at the surface might have been saturated. This was consistent with a previous study utilizing the class II hydrophobin HFBI fused to avidin, demonstrating by QCM measurements that 1.3 µM of the fusion protein were sufficient to saturate all binding sites at a polystyrene surface [268]. Additionally, previous studies revealed that the amount of hydrophobins adsorbed to a surface does not depend on the hydrophobin concentration above a certain threshold [169, 255]. Thus, the surface activity of the recombinant hydrophobins EAS and EAS-α was comparable to other hydrophobins.

Class I hydrophobins self-assemble into highly robust monolayers that are able to withstand harsh conditions. Only treatment with 100 % TFA or 100 % formic acid has been reported to effectively dissolve these layers [129-135]. Class I hydrophobin layers are known to resist hot SDS treatment whereas class II hydrophobin layers dissociate under these conditions. Therefore, the stability of the hydrophobin layers was evaluated by treatment of the functionalized surface with 2 % (w/v) SDS for 10 min at 80 °C.

Upon treatment of the functionalized surfaces with hot SDS, the water contact angle slightly increased to 72.0 ± 3.4° and 75.5 ± 3.2°, respectively, for substrates functionalized with EAS and EAS-α (Figure 5). This might result from partial extraction of the hydrophobins as observed for several class I hydrophobin layers treated with hot SDS [158, 213, 251, 257, 263, 280, 331, 396, 412-416]. However, the contact angles were still clearly reduced in comparison to unmodified polystyrene, indicating that the majority of the hydrophobins remained at the substrate. Taken together, these data indicated that the recombinant hydrophobins EAS and EAS-α displayed surface activity and self-assembly behavior similar to previously characterized class I hydrophobins.

3.1.2.2 Accessibility of peptide tags fused to recombinant hydrophobins

As a prerequisite for the implementation of an immunoassay for the α-factor utilizing hydrophobin-based surface functionalization, it was essential to prove that the α-factor is exposed at the functionalized surface. As shown above, the α-factor antibody recognized the fusion protein of the α-factor and the recombinant EAS-α hydrophobin (Figure 4 b). However, this finding was obtained upon electrophoretic separation under denaturing conditions that may affect the structure of the recombinant hydrophobin. Thus, it was of utmost importance to show that the α-factor was also exposed at a functionalized surface to provide accessible binding sites for cognate antibodies.

In order to evaluate the accessibility of peptide tags fused to the N-terminus and the C-terminus of EAS, a novel immunoassay was developed (section 2.8.3). First, hydrophobic polystyrene surfaces were functionalized with EAS, EAS-α or control proteins (BSA or lysozyme) and residual binding sites were blocked with BSA. Second, antibodies directed against the $(His)_6$-tag (fused to the N-terminus of both recombinant hydrophobins) or the α-factor (fused to the C-terminus of EAS-α) were applied to the functionalized surfaces, allowing for their attachment if their target epitope was accessible at the functionalized surface. The amount of bound antibodies was determined by the use of a secondary antibody linked to the HRP. Upon addition of suitable substrates, HRP catalyzes a colorimetric reaction that can be quantified by absorbance measurements. Absorbance values were normalized to surfaces consisting of 100 % EAS-α by calculating the antibody coverage of a specifically functionalized surface according to the equation:

$$\text{Antibody coverage} = \frac{\text{Absorbance value (functionalized surface)}}{\text{Absorbance value (100 \% EAS-α)}}$$

The entire setup for evaluating peptide tag accessibility is depicted in Figure 6 a. Comparable approaches have been used previously to prove the presence of hydrophobins on various substrates [248, 396, 417].

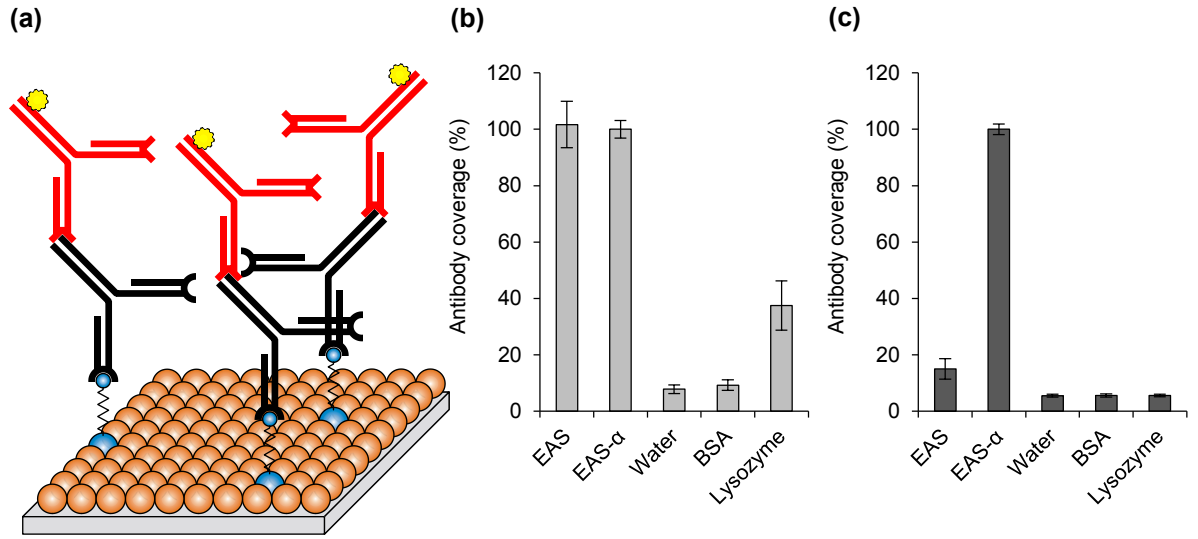

Figure 6: Analysis of the accessibility of peptide tags fused to the N-terminus or the C-terminus of EAS hydrophobin. (a) Schematic illustration of the immunoassay to determine the accessibility of peptide tags fused to the recombinant hydrophobins for cognate antibodies. Hydrophobic polystyrene substrates (gray) were functionalized with the recombinant hydrophobins EAS (orange) and EAS-α (blue) and treated with antibodies specific for the α-factor (black Y-shaped structures) or the $(His)_6$-tag (not shown). Bound antibodies were detected by the use of a secondary antibody (red Y-shaped structures) linked to HRP (yellow) that catalyzed a colorimetric reaction to quantify the antibody coverage. **(b)** Antibody coverage of surfaces functionalized with EAS, EAS-α or control proteins (BSA, lysozyme) determined by the use of the $(His)_6$-tag antibody. Data were normalized to surfaces consisting of EAS-α. **(c)** Antibody coverage for functionalized surfaces measured by employing the α-factor antibody. Data were normalized to surfaces consisting of EAS-α. All plotted values correspond to triplicate measurements of at least two independent experiments. Error bars indicate standard deviation.

The immunoassays strongly suggested that both the $(His)_6$-tag and the α-factor were exposed at the surface upon functionalization with the recombinant hydrophobins. Utilizing the $(His)_6$-tag antibody, high antibody coverage values were obtained when surfaces were functionalized with EAS or EAS-α whereas treatment with water or control proteins such as BSA or lysozyme resulted in low background signals (Figure 6 b). Surprisingly, polystyrene surfaces functionalized with lysozyme exhibited intermediate antibody coverage (37.5 % of the antibody coverage obtained with EAS-α). As histidine-rich stretches are not present in the primary structure of lysozyme (data not shown), this signal might have resulted from non-specific

interaction of the antibody with lysozyme-treated surfaces. Importantly, the values obtained for surfaces functionalized with EAS and EAS-α were very similar, indicating that both hydrophobins have self-assembled with a comparable packing density (Figure 6 b). In contrast, the α-factor antibody specifically bound to surfaces functionalized with EAS-α, while negligible signals were obtained for surfaces functionalized with control proteins (Figure 6 c). Similarly, polystyrene surfaces functionalized with the bare synthetic α-factor yielded only about 20 % of the antibody coverage obtained for EAS-α (data not shown), clearly underscoring the benefit of hydrophobin-based surface engineering. Notably, surfaces functionalized with 100 % EAS (lacking the pheromone tag) resulted in remarkably high antibody coverage values using the α-factor antibody, yielding 15.0 ± 3.6 % of the antibody coverage obtained for EAS-α (Figure 6 c). Most likely, this result reflected non-specific, predominantly ionic interactions between immunoglobulin G (IgG) antibodies and hydrophobin layers reported previously [280-282].

3.1.2.3 Analysis of pheromone activity of functionalized surfaces

Next, the pheromone activity of hydrophobic surface functionalized with EAS-α was evaluated (section 2.8.4). Given that the α-factor was accessible at the functionalized surfaces for cognate antibodies, it was of interest to analyze if the immobilized pheromone could elicit a pheromone response in yeast. To assess the pheromone activity of functionalized surfaces, pheromone-responsive yeast reporter cells (strain BY4741 *Δbar1 FIG1-tRFP*) were employed. Due to a deletion of the *BAR1* gene, encoding an extracellular protease cleaving the α-factor [370], the reporter cells were 20-fold more sensitive towards the α-factor than isogenic wild-type cells [418]. Additionally, the reporter cells carried the ORF encoding turbo red fluorescent protein (tRFP) under transcriptional control of the *FIG1* promoter that is almost 100-fold upregulated within 20 min after perception of the α-factor pheromone [357]. Hence, the reporter cells intracellularly accumulated tRFP, allowing for simple and quantitative read-out of the yeast pheromone response.

To determine the pheromone activity of the EAS-α hydrophobin layers, polystyrene petri dishes were functionalized with EAS-α and the reporter cells were grown in these petri dishes at 30 °C for 8 h without shaking. Finally, the pheromone response

was analyzed by flow cytometry (section 2.12.3), allowing for a rapid and quantitative analysis of a large population of cells. Flow cytometry results were confirmed qualitatively by fluorescence microscopy (section 2.12.4). For comparison, reporter cells were also grown on unmodified polystyrene surfaces in the presence or absence of synthetic α-factor (Figure 7).

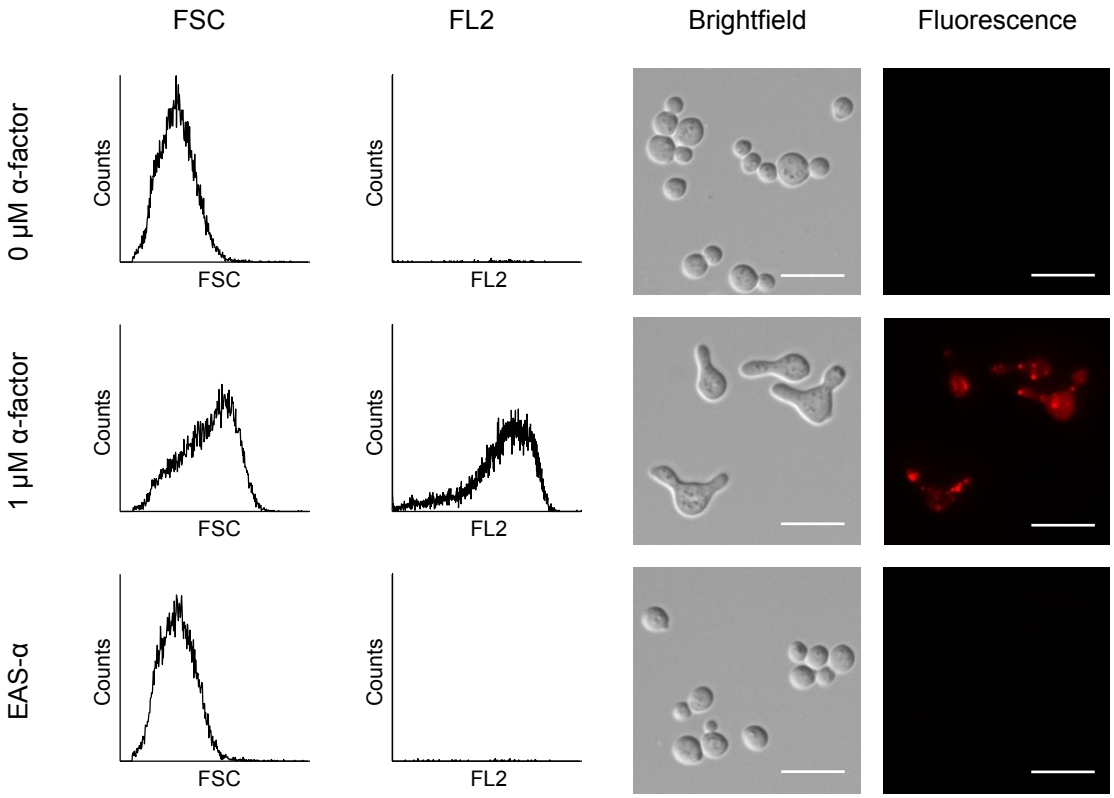

Figure 7. Assessment of the α-factor activity of surfaces functionalized with EAS-α by the use of pheromone-responsive *S. cerevisiae* reporter cells. Reporter cells of *S. cerevisiae* BY4741 *Δbar1 FIG1-tRFP* were grown in SD medium in a polystyrene dish functionalized with EAS-α. For control purposes, reporter cells were also grown in unmodified polystyrene dishes in the presence or absence of synthetic α-factor. Reporter cells were fixed after 8 h of incubation at 30 °C and cellular morphology as well as *tRFP* expression were analyzed by flow cytometry and fluorescence microscopy. Scale bars in microscopic images represent 10 µm.

In the absence of the synthetic α-factor, reporter cells exhibited the characteristics of vegetatively growing yeast cells (Figure 7, upper panel). A narrow size distribution of individual cells (quantified by the FSC measurements) was observed by flow cytometry, and only a minor fraction of the reporter cells (about 0.3 %) exhibited

measurable fluorescence. These data were confirmed by brightfield and fluorescence microscopy, since the characteristic morphology of growing yeast cells (including budding cells) was evident, but fluorescent cells could not be detected. In contrast, when reporter cells were treated with the synthetic α-factor for 8 h, a clearly altered cellular morphology was observed (Figure 7, middle panel). These cells formed mating projections, as evidenced by the broad size distribution in FSC measurements and the shmoo phenotype seen in brightfield microscopy. Some of the cells even exhibited multiple shmoo tips, a phenomenon frequently observed when high pheromone concentrations are applied in a uniform manner (*i.e.* in the absence of a pheromone gradient [419]). Additionally, the pheromone-dependent expression of *tRFP* was confirmed by flow cytometry with about 90 % of the cells showing fluorescence. Fluorescence microscopy revealed that the intracellular distribution of tRFP was not homogeneous and a rather speckled fluorescence pattern was observed. This may be caused by ethanol fixation and rehydration prior to flow cytometry and microscopy, as unfixed cells showed a rather homogeneous fluorescence distribution (data not shown). However, neither qualitative nor quantitative differences in size distribution or fluorescence of fixed and unfixed cells were observed. As indicated by the broad distribution in FL2, the deviation between individual cells regarding the expression of *tRFP* was relatively large, reflecting significant cell-to-cell variation in pheromone response as observed previously [420, 421].

When pheromone-responsive cells were grown on surfaces functionalized with EAS-α, their phenotype was indistinguishable from vegetatively growing cells in the absence of the pheromone, indicating that these cells did not undergo pheromone response (Figure 7, lower panel). The presence of vegetatively growing cells, however, confirmed that hydrophobin-functionalized surfaces did not exert cytotoxic effects [224, 248-253, 282, 290-294]. Apparently, there is a lack of correlation between the pheromone activity and the accessibility of the α-factor for cognate antibodies, most likely reflecting different recognition mechanisms of the pheromone receptor and the pheromone antibody (section 4.1.4). Steric effects might have contributed to the lack of pheromone activity of these surfaces, as yeast cells are surrounded by a rigid cell wall that pheromone molecules need to pass in order to be recognized by the pheromone receptor embedded in the plasma membrane. However, even yeast cells lacking the cell wall due to *in vitro* enzymatic degradation

did not undergo pheromone response when grown on EAS-α functionalized surfaces (Appendix B.1), indicating that additional effects rendered the α-factor exposed at the surface inactive (section 4.1.4).

3.2 Pheromone quantification by competitive ELISA measurements

3.2.1 Design and concept of the competitive ELISA

In order to quantify the α-factor pheromone by the use of the hydrophobin-based surface engineering technique, a novel immunoassay was developed (Figure 8). First, individual cavities of 96-well polystyrene microplates were functionalized with the recombinant hydrophobins EAS and EAS-α in different molar ratios (section 3.2.2) and residual protein binding sites of the wells were blocked with BSA. Subsequently, the α-factor antibody was allowed to specifically attach to the surface *via* binding to the immobilized α-factor (*i.e. via* binding to EAS-α). Application of a sample containing the α-factor pheromone was expected to trigger a competition between the soluble and the surface-immobilized α-factor, ultimately resulting in competitive detachment of the antibodies from the functionalized surface. Detached antibodies and dissolved α-factor were removed by extensive washing of the surface, while antibodies that were still bound to the surface were quantified by use of a secondary antibody linked to HRP. Thus, by competitively displacing antibodies from the functionalized surface, the concentration of the α-factor in the sample can be determined. As this immunoassay was closely related to the ELISA protocol and relied on competitive antibody detachment, this assay is referred to as competitive ELISA throughout this study.

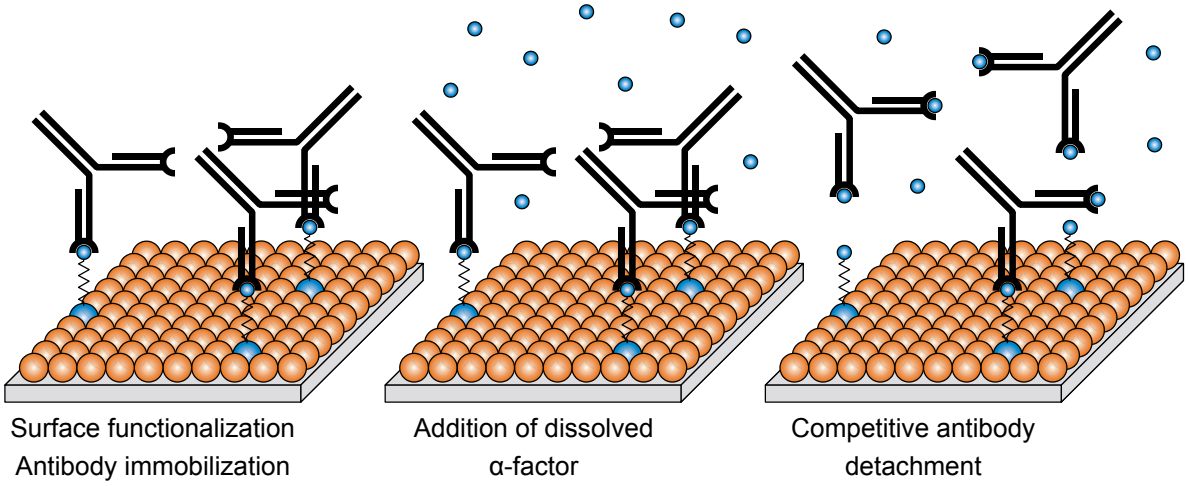

Figure 8. Schematic illustration of the concept of the competitive ELISA. First, hydrophobic polystyrene surfaces (gray) were functionalized with recombinant hydrophobins EAS (orange) and EAS-α (blue) in different molar ratios, and α-factor antibodies (black Y-shaped structures) were allowed to attach to the functionalized surfaces (left panel). Second, samples containing the α-factor (small blue spheres) were applied directly to the functionalized surfaces (middle panel). Due to the presence of dissolved α-factor in the close proximity of the functionalized surfaces, competition between the soluble and the surface-immobilized α-factor (*via* EAS-α) was triggered, resulting in competitive detachment of antibodies (right panel).

Comparable immunoassays, although using alternative methods to immobilize the target at the surface, have been used previously for the quantitative assessment of various analytes, including peptides present in the coating of the malaria parasite [422], disease biomarkers [423] or explosives [14].

3.2.2 Optimization of the hydrophobin layer composition

In order to yield a highly sensitive immunoassay for the detection and quantification of α-factor pheromone, hydrophobin-based surface functionalization required further optimization, in particular regarding the composition of the hydrophobin monolayer. Water contact angle measurements revealed that the formation and stability of mixed layers of EAS and EAS-α were indistinguishable to hydrophobin layers consisting exclusively of either hydrophobin, indicating that EAS and EAS-α can co-assemble into a mixed hydrophobin monolayer (data not shown). Therefore, the monolayer composition could be optimized by considering maximum antibody coverage and the

sensitivity of the immunoassay (Figure 9 a), following a proposal by Reimhult and Höök [12] that simple maximization of the density of immobilized recognition elements (*i.e.* the EAS-α content in this study) is not recommended. As steric hindrance or mutual interactions between individual recognition elements may affect the bioassay performance, optimization of the density of immobilized recognition elements might considerably enhance the sensitivity [12].

An ideal hydrophobin-based surface functionalization should allow for the specific attachment of a high number of α-factor antibodies per surface area (high antibody coverage, Figure 9 a). High antibody coverage was desirable as it determined the maximum signal intensity. Therefore, a high number of antibody binding sites at the surface (*i.e.* high EAS-α content of the monolayer) would be advantageous to maximize the attainable signal, although steric hindrance may prevent that all of the binding sites exposed at the surface can be occupied by an antibody. On the other hand, the competitive ELISA was based on competitive antibody detachment from the surface. Hence, excess of antibody binding sites at the functionalized surface should be avoided, given that these binding sites were expected to influence the competition and, consequently, to lower the sensitivity of the assay. Therefore, a rather low number of antibody binding sites (*i.e.* low EAS-α content of the monolayer) was desirable to obtain functionalized surfaces with the highest sensitivity. The optimized surface composition would thus allow for high antibody coverage with a minimum of binding sites present at the surface (Figure 9 a).

In order to identify the ideal surface composition, the recombinant hydrophobins EAS and EAS-α were mixed in several different molar ratios and used to functionalize polystyrene surfaces. These surfaces were treated with the α-factor antibody and a HRP-linked secondary antibody subsequently to determine the maximum antibody coverage (section 2.9.1, Figure 9 b,c). As can be deduced from the almost horizontal curve in Figure 9 b, the effect of the EAS-α content on the antibody coverage was barely visible within a wide range of EAS-α contents. Only within a narrow range of EAS-α concentrations (up to 2.0 % EAS-α), an obvious increase of the antibody coverage with an increasing EAS-α content of the mixed hydrophobin layer was observed (Figure 9 c).

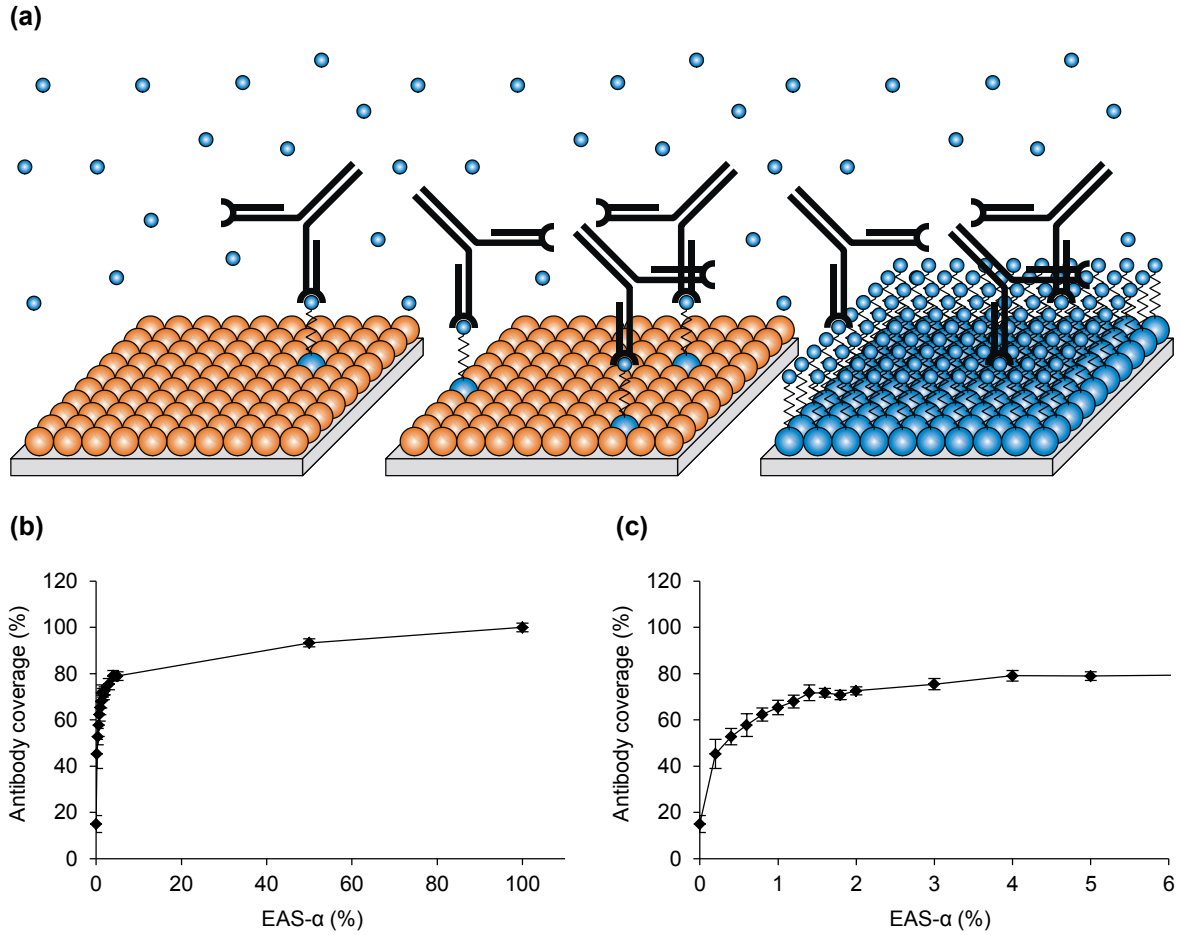

Figure 9. Optimization of the hydrophobin monolayer composition. (a) Schematic drawing of polystyrene surfaces (gray) functionalized with the recombinant hydrophobins EAS (orange) and EAS-α (blue) in different molar ratios to illustrate the concept of antibody coverage and sensitivity. High amounts of EAS-α will result in a high number of immobilized antibodies (black Y-shaped structures) per surface area (high antibody coverage), whereas the sensitivity of the assay towards soluble α-factor pheromone (small blue spheres) might be enhanced if low amounts of EAS-α are utilized (see text for details). **(b)** Influence of the EAS-α content of hydrophobin layers on the antibody coverage. Polystyrene surfaces were functionalized with EAS and EAS-α in different molar ratios and subsequently treated with the α-factor antibody and a HRP-linked secondary antibody (section 2.9.1). Antibody coverage was calculated by normalizing the data to surfaces consisting of 100 % EAS-α. **(c)** Enlarged image section of (b) to visualize the influence of low EAS-α content on the antibody coverage. All plotted values correspond to triplicate measurements of at least two independent experiments. Error bars indicate standard deviation.

Further increasing the EAS-α content (above 2.0 %) only caused a slight increase in antibody coverage, indicating that steric hindrance between the antibodies limited further binding. This might be attributed to the large differences in the size of IgG antibodies (about 10 nm × 14 nm × 5 nm [424]) and hydrophobin monomers

(diameter of 2.7 nm [146]). For an EAS-α content of up to 1.6 % (yielding 71.7 ± 1.9 % of the maximum antibody coverage), the increase in antibody coverage with increasing EAS-α content was rather steep, whereas the slope of the curve clearly decreased upon further increasing the EAS-α content (Figure 9 c). Therefore, a mixed hydrophobin layer encompassing 1.6 % EAS-α allowed for comparatively high antibody coverage with a low number of surface-exposed binding sites and was therefore considered to represent the optimized surface composition. Additionally, only minor differences in the slope of the curve between 1.4 % EAS-α and 2.0 % EAS-α were obtained (Figure 9 c). Thus, minor differences in the final surface composition, *e.g.* resulting from uncertainties in protein concentration determination, were not expected to dramatically affect the sensitivity of the assay.

3.2.3 Calibration of the competitive ELISA

Next, the competitive ELISA was calibrated with the synthetic α-factor pheromone (section 2.9.2). This immunoassay relied on the competitive detachment of antibodies from the hydrophobin-functionalized surface, triggered by the presence of soluble pheromone in the close proximity of the surface (Figure 8). Various concentrations of the synthetic α-factor were used to calibrate the competitive ELISA, and different hydrophobin monolayer compositions were utilized to validate the effect of the monolayer composition on the immunoassay sensitivity (Figure 10). The absorbance values were normalized to surfaces not treated with the pheromone to calculate the antibody coverage according to the equation:

$$\text{Antibody coverage} = \frac{\text{Absorbance value (pheromone-treated surface)}}{\text{Absorbance value (control surface not treated with the α-factor)}}$$

With increasing concentrations of the α-factor, the antibody coverage gradually decreased, in line with the competitive removal of α-factor antibodies from the functionalized surface (Figure 10). When the optimized hydrophobin monolayer composition (1.6 % EAS-α) was employed, a lower limit of detection (signal-to-noise ratio = 3) of 0.2 µM α-factor and a dynamic range of 0.2 – 100 µM α-factor were determined. In contrast, when the hydrophobin monolayers consisted of higher

amounts of EAS-α (16 % EAS-α or 100 % EAS-α), higher pheromone concentrations were required to yield a reduction in antibody coverage (Figure 10). Lower limits of detection of 2 µM and 10 µM α-factor were obtained for surfaces encompassing 16 % EAS-α and 100 % EAS-α, respectively. However, further lowering the EAS-α content of the monolayer (below 1.6 % EAS-α) did not result in enhanced sensitivity, mostly due to the low absorbance values obtained even in the absence of the pheromone (data not shown). Thus, these data unambiguously confirmed the aforementioned hypothesis that maximum antibody coverage and immunoassay sensitivity were interrelated and that optimization of the monolayer composition was advantageous for achieving the highest sensitivity. On the other hand, the possibility to modify the sensitivity by tuning the EAS-α content of the monolayer provided a tool for facile and precise adjustment of the sensitivity and the dynamic range of the assay. Thus, the sensitivity can be predefined according to the pheromone concentrations to be quantified.

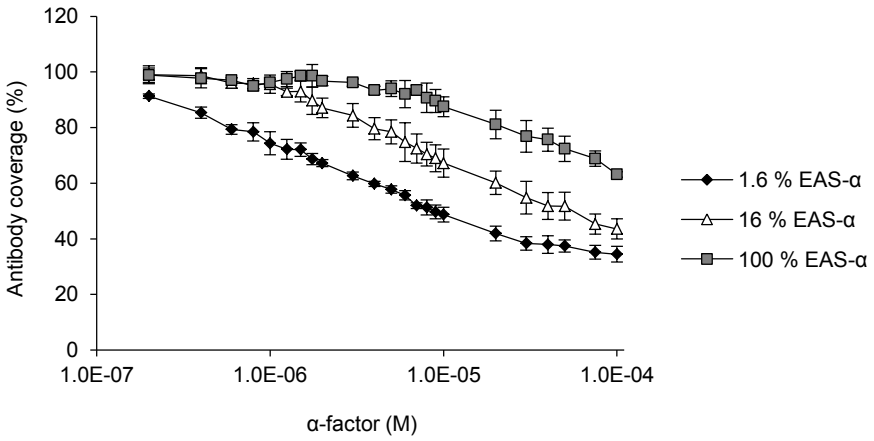

Figure 10. Calibration of the competitive ELISA. Individual wells of 96-well microplates were functionalized with the recombinant hydrophobins EAS and EAS-α in different molar ratios and used for competitive ELISA measurements (section 2.9.2). Antibody coverage was calculated by data normalization to surfaces not treated with the synthetic α-factor. Mean values, corresponding to triplicate measurements of at least two independent experiments, are plotted. Error bars indicate standard deviation.

Remarkably, even very high pheromone concentrations (100 µM α-factor) were not sufficient to completely remove the antibodies from the functionalized surface. This

may result from the non-specific interaction between antibodies and hydrophobin layers as observed in the course of evaluating the tag accessibility (Figure 6 c) and as reported previously [280-282]. Consequently, these non-specific interactions might be an issue for very high pheromone concentrations to be measured, *i.e.* in the case of very low antibody coverage values. However, these limitations could be overcome by increasing the EAS-α content of the monolayer, thereby shifting the dynamic range towards higher pheromone concentrations (Figure 10).

3.2.4 Evaluation of the competitive ELISA under varying conditions

Next, the influence of the sample matrix on the performance of the competitive ELISA was assessed. Any non-specific effect of the sample matrix on the competitive immunoassay may imply restrictions to the applicability of the assay, *e.g.* for the quantification of the α-factor in complex sample matrices such as the culture supernatants of yeast cells. On the other hand, it could be hypothesized that this approach might provide an opportunity to enhance the sensitivity of the assay. Particularly, if the affinity of the antibody to the immobilized pheromone (*i.e.* to EAS-α) can be reduced by applying certain conditions, lower concentrations of the dissolved α-factor will suffice to detach the antibodies from the surface, thereby lowering the limit of detection and enhancing the sensitivity of the assay.

In order to analyze the influence of the sample matrix, the competitive ELISA protocol was slightly modified to carry out the competition step under varying conditions (section 2.9.3). All other steps of the competitive ELISA were essentially similar to the standard protocol to avoid interference with the general immunoassay read-out. First, the influence of the pH value, the ionic strength and the detergent concentration of the sample matrix was addressed (Figure 11 a-d).

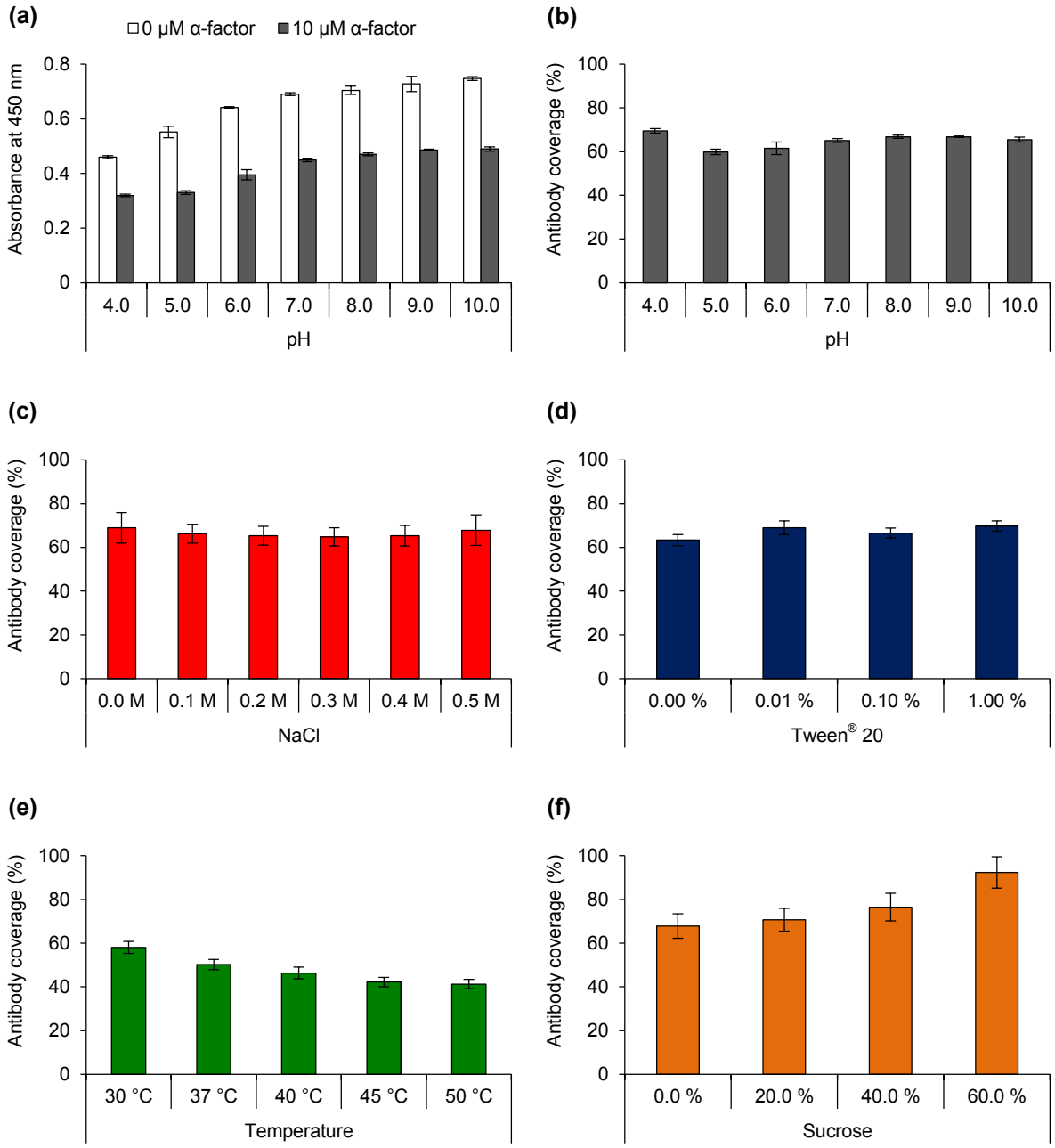

Figure 11. Evaluation of the competitive ELISA under varying conditions. (a) Influence of the sample matrix pH on the absorbance values. **(b)** Normalized data regarding the influence of the pH value. For data normalization, absorbance values obtained for samples containing 10 µM α-factor were normalized to absorbance values corresponding to control surfaces not treated with the pheromone. **(c)** Influence of the ionic strength on the competitive ELISA. Data were normalized according to (b). **(d)** Influence of the detergent concentration on the competitive ELISA. Data were normalized according to (b). **(e)** Influence of the temperature during the competition step. Data were normalized according to (b). **(f)** Influence of the sample viscosity – adjusted by sucrose addition – on the competitive ELISA. Data were normalized according to (b). All experiments were carried out using surfaces functionalized with recombinant hydrophobins in optimized composition (1.6 % EAS-α). Composition of the sample matrix buffers is shown in Table 18. Plotted values correspond to triplicate measurements of at least two independent experiments. Error bars indicate standard deviation.

Analysis of the influence of the pH value on the competitive ELISA revealed a biphasic behavior (Figure 11 a). No effect of the pH value on the absorbance values of both untreated and pheromone-treated surfaces was observed in the range of pH 7.0 – 10.0, while lowering the pH below 7.0 resulted in a gradual decrease of the absorbance values obtained. However, upon data normalization (*i.e.* calculating the antibody coverage of surfaces treated with 10 µM α-factor in relation to control surfaces not treated with the pheromone, Figure 11 b) the biphasic behavior was not evident, indicating that the competition efficiency was not dramatically altered in acidic conditions and that the α-factor could be reliably quantified in an acidic environment. The dependence of the absorbance values on the pH value in acidic conditions suggested that ionic interactions might be responsible for the observed behavior (section 4.2.3).

Next, the influence of the ionic strength and the detergent concentration of the sample matrix was analyzed. Strikingly, the competitive ELISA was highly robust against changes in these parameters, as neither the absorbance values (data not shown) nor the competition efficiency (Figure 11 c,d) were altered under these conditions. In summary, these data revealed that the competitive ELISA was largely robust against changes in the sample matrix composition and should therefore allow for highly sensitive α-factor quantification in various sample matrices, possibly including yeast culture supernatants.

Furthermore, the influence of varying physical conditions during the competition step was assessed. It was reasoned that physically increasing the diffusion rate might provide an opportunity to enhance the efficiency of the competition step. The diffusivity of the pheromone in the competitive immunoassay was defined by Brownian motion of individual molecules, given by the equation:

$$D = \frac{RT}{6\pi\eta rN}$$

where D represents the mass diffusivity, R and T are the universal gas constant and the absolute temperature, respectively, η defines the viscosity of the system, r represents the particle radius and N is the Avogadro constant [425]. Obviously,

temperature and viscosity of the system represented the only accessible parameters for elevating the diffusivity. Therefore, the influence of these parameters was addressed (Figure 11 e,f).

With increasing temperature during the competition step, the antibody coverage obtained for a fixed pheromone concentration was gradually decreased, indicating enhanced sensitivity of the assay at elevated temperatures (Figure 11 e). However, when the temperature was raised to 45 °C and 50 °C, a severe reduction in the absorbance values was observed (data not shown), most likely resulting from antibody denaturation at high temperatures. The increased assay sensitivity at elevated temperatures might reflect an altered stability of the antigen-antibody complex but may also result from enhanced diffusivity. In support of the latter hypothesis, increasing the sample viscosity by adding sucrose led to a marked reduction in sensitivity (Figure 11 f). These data were consistent with the hypothesis that the diffusion of the α-factor to the functionalized surface and the diffusion of detached antibodies into the bulk solution, both driven by Brownian motion, limited the sensitivity of the assay, while the interactive forces between the antibody and the α-factor were of minor importance in this regard. Taken together, the competitive ELISA proved to be highly robust against the sample matrix composition, and the highest assay sensitivity could be obtained by performing the competition step at elevated temperatures (40 °C).

3.2.5 Reusability of functionalized surfaces

Reusability of biological elements and functionalized surfaces is of high interest in biosensor development and commercialization. Provided that functionalized surfaces cannot be produced at very low cost, the development of single-use devices does not display an economically viable approach [6, 18]. However, the low dissociation constants of antibody-antigen complexes typically prevent the reuse of functionalized surfaces of affinity sensors based on antibodies or antibody fragments. Particularly, the regeneration procedures that need to be applied to remove the antibodies from a functionalized surface may affect the activity and stability of the surface functionalization and might dramatically affect the performance of the functionalized surface upon repeated use [18, 32].

Class I hydrophobins are known to self-assemble into highly robust monolayers that require harsh treatment (such as 100 % TFA or formic acid) to dissolve [129-135]. Monolayers of the EAS hydrophobin were found to resist treatment with hot detergents (Figure 5) or incubation in highly acidic or alkaline conditions [163]. Since antibodies show a clearly lower stability than hydrophobin layers, the possibility to reuse the hydrophobin-functionalized surfaces for multiple measurements was assessed. Therefore, after completion of a competitive ELISA measurement, the antibodies attached to the surface were stripped off by a combined treatment with a reducing agent, detergent and heat (section 2.9.4). Subsequently, the hydrophobin-functionalized surfaces were reused for competitive ELISA measurements and their performance upon repeated use was analyzed (Figure 12).

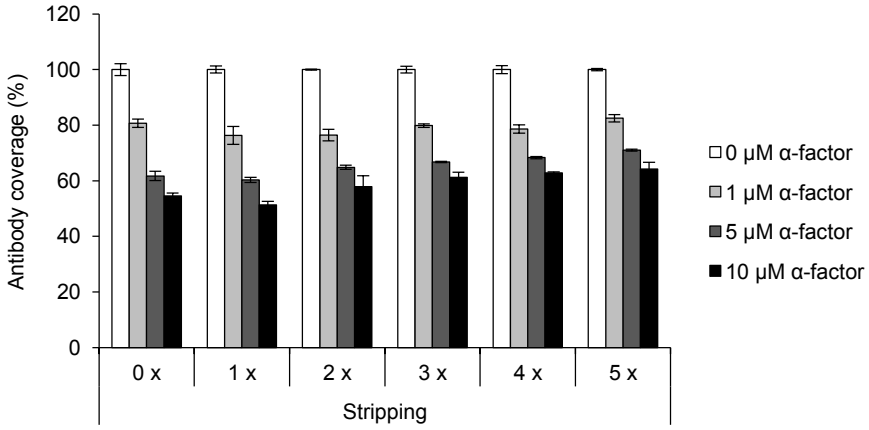

Figure 12. Analysis of the reusability of hydrophobin-functionalized surfaces. Polystyrene surfaces were functionalized with recombinant hydrophobins (1.6 % EAS-α) and used for competitive ELISA measurements. After measurement of the absorbance values, antibodies attached to the functionalized surfaces were removed by a combined treatment with reducing agents, detergents and heat (section 2.9.4). Functionalized surfaces were reused for competitive ELISA measurements the next day. Antibody coverage was calculated by normalizing the data to surfaces not treated with the pheromone. A representative set of data, corresponding to triplicate measurements for each condition, is plotted. Error bars indicate standard deviation. Qualitatively similar results were obtained in several independent experiments.

Evidently, the hydrophobin monolayers could be used for repeated competitive ELISA measurements (Figure 12). Even after five consecutive stripping cycles, the functionalized surfaces were still applicable for competitive ELISA measurements.

Importantly, the sensitivity of the immunoassay was not severely affected by multiple stripping events. These data indicated that the hydrophobin layers were not harmed by the antibody denaturation step, thereby offering the possibility to reuse the functionalized surfaces multiple times.

Compared to freshly functionalized surfaces, a 30 – 40 % reduction of the absorbance values was observed after the first stripping cycle (Appendix B.2), whereas no further decrease in signal intensity was seen after subsequent stripping events. The initial reduction in the signal intensity may result from partial extraction of the hydrophobins by the hot SDS treatment. Water contact angle measurements indicated that some of the recombinant hydrophobins were extracted during such a treatment (Figure 5), and partial extraction of class I hydrophobins by hot SDS treatment has been observed previously [158, 213, 251, 257, 263, 280, 331, 396, 412-416]. Quantitative analysis revealed that, depending on the hydrophobin, the substrate and the surface functionalization method, hot SDS extraction removed 7 – 85 % of the hydrophobins initially attached to the surface [158, 251, 331, 416]. As EAS and EAS-α did not exhibit any differences in their resistance against hot SDS treatment (Figure 5), it can be assumed that about 30 – 40 % of both hydrophobins were extracted during the first stripping cycle, whereas further extraction during additional stripping cycles was not evident (Appendix B.2). Therefore, the class I hydrophobin layers consisting of EAS and EAS-α were sufficiently robust to allow for multiple measurements with similar sensitivity.

3.3 Pheromone quantification by inverse ELISA measurements

3.3.1 Design and concept of the inverse ELISA

The competitive ELISA allowed for robust detection of the α-factor pheromone, largely independent on the sample matrix composition, with a lower limit of detection of 0.2 µM α-factor and wide dynamic range (section 3.2.3). However, the sensitivity of the competitive immunoassay may be insufficient, although several options may exist to considerably increase its sensitivity (sections 4.2.3 and 4.5.3). The competitive immunoassay relied on competitive detachment of antibodies from the hydrophobin-functionalized surface, implying that the antigen-antibody complex formed at the surface (*via* the α-factor exposed by EAS-α) had to dissociate to release the antibodies from the functionalized surface. Antigen-antibody complexes show very low dissociation constants, typically in the nanomolar to picomolar range [426-428]. Thus, the high stability of the complex between the α-factor antibody and its cognate antigen displayed at the functionalized surface may limit the sensitivity of the competitive immunoassay. To overcome this limitation, a second immunoassay based on hydrophobin-functionalized surfaces, but not relying on the dissociation of the antigen-antibody complex, was delevoped (Figure 13).

In this design, the α-factor antibodies were first added to a pheromone-containing sample and pre-incubated for 2 h. During this time frame, some of the available antigen binding sites of the α-factor antibodies were occupied by the soluble α-factor in the sample. In a second step, the pre-incubated samples were applied to polystyrene surfaces functionalized with EAS and EAS-α. In the absence of competition, only antibodies that still carried available antigen binding sites were capable of specifically binding to the surface (Figure 13). In this approach, competition between the α-factor in solution and the immobilized α-factor (*via* EAS-α) would be detrimental to the sensitivity. As competition efficiency is directly related to the diffusivity, being a function of the temperature (Figure 11 e), competition could be largely suppressed by performing the second step at 4 °C. Finally, the antibodies attached to the surface were quantified by the use of a secondary antibody linked to HRP.

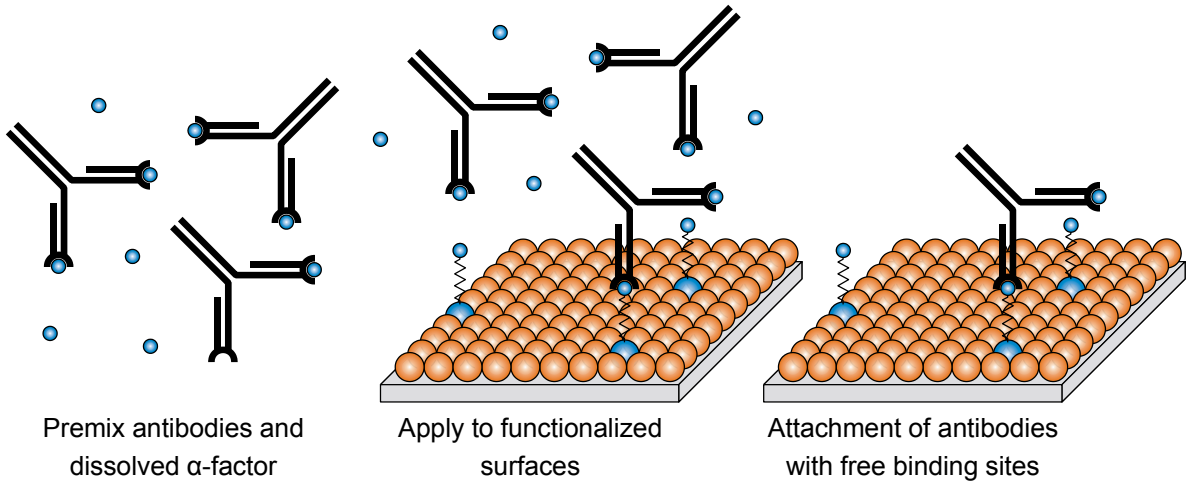

Figure 13. Schematic illustration of the concept of the inverse ELISA. First, α-factor antibodies (black Y-shaped structures) were added to samples containing the α-factor (small blue spheres) to occupy some of the available antigen binding sites of the antibodies (left panel). Second, the pre-incubated samples were applied to polystyrene surfaces (gray) functionalized with the recombinant hydrophobins EAS (orange) and EAS-α (blue) in advance (middle panel). During this step, only antibodies still carrying available antigen binding sites were able to specifically bind to the functionalized surfaces (right panel), allowing for quantification of the pheromone in the sample.

As the sequence of some of the reaction steps was inverted in comparison to the competitive ELISA, this immunoassay is referred to as the inverse ELISA throughout this study. Comparable immunoassays, although based on different strategies for target compound immobilization, have been established previously to quantify herbicides [429, 430] or explosives [14]. Additionally, a similar immunoassay was utilized to detect a hydrophobin from *Fusarium poae* in extracts of barley and malt to assess the risk of beer gushing [305].

3.3.2 Calibration of the inverse ELISA

In order to validate if the inverse ELISA was indeed more sensitive than the competitive ELISA, the inverse ELISA was calibrated with various dilutions of the synthetic α-factor (section 2.10.1). Different hydrophobin monolayer compositions were utilized for inverse ELISA calibration to evaluate the influence of the hydrophobin monolayer composition (Figure 14).

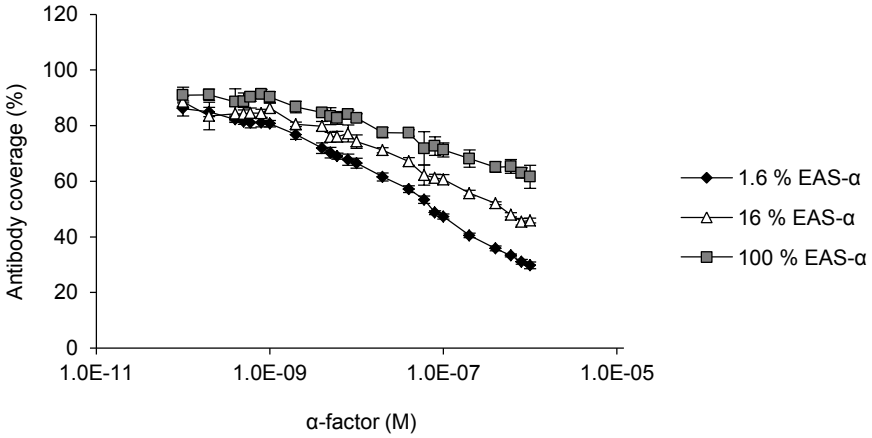

Figure 14. Calibration of the inverse ELISA. Serial dilutions of synthetic α-factor were pre-incubated with the α-factor antibody and subsequently applied to polystyrene surfaces functionalized with the recombinant hydrophobins EAS and EAS-α in different molar ratios. Antibody coverage was calculated by data normalization to samples not containing the pheromone. All plotted values correspond to triplicate measurements of at least two independent experiments. Error bars indicate standard deviation.

Evidently, increasing the pheromone concentration in the samples resulted in a gradual decrease in the antibody coverage, in line with fewer antibodies carrying available binding sites when pre-incubated with high amounts of the pheromone (Figure 14). Utilizing the optimized hydrophobin layer composition (1.6 % EAS-α), a lower limit of detection of 0.1 nM α-factor and a dynamic range of 0.1 nM – 1.0 µM α-factor were obtained. Thus, the limit of detection achieved by the inverse ELISA was about three orders of magnitude lower than the limit of detection obtained by the competitive ELISA (0.2 µM α-factor, Figure 10). Additionally, the dynamic range of the inverse ELISA, covering four orders of magnitude, was substantially larger than the dynamic range obtained for the competitive ELISA (0.2 µM – 100 µM, Figure 10). As observed for the competitive ELISA, the sensitivity of the inverse immunoassay could be tuned by adjusting the EAS-α content of the hydrophobin layer (Figure 14). Upon increasing EAS-α content of the monolayers, the slope of the calibration curve was reduced, indicating that the sensitivity and the dynamic range of the inverse immunoassay can be predefined by the choice of the EAS-α content of the hydrophobin monolayer. As the highest slope was obtained for hydrophobin layers encompassing 1.6 % EAS-α, this value was regarded as the optimized hydrophobin layer composition for the inverse ELISA as well. Although the second step of the

inverse ELISA, featuring attachment of antibodies with available binding sites to the functionalized surface, was performed at low temperatures to reduce competition between the soluble and the surface-immobilized pheromone, a distinct contribution of competition was still evident. In the absence of competition, the number of antibody binding sites exposed at the surface (*i.e.* the EAS-α content of the hydrophobin layer) would not be expected to affect the inverse ELISA performance above a specific threshold that guaranteed that all antibodies with available binding sites were able to attach. However, the slopes of the calibration curves obtained for different hydrophobin layer compositions differed remarkably (Figure 14), indicating that competition affected the inverse ELISA approach considerably (section 4.2.2).

3.3.3 Evaluation of the inverse ELISA under varying conditions

Next, the influence of the sample matrix composition on the behavior of the inverse ELISA was addressed, similar to the experiments performed to assess the robustness of the competitive immunoassay. Considering the high sensitivity of the inverse ELISA, this immunoassay should be ideally suited to quantify the α-factor in yeast culture supernatants in physiologically relevant concentrations. However, non-specific matrix effects have to be excluded to ensure reliable pheromone quantification. Therefore, the α-factor was diluted in various buffers with different pH values, ionic strength or detergent concentration (section 2.10.2) and the influence on the behavior of the inverse ELISA was evaluated (Figure 15).

Upon modification of the pH value of the sample matrix (Figure 15 a), the absorbance values showed a biphasic behavior, strikingly similar to the data obtained with the competitive ELISA (Figure 11 a). Again, an obvious reduction in the absorbance values was observed when the assay was performed in acidic conditions, whereas data normalization revealed that the sensitivity was not severely altered (Figure 15 b). These data suggested that antibody binding to the functionalized surfaces was limited under acidic conditions, possibly resulting from electrostatic repulsive forces between the antibody and the hydrophobin-functionalized surface (section 4.2.3). However, as the electrostatic forces were independent on the presence or absence of the pheromone, the absorbance values for pheromone-free

samples were similarly reduced, rendering the sensitivity of the immunoassays essentially unchanged.

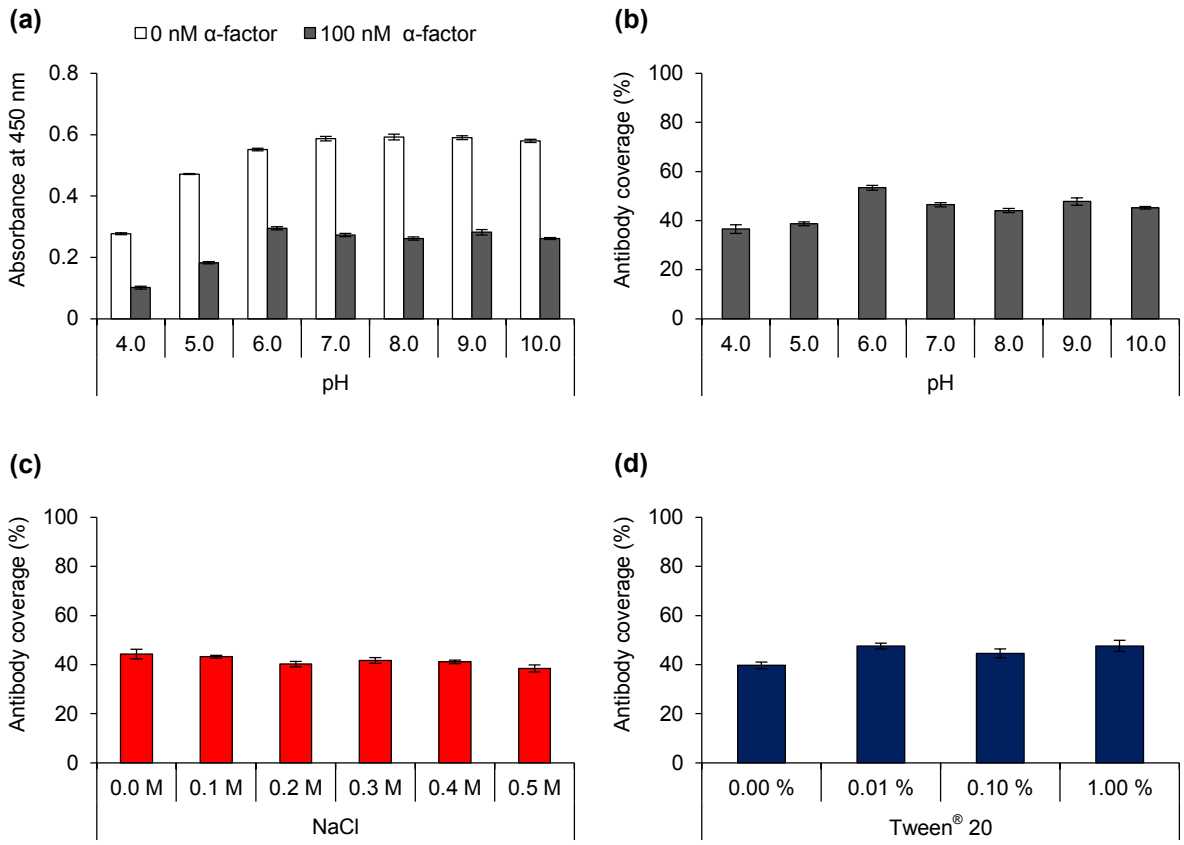

Figure 15. Evaluation of the inverse ELISA under varying conditions. (a) Influence of the pH on the absorbance values. **(b)** Normalized data concerning the influence of the pH value on the inverse ELISA behavior. For data normalization, values corresponding to pheromone-free samples were set to 100 % antibody coverage and values obtained for samples containing 100 nM α-factor were plotted. **(c)** Influence of the ionic strength on the performance of the inverse ELISA. Data normalization was carried out according to (b). **(d)** Influence of the detergent concentration on the behavior of the inverse ELISA. Data were normalized according to (b). All experiments were carried out using functionalized surfaces comprising the optimized hydrophobin layer composition (1.6 % EAS-α). The composition of the sample matrix buffers used in each set of experiments is detailed in Table 18. Plotted values correspond to triplicate measurements of at least two independent experiments. Error bars indicate standard deviation.

In contrast, the ionic strength or the detergent concentration of the buffer initially used to pre-incubate the α-factor and cognate antibodies did not show any influence on the inverse ELISA performance. Neither the absorbance values (data not shown)

nor the sensitivity (Figure 15 c,d) were affected by modifying these parameters in a wide range, consistent with the results obtained for the competitive ELISA. Thus, it can be concluded that the behavior of the inverse ELISA is highly independent on the sample matrix composition. Consequently, the inverse ELISA should be suitable to detect and quantify even very low α-factor concentrations in complex sample matrices such as yeast culture supernatants.

3.4 Pheromone quantification in yeast culture supernatants

3.4.1 Quantification of yeast pheromones by competitive and inverse ELISA measurements

Due to its sensitivity and its robustness against changes in sample matrix conditions, the inverse ELISA should be suitable to detect and quantify the α-factor pheromone in yeast culture supernatants. However, some pre-treatment of the cell-free culture supernatants was required to obtain high-quality results (section 2.10.3).

Yeast cells rapidly acidify their environment, resulting in acidic culture supernatants (pH 2.0 – 3.0, data not shown). As these conditions may cause antibody denaturation and both immunoassays suffered from low absorbance values when acidic samples were applied (Figures 11 a and 15 a), adjusting the culture supernatants to pH 8.0 proved to be mandatory. Increasing the pH value resulted in the formation of precipitates, most likely resulting from the poor solubility of certain calcium salts in neutral to alkaline environments. Thus, prior to increasing the pH value, EGTA was added to chelate calcium ions in the culture supernatants, thereby minimizing the formation of precipitates. Finally, protease inhibitors were added to the culture supernatants to prevent proteolytic degradation of the antibodies due to proteases secreted by yeast cells or released from lysed cells. Utilizing these sample treatment steps, the α-factor could be quantified in yeast culture supernatants by the competitive and the inverse ELISA technique. Importantly, the calibration curves were indistinguishable from the curves obtained when the α-factor was dissolved in

PBS-T (data not shown), again highlighting the robustness of both immunoassays against modifications in the sample matrix composition.

3.4.2 Pheromone secretion of wild-type and genetically engineered *S. cerevisiae* strains

First, the hydrophobin-based immunoassays were applied to study the pheromone secretion of wild-type strains of *S. cerevisiae*. To this end, yeast cells of the mating type α (BY4742) or mating type **a** (BY4741) were grown in SD medium and the cultures were sampled over time to analyze the α-factor concentration in the respective culture supernatants. At the indicated time points, cells were removed by centrifugation and the α-factor was quantified in cell-free culture supernatants by the inverse ELISA approach (Figure 16 a). Since individual cultures showed remarkable differences in their growth behavior (data not shown), pheromone concentrations of different cultures could not be averaged and representative curves are plotted. Due to the complexity of the biological system encompassing proliferation and death of pheromone-secreting cells as well as pheromone secretion and degradation, normalization of the α-factor concentration to the cell density at each time point did not prove to be appropriate.

As expected, the **a**-type strain of *S. cerevisiae* did not secrete measurable amounts of the α-factor throughout the time course of the experiment (Figure 16 a). Both α-factor pheromone precursor genes (*MFα1* and *MFα2*) are α-specific genes that are not expressed in **a**-type cells [340, 342, 343]. Hence, the inverse ELISA proved to be highly selective for the α-factor pheromone even in yeast culture supernatants.

In contrast, cells of the α-type strain secreted the α-factor, and 30 – 50 nM α-factor accumulated in the culture supernatants of these cells within 10 h of growth (Figure 16 a). The α-factor concentrations in the culture supernatant apparently paralleled the growth behavior of the α-type strain for the first 8 – 10 h (data not shown), suggesting that the pheromone was secreted at a constant rate as reported previously [431-433]. However, the pheromone concentrations declined upon further growth when the cells entered the late log phase or early stationary phase. This might reflect non-specific pheromone degradation in nutrient-limited surroundings as observed previously [368, 434-436] (section 4.3.1).

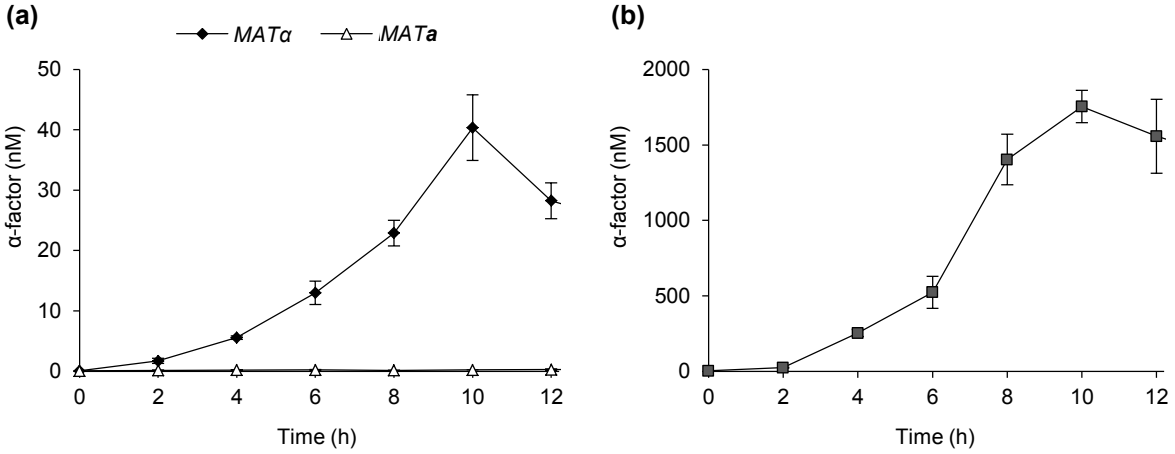

Figure 16. Pheromone secretion of wild-type and genetically engineered *S. cerevisiae* cells. (a) Secretion of the α-factor by wild-type *S. cerevisiae* cells. Haploid cells of the mating type **a** (BY4741) or α (BY4742) were grown in SD medium and the cultures were sampled at the indicated time points. The inverse ELISA technique was applied to quantify the α-factor pheromone in the respective culture supernatants by employing the optimized hydrophobin layer composition (1.6 % EAS-α). **(b)** Pheromone secretion of α-type cells engineered to secrete high amounts of the α-factor pheromone. *S. cerevisiae* BY4742 was transformed with the plasmid p426GPD-MFα1 and grown in SD medium. Pheromone concentrations were determined by the use of the inverse ELISA utilizing the optimized monolayer composition (1.6 % EAS-α) and appropriate sample dilutions. Representative curves, corresponding to triplicate measurements, are plotted. Error bars indicate standard deviation.

Next, the pheromone secretion of *S. cerevisiae* cells engineered to secrete high amounts of the α-factor was assessed (Figure 16 b). To this end, the *MFα1* ORF was cloned into p426GPD vector under transcriptional control of the strong *GPD* promoter, yielding the plasmid p426GPD-MFα1. *MFα1* was chosen as it encodes four copies of the α-factor, whereas only two α-factor units (one of them with two amino acid substitutions) are encoded by *MFα2* [348]. Furthermore, about 90 % of the α-factor secreted by α-type cells can be ascribed to *MFα1* expression [433, 434], indicating that *MFα1* might be superior to *MFα2* in terms of expression level, mRNA stability and/or the efficiency of translation, precursor processing and secretion. In addition, the yeast expression vector p426GPD carries the 2μ origin, conferring a high plasmid copy number in yeast cells [387, 437]. Consequently, upon transformation of the α-type strain BY4742 with p426GPD-MFα1, engineered yeast cells were expected to secrete high levels of the α-factor into their surroundings.

Analyzing the pheromone secretion of these cells by utilizing the hydrophobin-based immunoassays revealed that the α-type cells overexpressing *MFα1* indeed accumulated very high amounts of the α-factor, achieving about 1 – 2 µM α-factor within 10 h of growth (Figure 16 b). As observed for wild-type cells of the mating type α, there was a decline in the α-factor concentrations in the culture supernatants when the cells entered the stationary phase (10 – 12 h of growth), probably reflecting α-factor degradation (section 4.3.1). Despite comparable growth rates, certain deviations in the α-factor secretion were seen between individual cultures (data not shown), possibly resulting from the plasmid-based *MFα1* expression. Plasmid-based expression systems inherently cause a remarkable heterogeneity of the expression level in individual cells, mostly due to copy number differences and plasmid loss [73, 438, 439].

Notably, the α-factor concentrations in the culture supernatants of cells overexpressing *MFα1* markedly exceeded the dynamic range of the inverse ELISA utilizing the optimized hydrophobin layer composition (1.6 % EAS-α), and dilution of the culture supernatants was mandatory for reliable pheromone quantification. Alternatively, the α-factor concentrations could be determined by inverse ELISA measurements employing hydrophobin layers with increased EAS-α content, taking use of the possibility to shift the dynamic range by modulating the hydrophobin layer composition (Figure 14). Likewise, the competitive immunoassay could be employed to determine α-factor concentrations in the culture supernatants of *MFα1* overexpressing cells (data not shown).

3.4.3 Pheromone secretion of *S. cerevisiae* strains defective in pheromone maturation

Next, the selectivity and specificity of the inverse immunoassay were evaluated, in particular focusing on the importance of pheromone maturation with respect to the measurability by the hydrophobin-based immunoassays. To this end, α-type cells of *S. cerevisiae* defective in N-terminal or C-terminal pheromone maturation, *i.e.* carrying a deletion of the *KEX1* or the *STE13* gene, were used. Both genes encode peptidases involved in the processing of the α-factor precursor in the secretory pathway (Figure 1). In particular, Kex1p is responsible for C-terminal

maturation of the α-factor [354], cleaving off the C-terminal lysine-arginine moiety present at three of the four α-factor units of the Mfα1p precursor. In contrast, Ste13p carries out N-terminal processing of the α-factor by cleaving off dipeptide moieties [355]. To assess the influence of pheromone maturation, α-type cells lacking the *STE13* or *KEX1* gene were grown in SD medium and assayed for pheromone secretion by the inverse ELISA approach (Figure 17).

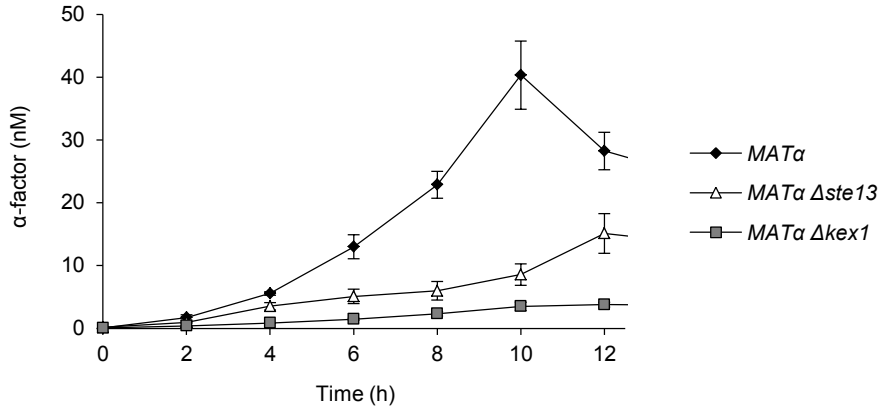

Figure 17. Pheromone secretion of yeast strains defective in pheromone maturation. Wild-type α-cells of *S. cerevisiae* (BY4742) or isogenic cells lacking the *KEX1* gene (BY4742 *Δkex1*) or the *STE13* gene (BY4742 *Δste13*) were grown in SD medium. Pheromone concentrations in the culture supernatants were determined by inverse ELISA measurement employing functionalized surfaces containing 1.6 % EAS-α. Representative curves, corresponding to triplicate measurements, are plotted. Error bars indicate standard deviation.

Yeast cells carrying a deletion of the *STE13* gene accumulated about 10 – 20 nM α-factor within 10 – 12 h of growth compared to 30 – 50 nM α-factor secreted by isogenic wild-type cells in a similar time frame (Figure 17). While a reduced affinity of the antibody towards the N-terminally immature α-factor could not be excluded, the reduced α-factor levels found in the supernatants of *Δste13* cells were most likely caused by differences in the growth rate of the wild-type and the *Δste13* strain. It was found that *Δste13* cells grew clearly slower than wild-type cells in minimal medium, achieving roughly 45 % of the cell density of the wild-type strain after 10 h of growth (data not shown). As cells carrying or lacking the *STE13* gene secrete the α-factor at a similar rate and with similar kinetics [355, 440], the comparatively low pheromone

concentrations detected in the culture supernatants of the *Δste13* strain might have resulted from the growth rate differences. However, as mentioned above, normalization of the pheromone concentration in the culture supernatants to the cell density did not provide evaluable data.

In marked contrast, the *Δkex1* strain accumulated very low levels of the α-factor in the culture supernatants, yielding a maximum of about 5 nM within 10 – 12 h of growth (Figure 17). The severe reduction in α-factor concentration in the supernatants of this strain could not be attributed to growth rate differences exclusively. Although the *Δkex1* strain was found to proliferate at a slightly reduced rate in comparison to wild-type cells, the *Δkex1* strain grew clearly faster than the *Δste13* strain that accumulated higher pheromone concentrations (Figure 17 and data not shown). Thus, the low α-factor concentrations determined by the inverse ELISA technique might have resulted from a severe reduction in the affinity of the antibody towards the C-terminally immature pheromone. A conclusive model addressing the importance of pheromone maturation on the measurability by hydrophobin-based immunoassays is given in the discussion (section 4.3.3).

3.5 Development of an artificial inter-species communication system

Artificial cell-cell communication represents an emerging tool in synthetic biology applications encompassing cellular consortia. Consortium-based approaches provide the unique possibility to share different tasks between specifically engineered cell populations, thereby reducing the metabolic burden for each cell type [373-377]. Artificial cell-cell communication might be a suitable approach to implement novel control elements in consortium-based approaches as cellular communication might be utilized to define the spatiotemporal sequence of actions taken by the consortium. In this study, a synthetic inter-species communication mode was developed, relying on engineered cells of the fission yeast *S. pombe* secreting the α-factor pheromone of *S. cerevisiae*. This system might represent a valuable tool for synthetic biology

applications as well as for the establishment of whole-cell sensors and cell-based sensor-actor systems. Employing the capabilities of distantly related species into a whole-cell sensor system might significantly enlarge the range of analytes and concentrations that could be detected, which would not be feasible with a single whole-cell sensor system [92] (section 4.4.1). Additionally, engineered *S. pombe* cells secreting the α-factor pheromone might be combined with the hydrophobin-based immunoassays, yielding a novel opportunity to create a whole-cell biosensor read-out (section 3.6.1).

3.5.1 Design, cloning and heterologous expression of α-factor pheromone precursor genes in *S. pombe*

Synthesis and secretion of the α-factor pheromone by *S. pombe* was realized by two different approaches. First, the authentic *S. cerevisiae MFα1* ORF was utilized to mediate α-factor expression in *S. pombe*. Similar routes have been taken previously to synthesize and secrete pheromones of *C. cinerea*, *Sordaria macrospora*, *Penicillium chrysogenum, S. pombe* and *S. commune* in *S. cerevisiae* host cells [432, 441-444]. In addition, a chimeric gene was generated (Figure 18 a) that was based on the *S. pombe map2* gene encoding the P-factor pheromone precursor [398]. Although the α-factor and the P-factor are highly different at the amino acid level, they share some structural similarities. Both pheromones represent unmodified peptides that are secreted *via* the standard secretory pathway [344]. Structurally, the precursors encoded by *S. cerevisiae MFα1* and *S. pombe map2* are similar, encompassing a signal peptide for import into the ER, four repeats of the mature pheromone and several N-linked glycosylation sites [347, 348, 398] (Figure 18 a). However, processing of the precursors is significantly different in *S. cerevisiae* and *S. pombe*, and the peptides spacing the pheromone units differ remarkably in their sequence [344]. The chimeric gene *map2/MFα1* was essentially identical to *S. pombe map2*, but the sequence encoding the mature P-factor pheromone was replaced by the sequence encoding the α-factor pheromone of *S. cerevisiae* in two of the four repeats (Figure 18 a, see Appendix A.3 for DNA and amino acid sequence). Hence, expression of the chimeric gene in *S. pombe* might result in synthesis and secretion of functional α-factor.

The ORFs encoding the authentic *S. cerevisiae* Mfα1p as well as the chimeric Map2/Mfα1p were integrated into fission yeast expression vector pJR1-3XL [388] under transcriptional control of the strong, thiamine-repressible *nmt1* promoter, yielding pJR1-MFα1 and pJR1-map2/MFα1. In the absence of thiamine, the *nmt1* promoter mediates high expression levels of downstream target genes [445]. The pheromone precursor genes were fused to the sequence encoding the hemagglutinin (HA) epitope to allow for immunological detection of the pheromone precursors upon expression in the heterologous host. Therefore, the respective ORFs were fused to the sequences encoding a flexible $(GGGGS)_3$ linker element and three repeats of the HA epitope at their 3' end and placed into pJR1-3XL, resulting in pJR1-MFα1-3HA and pJR1-map2/MFα1-3HA. Both plasmids were transformed into *S. pombe* HE620 and expression of the pheromone precursor genes was analyzed by SDS-PAGE and immunological detection (Figure 18 b). Colloidal Coomassie staining revealed that comparable amounts of proteins were loaded in each lane (data not shown).

Successful expression of both *MFα1-3HA* and *map2/MFα1-3HA* was evidenced by immunological detection of the pheromone precursors fused to the HA epitope. In contrast, no cross-reacting protein was observed in lysates of *S. pombe* cells transformed with an empty vector, indicating that the signals detected by the HA-tag antibody corresponded to the pheromone precursors (Figure 18 b). Upon heterologous expression of *MFα1* in *S. pombe*, a predominant signal at a molecular weight of about 35 kDa was evident. Additionally, a faint signal in the molecular weight of about 25 kDa could be detected. Remarkably, based on the primary structure, the molecular weight of the precursor encoded by *MFα1-3HA* was calculated to be 23.2 kDa and 21.2 kDa for the precursor carrying and lacking the N-terminal signal peptide, respectively [405]. The higher apparent molecular weight determined by SDS-PAGE might therefore indicate that the precursor underwent glycosylation. In its authentic host, the Mfα1p precursor is glycosylated at all three N-linked glycosylation sites [349-351]. Glycosylation of the precursor might also be carried out by *S. pombe* glycosyltransferases.

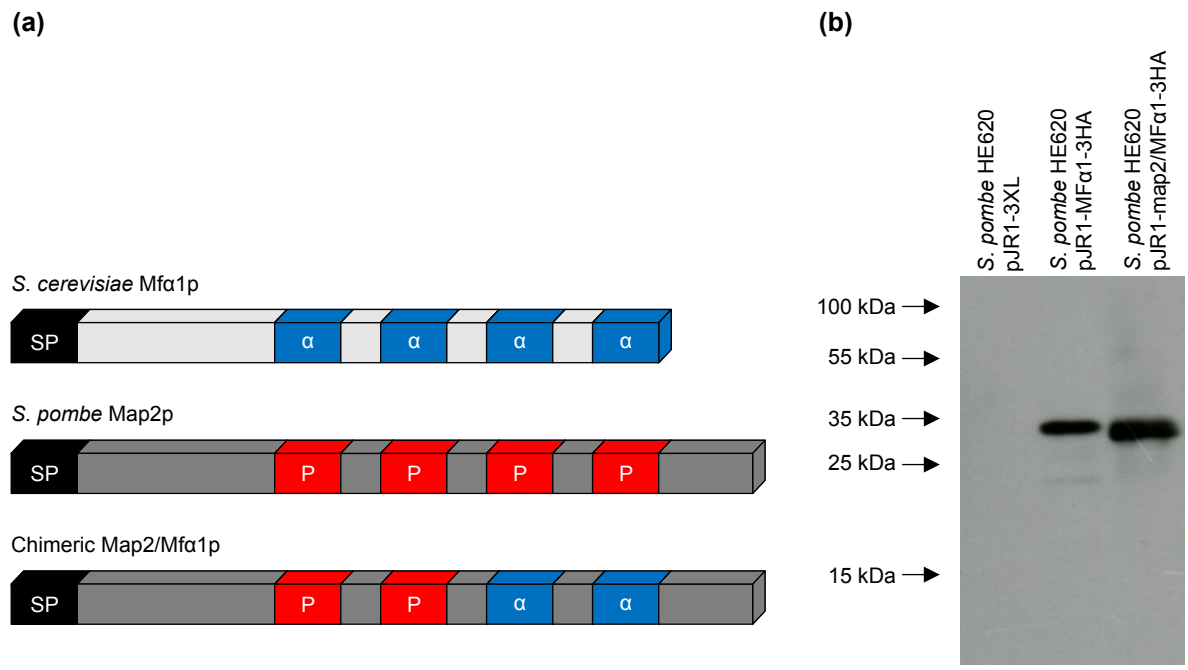

Figure 18. Structure and expression analysis of constructs for synthesis and secretion of the *S. cerevisiae* α-factor pheromone by *S. pombe*. (a) Schematic illustration of authentic and chimeric pheromone precursors. The authentic Mfα1p derived from *S. cerevisiae* carried an N-terminal signal peptide (SP) for import into the ER and four repeats of the α-factor pheromone. Likewise, the authentic *S. pombe* Map2p precursor harbored an N-terminal signal peptide and four copies of the mature P-factor pheromone. The chimeric Map2/Mfα1p precursor was highly similar to *S. pombe* Map2p, but two of the P-factor units were replaced by the sequence corresponding to the α-factor. Both *MFα1* and *map2/MFα1* were expressed in *S. pombe* to achieve synthesis and secretion of the α-factor pheromone in the heterologous host. **(b)** Expression analysis of pheromone precursor genes in *S. pombe.* To enable immunological detection of the pheromone precursors, the sequence encoding a $(GGGGS)_3$ linker as well as three repeats of the HA epitope were fused 3' to the sequence of the *MFα1* and *map2/MFα1* ORF to obtain *MFα1-3HA* and *map2/MFα1-3HA*, respectively. *S. pombe* HE620 was transformed with the empty vector (pJR1-3XL) or derivatives containing *MFα1-3HA* or *map2/MFα1-3HA*. Cellular lysates (25 µg total protein) were separated *via* SDS-PAGE and proteins were transferred to PVDF membranes and probed with the HA-tag antibody.

Upon expression of the chimeric *map2/MFα1-3HA* gene in *S. pombe*, a single band was detected in the molecular weight range of about 35 kDa (Figure 18 b). Again, this was different to the calculated molecular weight of the precursor carrying or lacking the N-terminal signal peptide (25.8 kDa and 23.8 kDa, respectively [405]), possibly due to glycosylation of the chimeric precursor. This precursor, derived from *S. pombe* Map2p, carries two N-linked glycosylation sites in the C-terminal part, and

glycosylation of these moieties has been demonstrated previously for the authentic *S. pombe* Map2p precursor [398, 446].

Reproducibly, the signal obtained for the chimeric pheromone precursor was slightly more intense than that for the authentic precursor encoded by *MFα1-3HA* (Figure 18 b), possibly indicating that the chimeric gene was expressed to a slightly higher level. However, it should be noted that the amount of a precursor detected immunologically does not necessarily reflect the expression level of the respective gene, since immunological detection of the C-terminal HA epitope might have been influenced dramatically by the efficiency and speed of precursor processing and trafficking through the secretory pathway (section 4.4.2).

3.5.2 Assessment of the α-factor pheromone activity in the culture supernatants of engineered *S. pombe* cells

Next, it was evaluated whether heterologous expression of the authentic *MFα1* or the chimeric *map2/MFα1* pheromone precursor genes in *S. pombe* resulted in synthesis and secretion of active α-factor pheromone. Therefore, *S. pombe* cells carrying the vectors pJR1-3XL (empty vector), pJR1-MFα1 or pJR1-map2/MFα1 were grown in EMM for 24 h and cell-free culture supernatants were obtained by centrifugation (section 2.11.1). Subsequently, pheromone-responsive reporter cells of *S. cerevisiae* were transferred into the culture supernatants of the engineered *S. pombe* cells (section 2.11.2). Using this approach, the cell-free culture supernatants of engineered *S. pombe* cells could be screened for α-factor activity by analyzing if the *S. cerevisiae* reporter cells underwent pheromone response. Comparable approaches have been carried out previously to verify the presence of a fungal pheromone in culture supernatants or to characterize the pheromone response of engineered reporter cells [384, 432, 443, 447].

Upon perception of a mating pheromone, haploid *S. cerevisiae* cells arrest in G1 phase of the cell cycle, thereby synchronizing the cell cycle of putative mating partners [342, 345, 358-364]. In order to analyze if engineered *S. pombe* cells secreted active α-factor, pheromone-responsive reporter cells of *S. cerevisiae* (BY4741 *Δbar1*) were shifted into the cell-free culture supernatants and cell cycle progression was monitored by quantitative DNA staining and flow cytometry (sections

2.12.2 and 2.12.3, Figure 19). The *FIG1-tRFP* reporter gene cassette was not present in this strain to avoid interference of tRFP fluorescence with the red propidium iodide dye used to stain yeast DNA.

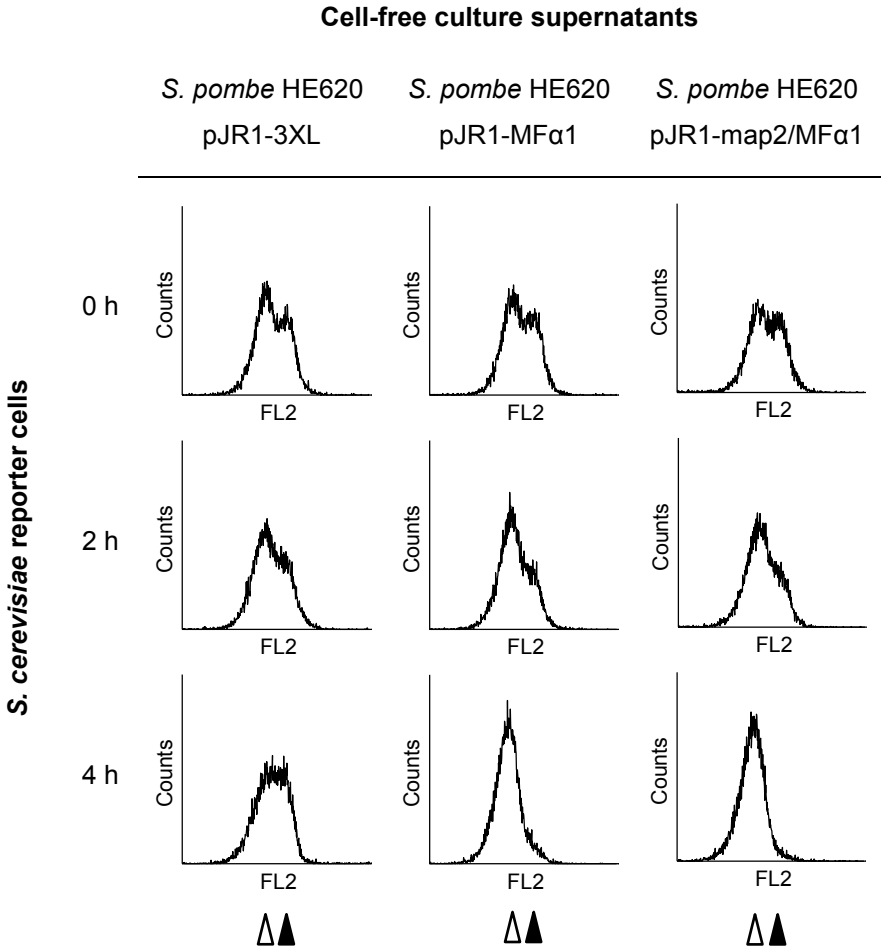

Figure 19. Cell cycle analysis of pheromone-responsive *S. cerevisiae* reporter cells transferred into culture supernatants of *S. pombe* cells engineered to secrete the α-factor pheromone. *S. pombe* HE620 was transformed with pJR1-3XL, pJR1-MFα1 or pJR1-map2/MFα1 and grown in EMM for 24 h prior to centrifugation to obtain cell-free culture supernatants. Pheromone-responsive reporter cells of *S. cerevisiae* BY4741 *Δbar1* were shifted into the culture supernatants and their cell cycle progression was monitored by quantitative DNA staining and flow cytometry. Open and filled arrow heads indicate G1 and G2 phase of the cell cycle, respectively.

Initially, *S. cerevisiae* reporter cells were distributed in both G1 and G2 phase of the cell cycle, with a slightly higher amount of cells in G1 phase (Figure 19). When reporter cells were transferred into a culture supernatant of *S. pombe* cells carrying

the empty vector, the amount of cells in G1 and G2 phase slightly changed over time, and the reporter cells were evenly distributed in G1 and G2 phase after 4 h. These data indicated that wild-type *S. pombe* cells did not secrete the α-factor pheromone or related peptides that could elicit a pheromone response in *S. cerevisiae*. In marked contrast, reporter cells shifted into the supernatants of *S. pombe* cells expressing *MFα1* or *map2/MFα1* clearly arrested the cell cycle in the G1 phase within 4 h, indicating that the reporter cells underwent pheromone response. After 4 h of incubation, the majority of reporter cells were arrested in the G1 phase of the cell cycle, consistent with previously reported data [448]. Upon further incubation, the reporter cells shifted into the supernatant of *MFα1*-expressing *S. pombe* cells gradually recovered from the cell cycle arrest and resumed growth, and almost equal populations could be assigned to the G1 and the G2 phase after 8 h (data not shown). In contrast, recovery was not evident for reporter cells shifted into supernatant of *map2/MFα1*-expressing cells, as they remained fully arrested for at least 8 h (data not shown). As the time required for recovery from pheromone-induced cell cycle arrest correlates with the pheromone concentration [449], these data suggested that the α-factor activity in the supernatants of *map2/MFα1*-expressing *S. pombe* cells was higher than the pheromone activity in the supernatants of *MFα1*-expressing cells.

The α-factor activity in the *S. pombe* culture supernatants was also assessed by monitoring the pheromone-dependent formation of mating projections and the pheromone-induced activation of the *FIG1* promoter in *S. cerevisiae* reporter cells. Therefore, reporter cells carrying the *FIG1-tRFP* cassette integrated into the genome (BY4741 *Δbar1 FIG1-tRFP*) were shifted into the culture supernatants of the engineered *S. pombe* cells, incubated for 8 h and the morphology and fluorescence of the reporter cells were analyzed by flow cytometry (section 2.12.3) and fluorescence microscopy (section 2.12.4, Figure 20).

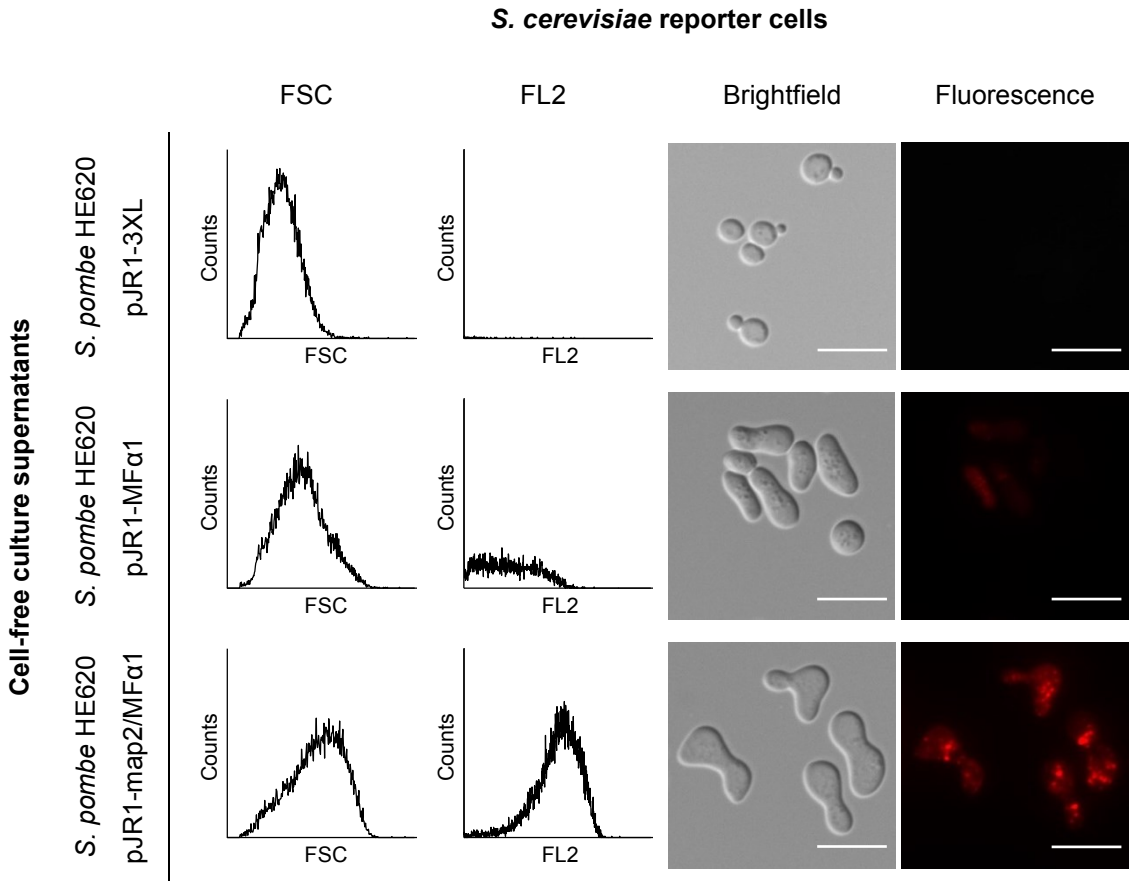

Figure 20. Analysis of the morphology and *tRFP* expression of *S. cerevisiae* reporter cells shifted into supernatants of *S. pombe* cells engineered to secrete the α-factor pheromone. Cells of *S. pombe* HE620 were transformed with the plasmids pJR1-3XL, pJR1-MFα1 or pJR1-map2/MFα1 and cell-free culture supernatants were obtained after 24 h of growth in EMM. Pheromone-responsive reporter cells of *S. cerevisiae* BY4741 *Δbar1 FIG1-tRFP* were transferred into culture supernatants and incubated for 8 h at 30 °C prior to fixation. Fixed cells were subjected to flow cytometry analysis and fluorescence microscopy to analyze their morphology and *tRFP* expression. Scale bars in microscopic images indicate 10 µm.

Reporter cells transferred into the supernatant of *S. pombe* cells carrying the empty vector showed the characteristic morphology of vegetatively growing cells, *i.e.* a narrow cell size distribution (quantified by FSC measurements) and the characteristic budding phenotype (Figure 20, top panel). Barely any fluorescent reporter cell was observed by flow cytometry and fluorescence microscopy, indicating that the *FIG1* promoter was not activated in these reporter cells. These data suggested that *S. pombe* cells did not secrete the α-factor or related compounds that could trigger the pheromone response in **a**-type *S. cerevisiae* cells. In contrast, reporter cells shifted to cell-free supernatants of *MFα1*-expressing *S. pombe* cells showed a

partially increased cell size (as evidenced by the broadened FSC distribution), and brightfield microscopy revealed that several reporter cells exhibited an elongated shape (Figure 20, middle panel). However, the reporter cells did not form the characteristic mating projections. The heterogeneity in the cellular morphology could be caused by physiological differences between individual cells, resulting in different responses to identical pheromone concentrations, in particular in the presence of low pheromone concentrations [420, 421]. About 30 % of the reporter cells exhibited a measurable fluorescence, indicating that about one-third of the reporter cells underwent pheromone-induced *tRFP* expression.

In contrast, *S. cerevisiae* reporter cells shifted to the culture supernatants of *S. pombe* cells expressing the chimeric *map2/MFα1* formed distinct mating projections resulting in an even wider cell size distribution, reflecting a hallmark feature of the yeast pheromone response (Figure 20, lower panel). Some of the reporter cells even formed multiple shmoo tips, a phenomenon observed upon application of very high pheromone concentrations (more than 50 nM α-factor for pheromone-hypersensitive *Δbar1* cells [419]). Additionally, about 90 % of the reporter cells showed fluorescence resulting from *tRFP* expression controlled by the pheromone-responsive *FIG1* promoter, and the mean *tRFP* expression of these reporter cells was clearly higher than the *tRFP* expression levels observed for reporter cells transferred into the supernatants of *MFα1*-expressing *S. pombe* cells. In summary, these data indicated that the expression of both *MFα1* and the chimeric *map2/MFα1* in *S. pombe* resulted in secretion of active α-factor, but that the pheromone activity was tremendously higher in the supernatants of *map2/MFα1* expressing *S. pombe* cells (sections 4.4.3 and 4.4.5).

3.5.3 Quantification of pheromones secreted by a heterologous host

Given the apparent differences in synthesis and secretion of biologically active α-factor upon expression of *MFα1* or *map2/MFα1* in *S. pombe*, it was of interest to study the pheromone secretion of the engineered *S. pombe* cells in further detail. Therefore, the hydrophobin-based inverse ELISA technique was applied to investigate the α-factor secretion of these cells during growth in minimal medium (section 2.10.3, Figure 21). Obviously, *S. pombe* cells carrying the empty vector did

not show any α-factor secretion (Figure 21), consistent with the absence of α-factor activity in the culture supernatants of these cells. Thus, it was confirmed that wild-type *S. pombe* cells did not secrete the α-factor pheromone or related compounds into the medium. Therefore, it can be concluded that the inverse ELISA is highly selective for the α-factor even in culture supernatants of *S. pombe* cells.

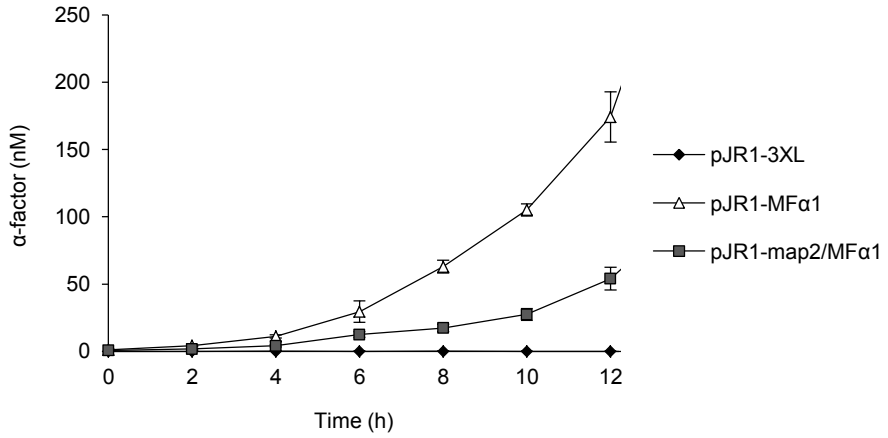

Figure 21. Quantification of the α-factor pheromone secreted by engineered *S. pombe* cells. Cells of *S. pombe* HE620 were transformed with pJR1-3XL, pJR1-MFα1 or pJR1-map2/MFα1 and grown in EMM. At the indicated time points, samples of the culture supernatants were taken and α-factor concentration was determined by inverse ELISA measurements featuring the optimized hydrophobin monolayer composition (1.6 % EAS-α). Representative curves, corresponding to triplicate measurements, are shown. Error bars indicate standard deviation.

Upon expression of *MFα1* in *S. pombe*, accumulation of the α-factor within culture supernatants was evident, yielding 150 – 300 nM α-factor after 12 h and 900 – 1500 nM α-factor after 24 h of growth. In contrast, upon expression of the chimeric *map2/MFα1* gene in *S. pombe*, about 30 – 50 nM α-factor and 400 – 600 nM α-factor accumulated within 12 h and 24 h, respectively (Figure 21). Some deviations between individual cultures were observed, most likely resulting from the plasmid-based expression system as was also observed for *S. cerevisiae* cells overexpressing *MFα1* (section 3.4.2). The pronounced difference in α-factor secretion in *S. pombe* cells expressing *MFα1* or *map2/MFα1* most likely reflects the difference in the number of α-factor repeats encoded by the respective genes (four copies in *MFα1* vs. two copies in *map2/MFα1*, Figure 18 a), although differences in

the expression level or the efficiency of trafficking through the secretory pathway cannot be excluded (sections 3.5.1 and 4.4.2). In marked contrast to *S. cerevisiae*, α-factor degradation upon entry into the stationary phase was not evident in *S. pombe* cultures, indicating that *S. pombe* cells do not express extracellular peptidases with suitable substrate specificity to degrade the α-factor pheromone.

Importantly, there was a striking discrepancy between the α-factor activity (determined by the use of pheromone-responsive reporter cells, section 3.5.2) and the α-factor concentration (assayed by the inverse ELISA) in the supernatants of *S. pombe* cells expressing *MFα1* or *map2/MFα1*. Although far higher α-factor concentrations were present in the supernatant of *MFα1*-expressing *S. pombe* cells, the pheromone activity was clearly lower in these supernatants. The apparent lack of correlation between α-factor concentration and activity is likely caused by inappropriate or incomplete processing of the Mfα1p precursor in *S. pombe*, leading to the secretion of immature or truncated derivatives of the α-factor upon expression of *MFα1* (section 4.4.5).

3.6 Applications of the hydrophobin-based surface engineering technique

Finally, further applications of the hydrophobin-based surface functionalization method for the development of immunoassays were investigated. First, a novel whole-cell sensor utilizing the α-factor to create the biosensor read-out was established. Exploiting the α-factor as a secreted peptide to generate the read-out signal of a whole-cell sensor might be advantageous as it provides the opportunity for signal transport, intrinsic signal amplification and sensor cell confinement (sections 1.4 and 4.5.1) and hydrophobin-based immunoassays might be compatible with various transducer technologies (section 4.5.3). In particular, *S. pombe* cells were engineered to modulate the α-factor secretion in response to thiamine (vitamin B1), thus developing a novel whole-cell sensor for the detection of trace amounts of thiamine (section 3.6.1).

Second, the versatility of the hydrophobin-based surface engineering technique for the development of novel immunoassays was investigated. It was demonstrated that hydrophobin-based immunoassays were not restricted to the detection of a yeast pheromone since comparable immunoassays for alternative analytes could be developed. In particular, hydrophobin-based immunoassays for the detection and quantification of the HA peptide and recombinant proteins fused to the HA epitope were established by employing a novel EAS derivative exposing the HA epitope upon self-assembly at a hydrophobic surface (section 3.6.2). Thus, functionalized surfaces encompassing this hydrophobin provided an opportunity to specifically attach HA-tag antibodies at the functionalized surface, paving the way for the development of competitive and inverse immunoassays.

3.6.1 Establishment of a novel whole-cell biosensor utilizing the α-factor pheromone to generate the sensor read-out

Due to the high sensitivity, robustness against sample matrix effects and suitability to quantify the α-factor in the culture supernatants of *S. cerevisiae* and *S. pombe*, the hydrophobin-based immunoassays could be employed to establish a novel whole-cell biosensor utilizing the α-factor pheromone to create the biosensor read-out signal. As a proof-of-concept, engineered *S. pombe* cells modulating the α-factor secretion in response to trace amounts of thiamine (vitamin B1) were employed. Thiamine is an important cofactor of several key metabolic enzymes [450] and thiamine deficiency has been linked to several human health issues, including systolic heart failure and arrhythmia [451], cancer [452] as well as dementia and Alzheimer`s disease [453]. Therefore, quantitative analysis of thiamine in various sample matrices is of high interest in healthcare applications.

S. pombe cells carrying the *MFα1* ORF under transcriptional control of the thiamine-repressible *nmt1* promoter (vector pJR1-MFα1) were employed as proof-of-principle whole-cell sensors. The authentic *MFα1* gene was chosen as cells expressing *MFα1* accumulated higher α-factor concentrations than *S. pombe* cells expressing *map2/MFα1* (Figure 21). Due to the positive regulation by the transcription factors Thi1p and Thi5p, the *S. pombe nmt1* promoter mediates very high transcription levels of a downstream target gene in the absence of thiamine in the extracellular

environment [454], whereas transcription from the *nmt1* promoter is suppressed by the action of Tnr1p, Tnr2p and Tnr3p in the presence of extracellular thiamine [455]. The regulation of the *nmt1* promoter by extracellular thiamine sources is consistent with the role of the Nmt1p protein in the synthesis of the pyrimidine moiety of thiamine [456]. The activity of the *nmt1* promoter can be regulated gradually in a narrow range of thiamine concentrations [457, 458], allowing for the implementation of a thiamine whole-cell sensor. Therefore, *S. pombe* cells carrying the vector pJR1-MFα1 were transferred to EMM supplemented with different amounts of thiamine and the pheromone secretion was monitored by the use of the inverse ELISA technique (section 2.10.3, Figure 22).

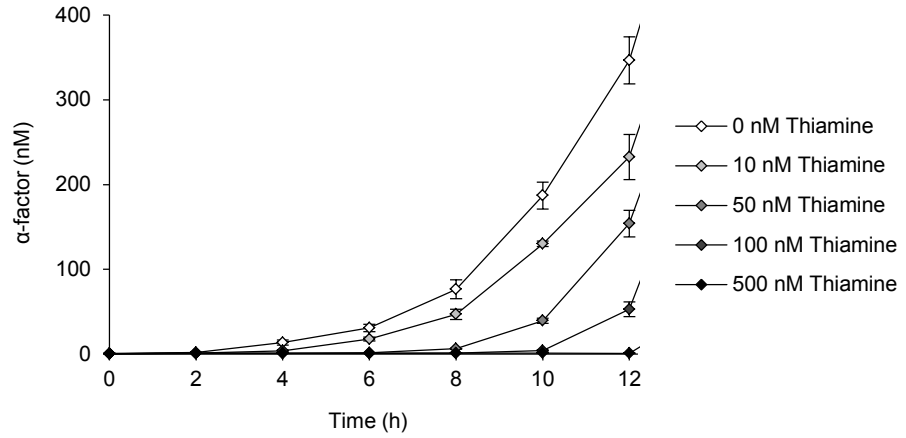

Figure 22. Secretion of the α-factor by engineered *S. pombe* sensor cells responding to extracellular thiamine by modulating *MFα1* expression. *S. pombe* HE620 was transformed with the vector pJR1-MFα1 containing the *MFα1* ORF under transcriptional control of the thiamine-repressible *nmt1* promoter. Transformed cells were pre-grown in EMM and shifted to EMM supplemented with different amounts of thiamine at time point zero. The α-factor present in the respective culture supernatants was quantified by inverse ELISA measurement employing the optimized hydrophobin layer composition (1.6 % EAS-α). A representative set of data, corresponding to triplicate measurements, is plotted. Error bars indicate standard deviation.

Gradual reduction in the α-factor accumulation in the culture supernatants of *S. pombe* cells carrying pJR1-MFα1 was observed upon increasing concentration of thiamine supplemented to the growth medium (Figure 22). Remarkably, thiamine concentrations as low as 10 nM were sufficient to decrease the α-factor secretion of

the sensor cells, resulting in reduced pheromone accumulation in the culture supernatants. These results were consistent with a thiamine-induced downregulation of the *nmt1* promoter activity. Thiamine itself did not affect the α-factor quantification by inverse ELISA measurements (data not shown). Additionally, thiamine has been reported to slightly stimulate the growth of *S. pombe* cells [456], which was also evident for the engineered *S. pombe* sensor cells (data not shown). Thus, it could be concluded that the thiamine-dependent reduction in α-factor accumulation in the culture supernatants was not caused by a thiamine-dependent reduction in the growth rate of the engineered sensor cells but instead resulted from thiamine-dependent downregulation of the activity of the *nmt1* promoter.

Obvious differences between the α-factor concentrations were evident already after 4 h of incubation in the presence or absence of thiamine (Figure 22), consistent with a previous report demonstrating the complete disappearance of the *nmt1* mRNA after 3 h of incubation in the presence of thiamine [459]. In summary, these data provide evidence that the hydrophobin-based immunoassays can be successfully combined with genetically engineered sensor cells to create a novel whole-cell sensor for the detection of thiamine. With a limit of detection in the range of 10 nM thiamine, this whole-cell sensor had a comparable sensitivity to previously reported whole-cell or protein-based sensors for thiamine [460, 461] and the use of the secreted peptide pheromone to create the sensor read-out might be beneficial compared to commonly employed whole-cell sensor read-out strategies (section 4.5.1).

3.6.2 Quantification of alternative analytes

Finally, the versatility of hydrophobin-based surface engineering for the development of novel immunoassays was evaluated. Using these techniques, it could be envisaged to invent novel immunoassays for a wide variety of analytes, including peptides, proteins or low molecular weight compounds such as herbicides, xenobiotics or explosives. Thus, it was analyzed whether hydrophobin-based immunoassays for the detection of an alternative analyte (different from the α-factor pheromone) could be developed. As a proof-of-concept, the HA epitope was chosen, possibly providing an opportunity to quantify the HA peptide as well as recombinant proteins fused to this epitope. These immunoassays could also serve to overcome

certain drawbacks of commonly employed protein quantification methods for the quantification of recombinant fusion proteins. Several of these methods rely on the reactivity of certain amino acid residues with specific substrates, yielding colorimetric reactions that can be quantified by absorbance measurements. However, these approaches depend on the presence of the reactive amino acids, thereby being highly dependent on the amino acid composition of the recombinant protein to be quantified. In contrast, the hydrophobin-based immunoassays would detect the HA epitope directly, independent on the amino acid composition of the recombinant protein.

3.6.2.1 Cloning, expression and purification of EAS-HA

In order to establish novel immunoassays for the quantification of the HA peptide and recombinant proteins fused to it, a third recombinant hydrophobin was created. The ORF encoding the recombinant EAS-HA hydrophobin was essentially similar to EAS-α, but the 3' sequence encoding yeast α-factor pheromone was replaced by the sequence encoding the HA epitope (Figure 23 a, see Appendix A.4 for DNA and amino acid sequence). Similar to EAS and EAS-α, the EAS-HA hydrophobin was expressed in *E. coli* strain T7 SHuffle® *lysY* (section 2.7.1.1) and purified under denaturing conditions by Ni^{2+} affinity chromatography using the N-terminal $(His)_6$-tag (section 2.7.2). Purity and integrity of the recombinant hydrophobin were evaluated by Tricine SDS-PAGE and immunological detection (Figure 23 b).

Upon electrophoretic separation of the recombinant EAS-HA, a predominant signal in the molecular weight range of 13 kDa was observed by colloidal Coomassie staining, consistent with the calculated molecular weight of the monomeric EAS-HA (12.72 kDa [405], Figure 23 b). However, a faint signal in the range of 11 kDa was reproducibly seen in purified fractions of EAS-HA, most likely representing a degradation product of EAS-HA. As this degradation product was recognized by the $(His)_6$-tag antibody but not by the HA-tag antibody, this protein might have corresponded to a C-terminal degradation product of EAS-HA.

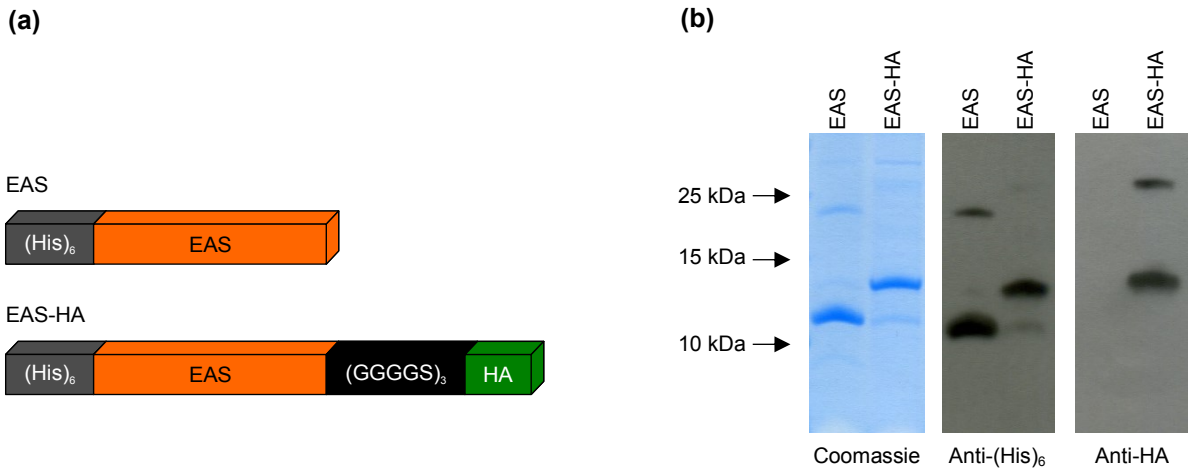

Figure 23. Design and purification of recombinant hydrophobins for the development of novel immunoassays to quantify the HA peptide and recombinant proteins fused to it. (a) Schematic illustration of the recombinant hydrophobins EAS and EAS-HA. Both proteins encompassed a $(His)_6$-tag at the N-terminus and the mature EAS hydrophobin. Additionally, EAS-HA harbored a flexible $(GGGGS)_3$ linker element and the HA epitope at its C-terminus. **(b)** Electrophoretic separation of recombinant hydrophobins. Fractions of the purified hydrophobins, corresponding to 3 µg of each purified protein, were separated by Tricine SDS-PAGE and proteins were visualized by colloidal Coomassie staining or transferred to PVDF membranes and probed with the indicated antibodies.

Similar to EAS and EAS-α, dimers of EAS-HA were observed upon separation in Tricine SDS-PAGE. Importantly, both EAS and EAS-HA were detected by the $(His)_6$-tag antibody whereas EAS-HA could additionally be detected by the HA-tag antibody. These data indicated that the HA-specific antibody was able to recognize its cognate antigen upon fusion to the C-terminus of the EAS hydrophobins, representing a prerequisite to develop the desired immunoassays.

3.6.2.2 Quantification of the HA peptide and recombinant proteins carrying the HA epitope

Next, competitive and inverse immunoassays for the quantification of the HA peptide and of recombinant fusion proteins carrying the HA-tag could be established, essentially following the route taken previously to develop immunoassays for the quantification of the α-factor pheromone. First, the composition of mixed hydrophobin layers consisting of EAS and EAS-HA was simultaneously optimized for high antibody coverage and ideal immunoassay sensitivity employing the HA-tag antibody

(Figure 24 a). To this end, the antibody coverage of mixed EAS/EAS-HA layers (in different molar ratios) was determined to optimize the layer composition. As expected, the antibody coverage was dependent on the EAS-HA content of the monolayer, and the curve was essentially very similar to the data obtained for mixed layers of EAS and EAS-α (compare Figure 9 c with Figure 24 a). For monolayers consisting of up to 1.6 % EAS-HA, a rather steep increase in antibody coverage with increasing the EAS-HA content was observed. In contrast, further increasing the EAS-HA content resulted in relatively constant antibody coverage values. Surprisingly, and in marked contrast to the data obtained for mixed EAS/EAS-α layers, the highest antibody coverage was obtained for monolayers consisting of 8 % EAS-HA, while the antibody coverage slightly declined upon further increasing the EAS-HA content (data not shown). This might indicate that EAS-HA formed less densely packed monolayers if insufficient EAS monomers were present to act as a molecular spacer between the EAS-HA monomers. As the HA-tag contains three aromatic and two negatively charged amino acids, self-assembly of EAS-HA into densely packed hydrophobin monolayers might be sterically impeded unless the mutual interactions between the HA epitopes are shielded by unmodified EAS monomers. Nevertheless, these data indicated that 1.6 % EAS-HA represented the ideal surface composition for highly sensitive detection of the HA peptide as well as of recombinant proteins fused to it. The composition of the optimized EAS/EAS-HA hydrophobin layer was therefore identical to the optimized EAS/EAS-α monolayer (section 3.2.2).

Next, competitive and inverse ELISA assays were established to detect and quantify the synthetic HA peptide, applying the protocols developed for the detection of the α-factor pheromone. A decrease in antibody coverage was observed upon increasing the concentration of the HA peptide applied in the competitive immunoassay (Figure 24 b), in line with competitive detachment of the HA-tag antibody from the hydrophobin-functionalized surface. Utilizing the optimized surface composition (1.6 % EAS-HA), a limit of detection of 0.2 µM HA peptide was observed, essentially identical to the sensitivity of the EAS/EAS-α based competitive ELISA for the α-factor (section 3.2.3). However, the dynamic range for the HA peptide was slightly narrower (0.2 – 20 µM HA peptide vs. 0.2 – 100 µM α-factor), and the shape of the calibration curve in the semi-logarithmic plot was rather sigmoidal compared to the rather linear calibration curve of the α-factor immunoassay in the respective semi-logarithmic plot

(compare Figure 10 and Figure 24 b). Nevertheless, these data unambiguously demonstrated that the competitive ELISA strategy, based on hydrophobin-functionalized surfaces, can be employed to quantify the HA peptide.

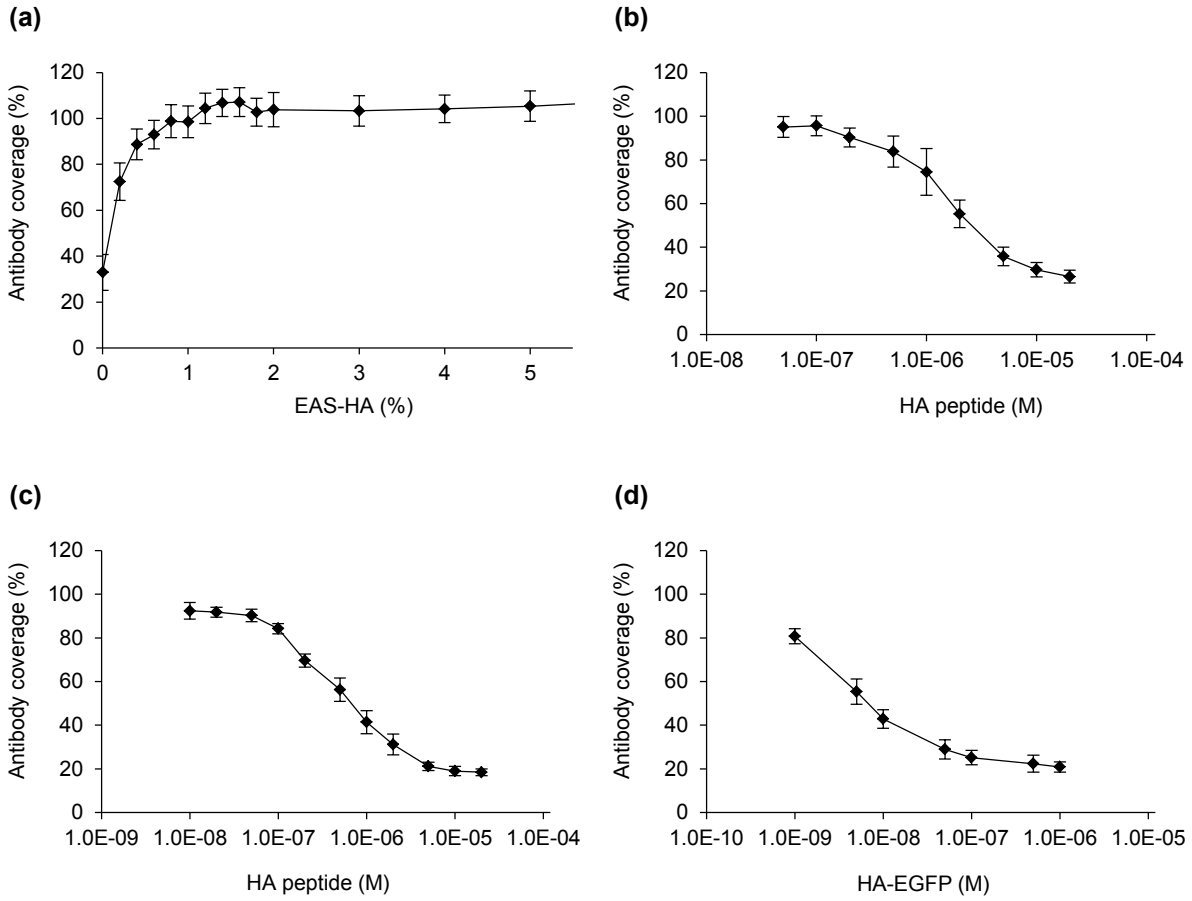

Figure 24. Hydrophobin-based immunoassays for the detection and quantification of the HA peptide and recombinant HA-EGFP. (a) Optimization of the hydrophobin layer composition. Recombinant hydrophobins EAS and EAS-HA were mixed in different molar ratios and utilized to functionalize polystyrene surfaces. The functionalized surfaces were treated with the HA-tag antibody and with a HRP-linked secondary antibody subsequently. Antibody coverage was calculated by normalizing the values to surfaces consisting of 100 % EAS-HA. **(b)** Calibration of the competitive ELISA for the detection of the HA peptide. Functionalized surfaces consisting of 1.6 % EAS-HA were utilized. Antibody coverage was calculated by data normalization to surfaces not treated with the HA peptide. **(c)** Calibration of the inverse ELISA for the quantification of the HA peptide. Functionalized surfaces were comprised of 1.6 % EAS-HA. Data normalization was applied to calculate the antibody coverage. **(d)** Calibration of the inverse ELISA for the quantification of the recombinant fusion protein HA-EGFP. Functionalized surfaces consisting of 1.6 % EAS-HA were employed. Antibody coverage was obtained by normalizing the measured values to samples lacking the recombinant HA-EGFP. All plotted values correspond to triplicate measurement of at least two experiments. Error bars indicate standard deviation.

Likewise, an inverse ELISA was set up to quantify the HA peptide (Figure 24 c). A gradual decrease in antibody coverage with increasing the amount of the HA peptide was observed, consistent with the inverse ELISA approach. When the optimized hydrophobin layer composition (1.6 % EAS-HA) was employed, a lower limit of detection of 50 nM HA peptide and a dynamic range of 0.05 – 20 µM HA peptide were observed. Remarkably, the inverse ELISA for the HA peptide was only about fourfold more sensitive than the competitive ELISA, and both immunoassays covered a comparable dynamic range. This was remarkably different from the competitive and inverse immunoassays for the α-factor, showing clearly different dynamic ranges and sensitivities, with the inverse ELISA being 2000-fold more sensitive than the competitive assay (sections 3.2.3 and 3.3.2). These striking differences may result from differences between the HA-tag antibody and the α-factor antibody regarding their affinity to their cognate antigen or the nature of the antibody (monoclonal HA-tag antibodies vs. polyclonal α-factor antibodies, section 4.2.2). However, it should be noted that the immunoassays for the HA peptide were not optimized regarding the sample matrix composition or physical conditions during the individual reaction steps, thus leaving significant room for optimization. Nevertheless, these data clearly indicate that both competitive and inverse immunoassays for the quantitative assessment of the HA peptide can be developed, suggesting that hydrophobin-based surface engineering represents a versatile technique to implement highly sensitive and specific immunoassays for a variety of target molecules (section 4.5.2).

Additionally, the applicability of the inverse ELISA technique for the quantification of recombinant proteins carrying the HA epitope was investigated. As a proof-of-concept, the recombinant fluorescent protein HA-EGFP, harboring an N-terminal HA-tag, was used (see Appendix A.5 for DNA and amino acid sequence of HA-EGFP). The expression vector pET23b-HA-EGFP, containing the ORF encoding the recombinant HA-EGFP, was transformed into *E. coli* BL21 (DE3) pLysS and expression of the *HA-EGFP* gene was induced by IPTG addition (section 2.7.1.2). The recombinant fusion protein was subsequently purified under native conditions by Ni^{2+} affinity chromatography, taking use of the C-terminal $(His)_6$-tag (section 2.7.2.3, see Appendix B.3 for examination of the purification process of HA-EGFP). Subsequently, a calibration curve of the inverse ELISA for several concentrations of the purified HA-EGFP was obtained (Figure 24 d). Evidently, increasing the amount of HA-EGFP gradually decreased the antibody coverage, indicating that HA-EGFP

could be detected by the inverse immunoassay. Notably, a limit of detection of about 1 nM HA-EGFP was observed when the optimized hydrophobin layer composition (1.6 % EAS-HA) was utilized. Thus, the inverse immunoassay was more sensitive towards HA-EGFP than towards the HA peptide, possibly resulting from beneficial steric effects or non-specific interaction of the HA-tag antibody and HA-EGFP apart from the HA-tag itself.

Nevertheless, these data revealed that hydrophobin-based immunoassays can be applied to determine the concentration of recombinant fusion proteins carrying the HA epitope, highlighting the versatility of the hydrophobin-based surface engineering approach for the development of novel immunoassays. Thus, it is conceivable that the hydrophobin-based surface functionalization technique harbors tremendous potential for utilization in commercial biosensor devices capable of detecting various target molecules (sections 4.5.2 and 4.5.3).

4 Discussion

In this study, a novel surface functionalization approach, based on self-assembling monolayers of recombinant hydrophobins, was employed to develop two types of immunoassays for the detection and quantification of the yeast α-factor pheromone. Both the competitive and the inverse immunoassay enabled quantitative assessment of the α-factor in a wide dynamic range that could be further tuned by adjusting the density of binding sites immobilized on the surface, *i.e.* the EAS-α content of the hydrophobin layer. Due to the superior stability of class I hydrophobin monolayers, the hydrophobin-functionalized surfaces could be reused for multiple measurements with similar sensitivity. Importantly, the hydrophobin-based immunoassays proved to be highly robust against changes in the sample matrix composition, allowing for pheromone quantification even in highly complex sample matrices such as yeast culture supernatants. Therefore, the pheromone secretion of wild-type and engineered *S. cerevisiae* cells could be studied. Additionally, cells of the fission yeast *S. pombe* were engineered to secrete the α-factor pheromone, yielding a synthetic inter-species communication mode, and the hydrophobin-based immunoassays could be employed to quantify the α-factor secretion by engineered *S. pombe* cells. Finally, a novel whole-cell sensor was developed, encompassing engineered *S. pombe* sensor cells secreting the α-factor in response to an environmental cue and the hydrophobin-based immunoassays to generate the whole-cell sensor read-out. Furthermore, the versatility of the hydrophobin-based surface engineering approach was demonstrated by developing novel immunoassays for the HA epitope as an alternative peptide analyte. In this chapter, the outcomes of this study are discussed, and advantages, limitations as well as future perspectives of the hydrophobin-based surface functionalization approach are highlighted.

4.1 Functionalization of hydrophobic surfaces with recombinant hydrophobins

4.1.1 Expression and purification of recombinant hydrophobins

The performance of hydrophobin-based immunoassays is crucially dependent on the surface functionalization with recombinant hydrophobins. Obviously, obtaining the recombinant hydrophobins in high purity and yield was an important prerequisite. Numerous proteins are able to bind strongly to hydrophobic surfaces, in particular due to unfolding and attachment *via* nonpolar residues. For example, it was reported previously that BSA, casein and collagen adsorbed strongly onto hydrophobic surfaces without any evidence of protein desorption even upon extensive rinsing [462]. Therefore, high amounts of contaminating proteins within the purified hydrophobin fractions may affect the density of the hydrophobin-based surface functionalization and the quality of the hydrophobin monolayers. Moreover, it was shown that β-casein interfered with the formation of interfacial layers by the class II hydrophobin HFBII, causing softening and fluidization of the protein layers [463-465]. Likewise, the chitin-binding protein cerato-platanin was reported previously to form hybrid layers with class I hydrophobins that differed from pure hydrophobin layers in several aspects [466]. Thus, it was of crucial importance to obtain the recombinant hydrophobins in high purity, allowing for the functionalization of biosensor surfaces in a reproducible and stable manner.

The recombinant hydrophobins EAS and EAS-α employed in this study were obtained in high purity upon heterologous expression in *E. coli* and Ni^{2+} affinity chromatography (section 3.1.1). Heterologous expression in *E. coli* (*e.g.* [146, 147, 246, 303, 467-475]) as well as purification by Ni^{2+} affinity chromatography (*e.g.* [146, 147, 246, 303, 473, 474, 476]) are commonly employed strategies to obtain purified hydrophobins. Thus, established protocols for heterologous expression and purification exist, allowing for rapid and facile application to novel recombinant hydrophobins. However, the insolubility of hydrophobins is the main disadvantage of heterologous expression in bacterial hosts, necessitating elaborate extraction, solubilization and purification steps. Previous studies revealed that recombinant hydrophobins form inclusion bodies in prokaryotic host cells and hence

were found almost exclusively in the insoluble fraction of cell lysates. However, some noticeable exceptions exist [153, 155, 164, 469, 471]. As expected, the recombinant hydrophobins EAS, EAS-α and EAS-HA were found to form inclusion bodies. Although the combination of heterologous expression in a bacterial host and purification by Ni^{2+} affinity chromatography could successfully be applied to yield highly pure recombinant hydrophobins (section 3.1.1), future studies might utilize alternative approaches for their expression and/or purification, in particular aiming at highly cost-effective and easily scalable methods for commercial applications.

In several studies, recombinant hydrophobins were fused to glutathione S-transferase (GST) and expressed in *E. coli* for subsequent affinity purification utilizing glutathione-functionalized matrices [171, 273, 467, 469, 471]. Due to the large size of the GST domain, some hydrophobin-GST fusion proteins were found in the soluble fraction of *E. coli* lysates, thereby simplifying the purification procedure [469, 471], whereas other hydrophobin-GST fusion proteins formed inclusion bodies [171, 273, 467]. In addition, steric issues may limit the applicability of recombinant hydrophobins carrying large fusion partners for affinity purification. It has been shown that hydrophobins fused to a large globular protein require unmodified hydrophobin monomers as molecular spacer to form hydrophobin layers with the characteristic features [274, 277-279]. For example, the formation of hydrophobin layers including MBP-HFBII – a fusion protein of the class II hydrophobin HFBII and the maltose binding protein (MBP) – was dependent on the presence of the unmodified HFBII since pure MBP-HFBII did not self-assemble into robust monolayers [277, 278]. Thus, fusion of the class I hydrophobin EAS (about 9 kDa) to the large GST tag (about 26 kDa [469, 471]) may have an impact on the formation of stable hydrophobin layers. Furthermore, the $(His)_6$-tag was exposed at the hydrophobin-functionalized surface (section 3.1.2.2), which would similarly be expected for large fusion partners, possibly restricting the accessibility of the immobilized α-factor (or alternative recognition elements) for cognate antibodies.

Thus, alternative strategies might be employed to obtain recombinant hydrophobins in sufficient purity and yield for commercial application. Heterologous gene expression was accomplished in fungal hosts, particularly focusing on *T. reesei* [415, 477] and *Pichia pastoris* (*e.g.* [253, 263, 307, 408, 410, 476-480]). Taking use of the authentic N-terminal signal peptide, the recombinant hydrophobins were

secreted into the extracellular environment, significantly simplifying the downstream purification protocol. Alternatively, heterologous expression in plants [293, 323-328] might be beneficial, given that targeting of the recombinant hydrophobin to the ER resulted in the formation of membrane-enveloped protein bodies that could be isolated easily and rapidly.

In addition, various alternative methods have been applied to purify recombinant hydrophobins, including preparative high-performance liquid chromatography (HPLC) [249, 253, 263, 410, 477, 478], electroelution from preparative electrophoresis [475] and foam separation in large scale fermenters [408]. Furthermore, hydrophobins have been purified by employing their unique surface activity, taking use of their strong interaction with hydrophobic column materials [167] or Teflon microbeads [157]. Another technique, based on aqueous two-phase systems (ATPS), could be utilized to purify hydrophobins in a convenient and cost-effective manner. Due to their unique properties, hydrophobins migrate to the detergent phase of ATPS systems, effectively separating them from contaminating proteins accumulating in the aqueous phase [293, 324, 326, 327, 481, 482]. Importantly, ATPS systems can easily be scaled-up to large volumes [326], making them highly attractive for low-cost mass production of recombinant hydrophobins for biosensor commercialization.

4.1.2 Hydrophobin-based surface functionalization

Hydrophobins can be modified at the N-terminus and the C-terminus [154, 246, 248-251, 263-265, 283, 294, 312, 408, 471, 483, 484] as well as within the flexible loop regions [147] without affecting their self-assembling properties. In fact, even fusion to highly polar sequences like the $(His)_6$-tag [246, 248, 303, 408, 414, 415, 472, 476] or highly charged peptides [265, 317] does not interfere with the self-assembly process of hydrophobins. In line with these studies, water contact angle measurements revealed that neither the N-terminal $(His)_6$-tag nor the C-terminal α-factor affected the self-assembly of the recombinant hydrophobins (section 3.1.2.1).

Upon functionalization with the recombinant hydrophobins, hydrophobic polystyrene supports showed a clear increase in hydrophilicity. Inversion of the wettability of solid substrates upon hydrophobin self-assembly represents a hallmark feature of this unique class of proteins [129-135]. In addition, contact angle measurements

indicated that the C-terminal α-factor exposed by EAS-α did not seem to influence the properties of the hydrophilic face of the hydrophobin. The water contact angles obtained for surfaces functionalized with EAS and EAS-α were essentially similar, suggesting that the packing densities of respective hydrophobin monolayers are comparable. This was further substantiated by analyzing the accessibility of tags fused to the hydrophobins (section 3.1.2.2). Similar antibody coverage values were obtained for surfaces functionalized with EAS or EAS-α when screened with the $(His)_6$-tag antibody, suggesting that the packing density was identical.

The monolayers formed by the recombinant hydrophobins proved to be highly robust, as only a slight increase in the water contact angle was observed upon hot SDS treatment (section 3.1.2.1). This was in line with previous reports for several class I hydrophobins [158, 213, 251, 257, 263, 280, 331, 396, 412-416], highlighting that the recombinant hydrophobins EAS and EAS-α resembled previously reported class I hydrophobins regarding the surface activity and the self-assembly into stable monolayers. Thus, it could be concluded that the recombinant hydrophobins adopted the characteristic hydrophobin fold, even upon heterologous expression in *E. coli* and purification from inclusion bodies. In contrast to class II hydrophobins, dissociating from a solid surface by applying detergents, ethanol or pressure [129-135], class I hydrophobin layers are extremely robust and require treatment with strong acids (100 % TFA or 100 % formic acid) to dissolve. The extremely high stability of the hydrophobin-functionalized surfaces might be of advantage for the development of immunoassays and biosensors since the functionalized surface will remain essentially unchanged even upon extended use (sections 3.2.5 and 4.2.4).

4.1.3 Hydrophobin-based surface engineering for peptide immobilization

Several previous studies exploited of recombinant hydrophobins to immobilize peptides at a functionalized surface [248-251, 263-265]. Likewise, recombinant hydrophobins were employed in this study to anchor the α-factor pheromone at a functionalized surface. Hydrophobin-based peptide immobilization might represent a suitable approach for future applications relying on peptide-based surface functionalization. The immobilization of peptides is often a challenging task due to their low molecular weight. In fact, non-specific adsorption of peptides may not be

feasible as peptides could desorb from the surface over time, possibly affecting extended storage and reusability, or may not be accessible any more upon adsorption [19, 20, 35]. As the immunoassays developed in this study rely on the recognition of the immobilized pheromone by cognate antibodies, appropriate orientation and accessibility of the α-factor at the functionalized surface were mandatory. Therefore, it was of crucial importance to obtain highly ordered protein films that expose the pheromone at the surface in a defined density to ensure accessibility for the antibodies. In contrast to other proteins that adsorb to solid supports in a random orientation [28], the amphipathic nature of hydrophobins causes uniform and predictable attachment to solid surfaces [129-135]. Thus, hydrophobins are well suited candidates for the functionalization of surfaces with protein layers in a defined and controlled manner.

A plethora of approaches for the site-specific immobilization of peptides have been proposed previously, most of them relying on the regio-selective modification of the peptide with a unique functional group subsequently used for immobilization. For example, peptides have been immobilized to solid supports by the use of terminal epoxy groups [485], cysteine residues [486] or fusion to alkanethiols that self-assembled into monolayers [487, 488]. Additional strategies included peptide embedding into silk fibroin layers, native chemical ligation, click chemistry or Staudinger ligation [19, 27-30, 489]. However, most of these methods depend on specific surface chemistries such as the presence of thiol groups [486] and alkynyl or azido groups [490, 491] at the substrate surface to ensure immobilization. Favorably, hydrophobin-based surface functionalization for peptide immobilization does not depend on the surface chemistry since hydrophobins self-assemble into robust monolayers at any hydrophobic surface [129-135]. Consistent with this, the competitive immunoassay for the α-factor could also be carried out on glass substrates modified with hydrophobic silanes or siloxanes (data not shown). Thus, the use of hydrophobins may provide an opportunity for more general application in protein-based surface engineering techniques, allowing for enhanced flexibility regarding the substrate material.

However, it should be noted that the use of recombinant hydrophobins might be laborious and time-consuming in comparison to some of the previously established peptide immobilization methods. In particular, suitable hydrophobin fusion proteins

need to be designed, expressed in a heterologous host and purified prior to surface functionalization. In contrast, solid phase synthesis of peptides and subsequent modification with unique functional groups for surface attachment are achieved rapidly and with high yields [19, 20]. However, both fermentation of host cells producing recombinant hydrophobins [303] and hydrophobin purification [326] could be scaled up to industrial levels. Thus, the use of recombinant hydrophobins for biosensor surface functionalization is certainly reasonable.

4.1.4 Accessibility and biological activity of the immobilized α-factor pheromone

Determination and prediction of the crystal structure of several hydrophobins revealed that both the N-terminus and the C-terminus of hydrophobins are localized at the hydrophilic face of the protein [146, 150-152, 492]. Likewise, previous studies provided strong evidence that the N-terminus [246, 294, 484, 493] as well as the C-terminus [408, 484, 494] point towards the hydrophilic site of hydrophobin monolayers and are thus accessible upon self-assembly at a hydrophobic surface. The results obtained for hydrophobic surfaces functionalized with EAS and EAS-α were consistent with these studies, confirming that both the $(His)_6$-tag and the α-factor were exposed at the functionalized surface and thus accessible for respective antibodies (section 3.1.2.2).

Previous reports highlighted that hydrophobins neither show cytotoxic effects towards mammalian cells [224, 248-253, 282, 290-294] nor serve as a suitable antigen for antibody production in mammals [224, 250, 290, 293]. In line with the biocompatibility of hydrophobin-functionalized surfaces, recombinant hydrophobins did not induce any obvious detrimental effect on yeast cells (section 3.1.2.3). However, polystyrene surfaces functionalized with EAS-α also did not show any evidence of pheromone activity towards pheromone-responsive *S. cerevisiae* reporter cells, pointing at a marked difference between the α-factor receptor and the α-factor antibody regarding their substrate recognition. Notably, these data were in contrast to several previous reports utilizing recombinant hydrophobins fused to specific peptides such as the RGD peptide (integrin receptor binding site) [248, 250, 251, 264], the LG3 peptide (integrin receptor binding site) [248] or the TPS peptide (peptide binding specifically

to human endothelial progenitor cells) [249, 263] for peptide immobilization at a functionalized surface. In these studies, the functionalized surfaces exerted the specific biological functions attributed to the peptides, indicating that the mammalian cells used in the respective studies were able to detect the peptides and to respond to this extracellular cue. In contrast, pheromone-responsive *S. cerevisiae* cells were apparently unable to detect the presence of the α-factor when fused to the EAS hydrophobin. In addition, these data suggested that the pheromone-responsive yeast cells did not secrete a protease capable of cleaving EAS-α to release the intact α-factor from the functionalized surface.

The lack of pheromone activity of solid supports functionalized with EAS-α could not be attributed solely to steric issues. Yeast cells are surrounded by a rigid and compact cell wall, possibly preventing the interaction of the Ste2p pheromone receptor (embedded in the plasma membrane) and the α-factor immobilized at the surface. However, spheroblasts (lacking the cell wall due to enzymatic degradation) similarly did not show any pheromone response when cultivated on substrates functionalized with EAS-α (Appendix B.1), indicating that the lack of pheromone activity did not result from restricted accessibility exclusively.

The N-terminus of the α-factor pheromone seems to be dispensable for binding of the pheromone to the Ste2p receptor, but is of crucial importance to induce the conformational change of the receptor, thereby triggering the initial step of yeast pheromone response [365]. Yeast cells of mating type α lacking the *STE13* gene are unable to perform N-terminal maturation of the α-factor, secreting pheromone molecules with four to six additional N-terminal residues that show at least 100-fold reduced biological activity compared to the mature α-factor [355]. Given the severe influence of four to six additional N-terminal residues, it is very likely that the presence of the EAS hydrophobin at the N-terminus of the α-factor in EAS-α has at least a similar effect on the pheromone activity. However, it is unlikely that a recombinant hydrophobin carrying the α-factor at its N-terminus would elicit the yeast pheromone response since the C-terminally immature α-factor does not show any biological activity [354]. Thus, in contrast to ligands detected by mammalian cells (see above), the α-factor might not be amenable to immobilization by fusion to hydrophobins.

4.2 Establishment of novel immunoassays for quantification of the yeast α-factor pheromone

4.2.1 Adjustment of immunoassay sensitivity by modifying the composition of mixed EAS/EAS-α hydrophobin layers

The stability of the class I hydrophobin layers as well as the accessibility of the immobilized α-factor towards the cognate antibody were prerequisites for the development of hydrophobin-based immunoassays (section 4.1). A competitive immunoassay, relying on the competitive detachment of antibodies from hydrophobin-functionalized surfaces by excess of the soluble pheromone (section 3.2.1), and an inverse immunoassay, based on pre-incubation of the α-factor and its cognate antibody and subsequent application to functionalized surfaces (section 3.3.1), were established and successfully applied for pheromone quantification. Evidently, optimum performance of both immunoassays was obtained when mixed hydrophobin layers encompassing EAS and EAS-α in a defined molar ratio were applied. It has been suggested previously that the density of the recognition elements immobilized at a functionalized surface should be considered to balance the influences of high surface density (maximum signal intensity) and low surface density (maximum assay sensitivity) for the development of bioassays with superior sensitivity [12]. Thus, careful optimization of the density of the EAS-α content was important to gain optimum performance of the novel hydrophobin-based immunoassays (section 3.2.2).

Although investigating a different parameter (enzyme activity instead of antibody coverage), Takatsuji *et al.* recently confirmed the importance of hydrophobin layer optimization [274]. The authors generated mixed hydrophobin layers consisting of the class II hydrophobin HFBI and a derivative fused to glucose oxidase (GOx) to immobilize the enzyme at the functionalized surface. Importantly, the enzymatic activity of protein layers consisting exclusively of GOx-HFBI was clearly lower than the activity obtained for mixed hydrophobin layers, and the highest enzyme activity was achieved for monolayers comprised of 5 – 50 % GOx-HFBI [274].

Mixed hydrophobin layers featuring a hydrophobin fused to a target compound – a protein of interest [274, 277-279, 321] or a gold nanoparticle [314] – and an unmodified hydrophobin as a molecular spacer have been reported previously. In several studies, the fused target compound was significantly larger than the hydrophobin itself, and the formation of protein layers consisting exclusively of the fusion protein was sterically impeded. Thus, the unmodified hydrophobin was indispensable to allow for the formation of stable hydrophobin layers [274, 277, 278]. Owing to the low molecular weight of the α-factor pheromone, the recombinant EAS-α employed in this study was able to form robust monolayers without the need for unmodified EAS (section 3.1.2.1). Thus, the use of peptides as a fusion partner provided a higher flexibility in terms of hydrophobin layer composition, given that EAS and EAS-α were able to co-assemble into stable hydrophobin layers in any molar ratio.

The optimized hydrophobin layers featured a surprisingly low amount of EAS-α (1.6 % molar content) and an excess of unmodified EAS monomers (section 3.2.2). These results might be attributed to the large difference in the size of antibodies [424] and hydrophobins [146]. Kwan *et al.* determined the diameter of the EAS hydrophobin in its soluble form (2.7 nm [146]), but the surface area occupied by a hydrophobin monomer upon self-assembly might be even lower, given that hydrophobins self-assemble into densely packed monolayers [131]. However, it should be noted that the hydrophobin layer composition was optimized for an ELISA-like approach that included a secondary HRP-linked antibody, implying that accessibility of the α-factor antibodies to the respective secondary antibodies was similarly important. It cannot be ruled out that the ideal hydrophobin layer composition for alternative read-out technologies not relying on a secondary antibody (*e.g.* based on labelled α-factor antibodies or on alternative transducers, section 4.5.3) would significantly differ from the ideal surface composition determined in this study. Almost identical data were obtained for mixed layers of EAS-HA and unmodified EAS (section 3.6.2.2), indicating that the packing density of EAS/EAS-α monolayers and EAS/EAS-HA monolayers may not be significantly different.

Employing the optimized surface composition allowed for the detection of 0.2 µM α-factor and 0.1 nM α-factor in the competitive and inverse immunoassay, respectively. Importantly, the dynamic range and sensitivity of both assays could be

tuned precisely by adjusting the amount of EAS-α within the hydrophobin monolayers (sections 3.2.3 and 3.3.2). This could be of particular importance for quantitative determination of high α-factor concentration, close to the upper limits of the dynamic range. In this regime, non-specific binding of antibodies to the functionalized surfaces was not negligible (see below). This limitation could be overcome by increasing the EAS-α content of the hydrophobin layer, thereby shifting the dynamic range of the assay towards higher pheromone concentrations.

Non-specific binding of antibodies to hydrophobin-functionalized surfaces was evident upon assessing the accessibility of tags fused to the recombinant hydrophobins. Remarkably high antibody coverage values were obtained when the α-factor antibody was applied to hydrophobin-functionalized surfaces consisting of EAS exclusively (*i.e.* lacking EAS-α, section 3.1.2.2). Similarly, non-specific binding might also be responsible for the flattening of the calibration curve upon employing the optimized hydrophobin surfaces (1.6 % EAS-α) for the detection of very high pheromone concentrations (50 – 100 µM α-factor) in the competitive ELISA (section 3.2.3). Previous studies highlighted that the adsorption of antibodies [280-282], enzymes [286] and fluorinated polymers [495] on hydrophobin layers was highly pH-dependent and most efficient when the hydrophobin layers and the target compound were oppositely charged. The recruitment of enzymes to hydrophobin layers, based on ionic interactions, is also employed by certain pathogenic fungi to immobilize degrading enzymes such as cutinases at their cellular surface [219, 220]. Monolayers of the recombinant EAS (with a calculated isoelectric point of 6.62 [405]) had a slightly negative net charge in PBS-T (pH 7.4), whereas IgG antibodies typically show an isoelectric point of 7.0 – 10.0 [496] and were hence expected to be positively charged under these conditions. Thus, non-specific attachment of the antibodies to hydrophobin layers might predominantly be mediated by ionic interactions. Future studies might investigate suitable strategies to weaken the non-specific interaction between the antibodies and the hydrophobin layer, possibly by performing the immunoassays in high-salt conditions that have been shown previously to effectively decrease protein adsorption to hydrophobin layers [281].

Future experiments may address the lateral composition of mixed hydrophobin layers with nanometer resolution. Although the formation of stable mixed layers of EAS and EAS-α was evident, their exact molecular composition remained elusive. In particular,

it should be determined if EAS-α was homogeneously integrated into the monolayer or if both hydrophobin variants clustered into distinct domains that assembled on the substrate side-by-side. Clustering was observed previously for class I hydrophobins and class II hydrophobins that were allowed to self-assemble at a common substrate [407], whereas the class II hydrophobin HFBII fused to MBP (MBP-HFBII) was homogeneously integrated into mixed layers with unmodified HFBII [277, 278]. However, the latter studies used fluorescent MBP-specific antibodies to evaluate layer homogeneity. Given that an individual antibody is far larger than a hydrophobin monomer, small clusters of MBP-HFBII would not have been resolved. Topography and recognition imaging (TREC) might represent a suitable technique to overcome these limitations [497]. This method is based on atomic force microscopy (AFM), but features an AFM tip modified with a specific recognition element (*e.g.* an antibody) to allow for mapping of individual molecular recognition events with nanometer resolution. This technique has been applied previously to study the molecular organization of mixed layers of self-assembling bacterial S-layer proteins (encompassing monomers of the S-layer proteins fused to the *Strep*-tagII and unmodified S-layer monomers [498]). Although the S-layer proteins employed in the previous study were far larger than hydrophobin monomers (four monomers of the S-layer protein self-assembled with square-lattice symmetry with a center-to-center spacing of 14 nm [498]), it would be conceivable to apply the TREC approach to study the molecular organization of EAS/EAS-α mixed hydrophobin layers.

4.2.2 Comparison of the competitive and the inverse immunoassay

Both the competitive and the inverse ELISA allowed for the quantification of the yeast α-factor pheromone with unique but partially overlapping dynamic ranges. While the competitive immunoassay covered a dynamic range of 0.2 µM – 100 µM α-factor (section 3.2.3), the inverse ELISA enabled the detection and quantification of 0.1 nM – 1 µM α-factor (section 3.3.2). Additionally, both techniques provided the opportunity to shift the dynamic range towards higher pheromone concentrations by increasing the EAS-α content of the hydrophobin layer employed for the measurements (section 4.2.1). Nevertheless, there was an obvious difference in the sensitivity of both immunoassays that might be attributed to the strong interaction

between antibodies and their cognate antigens, typically showing very low dissociation constants [426-428].

In the competitive ELISA approach, the antibodies were first immobilized at the surface *via* interaction with EAS-α and subsequently detached from the surface due to the presence of excess of the α-factor in solution, implying that the preformed complex of the antibody and EAS-α had to dissociate (section 3.2.1). In contrast, in the inverse ELISA method, available antigen binding sites of the antibodies were first occupied by the dissolved α-factor and the entire mixture of antibodies and soluble pheromones was applied to the hydrophobin-functionalized surfaces subsequently (section 3.3.1). Thus, whereas the competitive ELISA featured the formation and dissociation of antigen-antibody complexes, the inverse ELISA solely relied on their formation. It is conceivable that the difference in the reaction mode was the major reason for the difference in the assay sensitivity.

The differences in the reaction mode between the competitive and inverse ELISA were also reflected by an opposite dependency on competition between the soluble α-factor and immobilized pheromones. Whereas competition was mandatory for the functionality of the competitive immunoassay, it had a detrimental effect on the performance of the inverse ELISA. As competition in the hydrophobin-based immunoassays was dependent on Brownian motion, the efficiency of competition could be controlled by the temperature (section 4.2.3). Performing the competition step at elevated temperatures resulted in an increase in competition efficiency of the competitive ELISA. In contrast, the second reaction step of the inverse ELISA (*i.e.* the immobilization of antibodies with available binding sites) was carried out at 4 °C to limit the influence of competition. Nevertheless, an influence of competition was still obvious in the inverse immunoassay. Without the effect of competition, the sensitivity of the inverse ELISA would not be expected to depend on the density of immobilized pheromone molecules (*i.e.* on the EAS-α content) above a certain threshold, given that the inverse ELISA solely relied on the binding of antibodies that carry available binding sites. However, the slope of the calibration curve decreased considerably if hydrophobin layers with increased EAS-α content were employed (section 3.3.2), indicating that competition was not negligible. This hypothesis was further confirmed by considering the molar ratio of pheromone molecules and antibodies. An equimolar ratio of the α-factor and its cognate antibody would be

achieved at 2.67 nM α-factor, assuming a molecular weight of the antibody of 150 kDa [499]. As IgG antibodies harbor two antigen binding sites, all available antigen binding sites of the antibodies would theoretically be occupied by applying 5.34 nM α-factor and attachment to the hydrophobin-functionalized surfaces would not be possible if higher pheromone concentrations were present. However, the dynamic range of the inverse ELISA strikingly exceeded this value, indicating that competition contributed considerably to the behavior of the inverse ELISA.

It should be noted that the differences in the sensitivity of the competitive and inverse ELISA for the detection of HA peptides were far less pronounced, given that the inverse ELISA was only about fourfold more sensitive for the HA peptide and both immunoassays essentially covered a similar dynamic range (section 3.6.2.2). Hypothetically, the interaction between EAS-HA and the HA-tag antibody might be comparatively weak, showing high dissociation constants that would allow for efficient dissociation of the complex between the antibody and EAS-HA during the competition step. In this scenario, the HA peptide would represent the highly preferred antigen for the HA-tag antibody, resulting in high competition efficiencies. In support of this, the HA-tag antibody used in this study is characterized by a high affinity for the cognate antigenic peptide, showing a dissociation constant of 10^{-8} M [500]. However, further experiments should be carried out to validate this hypothesis. In this regard, it should be mentioned that the immunoassays for the HA peptide were not optimized concerning the sample matrix composition, leaving significant space for optimization of these immunoassays. Nevertheless, both competitive and inverse immunoassays could be conducted to quantify the α-factor as well as the HA peptide, implying that hydrophobin-based immunoassays may be invented to detect various, highly different analytes (section 4.5.2).

4.2.3 Robustness of the hydrophobin-based immunoassays against varying sample matrix conditions

Remarkably, both the competitive and the inverse immunoassay were highly robust against changes in the sample matrix composition (sections 3.2.4 and 3.3.3), allowing for α-factor quantification independent on the pH value, the ionic strength or the detergent concentration of the sample matrix. However, the influence of the

pH value on the signal intensity (*i.e.* the recorded absorbance values) should be examined in further detail. Compared to neutral or alkaline surroundings, the absorbance values were clearly decreased when the immunoassays were carried out in acidic conditions. In contrast, the influence of the pH value was not evident upon data normalization, indicating that both immunoassays were functional in acidic environments, albeit with lower signal intensity. Although partial denaturation of the antibodies in acidic conditions cannot be ruled out, it is tempting to speculate that the pH-dependent reduction in the affinity between the antibodies and the hydrophobin layer was caused by the $(His)_6$-tag exposed at the hydrophobin-functionalized surface.

Upon functionalization of hydrophobic supports with EAS and EAS-α, the N-terminal $(His)_6$-tag was accessible for cognate antibodies (section 3.1.2.2), in line with the $(His)_6$-tag exposed at the functionalized surface. As histidine residues possess a pK_a value of about 6.0, the imidazole side chains are essentially uncharged in neutral or alkaline conditions but become positively charged if the pH drops below 6.0. Thus, in acidic environments, the hydrophobin layer was expected to expose positive charges at the surface in high density. Although obvious effects on the stability or packing density of the hydrophobin layer were not observed, the charge cluster at the surface might reduce the affinity of the antibodies to the hydrophobin layers. As mentioned above, the adsorption of proteins on hydrophobin layers is most efficient when both are oppositely charged [280-282, 286]. However, due to their high isoelectric point, IgG antibodies are also positively charged in acidic surroundings [496], resulting in electrostatic repulsive forces between the hydrophobin layer and the antibodies. It is plausible that the reduced absorbance values determined in acidic conditions reflected these electrostatic repulsive forces. Utilizing recombinant hydrophobins lacking the $(His)_6$-tag, either by exploiting alternative fusion partners for protein purification (section 4.1.1) or by enzymatic cleavage of the recombinant hydrophobins to remove the $(His)_6$-tag, would provide suitable opportunities to unambiguously clarify the influence of the $(His)_6$-tag.

Analyzing the impact of the temperature during the competition step and the viscosity of the sample matrix revealed that the sensitivity of the competitive ELISA was mostly limited by Brownian motion, whereas the interactive forces between the antibody and EAS-α were of minor importance in this regard (section 3.2.4). In this study, the

competitive ELISA was performed under static conditions in 96-well microplates, implying that diffusion of the soluble α-factor to the functionalized surface and of detached antibodies into the bulk solution were solely driven by Brownian motion. A simple mathematical consideration revealed Brownian motion as a limiting parameter: Assuming a diameter of each hydrophobin monomer of 2.7 nm (diameter of EAS in solution [146]), a hydrophobin layer consisting of 25 × 25 monomers would cover an area of 67.5 nm × 67.5 nm including ten EAS-α monomers for the optimized surface composition (1.6 % EAS-α). As mentioned above, hydrophobins are tightly packed upon self-assembly [131], and the covered surface area might actually be even lower. Upon addition of 10 µM α-factor, 1.85 individual α-factor molecules would statistically be present in a cube of the respective dimensions (67.5 nm edge length). Thus, the majority of antibody binding sites would be immobilized at the surface (ten EAS-α monomers vs. 1.85 soluble pheromone molecules). However, the antibody coverage in the competitive ELISA measurements was reduced to 48.7 ± 2.6 % using this pheromone concentration, implicating that more than half of the antibodies were detached by the pheromone treatment. Thus, in a static system, the diffusion of the pheromone to the functionalized surface, triggering competitive antibody detachment, could not be neglected.

Therefore, increasing the diffusivity could be a promising approach to significantly enhance the sensitivity of the competitive ELISA. Increasing the efficiency of Brownian motion in a static system is limited (section 3.2.4), as further raising the temperature caused antibody denaturation and decreasing the viscosity of an aqueous solution is not straightforward. In addition, increasing the duration of the competition step was not desirable as it would result in an elevated time demand of the assay. Furthermore, doubling the time frame of the competition step did not alter the sensitivity of the competitive ELISA (data not shown). Transferring the competitive immunoassay approach to a fluidic system with a constant fluid stream might be an option to considerably improve the assay performance. Embedding the competitive immunoassay technology into microfluidic systems would be of particular interest, given the inherent advantages of microfluidic systems such as narrow sample volumes and the opportunity to implement miniaturized systems [7, 12]. In a constant fluid stream, active transport of the α-factor to the functionalized surface and removal of detached antibodies from the system may significantly reduce the assay time and enhance the sensitivity. Thus, it would be of high interest to develop

microfluidic devices encompassing hydrophobin-based competitive immunoassays, in particular for the establishment of miniaturized devices.

4.2.4 Reusability of hydrophobin-functionalized surfaces

The possibility to reuse the functionalized surfaces for multiple measurements with comparable sensitivity represented one of the main advantages of the hydrophobin-based immunoassays (section 3.2.5). Reusability of functionalized surfaces is highly desirable for the development of commercial biosensors with reasonable cost-efficiency [6, 18, 32]. In particular, if the biological functionalization of the biosensor surface cannot be produced at very low cost, single-use devices are economically not of interest, raising a tremendous demand for surface reusability [18]. Consequently, reuse of functionalized surfaces has been demonstrated in several studies aiming for sustainable and cost-effective biosensors [429, 487, 488]. However, regeneration of functionalized surfaces, in particular for immunoassays employing antibodies or antibody fragments, is a highly challenging task. As antigen-antibody complexes have very low dissociation constants [426-428] and antibodies are comparatively stable, appropriate regeneration protocols typically involve harsh conditions to denature the antibodies, possibly affecting the stability and activity of the functionalized surface [18, 32].

The use of class I hydrophobins for surface functionalization may represent a striking advantage in this regard since these proteins self-assemble into highly robust monolayers [129-135]. However, a recent study by Soikkeli *et al.* suggested that the use of class II hydrophobins for biosensor surface functionalization may also be advantageous for certain applications [265]. The authors argued that the hydrophobin layer could be removed easily after one measurement and the transducer surface could be re-functionalized with hydrophobins prior to a second measurement. This approach would offer the possibility to select the surface functionalization of a single transducer element immediately before the measurement is carried out. However, the stability of the biosensor against adverse sample matrix effects was not evaluated in this study [265]. It is conceivable that certain compounds, especially those present in complex sample matrices such as yeast culture supernatants, soil extracts or blood serum, might affect the class II hydrophobin layers in undesired ways, thereby

influencing the biosensor read-out. Thus, the utilization of class I hydrophobins like EAS and its derivatives may be more suitable for the development of robust biosensor devices.

Upon selective denaturation of the antibodies, EAS/EAS-α functionalized surfaces could be used for repeated competitive ELISA measurements without significantly affecting the sensitivity of the assay (section 3.2.5), indicating that class I hydrophobin layers were able to withstand the antibody denaturation procedure. However, close examination revealed that a slight increase in background signal was evident with an increasing number of stripping cycles (section 3.2.5), possibly caused by non-specific adsorption of denatured antibodies on hydrophobin layers that may still be recognized by secondary antibodies. An increase in background signal, resulting from irreversible adsorption of denatured antibodies, has similarly been observed in previous studies employing peptide-functionalized surfaces [487,488].

A loss in signal height of about 30 – 40 % was evident after the first stripping cycle (Appendix B.2). Water contact angle measurements (section 3.1.2.1) suggested that this effect might be attributed to partial extraction of the hydrophobins by hot SDS treatment, a phenomenon previously observed for numerous class I hydrophobins [158, 213, 251, 257, 263, 280, 331, 396, 412-416]. In these studies, quantitative analysis revealed that varying amounts of the hydrophobins were extracted, depending on the respective hydrophobin, the surface functionalization method, the substrate and the exact parameters of the hot SDS treatment. Consequently, the values reported in several studies differ dramatically, ranging from 7 – 85 % [158, 251, 331, 416] of the hydrophobin monomers detaching from the surface upon hot SDS treatment. The data obtained in this study suggested that 30 – 40 % of the recombinant hydrophobins were extracted during the first stripping cycle. Since water contact angle measurements revealed that the resistance of EAS and EAS-α towards hot SDS treatment was essentially similar (section 3.1.2.1), it could be assumed that both hydrophobins were extracted with similar efficiency. Remarkably, no further reduction in signal intensity was evident after subsequent stripping cycles (Appendix B.2), indicating that significant hydrophobin extraction did not occur during further stripping events. Taken together, these data unambiguously revealed that the hydrophobin-functionalized surfaces were sufficiently robust to allow for repeated use for competitive immunoassays with comparable sensitivity. In fact, hydrophobin-

functionalized surfaces could also be used for repeated inverse ELISA measurements and even performing competitive and inverse immunoassays alternately was feasible (data not shown), highlighting the flexibility of the functionalized surfaces for application in both immunoassays.

4.2.5 Comparison with previously established pheromone quantification methods

With a limit of detection of 0.1 nM α-factor, the inverse ELISA represented the most sensitive bioassay for the quantification of the α-factor pheromone currently available. Numerous approaches have been reported to quantitatively assess the presence of the pheromone, most of them focusing on the biological activity of the α-factor towards pheromone-responsive reporter cells. The limits of detection as well as the dynamic ranges of several methods for pheromone quantification are plotted in Figure 25. However, some of the previously developed assays were omitted if they were highly laborious, time-consuming and/or semi-quantitative and are thus not suitable for application in biosensor devices.

4.2.5.1 Quantification of the yeast pheromone based on its biological activity

Several studies analyzed the pheromone response of wild-type or engineered reporter cells depending on the pheromone concentration, yielding dose-response curves that enabled quantification of the pheromone. Most of these studies took use of pheromone-induced promoter elements to trigger the expression of a reporter gene, resulting in the intracellular accumulation of a reporter protein that could easily be quantified. This approach was also utilized in this study to semi-quantitatively analyze the α-factor activity of surfaces functionalized with EAS-α (section 3.1.2.3) and to study the α-factor secretion of engineered *S. pombe* cells (sections 3.5.2 and 4.4.3). Fluorescent proteins were most commonly employed [96, 366, 384, 420, 421, 431, 439, 501-506], but the use of luciferases [97] or β-galactosidases [507, 508] has also been reported. To mediate pheromone-responsive expression, the reporter genes were placed downstream of pheromone-induced promoter elements derived

from yeast genes such as *FUS1* [96, 97, 366, 384, 421, 431, 439, 503, 507, 508], *FIG1* [96, 97, 501, 504] or *PRM1* [420, 502, 505, 506].

In these studies, expression of the reporter gene was assessed by optical sensor devices, determining mean values for the entire cell population or analyzing individual cells (*e.g. via* flow cytometry or microscopy and image analysis [420, 431, 502, 505]). The limit of detection obtained in these assays differed according to the genotype of the pheromone-responsive reporter cells and the employed read-out technology (Figure 25). Pheromone response of wild-type cells was detected for α-factor concentrations of at least 0.1 – 0.5 µM α-factor [366, 384, 431, 439, 501, 503], while pheromone-hypersensitive reporter strains responded to pheromone concentrations as low as 5 – 10 nM α-factor [96, 97, 366, 384, 431, 439, 501, 503, 507] (Figure 25). Pheromone-hypersensitive reporter cells were obtained by numerous different approaches, *e.g.* by deletion of *SST2* [96, 97, 439, 501, 503, 507]. In *S. cerevisiae*, Sst2p is responsible for accelerating the GTP hydrolysis rate of the Gα subunit as an important step during pheromone signal adaptation and recovery from cell cycle arrest [509]. Other studies [366, 384, 431] employed the pheromone-hypersensitivity of *Δbar1* strains lacking the extracellular protease responsible for α-factor degradation [370]. Additionally, cells carrying the *gpa1-Ser302* allele [508] or encoding C-terminally truncated forms of the Ste2p α-factor receptor [510, 511] proved to be pheromone-hypersensitive.

The limits of detection reported for pheromone-hypersensitive reporter cells (5 – 10 nM α-factor, Figure 25) were strikingly consistent with the dissociation constant of the Ste2p pheromone receptor and the α-factor (2 – 13 nM [510-513]). However, the sensitivity of pheromone-response assays could be increased by an engineered positive feedback loop [501]. In this design, the initially weak pheromone response in the presence of low α-factor concentrations was amplified by placing the *STE4* gene (encoding the Gβ subunit) under the transcriptional control of the *FIG1* promoter. Pheromone-induced overexpression of *STE4* resulted in an excess of free Gβγ dimers, substantially reinforcing the signal. By this approach, the limit of detection could be reduced to 0.5 nM α-factor in *Δsst2* strains [501] (Figure 25).

An alternative approach to increase the sensitivity for the α-factor pheromone was realized by microscope-based cytometry [420, 502, 505]. This technique is based on a fluorescence microscope equipped with a high-quality CCD-camera and highly

sophisticated, customized image analysis to allow for the quantification of a single fluorescent molecule per image pixel [502]. By employing this technique, concentrations as low as 0.3 nM α-factor could be detected based on the pheromone response of *Δbar1* strains carrying reporter gene constructs relying on the *PRM1* promoter (Figure 25).

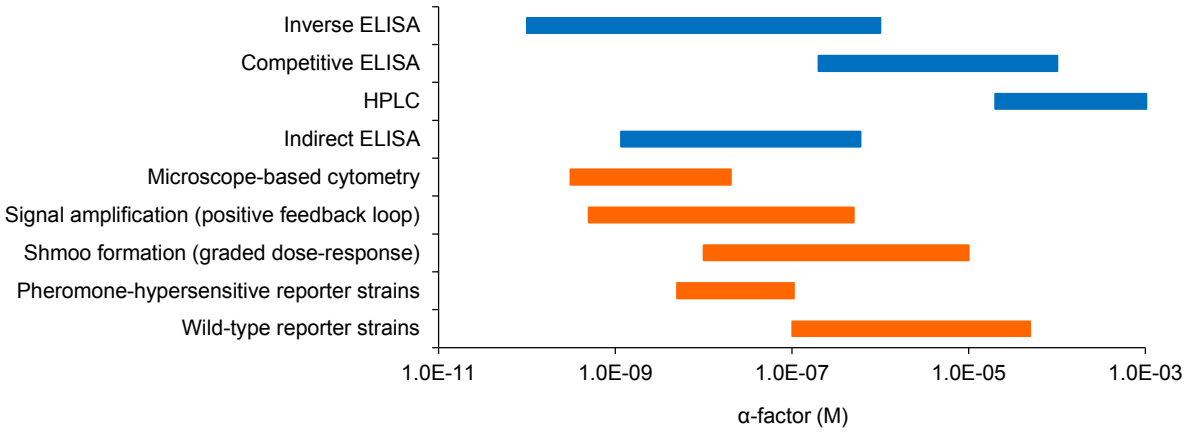

Figure 25. Limits of detection and dynamic ranges of different methods for α-factor quantification. The dynamic range of the indicated methods is plotted according to the results obtained in this study for the competitive ELISA (section 3.2.3), the inverse ELISA (section 3.3.2) and HPLC (Appendix B.4) or according to the values reported in the respective studies (see text for further information). Methods based on the biological activity of the pheromone are highlighted in orange, direct pheromone quantification methods are marked in blue.

Further approaches for the quantification of the yeast pheromone were based on the quantitative analysis of mating projection formation. In contrast to the pheromone-dependent reporter gene approaches, which show a graded dose-response curve, the formation of mating projections represents an all-or-nothing response [514], showing a very narrow dynamic range for pheromone quantification. By employing a modified version of the Ste5p scaffold protein (encoded by the $STE5^{ND}$ allele) that does not allow for the interaction between the Ste5p scaffold and the MAPK Fus3p, Malleshaiah *et al.* transformed the all-or-nothing response into a graded dose-response curve, enabling the quantification of the α-factor in a wide dynamic range (10 nM – 10 µM α-factor, Figure 25) [514]. However, quantitative assessment of

shmoo formation requires high-resolution microscopy and sophisticated image analysis and may therefore not be suitable for the use in biosensor devices.

Further approaches to quantify the yeast pheromone by evaluating the response of pheromone-reporter cells included the detection of pheromone-induced cell agglutination [510, 515, 516], assessment of Fus3p phosphorylation status by quantitative immunoblotting [517] or analysis of the pheromone-induced cell cycle arrest based on the halo assay, *i.e.* the formation of a growth inhibition zone around a pheromone source applied on an agar plate on which pheromone-responsive cells have been streaked [365, 510, 511, 518]. However, these assays are far too laborious and time-consuming for application in biosensors and do not allow for high-throughput screening. Additionally, halo assays are particularly dependent on the environmental conditions, including temperature, incubation time, depth and composition of the medium and the number of cells streaked onto the plates [433], thus necessitating highly reproducible conditions.

In addition to being less sensitive and more time-consuming than the immunoassays developed in this study, cell-based assays often suffer from a comparatively narrow dynamic range (Figure 25). Moreover, large cell-to-cell variations are typically observed, especially in the presence of very low pheromone concentrations [420, 421]. On the other hand, very high pheromone concentrations (≥ 60 µM α-factor for wild-type cells) were reported to cause programmed cell death in a subpopulation of pheromone-responding cells [519-521], thus posing the upper limit of pheromone concentrations that can be quantified.

4.2.5.2 Direct quantification of the α-factor pheromone

The α-factor pheromone could also be detected and quantified by highly sophisticated analytical chemistry methods. For example, HPLC [522] and mass spectrometry [434, 436] have been applied previously to detect the α-factor and its degradation products. Both techniques offer the possibility to detect the pheromone in very low sample volumes and to distinguish between the mature α-factor and related peptides, including proteolytic products and immature derivatives, whereas cell-based assays and the hydrophobin-based immunoassays do not allow to unambiguously identify all pheromone-related peptides. HPLC analysis was also

carried out in this study (Appendix B.4) to accurately quantify the α-factor based on its UV absorbance (due to the presence of aromatic amino acids) and its fluorescent properties (based on the intrinsic fluorescence of tryptophan residues). However, a limit of detection of about 20 µM α-factor was determined, about 100-fold and 200,000-fold higher than for the competitive and inverse ELISA technique, respectively (Appendix B.4, Figure 25). Mass spectrometry analysis was reported to be semi-quantitative, rendering precise pheromone quantification difficult [434]. In addition, as HPLC analysis and mass spectrometry require highly expensive instruments and are not amenable to miniaturization, their use is restricted to analytical laboratories and they cannot be integrated into field-deployable devices.

Numerous studies employed radioactively labeled α-factor, in combination with immunoprecipitation, HPLC or thin layer chromatography [350-352, 368, 440, 523]. Although radioactive labelling provides an opportunity to eminently increase the sensitivity, the use of radioactive labels is highly prohibitive for field-deployable, hand-held biosensor devices, owing to safety and waste disposal issues. Recently, an indirect ELISA method for the quantification of the α-factor pheromone was proposed [433] (Figure 25). In this approach, the α-factor was non-specifically adsorbed to polystyrene surfaces and the amount of adsorbed pheromone was subsequently quantified by the use of the α-factor antibody and a cognate secondary antibody. However, this assay required the use of specifically modified polystyrene microplates to achieve pheromone adsorption, and repeated use of these surfaces was not reported. Non-specific pheromone adsorption to the polystyrene plates required overnight incubation, rendering this assay more time-consuming than the hydrophobin-based immunoassays. Most importantly, the inverse ELISA technique was superior to the indirect ELISA [433] regarding the limit of detection (0.1 nM α-factor in the inverse ELISA vs. 1.2 nM α-factor in the indirect ELISA) and the dynamic range (0.1 – 1,000 nM α-factor in the inverse ELISA vs. 1.2 – 600 nM α-factor in the indirect ELISA, Figure 25). The indirect ELISA might also suffer from the lack of control regarding the orientation of the adsorbed pheromone. Due to non-specific pheromone adsorption, the α-factor may desorb over time and/or the epitope may be buried upon adsorption, thereby preventing pheromone recognition by the α-factor antibody.

In summary, the competitive and inverse immunoassays developed in this study were suitable to overcome a number of limitations of previously established pheromone quantification assays. Combining the competitive and the inverse ELISA approaches allowed for covering a wide dynamic range of α-factor concentrations (six orders of magnitude, Figure 25) that cannot be covered by any alternative method proposed so far. Both assays offered the unique possibility to tune the dynamic range and the sensitivity and enabled repeated use of the functionalized surfaces. Additionally, the immunoassays developed in this study might be amenable to miniaturization and compatible with numerous sophisticated transducer technologies (section 4.5.3) to yield portable devices for pheromone quantification. Thus, hydrophobin-based immunoassays might be valuable tools to detect and to quantify the yeast pheromone in basic research studies as well as in applied science, focusing *e.g.* on the development of novel whole-cell sensor read-out technologies (sections 3.6.1 and 4.5.1). As hydrophobin-based immunoassays were not restricted to the α-factor (section 3.6.2.2), they may be adapted to various analytes of choice, thereby providing broad applicability of the hydrophobin-based surface engineering technology for biosensor development.

4.3. Evaluation of the pheromone secretion of wild-type and engineered *S. cerevisiae* strains

4.3.1 Pheromone secretion of wild-type *S. cerevisiae* cells

As the inverse ELISA enabled highly sensitive quantification of the α-factor pheromone largely independent on the sample matrix composition, this technique was ideally suited to quantify the α-factor in the culture supernatants of wild-type and engineered *S. cerevisiae* cells. First, the inverse ELISA was first applied to study the pheromone secretion of wild-type *S. cerevisiae* cells of both mating types.

As expected, no α-factor pheromone could be detected in the culture supernatants of **a**-type yeast cells (section 3.4.2). As both α-factor pheromone precursor genes

(*MFα1* and *MFα2*) are α-specific genes, their expression requires the presence of the α1 transcriptional activator encoded by the *MATα* allele [338, 340-343]. Thus, neither *MFα1* nor *MFα2* are expressed in **a**-type cells carrying the *MAT**a*** allele at the mating locus. Consequently, **a**-type cells do not secrete the α-factor, consistent with the data obtained by inverse ELISA measurements. Hence, these measurements revealed that the inverse ELISA was highly selective for the α-factor pheromone even in rather complex sample matrices such as yeast culture supernatants.

In contrast, α-type cells accumulated about 30 – 50 nM α-factor in the culture supernatants (section 3.4.2), comparable to previously reported values calculated on the basis of simulations [431]. Consistent with α-factor secretion at a constant rate [431-433], pheromone concentrations in the culture supernatants paralleled the growth behavior of the α-type cells within the first 8 – 10 h. Upon entry into the stationary phase, the pheromone concentration declined, indicating that the α-factor was degraded by the α-type cells. It was reported previously that the α-factor activity in the supernatants of α-type cells does not correlate with the cell density of the culture upon entry into the stationary growth phase. Ciejek and Thorner noted that α-factor degradation by α-type cells was not evident within 4 h of growth at 25 °C, but a remarkably low pheromone activity was found in the supernatants of stationary phase cultures [368]. Likewise, Tanaka and Kita stated that the α-factor activity in the supernatants of α-type cells was highest during the late log or early stationary growth phase and declined thereafter [435]. These results are highly consistent with the data obtained in this study, confirming the growth-phase dependent α-factor degradation by α-type yeast cells. However, pheromone hydrolysis in acidic yeast culture supernatants might also contribute to the decline in α-factor concentration and activity.

A previous study highlighted that the decrease in pheromone activity upon entry into the stationary growth phase was accompanied by the appearance of pheromone-derived peptides resulting from cleavage between the sixth and the seventh residue (*i.e.* at the Leu6-Lys7 peptide bond [435]). Mass spectrometry analysis of culture supernatants of α-type cells revealed the presence of numerous α-factor related peptides in addition to the mature pheromone, including oxidation products (oxidation of Met12), C-terminally truncated species (lacking Tyr13) and two major degradation products corresponding to cleavage at the Leu6-Lys7 bond [434, 436]. Notably, the

amount of degradation products increased at later stages of growth whereas the concentration of intact α-factor declined during stationary growth phase [436]. The outcomes of these studies are in line with the results obtained by the inverse ELISA technique, highlighting the applicability of the hydrophobin-based immunoassays to study α-factor secretion and degradation. Future experiments might be conducted to study the mechanism and the biological significance of α-factor degradation by α-type cells in more detail, *e.g.* by adding protease inhibitors. It was reported that pepstatin, an inhibitor for aspartic proteases, significantly reduced the abundance of degradation products upon addition to growing yeast cultures, although the protease(s) targeted by this treatment were not identified [436]. In this regard, the inverse ELISA technique might provide a suitable approach to screen yeast mutant libraries for strains showing an altered α-factor degradation profile, serving to identify the enzyme(s) involved in this process.

Interestingly, the most prominent α-factor cleavage products observed in the supernatants of α-type cells corresponded to Leu6-Lys7 cleavage [434-436], essentially similar to the degradation products found upon cleavage of the α-factor by Bar1p protease [365]. However, the decrease in pheromone concentrations in the culture supernatants of α-type cells could not be ascribed to the expression of the **a**-specific *BAR1* gene [370, 372, 418, 518]. In support of this, neither intact Bar1p nor corresponding proteolytic fragments were found in supernatants of α-type cells by mass spectrometry [434]. Thus, enzymes other than Bar1p were responsible for pheromone degradation, although the protease(s) catalyzing this reaction are currently not known. Similarly, it is not clear if growth-dependent α-factor degradation resulted from the action of secreted protease(s) or from protease(s) released into the extracellular environment by cell lysis. It has been reported that degradation of the α-factor inside of the vacuole, resulting from endocytosis of the receptor-pheromone complex during adaptation to the pheromone signal, is a very rapid and efficient process [523]. Hypothetically, cell lysis might trigger α-factor degradation due to release of proteases that are naturally confined to the vacuole, although it is unclear if vacuolar proteases maintain any activity when released to the extracellular space.

4.3.2 Enhanced pheromone secretion upon overexpression of *MFα1* in α-type cells of *S. cerevisiae*

The inverse ELISA technique was further applied to study the pheromone secretion of engineered *S. cerevisiae* cells, in particular focusing on α-type cells engineered to secrete high amounts of the α-factor pheromone. To this end, the authentic *MFα1* ORF, responsible for 90 % of the α-factor secreted by α-type cells [433, 434], was placed under transcriptional control of the strong constitutive *GPD* promoter on a multi-copy yeast expression vector (p426GPD-MFα1). Respective transformants were expected to secrete high amounts of the α-factor. Assessment of the pheromone secretion by *MFα1*-overexpressing cells could serve to identify bottlenecks of pheromone synthesis, maturation and secretion. Upon utilization of *MFα1*-overexpressing cells, Julius *et al.* noted that N-terminal α-factor maturation by the Ste13p protease represents a rate-limiting activity in pheromone maturation [355]. Identification of bottlenecks in the pheromone synthesis might also provide an opportunity to increase the efficiency of α-factor secretion. This could be an important point to engineer sensor cells utilizing the secreted pheromone to generate the biosensor read-out signal (section 4.5.1).

Cell-free supernatants of α-type cells carrying the vector p426GPD-MFα1 contained very high amounts of the secreted pheromone. About 1 – 2 µM α-factor accumulated in the respective culture supernatants within 10 – 12 h (section 3.4.2). Further incubation resulted in decreasing pheromone concentrations, reflecting α-factor degradation as observed with wild-type cells of mating type α (section 4.3.1). Thus, transforming α-type cells with p426GPD-MFα1 resulted in a striking increase of α-factor secretion, indicating that pheromone maturation and secretion are very efficient processes. Apparently, engineering of *S. cerevisiae* sensor cells to create an α-factor-based whole-cell sensor read-out should be feasible. Previous studies reported that transformation of α-type cells with multi-copy plasmids carrying the *MFα1* gene (including its authentic promoter) resulted in a 25- to 30-fold increase in α-factor secretion [351, 352, 355], while transformation with the *MFα1* ORF under control of the strong *GPD* promoter caused roughly a 40-fold increase in pheromone secretion in this study (section 3.4.2). These data suggested that the activity of the authentic *MFα1* promoter might be comparatively high, which might also be anticipated considering the very high α-factor secretion rates (550 – 865 molecules

per cell and second [431-433]) and the low stability of the *MFα1* mRNA (half-time of 5 min [524]). However, differences in plasmid copy number might also be considered.

Upon transformation of α-type cells with p426GPD-MFα1, remarkable heterogeneity in the pheromone concentrations of the respective supernatants was observed, probably resulting from differences in plasmid copy number or plasmid loss. In line with these observations, recent reports on plasmid-based expression systems described marked cell-to-cell variations in the expression level [73, 437-439]. Moreover, α-type cells carrying the *MFα1* gene on a multi-copy plasmid tend to lose or integrate this plasmid rapidly (unpublished observation in [351]), possibly contributing to the observed heterogeneity.

4.3.3 The influence of pheromone maturation on the measurability by the hydrophobin-based immunoassays

Next, the specificity of the α-factor antibody was addressed. In particular, the impact of N- and C-terminal α-factor maturation on the measurability of the α-factor by the hydrophobin-based immunoassays was studied. This might be of interest for the development of novel whole-cell sensors relying on engineered sensor cells from yeast species other than *S. cerevisiae* that may be unable to carry out complete α-factor maturation and secrete an immature pheromone (sections 4.4.5 and 4.5.1). Thus, it was of interest to evaluate to what extent N- and C-terminal α-factor maturation is necessary to enable detection by hydrophobin-based immunoassays.

Therefore, the pheromone secretion of α-type strains of *S. cerevisiae* harboring a deletion of either the *KEX1* gene or the *STE13* gene was assessed by the inverse ELISA technique (section 3.4.3). The peptidases Kex1p and Ste13p are involved in α-factor maturation in yeast (Figures 1 and 26). In the Golgi network, the Mfα1p precursor is first cleaved by the Kex2p protease at two consecutive basic amino acids (lysine-arginine moiety [352]). Consequently, α-type cells lacking *KEX2* do not carry out proteolytic precursor processing and secrete the intact Mfα1p precursor in a highly glycosylated form [352] (Figure 26). However, given that the *KEX2* gene is highly conserved throughout the opisthokonts [344, 525], it is unlikely that *MFα1* expression in a heterologous (fungal) host would result in secretion of the full-length precursor protein. Therefore, the impact of the *kex2* deletion was not addressed in

this study, but respective deletion strains might be included in future experiments. Upon initial cleavage by Kex2p, the α-factor is processed simultaneously at its N-terminus (by Ste13p [355]) and at its C-terminus (by Kex1p [354]). Hence, the impact of respective deletion strains on the α-factor secretion was studied in more detail.

4.3.3.1 The influence of N-terminal pheromone processing

Notably, α-type cells lacking the *STE13* gene secreted about 10 – 20 nM α-factor within 10 – 12 h compared to 30 – 50 nM α-factor secreted by isogenic wild-type cells in the same time frame (section 3.4.3). Although a reduced affinity of the α-factor antibody towards the N-terminally immature α-factor cannot be completely ruled out, these differences most likely resulted from the different growth rates of both strains (data not shown). As wild-type cells and *Δste13* cells secrete the pheromone in similar amounts and with similar kinetics [355, 440], differences in α-factor concentrations could not be attributed to a reduced pheromone secretion of individual cells. Since the α-factor is secreted at a constant rate per cell [431-433], lower pheromone concentrations may have resulted from the reduced growth rate, given that fewer cells were present to secrete the pheromone.

Two lines of evidence further support the hypothesis that the affinity of the antibody towards the N-terminally immature pheromone was not severely reduced compared to the mature α-factor. First, the α-factor antibody was found to have a similar affinity towards the mature α-factor and the N-terminally immature pheromones secreted by *Δste13* strains [355]. Although certain differences between the polyclonal antibodies used in this study and the polyclonal antibodies employed by Julius *et al.* [355] cannot be excluded, it is unlikely that both antibodies recognized completely different epitopes of the α-factor. Since the α-factor encompasses only 13 amino acids, it may not have two distinct antigenic regions. In support of this hypothesis, prediction of putative epitopes based on different algorithms revealed that only one stretch of amino acids (LQLKPG) may have sufficient antigenic potential [526]. Provided that both antibodies showed comparable antigen specificities, both the N-terminally immature α-factor and the mature pheromone would be detected with comparable efficiency also by the antibody employed in this study. Second, previous experiments

based on SDS-PAGE and immunodetection (section 3.1.1) and based on immunoassays (section 3.1.2.2) demonstrated that the α-factor antibody showed a high affinity towards EAS-α. In contrast to the N-terminally immature α-factor secreted by *Δste13* strains, carrying four to six additional amino acids at its N-terminus, the α-factor present in EAS-α harbored 121 additional N-terminal amino acids including the EAS hydrophobin domain. Nevertheless, the α-factor antibody was able to specifically bind to EAS-α, indicating that binding of the α-factor antibody to its target did not depend on a mature N-terminus of the α-factor (Figure 26).

4.3.3.2 The influence of C-terminal pheromone processing

The pheromone secretion of α-type cells carrying a deletion of *KEX1* was significantly reduced in comparison to wild-type cells, as only about 5 nM α-factor accumulated within 10 – 12 h of growth (section 3.4.3). Although the *Δkex1* strain also proliferated at a slightly reduced rate compared to isogenic wild-type cells (data not shown), the severe differences in pheromone concentrations could not be attributed solely to growth rate differences. This was particularly evident as the *Δkex1* strain grew faster than the *Δste13* strain but accumulated less α-factor in the same time frame (section 3.4.3 and data not shown). These data therefore suggested that C-terminal maturation of the α-factor was essential for the interaction of the peptide pheromone with its cognate antibody, representing a prerequisite to ensure measurability by the hydrophobin-based immunoassays (Figure 26).

Due to the structure of the Mfα1p precursor, a lack of C-terminal pheromone processing leads to the secretion of two different types of α-factor molecules. Three of the four pheromone repeats are embedded within the Mfα1p precursor, while the fourth pheromone repeat is located at the C-terminal end of the precursor and does not carry additional C-terminal amino acids (Figures 1 and 26). In a *Δkex1* strain, the three internal pheromone copies will thus carry a lysine-arginine moiety at their C-terminal end upon secretion, while the fourth α-factor unit will have a mature C-terminus. It is tempting to speculate that the signal measured by the inverse ELISA resulted almost exclusively from the fourth α-factor repeat of the Mfα1p precursor and that the C-terminally immature pheromone copies barely contributed to the signal obtained by the inverse immunoassay (Figure 26).

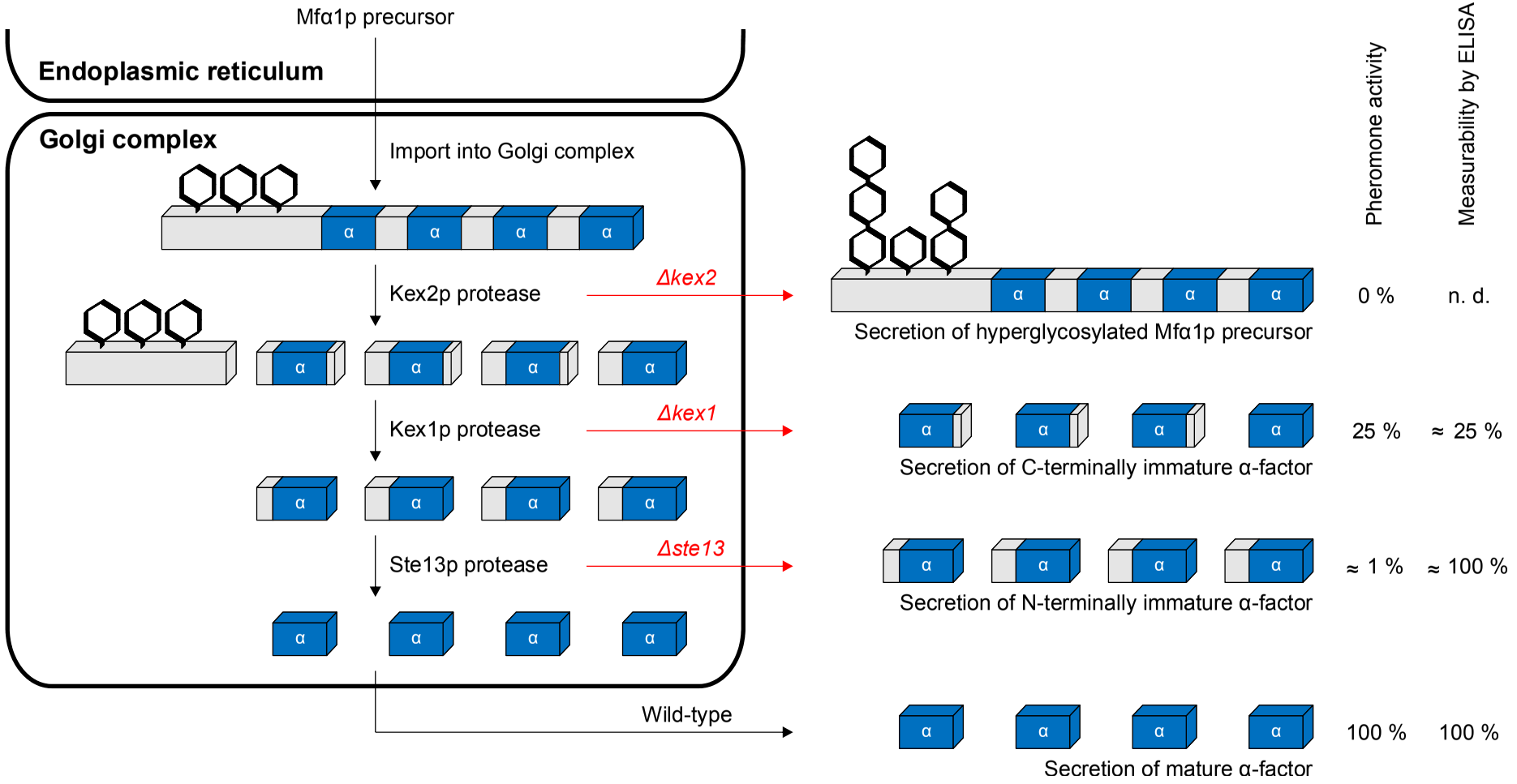

Figure 26. Pheromone precursor processing in wild-type and protease-deficient yeast strains and impact on the activity and measurability of the secreted peptides. The Mfα1p precursor is processed within the secretory pathway, encompassing glycosylation and proteolysis by Kex2p, Kex1p and Ste13p. Respective protease-deficient strains secrete incompletely processed pheromones. Detailed information on the secreted peptides as well as their biological activity and measurability by hydrophobin-based immunoassays are given in the text. Pheromone secretion by *Δkex2* strains was not determined (n. d.).

Genetic evidence further supported the hypothesis that C-terminal pheromone processing was mandatory for the interaction of the α-factor with its cognate antibody. The *MFα1-KR* gene, representing a modified allele of *MFα1* encoding an additional C-terminal lysine-arginine moiety, was integrated into the yeast expression vector p426GPD, yielding p426GPD-MFα1-KR (data not shown). Expression of *MFα1-KR* in *Δkex1* strains was expected to result in the secretion of four identical, C-terminally immature α-factor copies. By inverse ELISA measurements, it could be determined that α-type *Δkex1* strains overexpressing *MFα1* (upon transformation with p426GPD-MFα1) accumulated about 190 – 360 nM α-factor, whereas the same strain carrying p426GPD-MFα1-KR accumulated only about 7 – 9 nM α-factor in the same time frame (data not shown), essentially similar to *Δkex1* cells not carrying a plasmid (section 3.4.3). Thus, the residual pheromone accumulation in the *Δkex1* strain carrying p426GPD-MFα1-KR probably resulted from the expression of the chromosomal copies of *MFα1* and *MFα2*. Apparently, the presence of the C-terminal lysine-arginine moiety in C-terminally immature α-factor molecules was highly detrimental for the quantification by the inverse ELISA (Figure 26).

Additional support for this hypothesis was gained by the use of a fourth hydrophobin variant termed EAS-α-KR. This recombinant hydrophobin construct was based on EAS-α but carried an additional lysine-arginine moiety at its C-terminus (see Appendix A.6 for DNA and nucleic acid sequence and Appendix B.5 for schematic illustration). Thus, the pheromone present in EAS-α-KR resembled the C-terminally immature α-factor secreted by *Δkex1* strains. As determined by Western blot analysis, the affinity of the α-factor antibody towards EAS-α-KR was dramatically reduced compared to its affinity for EAS-α (Appendix B.5). These data provided additional evidence for the importance of C-terminal maturation for the interaction with the α-factor antibody, which is crucial to enable pheromone quantification by the hydrophobin-based immunoassays.

In summary, pheromone quantification of α-type *S. cerevisiae* strains deleted for *KEX1* or *STE13* provided sufficient data to establish a model regarding the importance of α-factor maturation for the interaction with the respective antibody (Figure 26). N-terminal pheromone maturation, carried out by Ste13p in *S. cerevisiae*, was highly important for pheromone activity, as N-terminally immature α-factor molecules are at least 100-fold reduced in pheromone activity [355]. However,

N-terminal maturation was dispensable for interaction with the α-factor antibody and therefore for the measurability by hydrophobin-based immunoassays. In contrast, C-terminal pheromone maturation was of crucial importance for pheromone activity as well as for measurability by competitive and inverse ELISA. The C-terminally immature α-factor derivative showed essentially no biological activity [354] and a severely reduced affinity to the α-factor antibody, being highly prohibitive for pheromone quantification by the immunoassays developed in this study. In the supernatants of *Δkex1* strains, both pheromone activity and the α-factor detected by hydrophobin-based immunoassays could therefore be exclusively attributed to the fourth pheromone repeat of Mfα1p. These data pointed at a lack of correlation of the pheromone activity of α-factor related peptides and their measurability by the hydrophobin-based immunoassays, highlighting significant differences between the pheromone receptor and the pheromone-specific antibody regarding their ligand/antigen specificity (Figure 26).

4.4 Yeast pheromone-based inter-species communication systems

4.4.1 Applications of artificial cell-cell communication systems for controlled inter-species communication between *S. pombe* and *S. cerevisiae*

Implementation of artificial cell-cell communication in synthetic biology applications is of growing interest, in particular as the functionalities engineered in synthetic biology circuits become increasingly complex [373-377]. The integration of multiple synthetic biology tools into a single cell is limited by the associated high metabolic burden, the intrinsic cellular gene expression noise and the increasing risk of circuit cross-talk. Distributing individual tasks to multiple subpopulations, each engineered to perform a specific function, and wiring these subpopulations in a sophisticated manner thus represents an emerging branch that could serve to overcome these limitations. However, tight control over the consortium behavior is mandatory for optimized performance. Artificial cell-cell communication might be a suitable approach to implement the essential control elements, regulating the sequence of reactions

performed by individual members of the consortium in an appropriate manner [373-377]. This may pave the way for synthetic biology applications in various disciplines, including biological computation, biomedicine and tissue engineering, the formation of synthetic patterns and ecosystems, bioprocess engineering as well as the development of biosensors and sensor-actor systems [375].

To expand the palette of available synthetic biology communication tools, an artificial inter-species communication mode between *S. cerevisiae* and *S. pombe*, based on the secretion of the *S. cerevisiae* α-factor pheromone by engineered *S. pombe* cells, was developed in this study. This is of interest not only for synthetic biology applications, but also for the establishment of whole-cell sensors and cell-based sensor-actor systems. Controlled cell-cell communication offers an outstanding opportunity for signal amplification in whole-cell biosensors and for establishing sensor-actor systems [385, 386]. Sensor-actor systems are comprised of a comparatively small population of engineered sensor cells (responding to an environmental cue by secreting the α-factor pheromone) and a large population of actor cells, responding to the secreted pheromone to create the biosensor read-out, significantly amplified in comparison to the use of whole-cell sensors featuring a single population of sensor cells [385].

Exemplarily, future applications of sensor-actor systems could also focus on combined biosensing and bioremediation featuring the detection and degradation of hazardous compounds such as herbicides, EDCs or xenobiotics. In this design, the sensor cells would be engineered to respond to the presence of the target compound by secreting the α-factor pheromone, and respective actor cells would respond with the expression of actor genes (*e.g.* encoding hydrolyzing enzymes) for target compound degradation [385]. In a previous study, Schofield *et al.* engineered two populations of *S. cerevisiae* cells for the detection and biodegradation of the organophosphate paraoxon [103]. A first population was engineered to detect paraoxon, whereas the second population expressed an organophosphate-degrading enzyme. The authors noted that implementation of paraoxon detection and degradation within a single yeast cell was not feasible, owing to the low genetic stability of three episomal plasmids in a single cell [103]. Therefore, distributing both tasks between two specifically engineered populations and wiring both populations

by the α-factor pheromone might represent an attractive approach to overcome this limitation.

The intrinsic abilities to detect or degrade certain analytes vary considerably between different species. Therefore, the use of multiple different species for the development of whole-cell sensors and sensor-actor systems could be highly advantageous, taking use of the inherent sensing and biodegrading capabilities of individual species. This could be of particular relevance when evolutionarily distant organisms are applied, differing greatly in life style, metabolic capabilities and signaling cascades. Recently, Wolf *et al.* utilized engineered *S. cerevisiae* and *S. pombe* sensor cells to detect EDCs with androgenic and anti-androgenic activities, observing marked differences in the sensitivity of both species to certain EDCs [92]. As the last common ancestor of the yeasts *S. cerevisiae* and *S. pombe* existed more than 1,000 million years ago [527, 528], combining the properties of both organisms significantly broadened the range of analytes and concentrations that could be detected, significantly exceeding the capabilities of a single whole-cell sensor system [92].

In this study, one-way communication between *S. pombe* and *S. cerevisiae* was implemented, based on the secretion of the α-factor pheromone by engineered *S. pombe* cells, whereas an alternative inter-species communication mode between both yeast species, focusing on the secretion of the P-factor pheromone by engineered *S. cerevisiae* cells, was reported previously [442]. By combining the artificial cell-cell communication modes between *S. cerevisiae* and *S. pombe* with the sensor-actor system approach, it could be envisaged to establish sensor-actor systems for a wide range of applications. These systems would benefit from a significantly enlarged range of metabolic capabilities in comparison to sensor-actor systems relying on a single species [92]. Additionally, engineered *S. pombe* cells capable of secreting the α-factor pheromone could be interfaced with the hydrophobin-based immunoassays, yielding a novel whole-cell biosensor read-out (sections 3.6.1 and 4.5.1).

4.4.2 Heterologous expression of α-factor pheromone precursor genes in *S. pombe*

In this study, an artificial cell-cell communication mode between *S. pombe* and *S. cerevisiae* was established, based on the synthesis and secretion of the *S. cerevisiae* α-factor pheromone by engineered *S. pombe* cells. Artificial cell-cell communication between fungal species, relying on the heterologous expression of fungal pheromones or pheromone receptors, has been implemented in several reports to study fungal mating [432, 441-444, 447, 529, 530]. Synthesis and secretion of the α-factor by *S. pombe* was achieved upon expression of both the authentic *S. cerevisiae MFα1* ORF and a chimeric *map2/MFα1* ORF (based on the *S. pombe map2* gene encoding the P-factor pheromone precursor, modified to encode two α-factor units, Figure 18 a). The presence of both the Mfα1p and the Map2/Mfα1p precursor upon heterologous expression of the respective genes in *S. pombe* could be detected immunologically (section 3.5.1). Both precursors appeared to be glycosylated upon expression in *S. pombe*, reflecting a key feature of precursor processing in *S. cerevisiae* and *S. pombe* [350, 446]. Although these data unambiguously proved that the pheromone precursor genes could successfully be expressed in *S. pombe*, it should be noted that the immunological detection of the respective precursors does not exclude inefficient precursor processing and pheromone secretion. In *S. cerevisiae*, the Mfα1p precursor cannot be detected immunologically due to the rapid passage through the secretory pathway [349, 350]. Therefore, immunological detection of the precursors may point to inefficient precursor processing and trafficking, possibly caused by overexpression due to the strong *nmt1* promoter and the expression system based on multi-copy plasmids. However, a detrimental effect of the C-terminal HA epitope cannot be ruled out.

4.4.3 Secretion of active α-factor pheromone by engineered *S. pombe* cells

Subsequent experiments, employing pheromone-responsive reporter cells of *S. cerevisiae*, revealed that the expression of both the authentic *MFα1* gene and the chimeric *map2/MFα1* gene in *S. pombe* resulted in the secretion of active α-factor pheromone, albeit at very different levels (section 3.5.2). Three key features of the yeast pheromone response, *i.e.* cell cycle arrest in G1 phase, the formation of mating

projections and the activation of pheromone-responsive promoter elements, were assessed to semi-quantitatively analyze the pheromone response of *S. cerevisiae* cells transferred to cell-free culture supernatants of the engineered *S. pombe* cells. Wild-type *S. pombe* cells did not secrete the α-factor or functionally related peptides and were consequently not able to elicit a pheromone response of *S. cerevisiae* reporter cells. Due to the large evolutionary distance between both organisms [527, 528], the peptide mating pheromones are chemically unrelated, *i.e.* the α-factor and the P-factor differ greatly in their amino acid sequence [348, 398]. In contrast, biological activity of the α-factor pheromone was present in the cell-free culture supernatants of *S. pombe* cells expressing *MFα1* or the chimeric *map2/MFα1*.

Heterologous expression of the authentic *S. cerevisiae MFα1* in *S. pombe* resulted in comparatively low α-factor activity in the cell-free supernatants. Pheromone-responsive *S. cerevisiae* reporter cells underwent a transient cell cycle arrest in G1 phase, exhibited an elongated cellular morphology (without forming the characteristic shmoo projections) and showed intermediate activity of the pheromone-induced *FIG1* promoter (section 3.5.2). Expression of the chimeric *map2/MFα1* gene in engineered *S. pombe* cells resulted in far higher α-factor activities in the culture supernatants, as shown by the sustained cell cycle arrest, the formation of mating projections and the high expression level of the *tRFP* gene under transcriptional control of the *FIG1* promoter in the *S. cerevisiae* reporter cells. Haploid *S. cerevisiae* cells modulate the pheromone response according to the sensed pheromone concentration. Low to intermediate α-factor concentrations lead to a transient arrest in the cell cycle and elongated growth, whereas high pheromone concentrations cause a substantial cell cycle arrest and the formation of mating projections [421, 531, 532]. These studies are in line with the hypothesis that the α-factor activity in the culture supernatants of *MFα1*-expressing cells was lower than in those of *map2/MFα1*-expressing cells. This hints at inefficient, inappropriate or incomplete processing of the Mfα1p precursor upon expression in a heterologous host (section 4.4.5), in agreement with the inefficient pheromone processing and/or secretion upon expression of authentic pheromone precursor genes of *C. cinerea*, *Sordaria macrospora* and *S. commune* in engineered *S. cerevisiae* strains [432, 444].

4.4.4 Quantitative assessment of α-factor pheromone secretion by engineered *S. pombe* cells

Application of the inverse ELISA approach allowed for the quantification of the α-factor pheromone in the culture supernatants of engineered *S. pombe* cells (section 3.5.3). As expected, wild-type *S. pombe* cells did not secrete any measurable α-factor, confirming the lack of α-factor activity in the respective cell-free supernatants and further highlighting the selectivity of the inverse ELISA technique. Surprisingly, the α-factor concentrations in the culture supernatants of *S. pombe* cells expressing the authentic *MFα1* gene were clearly higher than the pheromone concentrations obtained upon expression of the chimeric *map2/MFα1* gene in *S. pombe* (section 3.5.3). These differences may reflect the copy number of α-factor units encoded by the respective pheromone precursor genes (four units in Mfα1p vs. two units in Map2/Mfα1p, Figure 18 a), indicating that the expression levels of both genes as well as the efficiency of precursor processing and trafficking through the secretory pathway might be comparable. However, these data were in marked contrast to the observed α-factor activity (sections 3.5.2 and 4.4.3). Considering the knowledge on P-factor processing in *S. pombe* and the model established in section 4.3.3 (highlighting the importance of α-factor maturation for its measurability by the hydrophobin-based immunoassays), the discrepancy between pheromone concentration and activity upon expression of *MFα1* in *S. pombe* could be attributed to incomplete or inappropriate α-factor maturation.

4.4.5 A model for Mfα1p pheromone precursor processing in *S. pombe*

Proteolytic processing of the Mfα1p precursor in its authentic host requires the activity of three different proteases: Kex2p, Kex1p and Ste13p (Figures 1 and 26). The P-factor precursor of *S. pombe*, encoded by *map2*, is structurally similar to the Mfα1p precursor, encompassing an N-terminal signal peptide for ER import, N-linked glycosylation sites and four repeats of the mature pheromone separated by short spacer peptides [348, 398] (Figure 18 a). However, Map2p and Mfα1p differ considerably at the amino acid level. Importantly, the spacer peptides containing the recognition sites for the proteases carrying out pheromone maturation also differ in the amino acid sequence, consisting of the amino acid stretches KREA(E/D)AEA and

KKREFEAAP(A/E)K in *S. cerevisiae* Mfα1p and *S. pombe* Map2p, respectively [348, 398].

One of the initial steps of Mfα1p processing is carried out by Kex2p, cleaving the spacer peptides at a position C-terminal of the KR moieties [352] (Figure 27). Likewise, the first step of Map2p processing in *S. pombe* involves cleavage of the spacer peptides at the KKR moiety by Krp1p, a protease highly homologous to *S. cerevisiae* Kex2p [446]. Given the homology between Krp1p and Kex2p and the striking similarity of their cleavage sites, it is reasonable to assume that the initial step of Mfα1p processing was carried out by Krp1p upon heterologous expression in *S. pombe*. It has been reported that *S. cerevisiae* cells lacking the functional *KEX2* gene secrete a highly glycosylated form of the intact Mfα1p precursor that does not show any pheromone activity [352, 355, 533] (Figure 26). Thus, Kex2p-like cleavage of Mfα1p is mandatory to obtain α-factor activity in the cell-free supernatants. As heterologous expression of *MFα1* in *S. pombe* resulted in the secretion of active α-factor pheromones (sections 3.5.2 and 4.4.3), Kex2p-like cleavage was evidently carried out, most likely by *S. pombe* Krp1p (Figure 27).

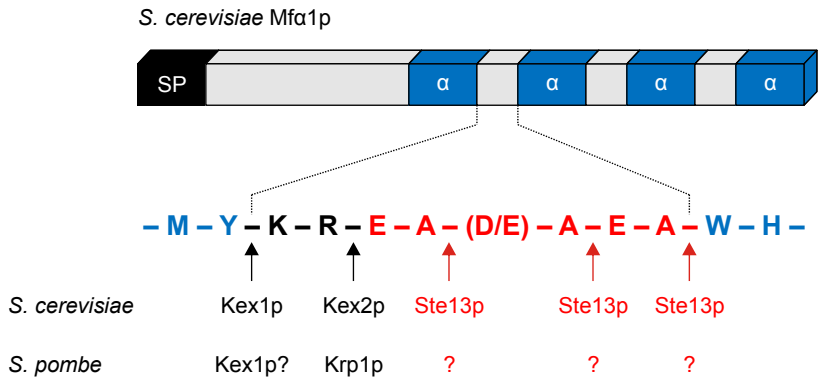

Figure 27. Processing of the Mfα1p precursor in *S. cerevisiae* and proposed model for proteolytic processing in *S. pombe*. In its authentic host, the Mfα1p precursor is proteolytically processed by Kex2p, Kex1p and Ste13p. After initial cleavage by Kex2p, the proteases Kex1p and Ste13p are responsible for C-terminal and N-terminal α-factor maturation, respectively. Upon heterologous expression of *MFα1* in *S. pombe*, Kex2p-like cleavage may be carried out by Krp1p, whereas *S. pombe* Kex1p might perform C-terminal pheromone maturation. Since *S. pombe* does not encode homologues of *S. cerevisiae* Ste13p, N-terminal pheromone maturation is unlikely to be carried out. Further details can be found in the text.

C-terminal α-factor maturation in *S. cerevisiae* requires the activity of the Kex1p protease, removing the C-terminal lysine-arginine moiety [354]. A related protease might be responsible for C-terminal maturation of the P-factor, given that the C-terminal extension of this pheromone upon Krp1p cleavage also consists exclusively of basic residues. Consistent with this assumption, the *S. cerevisiae KEX1* gene is conserved in all ascomycetes [525]. Although the fission yeast *KEX1* homologue (encoded by the *kex1* gene in *S. pombe*) has not been characterized so far, it is predicted to encode a serine protease [534] similar to *S. cerevisiae KEX1*. Thus, *S. pombe* Kex1p may carry out C-terminal P-factor maturation and might also perform C-terminal α-factor maturation upon heterologous expression of *MFα1* in *S. pombe* (Figure 27).

Additional experiments provided direct evidence that C-terminal α-factor maturation was carried out upon *MFα1* expression in *S. pombe*. Heterologous expression of *MFα1-KR* (a modified allele of *MFα1* encoding an additional C-terminal lysine-arginine moiety) in *S. pombe* resulted in a detectable α-factor activity in the respective culture supernatants (data not shown). Given that C-terminal pheromone maturation is mandatory for α-factor activity [354], these data indicated that C-terminal α-factor processing by a protease with Kex1p-like substrate specificity was realized. However, C-terminal pheromone maturation may be performed only in a fraction of the α-factor pheromone molecules.

N-terminal maturation of the α-factor in *S. cerevisiae* is catalyzed by the Ste13p protease that cleaves off dipeptide moieties [355] (Figure 27). Evidently, the *S. pombe* P-factor pheromone also undergoes N-terminal maturation prior to secretion, although the respective enzyme(s) still have to be identified. However, the substrate specificities of the peptidase(s) performing N-terminal processing of the α-factor and the P-factor might differ considerably [344]. Ste13p cleaves off N-terminal dipeptide repeats of an acidic amino acid (glutamic acid or aspartic acid) followed by an alanine residue, sequentially removing the EA(D/E)AEA stretch [355] (Figure 27). In contrast, the substrate specificity of the protease(s) involved in N-terminal P-factor maturation, removing the EFEAAP(A/E)K moiety, is less obvious. In fact, Imai and Yamamoto speculated that the lysine residue at the C-terminal end of the spacer peptide might be involved in spacer peptide cleavage [398]. Thus, N-terminal pheromone maturation might be entirely different in *S. cerevisiae* and

S. pombe. In line with this hypothesis, the *S. cerevisiae STE13* gene is only conserved within the *Saccharomycetaceae* family [525] and homologues of this gene are not encoded in the genome of *S. pombe* [535]. Therefore, it is tempting to speculate that N-terminal α-factor maturation was not carried out upon heterologous expression of *MFα1* in *S. pombe* (Figure 27). Importantly, this hypothesis is sufficient to explain the discrepancy between pheromone concentration and activity that was observed.

According to the model (section 4.3.3), N-terminal maturation of the α-factor was dispensable for its measurability by the hydrophobin-based immunoassays (Figure 26). In contrast, the N-terminally immature form is severely impaired in biological activity, being at least two orders of magnitude less active than the mature peptide [355]. Thus, the high pheromone concentrations observed in the supernatants of *MFα1*-expressing *S. pombe* cells (900 – 1500 nM α-factor after 24 h) might have resulted in a low but detectable pheromone activity in the absence of N-terminal processing. In marked contrast to the Mfα1p precursor, the chimeric Map2/Mfα1p precursor contained the authentic spacer peptides of the Map2p precursor and was therefore expected to undergo complete and efficient maturation by the proteases naturally involved in pheromone maturation in *S. pombe*. Thus, secretion of the mature α-factor was expected upon expression of the chimeric gene in *S. pombe*. Consequently, even comparatively low pheromone concentrations (as determined by the inverse ELISA) would have resulted in a significantly higher pheromone activity in the culture supernatants of *map2/MFα1*-expressing *S. pombe* cells, fully consistent with the experimental results.

Although the lack of N-terminal α-factor processing is sufficient to explain the results obtained by inverse ELISA measurements and pheromone activity determination, an alternative hypothesis should be considered. In particular, it cannot be excluded that the heterologous expression of *MFα1* in *S. pombe* resulted in the secretion of truncated derivatives of the α-factor pheromone. A C-terminally truncated species of the α-factor lacking Tyr13 shows a 40-fold reduction in biological activity, whereas an N-terminally truncated peptide lacking Trp1 has a tenfold reduced pheromone activity [522]. In contrast, α-factor related peptides lacking two amino acids at the N-terminus (Trp1 and His2) are acting as pheromone antagonists that still bind to the receptor but block signaling [522, 536]. The C-terminally truncated species lacking Met12 and

Tyr13 behaves as synergists for signaling, enhancing the signal of the mature pheromone, although neither being active on its own nor binding to the pheromone receptor [522, 536]. Therefore, the lack of correlation between α-factor concentration and pheromone activity in *MFα1*-expressing *S. pombe* strains could also result from inappropriate Mfα1p precursor processing or proteolytic digestion of the pheromone.

The exact nature of the α-factor-related peptide(s) present in the supernatants of *MFα1*-expressing cells could not be determined by the immunoassays developed in this study. Future experiments, including analytical techniques such as HPLC or mass spectrometry, may be conducted to clarify this issue. Additionally, further evidence for either of these hypotheses might be gained by genetic and/or biochemical methods. Notably, *S. pombe* cells co-expressing *MFα1* and *KEX1* or *STE13* did not show an increase in α-factor activity in comparison to *S. pombe* cells exclusively expressing *MFα1* (data not shown). Although this might support the hypothesis that inappropriate α-factor processing or proteolytic degradation occurred upon expression of *MFα1* in *S. pombe*, these data could also result from a lack of enzymatic activity of the heterologously expressed Kex1p and Ste13p.

It was demonstrated previously that *in vitro* treatment of immature α-factor molecules with respective proteases resulted in a significant increase in their pheromone activity. In particular, the reduced pheromone activity associated with the *Δste13* phenotype could be overcome by *in vitro* treatment of the N-terminally immature pheromone with V8 protease [355], whereas C-terminal pheromone maturation could be achieved by *in vitro* carboxypeptidase B treatment [354]. Thus, *in vitro* treatment of the α-factor-related peptides secreted by *MFα1*-expressing *S. pombe* cells with these enzymes might help to unravel Mfα1p processing in the heterologous host.

The abundance of the proteases naturally involved in pheromone processing in *S. pombe* could be an additional point of concern. Sexual differentiation in *S. pombe* is triggered by nutrient limitation, in particular by nitrogen starvation [537]. Consequently, mating-related genes such as *map2* (encoding the P-factor precursor) are not expressed during vegetative growth and their expression is induced upon nitrogen starvation [538]. In light of this, it is not clear if the proteases involved in pheromone maturation are expressed during vegetative growth. Consequently, processing of both Mfα1p and Map2/Mfα1p might be limited by the low abundance of suitable proteases. At least for Krp1p, the only protease involved in P-factor

maturation that has been characterized so far, expression during vegetative growth could be anticipated, given that a deletion of the *krp1* gene is lethal [446]. Thus, it would be interesting to see if *S. pombe* cells engineered to express *MFα1* or *map2/MFα1* showed higher pheromone concentrations or activities in their respective culture supernatants when starved for nitrogen.

4.5 Applications of hydrophobin-based immunoassays

4.5.1 Development of a novel whole-cell biosensor utilizing the α-factor pheromone to create the read-out signal

Employing the hydrophobin-based immunoassays developed in this study allowed for the implementation of a novel read-out possibility for whole-cell biosensors, in particular by combining engineered sensor cells (responding to an environmental cue by modulating the secretion of the α-factor) with the hydrophobin-based pheromone quantification assays (Figure 3). Changes in the pheromone secretion of the engineered sensor cells could be recorded by the use of hydrophobin-based immunoassays, thereby generating the whole-cell sensor read-out signal. Currently employed read-out strategies for whole-cell biosensors almost exclusively rely on fluorescent proteins or luciferases (section 1.1.3.3), thereby being dependent on optical transducer elements. In these systems, the use of sensor cells in high cell densities is unfavorable, as light scattering at the cellular envelop and compartments will deteriorate the biosensor performance. Unless low cell densities can be maintained to limit light absorption and scattering, parallel turbidity measurements are required to correct the whole-cell sensor signal [75, 116, 125].

The use of enzymes to create the whole-cell biosensor read-out has several inherent advantages, including the eminent signal amplification by enzymatic reactions. Furthermore, multiple transducer elements can be utilized if suitable substrates are available to generate colorimetric, fluorimetric, luminescent or electrochemical responses [3, 54]. However, the intracellular accumulation of enzymes often requires cell permeabilization or cell lysis, *e.g.* in the case of β-galactosidases in yeast cells

[75, 76, 79, 80, 91, 101, 115, 123, 124]. These limitations can be overcome by the use of secreted enzymes as reporter proteins as exemplified with phytase and tannase that have been used in *A. adeninivorans* [110-113]. However, enzyme-based sensors depend on the addition of complex, often expensive substrate molecules to create the read-out signal, thereby increasing the costs of a single measurement and preventing real-time monitoring of the whole-cell sensor response.

Hydrophobin-based immunoassays, in combination with sensor cells engineered to modulate pheromone synthesis, have the potential to overcome several limitations of whole-cell biosensors based on fluorescent proteins, luciferases or enzymes. First, employing the α-factor pheromone, which is naturally secreted with high efficiencies [431-433], neither disruption or permeabilization of the sensor cells nor the addition of expensive substrates are required. Furthermore, given the low molecular weight and the solubility of the α-factor, this pheromone can be transported *e.g.* in microfluidic devices, leading to spatial separation of the sensor cells and the read-out signal. This would enable the use of high sensor cell densities since light scattering by the sensor cells would not affect the read-out of the spatially separated hydrophobin-based immunoassays. However, as pheromone degradation was observed in yeast cultures with high cell densities (*i.e.* in stationary growth phase, section 3.4.2), these systems might include protease inhibitors [436] or suitable protease-deficient yeast strains to avoid extensive signal molecule degradation.

Additionally, spatial separation could serve to meet legal regulations when utilizing genetically modified sensor cells. The sensor cells could be entrapped in a confined space, allowing only small molecules such as yeast pheromones to exit. Microfluidic systems might be suitable to implement spatially separated systems, given that the α-factor pheromone can be transported across wide distances in microfluidic systems [382, 419, 421, 504, 531, 532, 539-542], whereas yeast cells can be efficiently entrapped in microfluidic chambers [421, 539]. Additionally, it has been reported previously that the yeast pheromone easily passes through alginate hydrogels whereas yeast cells can be entrapped in these matrices [385, 386], providing an alternative option to immobilize genetically engineered yeast cells in confined areas.

Moreover, the proposed whole-cell sensor read-out features intrinsic signal amplification, given that the α-factor is synthesized as a part of large precursor molecule carrying four copies of the mature pheromone (Figures 1 and 26). In future

studies, a synthetic *MFα1*-related gene containing even more pheromone repeats could be created and utilized to further amplify the read-out signal. Comparison of the pheromone secretion of engineered *S. pombe* cells suggested that increasing the number of α-factor molecules per pheromone precursor resulted in elevated pheromone secretion (section 3.5.3). The entire process of α-factor processing and secretion is highly efficient. Secretion rates of 550 – 865 pheromone molecules per cell and second have been reported [431-433], whereas the secretion of recombinant proteins, utilizing the Mfα1p propeptide to mediate trafficking through the secretory pathway, is clearly less efficient (30 – 50 molecules of a recombinant cytokine were secreted per cell and second upon overexpression of the corresponding gene [543]).

In addition, the kinetics of the pheromone secretion might be an advantage for the use in whole-cell biosensors. Synthesis of the α-factor pheromone is a rapid process: the entire cascade of translation, maturation, trafficking and secretion is completed within less than 20 min [440], comparing favorably with fluorescent proteins that require long maturation times to fold appropriately (section 1.1.3.3). Furthermore, fluorescent proteins and luciferases are comparatively stable, limiting their use in highly dynamic systems due to the time frames required for protein maturation and protein degradation for sensor regeneration (*i.e.* to reduce the signal to the background value after removal of the target analyte). In contrast, as the *MFα1* mRNA has a very short half-life (5 min [524]) and the α-factor precursors are processed rapidly [440], the signal increases and decreases rapidly. A simple washing step of the sensor cells would be sufficient to remove the secreted α-factor pheromone, efficiently setting the biosensor read-out signal to zero without relying on intracellular protein degradation. Therefore, the proposed biosensor read-out could be useful for application in highly dynamic systems, requiring short response times and/or short regeneration times. In summary, the secreted pheromone might represent a novel reporter to create a whole-cell sensor read-out, possibly contributing to increased sensitivity and broad applicability of yeast-based whole-cell sensors that are major demands in this branch of biosensors [62]. In addition, the hydrophobin-based immunoassays should be amenable to miniaturization and compatible with several different transducer elements (section 4.5.3), potentially providing an opportunity for label-free, real-time measurements of the secreted pheromone. Combining this detection platform with microfluidics and highly

integrated transducer elements could ultimately yield a novel, miniaturized whole-cell biosensor for real-time measurements in field-deployable devices.

The proposed whole-cell biosensor read-out crucially depends on the ability of engineered sensor cells to secrete the α-factor pheromone. It is conceivable that numerous species, especially prokaryotic hosts, are not inherently capable of secreting the yeast pheromone. Therefore, this read-out option might be restricted to fungal sensor cells, in contrast to commonly employed reporter genes encoding fluorescent proteins, luciferases or β-galactosidases that can be functionally expressed in almost all prokaryotic and eukaryotic host cells [3, 54]. However, the hydrophobin-based surface engineering technology could also be employed to develop novel immunoassays for alternative analytes (sections 3.6.2.2 and 4.5.2). If sensor cells can be engineered to secrete a specific target compound in response to an environmental cue, they could be combined with novel hydrophobin-based immunoassays for the detection of the secreted target compound to yield the whole-cell sensor read-out. Therefore, hydrophobin-based immunoassays might provide a more general strategy for the application in whole-cell biosensor devices.

As a proof-of-concept, engineered *S. pombe* cells were utilized in this study to detect trace amounts of thiamine (vitamin B1), an important enzyme cofactor involved in human diseases such as systolic heart failure, dementia and cancer [450-453]. Employing the thiamine-repressed *nmt1* promoter to control *MFα1* expression in *S. pombe* resulted in a thiamine-dependent reduction in α-factor secretion by the sensor cells that was quantified by the hydrophobin-based immunoassays (section 3.6.1), yielding a novel whole-cell biosensor for thiamine. Consistent with previous reports [457, 458], the activity of the *nmt1* promoter could be regulated gradually by the amount of extracellular thiamine. However, this may not directly reflect a gradual down-regulation of the *nmt1* promoter activity, but might result from deviations in the intracellular thiamine levels of individual cells. It has been suggested that the *nmt1* promoter is activated in a switch-like manner if the intracellular thiamine level drops below a certain threshold [457, 544]. In the presence of low extracellular thiamine concentrations, the thiamine pool of individual cells may oscillate around the threshold for *nmt1* promoter activation [457]. Thus, the thiamine-dependent reduction in α-factor synthesis may reflect a population-wide heterogeneity in *nmt1* promoter activity rather than gradual downregulation of the promoter activity.

Nevertheless, the novel whole-cell biosensor enabled thiamine quantification with a detection limit of 10 nM thiamine (section 3.6.1). This compares favorably with several previous approaches to quantify thiamine, *e.g.* utilizing fluorescent carbon dots [545], quantum dots [546], luminescent CdTe nanorods [547] or gold nanoparticles [548]. It should be noted that some of the previously established methods for thiamine detection were more sensitive than the novel whole-cell biosensor. For example, 0.6 nM thiamine could be detected by liquid chromatography systems encompassing post-column thiamine photolysis or pre-column thiamine oxidation [549, 550]. However, as these methods require bulky and highly expensive instruments as well as large volumes of pure solvents, their application is restricted to analytical laboratories. The development of field-deployable biosensors based on these technologies is not feasible.

Enzyme- and cell-based thiamine biosensors have also been reported. Akyilmaz and Yorganci took use of the thiamine-dependent stimulation of pyruvate oxidase activity to detect thiamine concentrations as low as 25 nM [461]. Furthermore, *S. cerevisiae* cells were shown to use thiamine as a carbon source in the absence of glucose. Therefore, monitoring cellular respiration by a dissolved oxygen probe allowed for the detection of thiamine with a lower limit of detection of 5 nM thiamine [460]. However, the latter approach might suffer from non-specific sample matrix effects. Although it was reported that the whole-cell sensor showed a lower response to other vitamins in comparison to thiamine [460], the impact of additional carbon sources or complex sample matrices was not tested. As the biosensor read-out was exclusively based on yeast respiration, this whole-cell sensor may show poor selectivity for thiamine. In contrast, the thiamine whole-cell sensor based on modulation of α-factor secretion is more robust, given that the hydrophobin-based immunoassays were not affected by the sample matrix composition (sections 3.2.4 and 3.3.3). However, the influence of the sample matrix on the activity of the *nmt1* promoter should be assessed in future studies.

Additionally, future efforts should focus on the integration of the *nmt1-MFα1* reporter gene cassette into the genome of the *S. pombe* sensor cells. Plasmid-based reporter gene assays result in a significant heterogeneity in the expression levels of individual cells [73, 437-439], which might be the reason for culture-to-culture deviations observed for plasmid-carrying *S. cerevisiae* and *S. pombe* cells in this study

(sections 3.4.2 and 3.5.3). Reporter gene cassettes integrated into the genome of the host cell are beneficial regarding the long-term genetic stability as well as the homogeneity in the response of individual cells [73, 437-439]. According to Yoo *et al.*, a constant copy number of the reporter gene is mandatory to enable quantification of the activity of the encoded reporter protein, thus necessitating integration of the reporter gene cassette into the host genome [115].

4.5.2 Versatility of the hydrophobin-based immunoassay technology

In this study, novel hydrophobin-based immunoassays for the detection and quantification of the yeast α-factor pheromone were developed. In addition, hydrophobin-based immunoassays for the quantitative assessment of alternative analytes, the HA peptide and recombinant proteins fused to the HA epitope, were established (section 3.6.2.2), highlighting the versatility of this technique. Although the immunoassays for the yeast pheromone and the HA peptide differed in several aspects (*i.e.* in the limit of detection of the inverse ELISA, the dynamic range and the shape of the calibration curves), both peptide analytes could be quantified reliably by the use of the respective hydrophobin-functionalized surfaces. Thus, the hydrophobin-based surface engineering technique might provide a general framework for the immobilization of a user-defined target compound to develop novel immunoassays for a wide variety of analytes. Importantly, previous studies highlighted that hydrophobins can be modified genetically (*i.e.* by the use of recombinant fusion proteins) or chemically (*e.g.* by covalent modification using additional N-terminal cysteine residues) with proteins [267-269, 273-279, 293, 322], peptides [236, 246, 248-251, 263-265, 317, 408], fluorophores [177, 294, 493], biotin [154, 484], dendrons [283], fluorous compounds [551] and polymers [312]. Thus, the hydrophobin-based surface engineering approach possesses an enormous potential for the development of novel biosensors for small molecules such as explosives, xenobiotics, EDCs or chemical warfare agents.

The hydrophobin-based immunoassays relied on the availability of suitable antibodies to detect the target compound. Given that antibodies cannot be raised against toxic, very small or non-immunogenic compounds, are comparatively unstable and their production requires elaborate, time-consuming as well as

expensive purification procedures, recent developments in the field of affinity biosensors increasingly focused on antibody substitutes (section 1.1.2). These include aptamers [15, 16], antibody fragments [12, 17, 18], engineered phages [21-24], peptides [19, 20] and “plastic antibodies” [8, 25, 26]. Potentially, such antibody substitutes can be combined with hydrophobin-functionalized surfaces to yield novel immunoassays.

4.5.3 Compatibility of the hydrophobin-based immunoassays with alternative transducer elements

As mentioned above, commonly employed reporter proteins in whole-cell sensor applications almost exclusively depend on optical transducers to create the read-out signal, representing a considerable limitation of these biosensors (section 1.1.3.3). Increased flexibility regarding the transducer element might be advantageous for whole-cell biosensors, allowing for the development of miniaturized, field-deployable devices. Likewise, novel hydrophobin-based immunoassays for the detection of alternative analytes would benefit from flexibility regarding the choice of the transducer element. Numerous transducers and read-out technologies for the use in affinity biosensors have been reported and most of them might be compatible with hydrophobin-based surface functionalization, ultimately implementing novel immunoassays for label-free, real-time monitoring.

In this study, the read-out of the hydrophobin-based immunoassays was based on the use of a secondary antibody linked to HRP to catalyze a colorimetric reaction. This approach was essentially similar to the commonly employed ELISA technique, benefitting from the intrinsic signal amplification of label-based bioassays (*i.e.* signal amplification by HRP-catalyzed colorimetric reactions [8, 12]). However, ELISA-based assays are comparatively laborious, time-consuming and depend on the use of microplate readers that are not amenable to miniaturization [6, 14, 18, 552]. Thus, ELISA-like approaches are restricted to the use in analytical laboratories and are not suitable for inexpensive and field-deployable biosensors for real-time analyte detection [18]. Consequently, alternative read-out strategies for the hydrophobin-based immunoassays should be investigated to facilitate their integration in commercially viable biosensor devices.

Among the read-out technologies that should be compatible with hydrophobin-based immunoassays, impedance spectroscopy or FET devices might be very promising [31, 32]. FET devices consist of a conductive channel formed by a doped semiconductor material that electrically connects the source and drain electrode. Possibly, functionalization of the conductive channel surface with the recombinant hydrophobins could be employed to yield a novel biosensor. Attachment or detachment of antibodies (or antibody substitutes) would alter the local current density at the surface of the conductive channel, thereby affecting its electrical properties. Recent approaches also focused on the use of nanomaterials such as CNTs or graphene layers in FET-based devices, owing to the excellent chemical stability, high electrical and thermal conductivity as well as a large surface-to-volume ratio [552-554]. Importantly, both CNTs [276, 294, 314-316] and graphene layers [265, 317] can be functionalized with hydrophobins, indicating that the development of novel hydrophobin-based biosensors relying on these nanomaterials may be feasible.

However, the applicability of several transducers relying on the attachment or detachment of charge carriers at a functionalized surface, such as FET devices utilizing CNTs [553, 554] as well as certain types of impedance biosensors [31, 32], is limited by the Debye length. The Debye length characterizes the distance over which these transducer elements can sense the presence of charged molecules at their surface. Remarkably, the Debye length is highly dependent on the ionic strength of the sample matrix, being about 7.3 nm in 0.01 × PBS but only about 0.7 nm in 1 × PBS [555]. Thus, this effect highlights the importance of the use of low ionic strength solvents and the functionalization of the transducer surfaces with very thin layers. The hydrophobin-based immunoassays might fulfill both requirements. The assay sensitivity was independent on the ionic strength of the sample matrix (sections 3.2.4 and 3.3.3). In addition, hydrophobin monolayers were reported to be very thin, as determined for monolayers of MPG1 (2.5 nm [154]), EAS (2.5 nm [149]) and NC2 (1.5 – 2 nm [155]).

Alternative transducers could also include SPR instruments [33, 34] or QCM devices [37, 38]. SPR devices detect a change in the refractive index upon adsorption or desorption of molecules at a functionalized surface and could thus be suitable to detect antibody attachment/detachment in a hydrophobin-based immunoassay. In

contrast to the optical phenomenon exploited in SPR instruments, QCM devices represent mass-based sensors relying on the inverse piezoelectric effect [37, 38]. Adsorption or desorption of molecules to the surface electrode of an oscillating quartz crystal result in a change in its resonance frequency that correlates with the mass change at the crystal surface. Notably, self-assembly of hydrophobins has been studied previously by QCM devices [169, 265, 268, 274, 279, 280, 288, 396, 462, 495], suggesting that QCM instruments might be compatible with hydrophobin-based immunoassays. Both SPR and QCM could offer the possibility for label-free and real-time measurement of antibody attachment/detachment to hydrophobin-functionalized surfaces. However, both techniques crucially depend on the suppression of non-specific protein binding to the functionalized surfaces. As hydrophobin layers support non-specific adsorption of proteins (section 1.2.3), further modification would be required. For example, PEG layers are often used to prevent biofouling of transducer surfaces [18, 31, 556]. Interestingly, hydrophobins can also be modified with PEG derivatives [312], suggesting that this strategy could be employed to reduce non-specific protein binding to hydrophobin-functionalized surfaces.

Further transducer elements that could potentially be employed include devices based on surface acoustic wave technology [39, 40], microcantilevers [41], silicon nanowires [555], surface-enhanced Raman scattering [36] or evanescent field excitation [35], among many others. Likewise, several nanomaterials such as quantum dots [43] or gold nanoparticles [42] could be employed to develop hydrophobin-based immunoassays for biosensor devices. Importantly, recent studies highlighted that nanoparticles [289, 309-313] and quantum dots [318] could also be functionalized with hydrophobins, suggesting that the development of hydrophobin-based immunoassays using these read-out platforms might similarly be feasible.

In summary, the hydrophobin-based immunoassays developed in this study could be employed for a wide variety of applications, either in combination with engineered sensor cells or for the detection of low molecular weight compounds, taking use of the proven versatility that hydrophobin-based immunoassays offer. Therefore, the hydrophobin-based surface engineering technology has tremendous potential for application in biosensor devices.

Summary

This study aimed at the development of a novel way to create a read-out signal in whole-cell biosensor applications. In contrast to protein-based biosensors, whole-cell sensors obviate the need for enzyme/antibody purification and provide the unique possibility to assess global parameters such as genotoxicity and bioavailability. Yeast species such as *S. cerevisiae* are ideal host organisms for whole-cell sensors. However, current approaches almost exclusively rely on analyte-induced expression of reporter genes encoding *e.g.* fluorescent proteins or luciferases that imply issues with light scattering and/or require the addition of expensive substrates. In this study, the yeast α-factor mating pheromone, a peptide pheromone involved in cell-cell communication in *S. cerevisiae*, was utilized to create the whole-cell sensor read-out signal, in particular by employing engineered sensor cells that couple the response to an environmental cue with the secretion of the α-factor.

Two novel immunoassays were developed to detect and quantify the α-factor yeast pheromone, relying on hydrophobin-based surface engineering. Hydrophobins are surface active, fungal proteins that self-assemble into robust monolayers at hydrophobic surfaces. Two recombinant hydrophobins, either lacking (EAS) or exposing the yeast α-factor pheromone (EAS-α) upon self-assembly, were purified upon heterologous expression in *E. coli* and used to functionalize polystyrene supports. In a first approach (competitive immunoassay), α-factor antibodies bound to the functionalized surface (due to the α-factor exposed by the hydrophobin layer) were competitively detached by soluble α-factor. In a second approach, pheromone-specific antibodies were first premixed with α-factor-containing samples and subsequently applied to functionalized surfaces, allowing for the attachment of antibodies that still carried available binding sites (inverse immunoassay).

Both immunoassays enabled quantitative assessment of the yeast pheromone in a unique but partially overlapping dynamic range and allowed for facile tuning of the assay sensitivity by adjustment of the EAS-α content of the hydrophobin monolayers. With a limit of detection of 0.1 nM α-factor, the inverse immunoassay proved to be

the most sensitive pheromone quantification assay reported so far. Due to the high stability of hydrophobin monolayers, the functionalized surfaces could be used for repeated measurements with comparable sensitivity. Favorably, both immunoassays proved to be highly robust against the sample matrix composition, allowing for α-factor quantification even in complex sample matrices such as yeast culture supernatants. Therefore, the hydrophobin-based immunoassays could be applied to study the pheromone secretion of wild-type and engineered *S. cerevisiae* strains.

In addition, a synthetic inter-species communication system, relying on the synthesis and secretion of the α-factor pheromone by engineered *S. pombe* cells, was established. Artificial cell-cell communication systems serve to implement novel control elements for cellular consortia, allowing for the realization of complex synthetic biology circuits and sensor-actor systems. Functional expression of the α-factor by engineered *S. pombe* cells could be demonstrated. In addition, the hydrophobin-based immunoassays were employed to quantify the pheromone secretion of these cells, providing novel insights into the processing of authentic and heterologous pheromone precursors in *S. pombe*.

Furthermore, *S. pombe* cells modulating the synthesis and secretion of the α-factor in response to an exogenous signal could be interfaced with the hydrophobin-based immunoassays to develop a proof-of-concept whole-cell sensor for thiamine. This whole-cell sensor, utilizing the secreted pheromone to create the read-out signal, showed a limit of detection of 10 nM thiamine, comparing favorably with previously developed thiamine quantification assays. This type of whole-cell sensors would also enable spatial separation of the sensor cells and the transducer element, overcoming light scattering issues and providing an opportunity for confinement of genetically modified sensor cells. In addition, this read-out strategy encompasses intrinsic signal amplification and enables flexible choice of the transducer element, contributing to the development of miniaturized, portable whole-cell sensors for on-site application.

Finally, the versatility of the hydrophobin-based immunoassays was demonstrated by developing novel immunoassays for an alternative peptide analyte. In summary, the hydrophobin-based surface engineering technique might harbor tremendous potential for the development of novel immunoassays and biosensors, allowing for the detection of proteins, peptides, nucleic acids and low molecular weight compounds in field-deployable biosensor devices for real-time analysis.

Bibliography

[1] Belkin S. Microbial whole-cell sensing systems of environmental pollutants. *Curr Opin Microbiol* **2003**, 6(3):206-212.

[2] Close DM, Ripp S, Sayler GS. Reporter proteins in whole-cell optical bioreporter detection systems, biosensor integrations, and biosensing applications. *Sensors (Basel)* **2009**, 9(11):9147-9174.

[3] D'Souza SF. Microbial biosensors. *Biosens Bioelectron* **2001**, 16(6):337-353.

[4] Lagarde F, Jaffrezic-Renault N. Cell-based electrochemical biosensors for water quality assessment. *Anal Bioanal Chem* **2011**, 400(4):947-964.

[5] Lei Y, Chen W, Mulchandani A. Microbial biosensors. *Anal Chim Acta* **2006**, 568(1-2):200-210.

[6] Mehrotra P. Biosensors and their applications - A review. *J Oral Biol Craniofac Res* **2016**, 6(2):153-159.

[7] Su L, Jia W, Hou C, Lei Y. Microbial biosensors: a review. *Biosens Bioelectron* **2011**, 26(5):1788-1799.

[8] Turner AP. Biosensors: sense and sensibility. *Chem Soc Rev* **2013**, 42(8):3184-3196.

[9] Vigneshvar S, Sudhakumari CC, Senthilkumaran B, Prakash H. Recent advances in biosensor technology for potential applications - an overview. *Front Bioeng Biotechnol* **2016**, 4:11.

[10] Gonchar M, Maidan M, Korpan Y, Sibirny V, Kotylak Z, Sibirny A. Metabolically engineered methylotrophic yeast cells and enzymes as sensor biorecognition elements. *FEMS Yeast Res* **2002**, 2(3):307-314.

[11] He W, Yuan S, Zhong WH, Siddikee MA, Dai CC. Application of genetically engineered microbial whole-cell biosensors for combined chemosensing. *Appl Microbiol Biotechnol* **2016**, 100(3):1109-1119.

[12] Reimhult E, Höök F. Design of surface modifications for nanoscale sensor applications. *Sensors (Basel)* **2015**, 15(1):1635-1675.

[13] Bereza-Malcolm LT, Mann G, Franks AE. Environmental sensing of heavy metals through whole cell microbial biosensors: a synthetic biology approach. *ACS Synth Biol* **2015**, 4(5):535-546.

[14] Smith RG, D'Souza N, Nicklin S. A review of biosensors and biologically-inspired systems for explosives detection. *Analyst* **2008**, 133(5):571-584.

[15] Kim YS, Raston NH, Gu MB. Aptamer-based nanobiosensors. *Biosens Bioelectron* **2016**, 76:2-19.

[16] Sun H, Zu Y. A highlight of recent advances in aptamer technology and its application. *Molecules* **2015**, 20(7):11959-11980.

[17] Gopinath SC, Tang TH, Citartan M, Chen Y, Lakshmipriya T. Current aspects in immunosensors. *Biosens Bioelectron* **2014**, 57:292-302.

[18] Holford TR, Davis F, Higson SP. Recent trends in antibody based sensors. *Biosens Bioelectron* **2012**, 34(1):12-24.

[19] Cretich M, Damin F, Pirri G, Chiari M. Protein and peptide arrays: recent trends and new directions. *Biomol Eng* **2006**, 23(2-3):77-88.

[20] Liu Q, Wang J, Boyd BJ. Peptide-based biosensors. *Talanta* **2015**, 136:114-127.

[21] Brigati J, Williams DD, Sorokulova IB, Nanduri V, Chen IH, Turnbough CL Jr, Petrenko VA. Diagnostic probes for *Bacillus anthracis* spores selected from a landscape phage library. *Clin Chem* **2004**, 50(10):1899-1906.

[22] Mao C, Liu A, Cao B. Virus-based chemical and biological sensing. *Angew Chem Int Ed Engl* **2009**, 48(37):6790-6810.

[23] Nanduri V, Sorokulova IB, Samoylov AM, Simonian AL, Petrenko VA, Vodyanoy V. Phage as a molecular recognition element in biosensors immobilized by physical adsorption. *Biosens Bioelectron* **2007**, 22(6):986-992.

[24] Petrenko VA, Smith GP. Phages from landscape libraries as substitute antibodies. *Protein Eng* **2000**, 13(8):589-592.

[25] Bedwell TS, Whitcombe MJ. Analytical applications of MIPs in diagnostic assays: future perspectives. *Anal Bioanal Chem* **2016**, 408(7):1735-1751.

[26] Uzun L, Turner AP. Molecularly-imprinted polymer sensors: realising their potential. *Biosens Bioelectron* **2016**, 76:131-144.

[27] Ansari SA, Husain Q. Potential applications of enzymes immobilized on/in nano materials: a review. *Biotechnol Adv* **2012**, 30(3):512-523.

[28] Camarero JA. Recent developments in the site-specific immobilization of proteins onto solid supports. *Biopolymers* **2008**, 90(3):450-458.

[29] Köhn M. Immobilization strategies for small molecule, peptide and protein microarrays. *J Pept Sci* **2009**, 15(6):393-397.

[30] Yeo DS, Panicker RC, Tan LP, Yao SQ. Strategies for immobilization of biomolecules in a microarray. *Comb Chem High Throughput Screen* **2004**, 7(3):213-221.

[31] Daniels JS, Pourmand N. Label-free impedance biosensors: opportunities and challenges. *Electroanalysis* **2007**, 19(12):1239-1257.

[32] Prodromidis MI. Impedimetric immunosensors – a review. *Electrochim Acta* **2010**, 55(14):4227-4233.

[33] Homola J. Surface plasmon resonance sensors for detection of chemical and biological species. *Chem Rev* **2008**, 108(2):462-493.

[34] Nguyen HH, Park J, Kang S, Kim M. Surface plasmon resonance: a versatile technique for biosensor applications. *Sensors (Basel)* **2015**, 15(5):10481-10510.

[35] Mukundan H, Anderson AS, Grace WK, Grace KM, Hartman N, Martinez JS, Swanson BI. Waveguide-based biosensors for pathogen detection. *Sensors (Basel)* **2009**, 9(7):5783-5809.

[36] McNay G, Eustace D, Smith WE, Faulds K, Graham D. Surface-enhanced Raman scattering (SERS) and surface-enhanced resonance Raman scattering (SERRS): a review of applications. *Appl Spectrosc* **2011**, 65(8):825-837.

[37] Cheng CI, Chang YP, Chu YH. Biomolecular interactions and tools for their recognition: focus on the quartz crystal microbalance and its diverse surface chemistries and applications. *Chem Soc Rev* **2012**, 41(5):1947-1971.

[38] Speight RE, Cooper MA. A survey of the 2010 quartz crystal microbalance literature. *J Mol Recognit* **2012**, 25(9):451-473.

[39] Länge K, Rapp BE, Rapp M. Surface acoustic wave biosensors: a review. *Anal Bioanal Chem* **2008**, 391(5):1509-1519.

[40] Voiculescu I, Nordin AN. Acoustic wave based MEMS devices for biosensing applications. *Biosens Bioelectron* **2012**, 33(1):1-9.

[41] Alvarez M, Lechuga LM. Microcantilever-based platforms as biosensing tools. *Analyst* **2010**, 135(5):827-836.

[42] Upadhyayula VK. Functionalized gold nanoparticle supported sensory mechanisms applied in detection of chemical and biological threat agents: a review. *Anal Chim Acta* **2012**, 715:1-18.

[43] Stanisavljevic M, Krizkova S, Vaculovicova M, Kizek R, Adam V. Quantum dots-fluorescence resonance energy transfer-based nanosensors and their application. *Biosens Bioelectron* **2015**, 74:562-574.

[44] Chong KF, Loh KP, Ang K, Ting YP. Whole cell environmental biosensor on diamond. *Analyst* **2008**, 133(6):739-743.

[45] Chouteau C, Dzyadevych S, Durrieu C, Chovelon JM. A bi-enzymatic whole cell conductometric biosensor for heavy metal ions and pesticides detection in water samples. *Biosens Bioelectron* **2005**, 21(2):273-281.

[46] Guedri H, Durrieu C. A self-assembled monolayers based conductometric algal whole cell biosensor for water monitoring. *Microchim Acta* **2008**, 163(3):179-184.

[47] Shitanda I, Takada K, Sakai Y, Tatsuma T. Compact amperometric algal biosensors for the evaluation of water toxicity. *Anal Chim Acta* **2005**, 530(2):191-197.

[48] Shitanda I, Tanaka K, Hoshi Y, Itagaki M. Electrochemical monitoring systems of demembranated flagellate algal motility for ATP sensing. *Analyst* **2014**, 139(4):721-723.

[49] Tatsuma T, Yoshida Y, Shitanda I, Notsu H. Algal biosensor array on a single electrode. *Analyst* **2009**, 134(2):223-225.

[50] Amaro F, Turkewitz AP, Martín-González A, Gutiérrez JC. Functional GFP-metallothionein fusion protein from *Tetrahymena thermophila*: a potential whole-cell biosensor for monitoring heavy metal pollution and a cell model to study metallothionein overproduction effects. *Biometals* **2014**, 27(1):195-205.

[51] Lagido C, Pettitt J, Porter AJ, Paton GI, Glover LA. Development and application of bioluminescent *Caenorhabditis elegans* as multicellular eukaryotic biosensors. *FEBS Lett* **2001**, 493(1):36-39.

[52] Ben-Yoav H, Melamed S, Freeman A, Shacham-Diamand Y, Belkin S. Whole-cell biochips for bio-sensing: integration of live cells and inanimate surfaces. *Crit Rev Biotechnol* **2011**, 31(4):337-353.

[53] Baronian KH. The use of yeast and moulds as sensing elements in biosensors. *Biosens Bioelectron* **2004**, 19(9):953-962.

[54] Daunert S, Barrett G, Feliciano JS, Shetty RS, Shrestha S, Smith-Spencer W. Genetically engineered whole-cell sensing systems: coupling biological recognition with reporter genes. *Chem Rev* **2000**, 100(7):2705-2738.

[55] Michelini E, Cevenini L, Calabretta MM, Spinozzi S, Camborata C, Roda A. Field-deployable whole-cell bioluminescent biosensors: so near and yet so far. *Anal Bioanal Chem* **2013**, 405(19):6155-6163.

[56] Park M, Tsai SL, Chen W. Microbial biosensors: engineered microorganisms as the sensing machinery. *Sensors (Basel)* **2013**, 13(5):5777-5795.

[57] Adeniran A, Sherer M, Tyo KE. Yeast-based biosensors: design and applications. *FEMS Yeast Res* **2014**, 15:1-15.

[58] Zacharewski T. *In vitro* bioassays for assessing estrogenic substances. *Environ Sci Technol* **1997**, 31(3):613-623.

[59] Fernandez-López R, Ruiz R, de la Cruz F, Moncalián G. Transcription factor-based biosensors enlightened by the analyte. *Front Microbiol* **2015**, 6:648.

[60] Hynninen A, Virta M. Whole-cell bioreporters for the detection of bioavailable metals. *Adv Biochem Eng Biotechnol* **2010**, 118:31-63.

[61] Merulla D, Buffi N, Beggah S, Truffer F, Geiser M, Renaud P, van der Meer JR. Bioreporters and biosensors for arsenic detection. Biotechnological solutions for a world-wide pollution problem. *Curr Opin Biotechnol* **2013**, 24(3):534-541.

[62] Jarque S, Bittner M, Blaha L, Hilscherova K. Yeast biosensors for detection of environmental pollutants: current state and limitations. *Trends Biotechnol* **2016**, 34(5):408-419.

[63] Bovee TF, Helsdingen RJ, Hamers AR, van Duursen MB, Nielen MW, Hoogenboom RL. A new highly specific and robust yeast androgen bioassay for the detection of agonists and antagonists. *Anal Bioanal Chem* **2007**, 389(5):1549-1558.

[64] U.S. Food and Drug Administration, Inventory of GRAS notices. Available online: http://www.accessdata.fda.gov/scripts/fdcc/?set=GRASNotices (last accessed: 7 July 2016).

[65] Bakhrat A, Eltzov E, Finkelstein Y, Marks RS, Raveh D. UV and arsenate toxicity: a specific and sensitive yeast bioluminescence assay. *Cell Biol Toxicol* **2011**, 27(3):227-236.

[66] Lehmann M, Riedel K, Adler K, Kunze G. Amperometric measurement of copper ions with a deputy substrate using a novel *Saccharomyces cerevisiae* sensor. *Biosens Bioelectron* **2000**, 15(3-4):211-219.

[67] Leskinen P, Virta M, Karp M. One-step measurement of firefly luciferase activity in yeast. *Yeast* **2003**, 20(13):1109-1113.

[68] Park JN, Sohn MJ, Oh DB, Kwon O, Rhee SK, Hur CG, Lee SY, Gellissen G, Kang HA. Identification of the cadmium-inducible *Hansenula polymorpha SEO1* gene promoter by

transcriptome analysis and its application to whole-cell heavy-metal detection systems. *Appl Environ Microbiol* **2007**, 73(19):5990-6000.

[69] Peltola P, Ivask A, Aström M, Virta M. Lead and Cu in contaminated urban soils: extraction with chemical reagents and bioluminescent bacteria and yeast. *Sci Total Environ* **2005**, 350(1-3):194-203.

[70] Roda A, Roda B, Cevenini L, Michelini E, Mezzanotte L, Reschiglian P, Hakkila K, Virta M. Analytical strategies for improving the robustness and reproducibility of bioluminescent microbial bioreporters. *Anal Bioanal Chem* **2011**, 401(1):201-211.

[71] Shetty RS, Deo SK, Liu Y, Daunert S. Fluorescence-based sensing system for copper using genetically engineered living yeast cells. *Biotechnol Bioeng* **2004**, 88(5):664-670.

[72] Tag K, Riedel K, Bauer HJ, Hanke G, Baronian KH, Kunze G. Amperometric detection of Cu^{2+} by yeast biosensors using flow injection analysis (FIA). *Sensors Actuat B Chem* **2007**, 122(2):403-409.

[73] Benton MG, Glasser NR, Palecek SP. The utilization of a *Saccharomyces cerevisiae HUG1P*-GFP promoter-reporter construct for the selective detection of DNA damage. *Mutat Res* **2007**, 633(1):21-34.

[74] Cahill PA, Knight AW, Billinton N, Barker MG, Walsh L, Keenan PO, Williams CV, Tweats DJ, Walmsley RM. The GreenScreen® genotoxicity assay: a screening validation programme. *Mutagenesis* **2004**, 19(2):105-119.

[75] Ichikawa K, Eki T. A novel yeast-based reporter assay system for the sensitive detection of genotoxic agents mediated by a DNA damage-inducible LexA-GAL4 protein. *J Biochem* **2006**, 139(1):105-112.

[76] Jia X, Zhu Y, Xiao W. A stable and sensitive genotoxic testing system based on DNA damage induced gene expression in *Saccharomyces cerevisiae*. *Mutat Res* **2002**, 519(1-2):83-92.

[77] Wei T, Zhang C, Xu X, Hanna M, Zhang X, Wang Y, Dai H, Xiao W. Construction and evaluation of two biosensors based on yeast transcriptional response to genotoxic chemicals. *Biosens Bioelectron* **2013**, 44:138-145.

[78] Yang HC, Lim BS, Lee YK. *In vitro* assessment of biocompatibility of biomaterials by using fluorescent yeast biosensor. *Curr Appl Phys* **2005**, 5(5):444-448.

[79] Zhang M, Zhang C, Li J, Hanna M, Zhang X, Dai H, Xiao W. Inactivation of *YAP1* enhances sensitivity of the yeast *RNR3-lacZ* genotoxicity testing system to a broad range of DNA-damaging agents. *Toxicol Sci* **2011**, 120(2):310-321.

[80] Erickson JR, Wu JJ, Goddard JG, Tigyi G, Kawanishi K, Tomei LD, Kiefer MC. Edg-2/Vzg-1 couples to the yeast pheromone response pathway selectively in response to lysophosphatidic acid. *J Biol Chem* **1998**, 273(3):1506-1510.

[81] Erlenbach I, Kostenis E, Schmidt C, Hamdan FF, Pausch MH, Wess J. Functional expression of M_1, M_3 and M_5 muscarinic acetylcholine receptors in yeast. *J Neurochem* **2001**, 77(5):1327-1337.

[82] Iguchi Y, Ishii J, Nakayama H, Ishikura A, Izawa K, Tanaka T, Ogino C, Kondo A. Control of signalling properties of human somatostatin receptor subtype-5 by additional signal sequences on its amino-terminus in yeast. *J Biochem* **2010**, 147(6):875-884.

[83] Miret JJ, Rakhilina L, Silverman L, Oehlen B. Functional expression of heteromeric calcitonin gene-related peptide and adrenomedullin receptors in yeast. *J Biol Chem* **2002**, 277(9):6881-6887.

[84] Baronian KH, Gurazada S. Electrochemical detection of wild type *Saccharomyces cerevisiae* responses to estrogens. *Biosens Bioelectron* **2007**, 22(11):2493-2499.

[85] Beck V, Reiter E, Jungbauer A. Androgen receptor transactivation assay using green fluorescent protein as a reporter. *Anal Biochem* **2008**, 373(2):263-271.

[86] Eldridge ML, Sanseverino J, Layton AC, Easter JP, Schultz TW, Sayler GS. *Saccharomyces cerevisiae* BLYAS, a new bioluminescent bioreporter for detection of androgenic compounds. *Appl Environ Microbiol* **2007**, 73(19):6012-6018.

[87] Ino K, Kitagawa Y, Watanabe T, Shiku H, Koide M, Itayama T, Yasukawa T, Matsue T. Detection of hormone active chemicals using genetically engineered yeast cells and microfluidic devices with interdigitated array electrodes. *Electrophoresis* **2009**, 30(19):3406-3412.

[88] Michelini E, Leskinen P, Virta M, Karp M, Roda A. A new recombinant cell-based bioluminescent assay for sensitive androgen-like compound detection. *Biosens Bioelectron* **2005**, 20(11):2261-2267.

[89] Sanseverino J, Gupta RK, Layton AC, Patterson SS, Ripp SA, Saidak L, Simpson ML, Schultz TW, Sayler GS. Use of *Saccharomyces cerevisiae* BLYES expressing bacterial bioluminescence for rapid, sensitive detection of estrogenic compounds. *Appl Environ Microbiol* **2005**, 71(8):4455-4460.

[90] Sanseverino J, Eldridge ML, Layton AC, Easter JP, Yarbrough J, Schultz TW, Sayler GS. Screening of potentially hormonally active chemicals using bioluminescent yeast bioreporters. *Toxicol Sci* **2009**, 107(1):122-134.

[91] Schwartz-Mittelman A, Baruch A, Neufeld T, Buchner V, Rishpon J. Electrochemical detection of xenoestrogenic and antiestrogenic compounds using a yeast two-hybrid-17-β-estradiol system. *Bioelectrochemistry* **2005**, 65(2):149-156.

[92] Wolf S, Rataj F, Zierau O, Ostermann K, Diel P, Parr MK, Vollmer G, Rödel G. A novel combined approach to detect androgenic activities with yeast based assays in *Schizosaccharomyces pombe* and *Saccharomyces cerevisiae*. *Toxicol Lett* **2010**, 199(3):410-415.

[93] Fukutani Y, Hori A, Tsukada S, Sato R, Ishii J, Kondo A, Matsunami H, Yohda M. Improving the odorant sensitivity of olfactory receptor-expressing yeast with accessory proteins. *Anal Biochem* **2015**, 471:1-8.

[94] Minic J, Persuy MA, Godel E, Aioun J, Connerton I, Salesse R, Pajot-Augy E. Functional expression of olfactory receptors in yeast and development of a bioassay for odorant screening. *FEBS J* **2005**, 272(2):524-537.

[95] Radhika V, Proikas-Cezanne T, Jayaraman M, Onesime D, Ha JH, Dhanasekaran DN. Chemical sensing of DNT by engineered olfactory yeast strain. *Nat Chem Biol* **2007**, 3(6):325-330.

[96] Mukherjee K, Bhattacharyya S, Peralta-Yahya P. GPCR-based chemical biosensors for medium-chain fatty acids. *ACS Synth Biol* **2015**, 4(12):1261-1269.

[97] Fukutani Y, Ishii J, Noguchi K, Kondo A, Yohda M. An improved bioluminescence-based signaling assay for odor sensing with a yeast expressing a chimeric olfactory receptor. *Biotechnol Bioeng* **2012**, 109(12):3143-3151.

[98] Thierfelder S, Ostermann K, Göbel A, Rödel G. Vectors for glucose-dependent protein expression in *Saccharomyces cerevisiae*. *Appl Biochem Biotechnol* **2011**, 163(8):954-964.

[99] Wang H, Lang Q, Li L, Liang B, Tang X, Kong L, Mascini M, Liu A. Yeast surface displaying glucose oxidase as whole-cell biocatalyst: construction, characterization, and its electrochemical glucose sensing application. *Anal Chem* **2013**, 85(12):6107-6112.

[100] Weaver AA, Halweg S, Joyce M, Lieberman M, Goodson HV. Incorporating yeast biosensors into paper-based analytical tools for pharmaceutical analysis. *Anal Bioanal Chem* **2015**, 407(2):615-619.

[101] Fujita K, Iwahashi H, Kawai R, Komatsu Y. Hsp104 expression and morphological changes associated with disinfectants in *Saccharomyces cerevisiae*: Environmental bioassay using stress response. *Water Sci Technol* **1998**, 38(7):237-243.

[102] Leskinen P, Hilscherova K, Sidlova T, Kiviranta H, Pessala P, Salo S, Verta M, Virta M. Detecting AhR ligands in sediments using bioluminescent reporter yeast. *Biosens Bioelectron* **2008**, 23(12):1850-1855.

[103] Schofield DA, Westwater C, Barth JL, DiNovo AA. Development of a yeast biosensor-biocatalyst for the detection and biodegradation of the organophosphate paraoxon. *Appl Microbiol Biotechnol* **2007**, 76(6):1383-1394.

[104] Richter I, Fidler AE. Detection of marine microalgal biotoxins using bioassays based on functional expression of tunicate xenobiotic receptors in yeast. *Toxicon* **2015**, 95:13-22.

[105] Välimaa AL, Kivistö AT, Leskinen PI, Karp MT. A novel biosensor for the detection of zearalenone family mycotoxins in milk. *J Microbiol Methods* **2010**, 80(1):44-48.

[106] Venkatesh AG, Sun A, Brickner H, Looney D, Hall DA, Aronoff-Spencer E. Yeast dual-affinity biobricks: Progress towards renewable whole-cell biosensors. *Biosens Bioelectron* **2015**, 70:462-468.

[107] Goldblum DK, Holodnick SE, Mancy KH, Briggs DE. Oxygen transport in biofilm electrodes for screening of toxic chemicals. *AIChE J* **1990**, 36(1):19-28.

[108] Garjonyte R, Melvydas V, Malinauskas A. Mediated amperometric biosensors for lactic acid based on carbon paste electrodes modified with baker's yeast *Saccharomyces cerevisiae*. *Bioelectrochemistry* **2006**, 68(2):191-196.

[109] Chan C, Lehmann M, Chan K, Chan P, Chan C, Gruendig B, Kunze G, Renneberg R. Designing an amperometric thick-film microbial BOD sensor. *Biosens Bioelectron* **2000**, 15(7-8):343-353.

[110] Gerlach T, Knaust J, Kaiser C, Körner M, Hettwer K, Uhlig S, Simon K, Baronian K, Kunze G. Development and assessment of a novel *Arxula adeninivorans* androgen screen (A-YAS) assay and its application in analysis of cattle urine. *Sci Total Environ* **2014**, 490:1073-1081.

[111] Hahn T, Tag K, Riedel K, Uhlig S, Baronian K, Gellissen G, Kunze G. A novel estrogen sensor based on recombinant *Arxula adeninivorans* cells. *Biosens Bioelectron* **2006**, 21(11):2078-2085.

[112] Kaiser C, Uhlig S, Gerlach T, Körner M, Simon K, Kunath K, Florschütz K, Baronian K, Kunze G. Evaluation and validation of a novel *Arxula adeninivorans* estrogen screen (nAES) assay and its application in analysis of wastewater, seawater, brackish water and urine. *Sci Total Environ* **2010**, 408(23):6017-6026.

[113] Pham HT, Giersberg M, Uhlig S, Hanke G, Simon K, Kunath K, Baronian K, Kunze G. EstraMonitor – A monitor for amperometric detection of estrogenic activity with *Arxula adeninivorans* yeast cells as the biocomponent. *Sensors Actuat B Chem* **2012**, 161(1):137-145.

[114] Jiao B, Yeung EK, Chan CB, Cheng CH. Establishment of a transgenic yeast screening system for estrogenicity and identification of the anti-estrogenic activity of malachite green. *J Cell Biochem* **2008**, 105(6):1399-1409.

[115] Yoo EJ, Jang YK, Kimm HS, Choi ES, Park SD. Development of a new xenoestrogen screening system using fission yeast *Schizosaccharomyces pombe*. *Mol Cells* **2002**, 13(1):148-153.

[116] Webb JS, Barratt SR, Sabev H, Nixon M, Eastwood IM, Greenhalgh M, Handley PS, Robson GD. Green fluorescent protein as a novel indicator of antimicrobial susceptibility in *Aureobasidium pullulans*. *Appl Environ Microbiol* **2001**, 67(12):5614-5620.

[117] Weitz HJ, Campbell CD, Killham K. Development of a novel, bioluminescence-based, fungal bioassay for toxicity testing. *Environ Microbiol* **2002**, 4(7):422-429.

[118] Choe SI, Gravelat FN, Al Abdallah Q, Lee MJ, Gibbs BF, Sheppard DC. Role of *Aspergillus niger acrA* in arsenic resistance and its use as the basis for an arsenic biosensor. *Appl Environ Microbiol* **2012**, 78(11):3855-3863.

[119] Akyilmaz E, Dinçkaya E. An amperometric microbial biosensor development based on *Candida tropicalis* yeast cells for sensitive determination of ethanol. *Biosens Bioelectron* **2005**, 20(7):1263-1269.

[120] Akyilmaz E, Turemis M, Yasa I. Voltammetric determination of epinephrine by White rot fungi (*Phanerochaete chrysosporium* ME446) cells based microbial biosensor. *Biosens Bioelectron* **2011**, 26(5):2590-2594.

[121] Whiting JG, de Lacy Costello B, Adamatzky A. Development and initial testing of a novel slime mould biosensor. *Conf Proc IEEE Eng Med Biol Soc* **2014**, 2014:4042-4045.

[122] Frommer WB, Davidson MW, Campbell RE. Genetically encoded biosensors based on engineered fluorescent proteins. *Chem Soc Rev* **2009**, 38(10):2833-2841.

[123] Bazin I, Seo HB, Suehs CM, Ramuz M, De Waard M, Gu MB. Profiling the biological effects of wastewater samples *via* bioluminescent bacterial biosensors combined with estrogenic assays. *Environ Sci Pollut Res Int* **2016**, in press.

[124] King K, Dohlman HG, Thorner J, Caron MG, Lefkowitz RJ. Control of yeast mating signal transduction by a mammalian β_2-adrenergic receptor and G_S α subunit. *Science* **1990**, 250(4977):121-123.

[125] Riether KB, Dollard MA, Billard P. Assessment of heavy metal bioavailability using *Escherichia coli zntAp::lux* and *copAp::lux*-based biosensors. *Appl Microbiol Biotechnol* **2001**, 57(5-6):712-716.

[126] Melcher K, Sharma B, Ding WV, Nolden M. Zero background yeast reporter plasmids. *Gene* **2000**, 247(1-2):53-61.

[127] Ochi Y, Sugawara H, Iwami M, Tanaka M, Eki T. Sensitive detection of chemical-induced genotoxicity by the *Cypridina* secretory luciferase reporter assay, using DNA repair-deficient strains of *Saccharomyces cerevisiae*. *Yeast* **2011**, 28(4):265-278.

[128] Tochigi Y, Sato N, Sahara T, Wu C, Saito S, Irie T, Fujibuchi W, Goda T, Yamaji R, Ogawa M, Ohmiya Y, Ohgiya S. Sensitive and convenient yeast reporter assay for high-throughput analysis by using a secretory luciferase from *Cypridina noctiluca*. *Anal Chem* **2010**, 82(13):5768-5776.

[129] Kershaw MJ, Talbot NJ. Hydrophobins and repellents: proteins with fundamental roles in fungal morphogenesis. *Fungal Genet Biol* **1998**, 23(1):18-33.

[130] Linder MB, Szilvay GR, Nakari-Setälä T, Penttilä ME. Hydrophobins: the protein-amphiphiles of filamentous fungi. *FEMS Microbiol Rev* **2005**, 29(5):877-896.

[131] Ren Q, Kwan AH, Sunde M. Two forms and two faces, multiple states and multiple uses: Properties and applications of the self-assembling fungal hydrophobins. *Biopolymers* **2013**, 100(6):601-612.

[132] Sunde M, Kwan AH, Templeton MD, Beever RE, Mackay JP. Structural analysis of hydrophobins. *Micron* **2008**, 39(7):773-784.

[133] Wösten HA, de Vocht ML. Hydrophobins, the fungal coat unravelled. *Biochim Biophys Acta* **2000**, 1469(2):79-86.

[134] Wösten HA. Hydrophobins: multipurpose proteins. *Annu Rev Microbiol* **2001**, 55:625-646.

[135] Zampieri F, Wösten HA, Scholtmeijer K. Creating surface properties using a palette of hydrophobins. *Materials* **2010**, 3(9):4607-4625.

[136] Wessels J, De Vries O, Asgeirsdottir SA, Schuren F. Hydrophobin genes involved in formation of aerial hyphae and fruit bodies in *Schizophyllum*. *Plant Cell* **1991**, 3(8):793-799.

[137] Grünbacher A, Throm T, Seidel C, Gutt B, Röhrig J, Strunk T, Vincze P, Walheim S, Schimmel T, Wenzel W, Fischer R. Six hydrophobins are involved in hydrophobin rodlet formation in *Aspergillus nidulans* and contribute to hydrophobicity of the spore surface. *PLoS One* **2014**, 9(4):e94546.

[138] Jensen BG, Andersen MR, Pedersen MH, Frisvad JC, Søndergaard I. Hydrophobins from *Aspergillus* species cannot be clearly divided into two classes. *BMC Res Notes* **2010**, 3:344.

[139] Littlejohn KA, Hooley P, Cox PW. Bioinformatics predicts diverse *Aspergillus hydrophobins* with novel properties. *Food Hydrocolloid* **2012**, 27(2):503-516.

[140] Seidl-Seiboth V, Gruber S, Sezerman U, Schwecke T, Albayrak A, Neuhof T, von Döhren H, Baker SE, Kubicek CP. Novel hydrophobins from *Trichoderma* define a new hydrophobin subclass: protein properties, evolution, regulation and processing. *J Mol Evol* **2011**, 72(4):339-351.

[141] Hektor HJ, Scholtmeijer K. Hydrophobins: proteins with potential. *Curr Opin Biotechnol* **2005**, 16(4):434-439.

[142] Whiteford JR, Spanu PD. Hydrophobins and the interactions between fungi and plants. *Mol Plant Pathol* **2002**, 3(5):391-400.

[143] Segers GC, Hamada W, Oliver RP, Spanu PD. Isolation and characterisation of five different hydrophobin-encoding cDNAs from the fungal tomato pathogen *Cladosporium fulvum*. *Mol Gen Genet* **1999**, 261(4-5):644-652.

[144] Bell-Pedersen D, Dunlap JC, Loros JJ. The *Neurospora* circadian clock-controlled gene, *ccg-2*, is allelic to *eas* and encodes a fungal hydrophobin required for formation of the conidial rodlet layer. *Genes Dev* **1992**, 6(12A):2382-2394.

[145] Lauter FR, Russo VE, Yanofsky C. Developmental and light regulation of *eas*, the structural gene for the rodlet protein of *Neurospora*. *Genes Dev* **1992**, 6(12A):2373-2381.

[146] Kwan AH, Winefield RD, Sunde M, Matthews JM, Haverkamp RG, Templeton MD, Mackay JP. Structural basis for rodlet assembly in fungal hydrophobins. *Proc Natl Acad Sci USA* **2006**, 103(10):3621-3626.

[147] Kwan AH, Macindoe I, Vukasin PV, Morris VK, Kass I, Gupte R, Mark AE, Templeton MD, Mackay JP, Sunde M. The Cys3-Cys4 loop of the hydrophobin EAS is not required for rodlet formation and surface activity. *J Mol Biol* **2008**, 382(3):708-720.

[148] De Simone A, Kitchen C, Kwan AH, Sunde M, Dobson CM, Frenkel D. Intrinsic disorder modulates protein self-assembly and aggregation. *Proc Natl Acad Sci USA* **2012**, 109(18):6951-6956.

[149] Macindoe I, Kwan AH, Ren Q, Morris VK, Yang W, Mackay JP, Sunde M. Self-assembly of functional, amphipathic amyloid monolayers by the fungal hydrophobin EAS. *Proc Natl Acad Sci USA* **2012**, 109(14):E804-811.

[150] Hakanpää J, Paananen A, Askolin S, Nakari-Setälä T, Parkkinen T, Penttilä M, Linder MB, Rouvinen J. Atomic resolution structure of the HFBII hydrophobin, a self-assembling amphiphile. *J Biol Chem* **2004**, 279(1):534-539.

[151] Hakanpää J, Linder M, Popov A, Schmidt A, Rouvinen J. Hydrophobin HFBII in detail: ultrahigh-resolution structure at 0.75 Å. *Acta Crystallogr D Biol Crystallogr* **2006**, 62(Pt 4):356-367.

[152] Hakanpää J, Szilvay GR, Kaljunen H, Maksimainen M, Linder M, Rouvinen J. Two crystal structures of *Trichoderma reesei* hydrophobin HFBI - the structure of a protein amphiphile with and without detergent interaction. *Protein Sci* **2006**, 15(9):2129-2140.

[153] Morris VK, Kwan AH, Sunde M. Analysis of the structure and conformational states of DewA gives insight into the assembly of the fungal hydrophobins. *J Mol Biol* **2013**, 425(2):244-256.

[154] Pham CL, Rey A, Lo V, Soulès M, Ren Q, Meisl G, Knowles TP, Kwan AH, Sunde M. Self-assembly of MPG1, a hydrophobin protein from the rice blast fungus that forms functional amyloid coatings, occurs by a surface-driven mechanism. *Sci Rep* **2016**, 6:25288.

[155] Ren Q, Kwan AH, Sunde M. Solution structure and interface-driven self-assembly of NC2, a new member of the Class II hydrophobin proteins. *Proteins* **2014**, 82(6):990-1003.

[156] Asgeirsdóttir SA, de Vries OM, Wessels JG. Identification of three differentially expressed hydrophobins in *Pleurotus ostreatus* (oyster mushroom). *Microbiology* **1998**, 144 (Pt 11):2961-2969.

[157] Kupčík R, Zelená M, Řehulka P, Bílková Z, Česlová L. Selective isolation of hydrophobin SC3 by solid-phase extraction with polytetrafluoroethylene microparticles and subsequent mass spectrometric analysis. *J Sep Sci* **2016**, 39(4):717-724.

[158] de Vocht ML, Scholtmeijer K, van der Vegte EW, de Vries OM, Sonveaux N, Wösten HA, Ruysschaert JM, Hadziloannou G, Wessels JG, Robillard GT. Structural characterization of the hydrophobin SC3, as a monomer and after self-assembly at hydrophobic/hydrophilic interfaces. *Biophys J* **1998**, 74(4):2059-2068.

[159] De Vries OM, Moore S, Arntz C, Wessels JG, Tudzynski P. Identification and characterization of a tri-partite hydrophobin from *Claviceps fusiformis*. A novel type of class II hydrophobin. *Eur J Biochem* **1999**, 262(2):377-385.

[160] Mey G, Correia T, Oeser B, Kershaw MJ, Garre V, Arntz C, Talbot NJ, Tudzynski P. Structural and functional analysis of an oligomeric hydrophobin gene from *Claviceps purpurea*. *Mol Plant Pathol* **2003**, 4(1):31-41.

[161] Mackay JP, Matthews JM, Winefield RD, Mackay LG, Haverkamp RG, Templeton MD. The hydrophobin EAS is largely unstructured in solution and functions by forming amyloid-like structures. *Structure* **2001**, 9(2):83-91.

[162] Morris VK, Linser R, Wilde KL, Duff AP, Sunde M, Kwan AH. Solid-state NMR spectroscopy of functional amyloid from a fungal hydrophobin: a well-ordered β-sheet core amidst structural heterogeneity. *Angew Chem Int Ed Engl* **2012**, 51(50):12621-12625.

[163] Lo VC, Ren Q, Pham CL, Morris VK, Kwan AH, Sunde M. Fungal hydrophobin proteins produce self-assembling protein films with diverse structure and chemical stability. *Nanomaterials* **2014**, 4(3):827-843.

[164] Morris VK, Ren Q, Macindoe I, Kwan AH, Byrne N, Sunde M. Recruitment of class I hydrophobins to the air:water interface initiates a multi-step process of functional amyloid formation. *J Biol Chem* **2011**, 286(18):15955-15963.

[165] Ley K, Christofferson A, Penna M, Winkler D, Maclaughlin S, Yarovsky I. Surface-water interface induces conformational changes critical for protein adsorption: implications for monolayer formation of EAS hydrophobin. *Front Mol Biosci* **2015**, 2:64.

[166] de Vocht ML, Reviakine I, Ulrich WP, Bergsma-Schutter W, Wösten HA, Vogel H, Brisson A, Wessels JG, Robillard GT. Self-assembly of the hydrophobin SC3 proceeds *via* two structural intermediates. *Protein Sci* **2002**, 11(5):1199-1205.

[167] Martin GG, Cannon GC, McCormick CL. Sc3p hydrophobin organization in aqueous media and assembly onto surfaces as mediated by the associated polysaccharide schizophyllan. *Biomacromolecules* **2000**, 1(1):49-60.

[168] Scholtmeijer K, de Vocht ML, Rink R, Robillard GT, Wösten HA. Assembly of the fungal SC3 hydrophobin into functional amyloid fibrils depends on its concentration and is promoted by cell wall polysaccharides. *J Biol Chem* **2009**, 284(39):26309-26314.

[169] Paslay LC, Falgout L, Savin DA, Heinhorst S, Cannon GC, Morgan SE. Kinetics and control of self-assembly of ABH1 hydrophobin from the edible white button mushroom. *Biomacromolecules* **2013**, 14(7):2283-2293.

[170] Gravagnuolo AM, Longobardi S, Luchini A, Appavou MS, De Stefano L, Notomista E, Paduano L, Giardina P. Class I hydrophobin Vmh2 adopts atypical mechanisms to self-assemble into functional amyloid fibrils. *Biomacromolecules* **2016**, 17(3):954-964.

[171] Longobardi S, Picone D, Ercole C, Spadaccini R, De Stefano L, Rea I, Giardina P. Environmental conditions modulate the switch among different states of the hydrophobin Vmh2 from *Pleurotus ostreatus*. *Biomacromolecules* **2012**, 13(3):743-750.

[172] Paananen A, Vuorimaa E, Torkkeli M, Penttilä M, Kauranen M, Ikkala O, Lemmetyinen H, Serimaa R, Linder MB. Structural hierarchy in molecular films of two class II hydrophobins. *Biochemistry* **2003**, 42(18):5253-5258.

[173] Kisko K, Torkkeli M, Vuorimaa E, Lemmetyinen H, Seeck OH, Linder M, Serimaa R. Langmuir–Blodgett films of hydrophobins HFBI and HFBII. *Surf Sci* **2005**, 584(1):35-40.

[174] Kisko K, Szilvay GR, Vuorimaa E, Lemmetyinen H, Linder MB, Torkkeli M, Serimaa R. Self-assembled films of hydrophobin protein HFBIII from *Trichoderma reesei*. *J Appl Cryst* **2007**, 40:355-360.

[175] Oude Vrielink AS, Bomans PH, Vredenbregt EJ, Wirix MJ, Sommerdijk NA, Luiten OJ, Voets IK. Suspended crystalline films of protein hydrophobin I (HFBI). *J Colloid Interface Sci* **2015**, 447:107-112.

[176] Yamasaki R, Takatsuji Y, Lienemann M, Asakawa H, Fukuma T, Linder M, Haruyama T. Electrochemical properties of honeycomb-like structured HFBI self-organized membranes on HOPG electrodes. *Colloids Surf B Biointerfaces* **2014**, 123:803-808.

[177] Yamasaki R, Takatsuji Y, Asakawa H, Fukuma T, Haruyama T. Flattened-top domical water drops formed through self-organization of hydrophobin membranes: a structural and mechanistic study using atomic force microscopy. *ACS Nano* **2016**, 10(1):81-87.

[178] Alexandrov NA, Marinova KG, Gurkov TD, Danov KD, Kralchevsky PA, Stoyanov SD, Blijdenstein TB, Arnaudov LN, Pelan EG, Lips A. Interfacial layers from the protein HFBII hydrophobin: dynamic surface tension, dilatational elasticity and relaxation times. *J Colloid Interface Sci* **2012**, 376(1):296-306.

[179] Blijdenstein TB, Ganzevles RA, de Groot PW, Stoyanov SD. On the link between surface rheology and foam disproportionation in mixed hydrophobin HFBII and whey protein systems. *Colloid Surf A* **2013**, 438:13-20.

[180] Sbrana F, Fanelli D, Vassalli M, Carresi L, Scala A, Pazzagli L, Cappugi G, Tiribilli B. Progressive pearl necklace collapse mechanism for cerato-ulmin aggregation film. *Eur Biophys J* **2010**, 39(6):971-977.

[181] Templeton MD, Greenwood DR, Beever RE. Solubilization of *Neurospora crassa* rodlet proteins and identification of the predominant protein as the proteolytically processed *eas* (*ccg-2*) gene product. *Exp Mycol* **1995**, 19(2):166-169.

[182] Dyer PS. Hydrophobins in the lichen symbiosis. *New Phytol* **2002**, 154(1):1-4.

[183] Ebbole DJ. Hydrophobins and fungal infection of plants and animals. *Trends Microbiol* **1997**, 5(10):405-408.

[184] Talbot NJ. Growing into the air. *Curr Biol* **1997**, 7(2):R78-R81.

[185] Tucker SL, Talbot NJ. Surface attachment and pre-penetration stage development by plant pathogenic fungi. *Annu Rev Phytopathol* **2001**, 39:385-417.

[186] Wösten HA, Wessels JG. Hydrophobins, from molecular structure to multiple functions in fungal development. *Mycoscience* **1997**, 38(3):363-374.

[187] Wösten HA, Willey JM. Surface-active proteins enable microbial aerial hyphae to grow into the air. *Microbiology* **2000**, 146 (Pt 4):767-773.

[188] Mikus M, Hatvani L, Neuhof T, Komoń-Zelazowska M, Dieckmann R, Schwecke T, Druzhinina IS, von Döhren H, Kubicek CP. Differential regulation and posttranslational processing of the class II hydrophobin genes from the biocontrol fungus *Hypocrea atroviridis*. *Appl Environ Microbiol* **2009**, 75(10):3222-3229.

[189] Mgbeahuruike AC, Kovalchuk A, Asiegbu FO. Comparative genomics and evolutionary analysis of hydrophobins from three species of wood-degrading fungi. *Mycologia* **2013**, 105(6):1471-1478.

[190] Mgbeahuruike AC, Kovalchuk A, Chen H, Ubhayasekera W, Asiegbu FO. Evolutionary analysis of hydrophobin gene family in two wood-degrading basidiomycetes, *Phlebia brevispora* and *Heterobasidion annosum* s.l. *BMC Evol Biol* **2013**, 13:240.

[191] Stajich JE, Wilke SK, Ahrén D, Au CH, Birren BW, Borodovsky M, Burns C, Canbäck B, Casselton LA, Cheng CK, Deng J, Dietrich FS, Fargo DC, Farman ML, Gathman AC, Goldberg J, Guigó R, Hoegger PJ, Hooker JB, Huggins A, James TY, Kamada T, Kilaru S, Kodira C, Kües U, Kupfer D, Kwan HS, Lomsadze A, Li W, Lilly WW, Ma LJ, Mackey AJ, Manning G, Martin F, Muraguchi H, Natvig DO, Palmerini H, Ramesh MA, Rehmeyer CJ, Roe BA, Shenoy N, Stanke M, Ter-Hovhannisyan V, Tunlid A, Velagapudi R, Vision TJ, Zeng Q, Zolan ME, Pukkila PJ. Insights into evolution of multicellular fungi from the assembled chromosomes of the mushroom *Coprinopsis cinerea* (*Coprinus cinereus*). *Proc Natl Acad Sci USA* **2010**, 107(26):11889-11894.

[192] Kershaw MJ, Wakley G, Talbot NJ. Complementation of the Mpg1 mutant phenotype in *Magnaporthe grisea* reveals functional relationships between fungal hydrophobins. *EMBO J* **1998**, 17(14):3838-3849.

[193] Corvis Y, Brezesinski G, Rink R, Walcarius A, Van der Heyden A, Mutelet F, Rogalska E. Analytical investigation of the interactions between SC3 hydrophobin and lipid layers: elaborating of nanostructured matrixes for immobilizing redox systems. *Anal Chem* **2006**, 78(14):4850-4864.

[194] van der Vegt W, van der Mei HC, Wösten HA, Wessels JG, Busscher HJ. A comparison of the surface activity of the fungal hydrophobin SC3p with those of other proteins. *Biophys Chem* **1996**, 57(2-3):253-260.

[195] Wösten HA, van Wetter MA, Lugones LG, van der Mei HC, Busscher HJ, Wessels JG. How a fungus escapes the water to grow into the air. *Curr Biol* **1999**, 9(2):85-88.

[196] Askolin S, Penttilä M, Wösten HA, Nakari-Setälä T. The *Trichoderma reesei* hydrophobin genes *hfb1* and *hfb2* have diverse functions in fungal development. *FEMS Microbiol Lett* **2005**, 253(2):281-288.

[197] Tillotson RD, Wösten HA, Richter M, Willey JM. A surface active protein involved in aerial hyphae formation in the filamentous fungus *Schizophyllum commune* restores the capacity of a bald mutant of the filamentous bacterium *Streptomyces coelicolor* to erect aerial structures. *Mol Microbiol* **1998**, 30(3):595-602.

[198] van Wetter MA, Wösten HA, Wessels JG. SC3 and SC4 hydrophobins have distinct roles in formation of aerial structures in dikaryons of *Schizophyllum commune*. *Mol Microbiol* **2000**, 36(1):201-210.

[199] Asgeirsdóttir SA, Halsall JR, Casselton LA. Expression of two closely linked hydrophobin genes of *Coprinus cinereus* is monokaryon-specific and down-regulated by the *oid-1* mutation. *Fungal Genet Biol* **1997**, 22(1):54-63.

[200] Terhem RB, van Kan JA. Functional analysis of hydrophobin genes in sexual development of *Botrytis cinerea*. *Fungal Genet Biol* **2014**, 71:42-51.

[201] Girardin H, Paris S, Rault J, Bellon-Fontaine MN, Latgé JP. The role of the rodlet structure on the physicochemical properties of *Aspergillus* conidia. *Lett Appl Microbiol* **1999**, 29(6):364-369.

[202] Hamada W, Spanu PD. Co-suppression of the hydrophobin gene *HCf-1* is correlated with antisense RNA biosynthesis in *Cladosporium fulvum*. *Mol Gen Genet* **1998**, 259(6):630-638.

[203] Minenko E, Vogel RF, Niessen L. Significance of the class II hydrophobin FgHyd5p for the life cycle of *Fusarium graminearum*. *Fungal Biol* **2014**, 118(4):385-393.

[204] Spanu P. Deletion of *HCf-1*, a hydrophobin gene of *Cladosporium fulvum*, does not affect pathogenicity on tomato. *Physiol Mol Plant P* **1998**, 52(5):323-334.

[205] Stringer MA, Dean RA, Sewall TC, Timberlake WE. *Rodletless*, a new *Aspergillus* developmental mutant induced by directed gene inactivation. *Genes Dev* **1991**, 5(7):1161-1171.

[206] Talbot NJ, Ebbole DJ, Hamer JE. Identification and characterization of *MPG1*, a gene involved in pathogenicity from the rice blast fungus *Magnaporthe grisea*. *Plant Cell* **1993**, 5(11):1575-1590.

[207] Talbot NJ, Kershaw MJ, Wakley GE, De Vries O, Wessels J, Hamer JE. *MPG1* encodes a fungal hydrophobin involved in surface interactions during infection-related development of *Magnaporthe grisea*. *Plant Cell* **1996**, 8(6):985-999.

[208] Thau N, Monod M, Crestani B, Rolland C, Tronchin G, Latgé JP, Paris S. *rodletless* mutants of *Aspergillus fumigatus*. *Infect Immun* **1994**, 62(10):4380-4388.

[209] van Wetter MA, Schuren FH, Schuurs TA, Wessels JG. Targeted mutation of the SC3 hydrophobin gene of *Schizophyllum commune* affects formation of aerial hyphae. *FEMS Microbiol Lett* **1996**, 140(2-3):265-269.

[210] Whiteford JR, Spanu PD. The hydrophobin HCf-1 of *Cladosporium fulvum* is required for efficient water-mediated dispersal of conidia. *Fungal Genet Biol* **2001**, 32(3):159-168.

[211] Zhang S, Xia YX, Kim B, Keyhani NO. Two hydrophobins are involved in fungal spore coat rodlet layer assembly and each play distinct roles in surface interactions, development and pathogenesis in the entomopathogenic fungus, *Beauveria bassiana*. *Mol Microbiol* **2011**, 80(3):811-826.

[212] Beever RE, Dempsey GP. Function of rodlets on the surface of fungal spores. *Nature* **1978**, 272(5654):608-610.

[213] Lugones LG, Wösten HA, Birkenkamp KU, Sjollema KA, Zagers J, Wessels JG. Hydrophobins line air channels in fruiting bodies of *Schizophyllum commune* and *Agaricus bisporus*. *Mycol Res* **1999**, 103(5):635-640.

[214] Scherrer S, De Vries OM, Dudler R, Wessels JG, Honegger R. Interfacial self-assembly of fungal hydrophobins of the lichen-forming ascomycetes *Xanthoria parietina* and *X. ectaneoides*. *Fungal Genet Biol* **2000**, 30(1):81-93.

[215] Trembley ML, Ringli C, Honegger R. Hydrophobins DGH1, DGH2, and DGH3 in the lichen-forming basidiomycete *Dictyonema glabratum*. *Fungal Genet Biol* **2002**, 35(3):247-259.

[216] Beckerman JL, Ebbole DJ. *MPG1*, a gene encoding a fungal hydrophobin of *Magnaporthe grisea*, is involved in surface recognition. *Mol Plant Microbe Interact* **1996**, 9(6):450-456.

[217] Izumitsu K, Kimura S, Kobayashi H, Morita A, Saitoh Y, Tanaka C. Class I hydrophobin BcHpb1 is important for adhesion but not for later infection of *Botrytis cinerea. J Gen Plant Pathol* **2010**, 76(4):254-260.

[218] Temple B, Horgen PA, Bernier L, Hintz WE. Cerato-ulmin, a hydrophobin secreted by the causal agents of Dutch elm disease, is a parasitic fitness factor. *Fungal Genet Biol* **1997**, 22(1):39-53.

[219] Takahashi T, Maeda H, Yoneda S, Ohtaki S, Yamagata Y, Hasegawa F, Gomi K, Nakajima T, Abe K. The fungal hydrophobin RolA recruits polyesterase and laterally moves on hydrophobic surfaces. *Mol Microbiol* **2005**, 57(6):1780-1796.

[220] Takahashi T, Tanaka T, Tsushima Y, Muragaki K, Uehara K, Takeuchi S, Maeda H, Yamagata Y, Nakayama M, Yoshimi A, Abe K. Ionic interaction of positive amino acid residues of fungal hydrophobin RolA with acidic amino acid residues of cutinase CutL1. *Mol Microbiol* **2015**, 96(1):14-27.

[221] Kazmierczak P, Kim DH, Turina M, Van Alfen NK. A hydrophobin of the chestnut blight fungus, *Cryphonectria parasitica*, is required for stromal pustule eruption. *Eukaryot Cell* **2005**, 4(5):931-936.

[222] Kim S, Ahn IP, Rho HS, Lee YH. *MHP1*, a *Magnaporthe grisea* hydrophobin gene, is required for fungal development and plant colonization. *Mol Microbiol* **2005**, 57(5):1224-1237.

[223] Sevim A, Donzelli BG, Wu D, Demirbag Z, Gibson DM, Turgeon BG. Hydrophobin genes of the entomopathogenic fungus, *Metarhizium brunneum*, are differentially expressed and corresponding mutants are decreased in virulence. *Curr Genet* **2012**, 58(2):79-92.

[224] Aimanianda V, Bayry J, Bozza S, Kniemeyer O, Perruccio K, Elluru SR, Clavaud C, Paris S, Brakhage AA, Kaveri SV, Romani L, Latgé JP. Surface hydrophobin prevents immune recognition of airborne fungal spores. *Nature* **2009**, 460(7259):1117-1121.

[225] Bruns S, Kniemeyer O, Hasenberg M, Aimanianda V, Nietzsche S, Thywissen A, Jeron A, Latgé JP, Brakhage AA, Gunzer M. Production of extracellular traps against *Aspergillus fumigatus in vitro* and in infected lung tissue is dependent on invading neutrophils and influenced by hydrophobin RodA. *PLoS Pathog* **2010**, 6(4):e1000873.

[226] Dagenais TR, Giles SS, Aimanianda V, Latgé JP, Hull CM, Keller NP. *Aspergillus fumigatus* LaeA-mediated phagocytosis is associated with a decreased hydrophobin layer. *Infect Immun* **2010**, 78(2):823-829.

[227] Paris S, Debeaupuis JP, Crameri R, Carey M, Charlès F, Prévost MC, Schmitt C, Philippe B, Latgé JP. Conidial hydrophobins of *Aspergillus fumigatus*. *Appl Environ Microbiol* **2003**, 69(3):1581-1588.

[228] Rambach G, Blum G, Latgé JP, Fontaine T, Heinekamp T, Hagleitner M, Jeckström H, Weigel G, Würtinger P, Pfaller K, Krappmann S, Löffler J, Lass-Flörl C, Speth C. Identification of *Aspergillus fumigatus* surface components that mediate interaction of conidia and hyphae with human platelets. *J Infect Dis* **2015**, 212(7):1140-1149.

[229] Klimes A, Dobinson KF. A hydrophobin gene, *VDH1*, is involved in microsclerotial development and spore viability in the plant pathogen *Verticillium dahliae*. *Fungal Genet Biol* **2006**, 43(4):283-294.

[230] van Wetter MA, Wösten HA, Sietsma JH, Wessels JG. Hydrophobin gene expression affects hyphal wall composition in *Schizophyllum commune*. *Fungal Genet Biol* **2000**, 31(2):99-104.

[231] Fuchs U, Czymmek KJ, Sweigard JA. Five hydrophobin genes in *Fusarium verticillioides* include two required for microconidial chain formation. *Fungal Genet Biol* **2004**, 41(9):852-864.

[232] Brown NA, Ries LN, Reis TF, Rajendran R, Corrêa Dos Santos RA, Ramage G, Riaño-Pachón DM, Goldman GH. RNAseq reveals hydrophobins that are involved in the adaptation of *Aspergillus nidulans* to lignocellulose. *Biotechnol Biofuels* **2016**, 9:145.

[233] Mankel A, Krause K, Kothe E. Identification of a hydrophobin gene that is developmentally regulated in the ectomycorrhizal fungus *Tricholoma terreum*. *Appl Environ Microbiol* **2002**, 68(3):1408-1413.

[234] Dubey MK, Jensen DF, Karlsson M. Hydrophobins are required for conidial hydrophobicity and plant root colonization in the fungal biocontrol agent *Clonostachys rosea*. *BMC Microbiol* **2014**, 14:18.

[235] Huang Y, Mijiti G, Wang Z, Yu W, Fan H, Zhang R, Liu Z. Functional analysis of the class II hydrophobin gene *HFB2-6* from the biocontrol agent *Trichoderma asperellum* ACCC30536. *Microbiol Res* **2015**, 171:8-20.

[236] Viterbo A, Chet I. *TasHyd1*, a new hydrophobin gene from the biocontrol agent *Trichoderma asperellum*, is involved in plant root colonization. *Mol Plant Pathol* **2006**, 7(4):249-258.

[237] Bromley KM, Morris RJ, Hobley L, Brandani G, Gillespie RM, McCluskey M, Zachariae U, Marenduzzo D, Stanley-Wall NR, MacPhee CE. Interfacial self-assembly of a bacterial hydrophobin. *Proc Natl Acad Sci USA* **2015**, 112(17):5419-5424.

[238] Hobley L, Ostrowski A, Rao FV, Bromley KM, Porter M, Prescott AR, MacPhee CE, van Aalten DM, Stanley-Wall NR. BslA is a self-assembling bacterial hydrophobin that coats the *Bacillus subtilis* biofilm. *Proc Natl Acad Sci USA* **2013**, 110(33):13600-13605.

[239] Kobayashi K, Iwano M. BslA(YuaB) forms a hydrophobic layer on the surface of *Bacillus subtilis* biofilms. *Mol Microbiol* **2012**, 85(1):51-66.

[240] Elliot MA, Talbot NJ. Building filaments in the air: aerial morphogenesis in bacteria and fungi. *Curr Opin Microbiol* **2004**, 7(6):594-601.

[241] Teertstra WR, Deelstra HJ, Vranes M, Bohlmann R, Kahmann R, Kämper J, Wösten HA. Repellents have functionally replaced hydrophobins in mediating attachment to a hydrophobic surface and in formation of hydrophobic aerial hyphae in *Ustilago maydis*. *Microbiology* **2006**, 152(Pt 12):3607-3612.

[242] Teertstra WR, van der Velden GJ, de Jong JF, Kruijtzer JA, Liskamp RM, Kroon-Batenburg LM, Müller WH, Gebbink MF, Wösten HA. The filament-specific Rep1-1 repellent of the phytopathogen *Ustilago maydis* forms functional surface-active amyloid-like fibrils. *J Biol Chem* **2009**, 284(14):9153-9159.

[243] Wösten HA, Bohlmann R, Eckerskorn C, Lottspeich F, Bölker M, Kahmann R. A novel class of small amphipathic peptides affect aerial hyphal growth and surface hydrophobicity in *Ustilago maydis*. *EMBO J* **1996**, 15(16):4274-4281.

[244] Khalesi M, Gebruers K, Derdelinckx G. Recent advances in fungal hydrophobin towards using in industry. *Protein J* **2015**, 34(4):243-255.

[245] Scholtmeijer K, Wessels JG, Wösten HA. Fungal hydrophobins in medical and technical applications. *Appl Microbiol Biotechnol* **2001**, 56(1-2):1-8.

[246] Gruner LJ, Ostermann K, Rödel G. Layer thickness of hydrophobin films leads to oscillation in wettability. *Langmuir* **2012**, 28(17):6942-6949.

[247] Bimbo LM, Mäkilä E, Raula J, Laaksonen T, Laaksonen P, Strommer K, Kauppinen EI, Salonen J, Linder MB, Hirvonen J, Santos HA. Functional hydrophobin-coating of thermally hydrocarbonized porous silicon microparticles. *Biomaterials* **2011**, 32(34):9089-9099.

[248] Boeuf S, Throm T, Gutt B, Strunk T, Hoffmann M, Seebach E, Mühlberg L, Brocher J, Gotterbarm T, Wenzel W, Fischer R, Richter W. Engineering hydrophobin DewA to generate surfaces that enhance adhesion of human but not bacterial cells. *Acta Biomater* **2012**, 8(3):1037-1047.

[249] Huang Y, Zhang S, Niu B, Wang D, Wang Z, Feng S, Xu H, Kong D, Qiao M. Poly(ε-caprolactone) modified with fusion protein containing self-assembled hydrophobin and functional peptide for selective capture of human blood outgrowth endothelial cells. *Colloids Surf B Biointerfaces* **2013**, 101:361-369.

[250] Janssen MI, van Leeuwen MB, Scholtmeijer K, van Kooten TG, Dijkhuizen L, Wösten HA. Coating with genetic engineered hydrophobin promotes growth of fibroblasts on a hydrophobic solid. *Biomaterials* **2002**, 23(24):4847-4854.

[251] Janssen MI, van Leeuwen MB, van Kooten TG, de Vries J, Dijkhuizen L, Wösten HA. Promotion of fibroblast activity by coating with hydrophobins in the β-sheet end state. *Biomaterials* **2004**, 25(14):2731-2739.

[252] Sarparanta MP, Bimbo LM, Mäkilä EM, Salonen JJ, Laaksonen PH, Helariutta AM, Linder MB, Hirvonen JT, Laaksonen TJ, Santos HA, Airaksinen AJ. The mucoadhesive and gastroretentive properties of hydrophobin-coated porous silicon nanoparticle oral drug delivery systems. *Biomaterials* **2012**, 33(11):3353-3362.

[253] Wang Z, Feng S, Huang Y, Li S, Xu H, Zhang X, Bai Y, Qiao M. Expression and characterization of a *Grifola frondosa* hydrophobin in *Pichia pastoris*. *Protein Expr Purif* **2010**, 72(1):19-25.

[254] Hakala TJ, Laaksonen P, Saikko V, Ahlroos T, Helle A, Mahlberg R, Hähl H, Jacobs K, Kuosmanen P, Linder MB, Holmberg K. Adhesion and tribological properties of hydrophobin proteins in aqueous lubrication on stainless steel surfaces. *RSC Adv* **2012**, 2:9867-9872.

[255] Lee S, Røn T, Pakkanen KI, Linder M. Hydrophobins as aqueous lubricant additive for a soft sliding contact. *Colloids Surf B Biointerfaces* **2015**, 125:264-269.

[256] Misra R, Li J, Cannon GC, Morgan SE. Nanoscale reduction in surface friction of polymer surfaces modified with Sc3 hydrophobin from *Schizophyllum commune*. *Biomacromolecules* **2006**, 7(5):1463-1470.

[257] Hou S, Li X, Li X, Feng XZ, Wang R, Wang C, Yu L, Qiao MQ. Surface modification using a novel type I hydrophobin HGFI. *Anal Bioanal Chem* **2009**, 394(3):783-789.

[258] Laaksonen P, Kivioja J, Paananen A, Kainlauri M, Kontturi K, Ahopelto J, Linder MB. Selective nanopatterning using citrate-stabilized Au nanoparticles and cystein-modified amphiphilic protein. *Langmuir* **2009**, 25(9):5185-5192.

[259] Li X, Hou S, Feng X, Yu Y, Ma J, Li L. Patterning of neural stem cells on poly(lactic-co-glycolic acid) film modified by hydrophobin. *Colloids Surf B Biointerfaces* **2009**, 74(1):370-374.

[260] Qin M, Hou S, Wang L, Feng X, Wang R, Yang Y, Wang C, Yu L, Shao B, Qiao M. Two methods for glass surface modification and their application in protein immobilization. *Colloids Surf B Biointerfaces* **2007**, 60(2):243-249.

[261] Qin M, Wang LK, Feng XZ, Yang YL, Wang R, Wang C, Yu L, Shao B, Qiao MQ. Bioactive surface modification of mica and poly(dimethylsiloxane) with hydrophobins for protein immobilization. *Langmuir* **2007**, 23(8):4465-4471.

[262] Longobardi S, Gravagnuolo AM, Rea I, De Stefano L, Marino G, Giardina P. Hydrophobin-coated plates as matrix-assisted laser desorption/ionization sample support for peptide/protein analysis. *Anal Biochem* **2014**, 449:9-16.

[263] Niu B, Huang Y, Zhang S, Wang D, Xu H, Kong D, Qiao M. Expression and characterization of hydrophobin HGFI fused with the cell-specific peptide TPS in *Pichia pastoris*. *Protein Expr Purif* **2012**, 83(1):92-97.

[264] Scholtmeijer K, Janssen MI, Gerssen B, de Vocht ML, van Leeuwen BM, van Kooten TG, Wösten HA, Wessels JG. Surface modifications created by using engineered hydrophobins. *Appl Environ Microbiol* **2002**, 68(3):1367-1373.

[265] Soikkeli M, Kurppa K, Kainlauri M, Arpiainen S, Paananen A, Gunnarsson D, Joensuu JJ, Laaksonen P, Prunnila M, Linder MB, Ahopelto J. Graphene biosensor programming with genetically engineered fusion protein monolayers. *ACS Appl Mater Interfaces* **2016**, 8(12):8257-8264.

[266] De Stefano L, Rea I, De Tommasi E, Rendina I, Rotiroti L, Giocondo M, Longobardi S, Armenante A, Giardina P. Bioactive modification of silicon surface using self-assembled hydrophobins from *Pleurotus ostreatus*. *Eur Phys J E Soft Matter* **2009**, 30(2):181-185.

[267] Fokina O, Fenchel A, Winandy L, Fischer R. Immobilization of LccC laccase from *Aspergillus nidulans* on hard surfaces using fungal hydrophobins. *Appl Environ Microbiol* **2016**, 82(21):6395-6402.

[268] Kurppa K, Hytönen VP, Nakari-Setälä T, Kulomaa MS, Linder MB. Molecular engineering of avidin and hydrophobin for functional self-assembling interfaces. *Colloids Surf B Biointerfaces* **2014**, 120:102-109.

[269] Linder M, Szilvay GR, Nakari-Setälä T, Söderlund H, Penttilä M. Surface adhesion of fusion proteins containing the hydrophobins HFBI and HFBII from *Trichoderma reesei*. *Protein Sci* **2002**, 11(9):2257-2266.

[270] Longobardi S, Gravagnuolo AM, Funari R, Della Ventura B, Pane F, Galano E, Amoresano A, Marino G, Giardina P. A simple MALDI plate functionalization by Vmh2 hydrophobin for serial multi-enzymatic protein digestions. *Anal Bioanal Chem* **2015**, 407(2):487-496.

[271] Palomo JM, Peñas MM, Fernández-Lorente G, Mateo C, Pisabarro AG, Fernández-Lafuente R, Ramírez L, Guisán JM. Solid-phase handling of hydrophobins: immobilized hydrophobins as a new tool to study lipases. *Biomacromolecules* **2003**, 4(2):204-210.

[272] Patel E, Cicatiello P, Deininger L, Clench MR, Marino G, Giardina P, Langenburg G, West A, Marshall P, Sears V, Francese S. A proteomic approach for the rapid, multi-informative and reliable identification of blood. *Analyst* **2016**, 141(1):191-198.

[273] Piscitelli A, Pennacchio A, Longobardi S, Velotta R, Giardina P. Vmh2 hydrophobin as a tool for the development of "self-immobilizing" enzymes for biosensing. *Biotechnol Bioeng* **2016**, in press.

[274] Takatsuji Y, Yamasaki R, Iwanaga A, Lienemann M, Linder MB, Haruyama T. Solid-support immobilization of a "swing" fusion protein for enhanced glucose oxidase catalytic activity. *Colloids Surf B Biointerfaces* **2013**, 112:186-191.

[275] Piscitelli A, Pennacchio A, Cicatiello P, Politi J, De Stefano L, Giardina P. Rapid and ultrasensitive detection of active thrombin based on the Vmh2 hydrophobin fused to a green fluorescent protein. *Biosens Bioelectron* **2016**, 87:816-822.

[276] Zhao L, Liu J, Song D, Wang X, Tai F, Xu H, Qiao M. A visualized fusion protein based on self-assembly hydrophobin HGFI. *Chem Res Chinese U* **2015**, 31(5):781-786.

[277] Asakawa H, Tahara S, Nakamichi M, Takehara K, Ikeno S, Linder MB, Haruyama T. The amphiphilic protein HFBII as a genetically taggable molecular carrier for the formation of a self-organized functional protein layer on a solid surface. *Langmuir* **2009**, 25(16):8841-8844.

[278] Iwanaga A, Asakawa H, Fukuma T, Nakamichi M, Shigematsu S, Linder MB, Haruyama T. Ordered nano-structure of a stamped self-organized protein layer on a HOPG surface using a HFB carrier. *Colloids Surf B Biointerfaces* **2011**, 84(2):395-399.

[279] Varjonen S, Laaksonen P, Paananen A, Valo H, Hähl H, Laaksonen T, Linder MB. Self-assembly of cellulose nanofibrils by genetically engineered fusion proteins. *Soft Matter* **2011**, 7:2402-2411.

[280] Wang Z, Huang Y, Li S, Xu H, Linder MB, Qiao M. Hydrophilic modification of polystyrene with hydrophobin for time-resolved immunofluorometric assay. *Biosens Bioelectron* **2010**, 26(3):1074-1079.

[281] Wang Z, Lienemann M, Qiau M, Linder MB. Mechanisms of protein adhesion on surface films of hydrophobin. *Langmuir* **2010**, 26(11):8491-8496.

[282] Zhang M, Wang Z, Wang Z, Feng S, Xu H, Zhao Q, Wang S, Fang J, Qiao M, Kong D. Immobilization of anti-CD31 antibody on electrospun poly(ε-caprolactone) scaffolds through hydrophobins for specific adhesion of endothelial cells. *Colloids Surf B Biointerfaces* **2011**, 85(1):32-39.

[283] Kostiainen MA, Szilvay GR, Smith DK, Linder MB, Ikkala O. Multivalent dendrons for high-affinity adhesion of proteins to DNA. *Angew Chem Int Ed Engl* **2006**, 45(21):3538-3542.

[284] Bilewicz R, Witomski J, Van der Heyden A, Tagu D, Palin B, Rogalska E. Modification of electrodes with self-assembled hydrophobin layers. *J Phys Chem B* **2001**, 105(40):9772-9777.

[285] Corvis Y, Walcarius A, Rink R, Mrabet NT, Rogalska E. Preparing catalytic surfaces for sensing applications by immobilizing enzymes *via* hydrophobin layers. *Anal Chem* **2005**, 77(6):1622-1630.

[286] Zhao ZX, Qiao MQ, Yin F, Shao B, Wu BY, Wang YY, Wang XS, Qin X, Li S, Yu L, Chen Q. Amperometric glucose biosensor based on self-assembly hydrophobin with high efficiency of enzyme utilization. *Biosens Bioelectron* **2007**, 22(12):3021-3027.

[287] Zhao ZX, Wang HC, Qin X, Wang XS, Qiao MQ, Anzai J, Chen Q. Self-assembled film of hydrophobins on gold surfaces and its application to electrochemical biosensing. *Colloids Surf B Biointerfaces* **2009**, 71(1):102-106.

[288] Della Ventura B, Rea I, Caliò A, Giardina P, Gravagnuolo AM, Funari R, Altucci C, Velotta R, De Stefano L. Vmh2 hydrophobin layer entraps glucose: a quantitative characterization by label-free optical and gravimetric methods. *Appl Surf Sci* **2016**, 364:201-207.

[289] Politi J, De Stefano L, Rea I, Gravagnuolo AM, Giardina P, Methivier C, Casale S, Spadavecchia J. One-pot synthesis of a gold nanoparticle-Vmh2 hydrophobin nanobiocomplex for glucose monitoring. *Nanotechnology* **2016**, 27(19):195701.

[290] Akanbi MH, Post E, van Putten SM, de Vries L, Smisterova J, Meter-Arkema AH, Wösten HA, Rink R, Scholtmeijer K. The antitumor activity of hydrophobin SC3, a fungal protein. *Appl Microbiol Biotechnol* **2013**, 97(10):4385-4392.

[291] Carpenter CE, Mueller RJ, Kazmierczak P, Zhang L, Villalon DK, Van Alfen NK. Effect of a virus on accumulation of a tissue-specific cell-surface protein of the fungus *Cryphonectria* (*Endothia*) *parasitica*. *Mol Plant Microbe Interact* **1992**, 5(1):55-61.

[292] Fang G, Tang B, Liu Z, Gou J, Zhang Y, Xu H, Tang X. Novel hydrophobin-coated docetaxel nanoparticles for intravenous delivery: *in vitro* characteristics and *in vivo* performance. *Eur J Pharm Sci* **2014**, 60:1-9.

[293] Jacquet N, Navarre C, Desmecht D, Boutry M. Hydrophobin fusion of an influenza virus hemagglutinin allows high transient expression in *Nicotiana benthamiana*, easy purification and immune response with neutralizing activity. *PLoS One* **2014**, 9(12):e115944.

[294] Yang W, Ren Q, Wu YN, Morris VK, Rey AA, Braet F, Kwan AH, Sunde M. Surface functionalization of carbon nanomaterials by self-assembling hydrophobin proteins. *Biopolymers* **2013**, 99(1):84-94.

[295] Hou S, Li X, Li X, Feng X. Coating of hydrophobins on three-dimensional electrospun poly(lactic-co-glycolic acid) scaffolds for cell adhesion. *Biofabrication* **2009**, 1(3):035004.

[296] Milani R, Monogioudi E, Baldrighi M, Cavallo G, Arima V, Marra L, Zizzari A, Rinaldi R, Linder M, Resnati G, Metrangolo P. Hydrophobin: fluorosurfactant-like properties without fluorine. *Soft Matter* **2013**, 9:6505-6514.

[297] Reger M, Sekine T, Okamoto T, Hoffmann H. Unique emulsions based on biotechnically produced hydrophobins. *Soft Matter* **2011**, 7:8248-8257.

[298] Reger M, Hoffmann H. Hydrophobin coated boehmite nanoparticles stabilizing oil in water emulsions. *J Colloid Interface Sci* **2012**, 368(1):378-386.

[299] Schulz A, Liebeck BM, John D, Heiss A, Subkowski T, Böker A. Protein-mineral hybrid capsules from emulsions stabilized with an amphiphilic protein. *J Mater Chem* **2011**, 21:9731-9736.

[300] Tchuenbou-Magaia FL, Norton IT, Cox PW. Hydrophobins stabilised air-filled emulsions for the food industry. *Food Hydrocolloid* **2009**, 23(7):1877-1885.

[301] Cox AR, Aldred DL, Russell AB. Exceptional stability of food foams using class II hydrophobin HFBII. *Food Hydrocolloid* **2009**, 23(2):366-376.

[302] Crilly JF, Russell AB, Cox AR, Cebula DJ. Designing multiscale structures for desired properties of ice cream. *Ind Eng Chem Res* **2008**, 47(17):6362-6367.

[303] Wohlleben W, Subkowski T, Bollschweiler C, von Vacano B, Liu Y, Schrepp W, Baus U. Recombinantly produced hydrophobins from fungal analogues as highly surface-active performance proteins. *Eur Biophys J* **2010**, 39(3):457-468.

[304] Lutterschmid G, Muranyi M, Stübner M, Vogel RF, Niessen L. Heterologous expression of surface-active proteins from barley and filamentous fungi in *Pichia pastoris* and characterization of their contribution to beer gushing. *Int J Food Microbiol* **2011**, 147(1):17-25.

[305] Sarlin T, Nakari-Setälä T, Linder M, Penttilä M, Haikara A. Fungal hydrophobins as predictors of the gushing activity of malt. *J I Brewing* **2005**, 111(2):105-111.

[306] Shokribousjein Z, Riveros Galan D, Losada-Pérez P, Wagner P, Lammertyn J, Arghir I, Golreihan A, Verachtert H, Aydın AA, De Maeyer M, Titze J, Ilberg V, Derdelinckx G. Mechanism of nonpolar model substances to inhibit primary gushing induced by hydrophobin HFBI. *J Agric Food Chem* **2015**, 63(18):4673-4682.

[307] Stübner M, Lutterschmid G, Vogel RF, Niessen L. Heterologous expression of the hydrophobin FcHyd5p from *Fusarium culmorum* in *Pichia pastoris* and evaluation of its surface activity and contribution to gushing of carbonated beverages. *Int J Food Microbiol* **2010**, 141(1-2):110-115.

[308] Zapf MW, Theisen S, Vogel RF, Niessen L. Cloning of wheat LTP1500 and two *Fusarium culmorum* hydrophobins in *Saccharomyces cerevisiae* and assessment of their gushing inducing potential in experimental wort fermentation. *J I Brewing* **2006**, 112(3):237-245.

[309] Grunér MS, Kauscher U, Linder MB, Monopoli MP. An environmental route of exposure affects the formation of nanoparticle coronas in blood plasma. *J Proteomics* **2016**, 137:52-58.

[310] Peters R, Sandiford L, Owen DM, Kemal E, Bourke S, Dailey LA, Green M. Red-emitting protein-coated conjugated polymer nanoparticles. *Photochem Photobiol Sci* **2016**, in press.

[311] Pigliacelli C, D'Elicio A, Milani R, Terraneo G, Resnati G, Bombelli FB, Metrangolo P. Hydrophobin-stabilized dispersions of PVDF nanoparticles in water. *J Fluorine Chem* **2015**, 177:62-69.

[312] Politi J, De Stefano L, Longobardi S, Giardina P, Rea I, Methivier C, Pradier CM, Casale S, Spadavecchia J. The amphiphilic hydrophobin Vmh2 plays a key role in one step synthesis of hybrid protein-gold nanoparticles. *Colloids Surf B Biointerfaces* **2015**, 136:214-221.

[313] Wang K, Xiao Y, Wang Y, Feng Y, Chen C, Zhang J, Zhang Q, Meng S, Wang Z, Yang H. Self-assembled hydrophobin for producing water-soluble and membrane permeable fluorescent dye. *Sci Rep* **2016**, 6:23061.

[314] Kurppa K, Jiang H, Szilvay GR, Nasibulin AG, Kauppinen EI, Linder MB. Controlled hybrid nanostructures through protein-mediated noncovalent functionalization of carbon nanotubes. *Angew Chem Int Ed Engl* **2007**, 46(34):6446-6449.

[315] Wang X, Wang H, Huang Y, Zhao Z, Qin X, Wang Y, Miao Z, Chen Q, Qiao M. Noncovalently functionalized multi-wall carbon nanotubes in aqueous solution using the hydrophobin HFBI and their electroanalytical application. *Biosens Bioelectron* **2010**, 26(3):1104-1108.

[316] Yotprayoonsak P, Szilvay GR, Laaksonen P, Linder MB, Ahlskog M. The effect of hydrophobin protein on conductive properties of carbon nanotube field-effect transistors: first study on sensing mechanism. *J Nanosci Nanotechnol* **2015**, 15(3):2079-2087.

[317] Laaksonen P, Kainlauri M, Laaksonen T, Shchepetov A, Jiang H, Ahopelto J, Linder MB. Interfacial engineering by proteins: exfoliation and functionalization of graphene by hydrophobins. *Angew Chem Int Ed Engl* **2010**, 49(29):4946-4949.

[318] Taniguchi S, Sandiford L, Cooper M, Rosca EV, Ahmad Khanbeigi R, Fairclough SM, Thanou M, Dailey LA, Wohlleben W, von Vacano B, de Rosales RT, Dobson PJ, Owen DM, Green M. Hydrophobin-encapsulated quantum dots. *ACS Appl Mater Interfaces* **2016**, 8(7):4887-4893.

[319] Haas Jimoh Akanbi M, Post E, Meter-Arkema A, Rink R, Robillard GT, Wang X, Wösten HA, Scholtmeijer K. Use of hydrophobins in formulation of water insoluble drugs for oral administration. *Colloids Surf B Biointerfaces* **2010**, 75(2):526-531.

[320] Israeli-Lev G, Livney YD. Self-assembly of hydrophobin and its co-assembly with hydrophobic nutraceuticals in aqueous solutions: towards application as delivery systems. *Food Hydrocolloid* **2014**, 35:28-35.

[321] Valo HK, Laaksonen PH, Peltonen LJ, Linder MB, Hirvonen JT, Laaksonen TJ. Multifunctional hydrophobin: toward functional coatings for drug nanoparticles. *ACS Nano* **2010**, 4(3):1750-1758.

[322] Valo H, Kovalainen M, Laaksonen P, Häkkinen M, Auriola S, Peltonen L, Linder M, Järvinen K, Hirvonen J, Laaksonen T. Immobilization of protein-coated drug nanoparticles in nanofibrillar cellulose matrices - enhanced stability and release. *J Control Release* **2011**, 156(3):390-397.

[323] Gutiérrez SP, Saberianfar R, Kohalmi SE, Menassa R. Protein body formation in stable transgenic tobacco expressing elastin-like polypeptide and hydrophobin fusion proteins. *BMC Biotechnol* **2013**, 13:40.

[324] Joensuu JJ, Conley AJ, Lienemann M, Brandle JE, Linder MB, Menassa R. Hydrophobin fusions for high-level transient protein expression and purification in *Nicotiana benthamiana*. *Plant Physiol* **2010**, 152(2):622-633.

[325] Phan HT, Hause B, Hause G, Arcalis E, Stoger E, Maresch D, Altmann F, Joensuu J, Conrad U. Influence of elastin-like polypeptide and hydrophobin on recombinant hemagglutinin accumulations in transgenic tobacco plants. *PLoS One* **2014**, 9(6):e99347.

[326] Reuter LJ, Bailey MJ, Joensuu JJ, Ritala A. Scale-up of hydrophobin-assisted recombinant protein production in tobacco BY-2 suspension cells. *Plant Biotechnol J* **2014**, 12(4):402-410.

[327] Reuter L, Ritala A, Linder M, Joensuu J. Novel hydrophobin fusion tags for plant-produced fusion proteins. *PLoS One* **2016**, 11(10):e0164032.

[328] Saberianfar R, Joensuu JJ, Conley AJ, Menassa R. Protein body formation in leaves of *Nicotiana benthamiana*: a concentration-dependent mechanism influenced by the presence of fusion tags. *Plant Biotechnol J* **2015**, 13(7):927-937.

[329] Mustalahti E, Saloheimo M, Joensuu JJ. Intracellular protein production in *Trichoderma reesei* (*Hypocrea jecorina*) with hydrophobin fusion technology. *N Biotechnol* **2013**, 30(2):262-268.

[330] Opwis K, Gutmann JS. Surface modification of textile materials with hydrophobins. *Text Res J* **2011**, 81(15):1594-1602.

[331] De Stefano L, Rea I, Armenante A, Giardina P, Giocondo M, Rendina I. Self-assembled biofilm of hydrophobins protects the silicon surface in the KOH wet etch process. *Langmuir* **2007**, 23(15):7920-7922.

[332] Heinonen H, Laaksonen P, Linder M, Hentze H. Engineered hydrophobin for biomimetic mineralization of functional calcium carbonate microparticles. *J Biomater Nanobiotechnol* **2014**, 5(1):1-7.

[333] Melcher M, Facey SJ, Henkes TM, Subkowski T, Hauer B. Accelerated nucleation of hydroxyapatite using an engineered hydrophobin fusion protein. *Biomacromolecules* **2016**, 17(5):1716-1726.

[334] Schulz S, Schumacher D, Raszkowski D, Girhard M, Urlacher VB. Fusion to hydrophobin HFBI improves the catalytic performance of a cytochrome P450 system. *Front Bioeng Biotechnol* **2016**, 4:57.

[335] Zhao L, Xu H, Li Y, Song D, Wang X, Qiao M, Gong M. Novel application of hydrophobin in medical science: a drug carrier for improving serum stability. *Sci Rep* **2016**, 6:26461.

[336] Lohrasbi-Nejad A, Torkzadeh-Mahani M, Hosseinkhani S. Hydrophobin-1 promotes thermostability of firefly luciferase. *FEBS J* **2016**, 283(13):2494-2507.

[337] Herskowitz I. Life cycle of the budding yeast *Saccharomyces cerevisiae*. *Microbiol Rev* **1988**, 52(4):536-553.

[338] Souza CA, Silva CC, Ferreira AV. Sex in fungi: lessons of gene regulation. *Genet Mol Res* **2003**, 2(1):136-147.

[339] Haber JE. Mating-type gene switching in *Saccharomyces cerevisiae*. *Annu Rev Genet* **1998**, 32:561-599.

[340] Herskowitz I. A regulatory hierarchy for cell specialization in yeast. *Nature* **1989**, 342(6251):749-757.

[341] Strathern J, Hicks J, Herskowitz I. Control of cell type in yeast by the mating type locus. The α1-α2 hypothesis. *J Mol Biol* **1981**, 147(3):357-372.

[342] Dolan JW, Fields S. Cell-type-specific transcription in yeast. *Biochim Biophys Acta* **1991**, 1088(2):155-169.

[343] Johnson AD. Molecular mechanisms of cell-type determination in budding yeast. *Curr Opin Genet Dev* **1995**, 5(5):552-558.

[344] Davey J, Davis K, Hughes M, Ladds G, Powner D. The processing of yeast pheromones. *Semin Cell Dev Biol* **1998**, 9(1):19-30.

[345] Jones SK Jr, Bennett RJ. Fungal mating pheromones: choreographing the dating game. *Fungal Genet Biol* **2011**, 48(7):668-676.

[346] Chen P, Sapperstein SK, Choi JD, Michaelis S. Biogenesis of the *Saccharomyces cerevisiae* mating pheromone **a**-factor. *J Cell Biol* **1997**, 136(2):251-269.

[347] Kurjan J, Herskowitz I. Structure of a yeast pheromone gene (*MFα*): a putative α-factor precursor contains four tandem copies of mature α-factor. *Cell* **1982**, 30(3):933-943.

[348] Singh A, Chen EY, Lugovoy JM, Chang CN, Hitzeman RA, Seeburg PH. *Saccharomyces cerevisiae* contains two discrete genes coding for the α-factor pheromone. *Nucleic Acids Res* **1983**, 11(12):4049-4063.

[349] Waters MG, Evans EA, Blobel G. Prepro-α-factor has a cleavable signal sequence. *J Biol Chem* **1988**, 263(13):6209-6214.

[350] Caplan S, Green R, Rocco J, Kurjan J. Glycosylation and structure of the yeast *MFα1* α-factor precursor is important for efficient transport through the secretory pathway. *J Bacteriol* **1991**, 173(2):627-635.

[351] Julius D, Schekman R, Thorner J. Glycosylation and processing of prepro-α-factor through the yeast secretory pathway. *Cell* **1984**, 36(2):309-318.

[352] Julius D, Brake A, Blair L, Kunisawa R, Thorner J. Isolation of the putative structural gene for the lysine-arginine-cleaving endopeptidase required for processing of yeast prepro-α-factor. *Cell* **1984**, 37(3):1075-1089.

[353] Redding K, Holcomb C, Fuller RS. Immunolocalization of Kex2 protease identifies a putative late Golgi compartment in the yeast *Saccharomyces cerevisiae*. *J Cell Biol* **1991**, 113(3):527-538.

[354] Dmochowska A, Dignard D, Henning D, Thomas DY, Bussey H. Yeast *KEX1* gene encodes a putative protease with a carboxypeptidase B-like function involved in killer toxin and α-factor precursor processing. *Cell* **1987**, 50(4):573-584.

[355] Julius D, Blair L, Brake A, Sprague G, Thorner J. Yeast α factor is processed from a larger precursor polypeptide: the essential role of a membrane-bound dipeptidyl aminopeptidase. *Cell* **1983**, 32(3):839-852.

[356] Erdman S, Lin L, Malczynski M, Snyder M. Pheromone-regulated genes required for yeast mating differentiation. *J Cell Biol* **1998**, 140(3):461-483.

[357] Roberts CJ, Nelson B, Marton MJ, Stoughton R, Meyer MR, Bennett HA, He YD, Dai H, Walker WL, Hughes TR, Tyers M, Boone C, Friend SH. Signaling and circuitry of multiple MAPK pathways revealed by a matrix of global gene expression profiles. *Science* **2000**, 287(5454):873-880.

[358] Alvaro CG, Thorner J. Heterotrimeric G protein-coupled receptor signaling in yeast mating pheromone response. *J Biol Chem* **2016**, 291(15):7788-7795.

[359] Bardwell L. A walk-through of the yeast mating pheromone response pathway. *Peptides* **2005**, 26(2):339-350.

[360] Dohlman HG, Thorner JW. Regulation of G protein-initiated signal transduction in yeast: paradigms and principles. *Annu Rev Biochem* **2001**, 70:703-754.

[361] Elion EA. Pheromone response, mating and cell biology. *Curr Opin Microbiol* **2000**, 3(6):573-581.

[362] Gustin MC, Albertyn J, Alexander M, Davenport K. MAP kinase pathways in the yeast *Saccharomyces cerevisiae*. *Microbiol Mol Biol Rev* **1998**, 62(4):1264-1300.

[363] Marsh L, Neiman AM, Herskowitz I. Signal transduction during pheromone response in yeast. *Annu Rev Cell Biol* **1991**, 7:699-728.

[364] Merlini L, Dudin O, Martin SG. Mate and fuse: how yeast cells do it. *Open Biol* **2013**, 3(3):130008.

[365] Naider F, Becker JM. The α-factor mating pheromone of *Saccharomyces cerevisiae*: a model for studying the interaction of peptide hormones and G protein-coupled receptors. *Peptides* **2004**, 25(9):1441-1463.

[366] Banderas A, Koltai M, Anders A, Sourjik V. Sensory input attenuation allows predictive sexual response in yeast. *Nat Commun* **2016**, 7:12590.

[367] Chan RK, Otte CA. Physiological characterization of *Saccharomyces cerevisiae* mutants supersensitive to G1 arrest by **a** factor and α factor pheromones. *Mol Cell Biol* **1982**, 2(1):21-29.

[368] Ciejek E, Thorner J. Recovery of *S. cerevisiae* **a** cells from G1 arrest by α factor pheromone requires endopeptidase action. *Cell* **1979**, 18(3):623-635.

[369] Jin M, Errede B, Behar M, Mather W, Nayak S, Hasty J, Dohlman HG, Elston TC. Yeast dynamically modify their environment to achieve better mating efficiency. *Sci Signal* **2011**, 4(186):ra54.

[370] MacKay VL, Welch SK, Insley MY, Manney TR, Holly J, Saari GC, Parker ML. The *Saccharomyces cerevisiae BAR1* gene encodes an exported protein with homology to pepsin. *Proc Natl Acad Sci USA* **1988**, 85(1):55-59.

[371] Rappaport N, Barkai N. Disentangling signaling gradients generated by equivalent sources. *J Biol Phys* **2012**, 38(2):267-278.

[372] Sprague GF Jr, Herskowitz I. Control of yeast cell type by the mating type locus. I. Identification and control of expression of the **a**-specific gene *BAR1*. *J Mol Biol* **1981**, 153(2):305-321.

[373] Bacchus W, Fussenegger M. Engineering of synthetic intercellular communication systems. *Metab Eng* **2013**, 16:33-41.

[374] Chuang JS. Engineering multicellular traits in synthetic microbial populations. *Curr Opin Chem Biol* **2012**, 16(3-4):370-378.

[375] Hennig S, Rödel G, Ostermann K. Artificial cell-cell communication as an emerging tool in synthetic biology applications. *J Biol Eng* **2015**, 9:13.

[376] Song H, Payne S, Tan C, You L. Programming microbial population dynamics by engineered cell-cell communication. *Biotechnol J* **2011**, 6(7):837-849.

[377] Song H, Ding MZ, Jia XQ, Ma Q, Yuan YJ. Synthetic microbial consortia: from systematic analysis to construction and applications. *Chem Soc Rev* **2014**, 43(20):6954-6981.

[378] Regot S, Macia J, Conde N, Furukawa K, Kjellén J, Peeters T, Hohmann S, de Nadal E, Posas F, Solé R. Distributed biological computation with multicellular engineered networks. *Nature* **2011**, 469(7329):207-211.

[379] Hoffman-Sommer M, Supady A, Klipp E. Cell-to-cell communication circuits: quantitative analysis of synthetic logic gates. *Front Physiol* **2012**, 3:287.

[380] Macia J, Manzoni R, Conde N, Urrios A, de Nadal E, Solé R, Posas F. Implementation of complex biological logic circuits using spatially distributed multicellular consortia. *PLoS Comput Biol* **2016**, 12(2):e1004685.

[381] Sardanyés J, Bonforti A, Conde N, Solé R, Macia J. Computational implementation of a tunable multicellular memory circuit for engineered eukaryotic consortia. *Front Physiol* **2015**, 6:281.

[382] Urrios A, Macia J, Manzoni R, Conde N, Bonforti A, de Nadal E, Posas F, Solé R. A synthetic multicellular memory device. *ACS Synth Biol* **2016**, 5(8):862-873.

[383] Youk H, Lim WA. Secreting and sensing the same molecule allows cells to achieve versatile social behaviors. *Science* **2014**, 343(6171):1242782.

[384] Williams TC, Nielsen LK, Vickers CE. Engineered quorum sensing using pheromone-mediated cell-to-cell communication in *Saccharomyces cerevisiae*. *ACS Synth Biol* **2013**, 2(3):136-149.

[385] Gross A, Rödel G, Ostermann K. Application of the yeast pheromone system for controlled cell-cell communication and signal amplification. *Lett Appl Microbiol* **2011**, 52(5):521-526.

[386] Jahn M, Mölle A, Rödel G, Ostermann K. Temporal and spatial properties of a yeast multi-cellular amplification system based on signal molecule diffusion. *Sensors (Basel)* **2013**, 13(11):14511-14522.

[387] Mumberg D, Müller R, Funk M. Yeast vectors for the controlled expression of heterologous proteins in different genetic backgrounds. *Gene* **1995**, 156(1):119-122.

[388] Moreno MB, Durán A, Ribas JC. A family of multifunctional thiamine-repressible expression vectors for fission yeast. *Yeast* **2000**, 16(9):861-872.

[389] Heim L. Construction of an h^{+S} strain of *Schizosaccharomyces pombe*. *Curr Genet* **1990**, 17(1):13-19.

[390] Forsburg SL, Rhind N. Basic methods for fission yeast. *Yeast* **2006**, 23(3):173-183.

[391] Gietz RD, Woods RA. Transformation of yeast by lithium acetate/single-stranded carrier DNA/polyethylene glycol method. *Methods Enzymol* **2002**, 350:87-96.

[392] Ornstein L. Disc electrophoresis. I. Background and theory. *Ann N Y Acad Sci* **1964**, 121:321-349.

[393] Schägger H. Tricine-SDS-PAGE. *Nat Protoc* **2006**, 1(1):16-22.

[394] Neuhoff V, Arold N, Taube D, Ehrhardt W. Improved staining of proteins in polyacrylamide gels including isoelectric focusing gels with clear background at nanogram sensitivity using Coomassie Brilliant Blue G-250 and R-250. *Electrophoresis* **1988**, 9(6):255-262.

[395] Bradford MM. A rapid and sensitive method for the quantitation of microgram quantities of protein utilizing the principle of protein-dye binding. *Anal Biochem* **1976**, 72:248-254.

[396] Rieder A, Ladnorg T, Wöll C, Obst U, Fischer R, Schwartz T. The impact of recombinant fusion-hydrophobin coated surfaces on *E. coli* and natural mixed culture biofilm formation. *Biofouling* **2011**, 27(10):1073-1085.

[397] Santhiya D, Burghard Z, Greiner C, Jeurgens LP, Subkowski T, Bill J. Bioinspired deposition of TiO_2 thin films induced by hydrophobins. *Langmuir* **2010**, 26(9):6494-6502.

[398] Imai Y, Yamamoto M. The fission yeast mating pheromone P-factor: its molecular structure, gene structure, and ability to induce gene expression and G_1 arrest in the mating partner. *Genes Dev* **1994**, 8(3):328-338.

[399] Haase SB, Reed SI. Improved flow cytometric analysis of the budding yeast cell cycle. *Cell Cycle* **2002**, 1(2):132-136.

[400] Hall TA. BioEdit: a user-friendly biological sequence alignment editor and analysis program for Windows 95/98/NT. *Nucl Acids Symp Ser* **1999**, 41:95-98.

[401] Maloy S, Stewart V, Taylor R. Genetic analysis of pathogenic bacteria: a laboratory manual. *Cold Spring Harbor Laboratory Press*. New York, NY, USA, **1996**.

[402] Prinz WA, Aslund F, Holmgren A, Beckwith J. The role of the thioredoxin and glutaredoxin pathways in reducing protein disulfide bonds in the *Escherichia coli* cytoplasm. *J Biol Chem* **1997**, 272(25):15661-15667.

[403] de Vocht ML, Reviakine I, Wösten HA, Brisson A, Wessels JG, Robillard GT. Structural and functional role of the disulfide bridges in the hydrophobin SC3. *J Biol Chem* **2000**, 275(37):28428-28432.

[404] Kershaw MJ, Thornton CR, Wakley GE, Talbot NJ. Four conserved intramolecular disulphide linkages are required for secretion and cell wall localization of a hydrophobin during fungal morphogenesis. *Mol Microbiol* **2005**, 56(1):117-125.

[405] ExPASy Compute pI/Mw tool. Available online: http://web.expasy.org/compute_pi/ (last accessed: 5 July 2016).

[406] Askolin S, Nakari-Setälä T, Tenkanen M. Overproduction, purification, and characterization of the *Trichoderma reesei* hydrophobin HFBI. *Appl Microbiol Biotechnol* **2001**, 57(1-2):124-130.

[407] Askolin S, Linder M, Scholtmeijer K, Tenkanen M, Penttilä M, de Vocht ML, Wösten HA. Interaction and comparison of a class I hydrophobin from *Schizophyllum commune* and class II hydrophobins from *Trichoderma reesei*. *Biomacromolecules* **2006**, 7(4):1295-1301.

[408] Kottmeier K, Günther TJ, Weber J, Kurtz S, Ostermann K, Rödel G, Bley T. Constitutive expression of hydrophobin HFB1 from *Trichoderma reesei* in *Pichia pastoris* and its pre-purification by foam separation during cultivation. *Eng Life Sci* **2012**, 12(2):162-170.

[409] Nakari-Setälä T, Aro N, Kalkkinen N, Alatalo E, Penttilä M. Genetic and biochemical characterization of the *Trichoderma reesei* hydrophobin HFBI. *Eur J Biochem* **1996**, 235(1-2):248-255.

[410] Song D, Gao Z, Zhao L, Wang X, Xu H, Bai Y, Zhang X, Linder MB, Feng H, Qiao M. High-yield fermentation and a novel heat-precipitation purification method for hydrophobin HGFI from *Grifola frondosa* in *Pichia pastoris*. *Protein Expr Purif* **2016**, 128:22-28.

[411] Yu L, Zhang B, Szilvay GR, Sun R, Jänis J, Wang Z, Feng S, Xu H, Linder MB, Qiao M. Protein HGFI from the edible mushroom *Grifola frondosa* is a novel 8 kDa class I hydrophobin that forms rodlets in compressed monolayers. *Microbiology* **2008**, 154(Pt 6):1677-1685.

[412] Gunning AP, De Groot PW, Visser J, Morris VJ. Atomic force microscopy of a hydrophobin protein from the edible mushroom *Agaricus bisporus. J Colloid Interf Sci* **1998**, 201(2):118-126.

[413] Lugones LG, Wösten HA, Wessels JG. A hydrophobin (ABH3) specifically secreted by vegetatively growing hyphae of *Agaricus bisporus* (common white button mushroom). *Microbiology* **1998**, 144 (Pt 8):2345-2353.

[414] Pedersen MH, Borodina I, Moresco JL, Svendsen WE, Frisvad JC, Søndergaard I. High-yield production of hydrophobins RodA and RodB from *Aspergillus fumigatus* in *Pichia pastoris*. *Appl Microbiol Biotechnol* **2011**, 90(6):1923-1932.

[415] Schmoll M, Seibel C, Kotlowski C, Wöllert Genannt Vendt F, Liebmann B, Kubicek CP. Recombinant production of an *Aspergillus nidulans* class I hydrophobin (DewA) in *Hypocrea jecorina* (*Trichoderma reesei*) is promoter-dependent. *Appl Microbiol Biotechnol* **2010**, 88(1):95-103.

[416] Wösten HA, Schuren FH, Wessels JG. Interfacial self-assembly of a hydrophobin into an amphipathic protein membrane mediates fungal attachment to hydrophobic surfaces. *EMBO J* **1994**, 13(24):5848-5854.

[417] Weickert U, Wiesend F, Subkowski T, Eickhoff A, Reiss G. Optimizing biliary stent patency by coating with hydrophobin alone or hydrophobin and antibiotics or heparin: an *in vitro* proof of principle study. *Adv Med Sci* **2011**, 56(2):138-144.

[418] Chan RK, Otte CA. Isolation and genetic analysis of *Saccharomyces cerevisiae* mutants supersensitive to G1 arrest by a factor and α factor pheromones. *Mol Cell Biol* **1982**, 2(1):11-20.

[419] Moore TI, Chou CS, Nie Q, Jeon NL, Yi TM. Robust spatial sensing of mating pheromone gradients by yeast cells. *PLoS One* **2008**, 3(12):e3865.

[420] Colman-Lerner A, Gordon A, Serra E, Chin T, Resnekov O, Endy D, Pesce CG, Brent R. Regulated cell-to-cell variation in a cell-fate decision system. *Nature* **2005**, 437(7059):699-706.

[421] Paliwal S, Iglesias PA, Campbell K, Hilioti Z, Groisman A, Levchenko A. MAPK-mediated bimodal gene expression and adaptive gradient sensing in yeast. *Nature* **2007**, 446(7131):46-51.

[422] Gizeli E, Lowe CR, Liley M, Vogel H. Detection of supported lipid layers with the acoustic Love waveguide device: application to biosensors. *Sensors Actuat B Chem* **1996**, 34(1-3):295-300.

[423] Shi M, Chen J, Huang Y, Hu K, Zhao S, Chen ZF, Liang H. A multicolor nano-immunosensor for the detection of multiple targets. *RSC Adv* **2013**, 3:13884-13890.

[424] Silverton EW, Navia MA, Davies DR. Three-dimensional structure of an intact human immunoglobulin. *Proc Natl Acad Sci USA* **1977**, 74(11):5140-5144.

[425] Einstein A. Über die von der molekularkinetischen Theorie der Wärme geforderte Bewegung von in ruhenden Flüssigkeiten suspendierten Teilchen. *Ann Phys Berlin* **1905**, 17:549-560.

[426] Rocha LB, Luz DE, Moraes CT, Caravelli A, Fernandes I, Guth BE, Horton DS, Piazza RM. Interaction between Shiga toxin and monoclonal antibodies: binding characteristics and *in vitro* neutralizing abilities. *Toxins (Basel)* **2012**, 4(9):729-747.

[427] Tu T, Drăguşanu M, Petre BA, Rempel DL, Przybylski M, Gross ML. Protein-peptide affinity determination using an H/D exchange dilution strategy: application to antigen-antibody interactions. *J Am Soc Mass Spectrom* **2010**, 21(10):1660-1667.

[428] Zhao Q, Feng Y, Zhu Z, Dimitrov DS. Human monoclonal antibody fragments binding to insulin-like growth factors I and II with picomolar affinity. *Mol Cancer Ther* **2011**, 10(9):1677-1685.

[429] Tom-Moy M, Baer RL, Spira-Solomon D, Doherty TP. Atrazine measurements using surface transverse wave devices. *Anal Chem* **1995**, 67(9):1510-1516.

[430] Wijaya IP, Nie TJ, Gandhi S, Boro R, Palaniappan A, Hau GW, Rodriguez I, Suri CR, Mhaisalkar SG. Femtomolar detection of 2,4-dichlorophenoxyacetic acid herbicides *via* competitive immunoassays using microfluidic based carbon nanotube liquid gated transistor. *Lab Chip* **2010**, 10(5):634-638.

[431] Diener C, Schreiber G, Giese W, del Rio G, Schröder A, Klipp E. Yeast mating and image-based quantification of spatial pattern formation. *PLoS Comput Biol* **2014**, 10(6):e1003690.

[432] Gonçalves-Sá J, Murray A. Asymmetry in sexual pheromones is not required for ascomycete mating. *Curr Biol* **2011**, 21(16):1337-1346.

[433] Rogers DW, McConnell E, Greig D. Molecular quantification of *Saccharomyces cerevisiae* α-pheromone secretion. *FEMS Yeast Res* **2012**, 12(6):668-674.

[434] Bener Aksam E, Pinkse MW, Verhaert PD. Molecular characterization of *Saccharomyces cerevisiae* α-pheromone by mass spectrometry-based peptidomics. *FEMS Yeast Res* **2013**, 13(3):350-353.

[435] Tanaka T, Kita H. Degradation of mating factor by α-mating type cells of *Saccharomyces cerevisiae*. *J Biochem* **1977**, 82:1689-1693.

[436] Weber E, Pinkse MW, Bener-Aksam E, Vellekoop MJ, Verhaert PD. Miniaturized mass-spectrometry-based analysis system for fully automated examination of conditioned cell culture media. *Int J Proteomics* **2012**, 2012:290457.

[437] Karim AS, Curran KA, Alper HS. Characterization of plasmid burden and copy number in *Saccharomyces cerevisiae* for optimization of metabolic engineering applications. *FEMS Yeast Res* **2013**, 13(1):107-116.

[438] Jensen NB, Strucko T, Kildegaard KR, David F, Maury J, Mortensen UH, Forster J, Nielsen J, Borodina I. EasyClone: method for iterative chromosomal integration of multiple genes in *Saccharomyces cerevisiae*. *FEMS Yeast Res* **2014**, 14(2):238-248.

[439] Poritz MA, Malmstrom S, Kim MK, Rossmeissl PJ, Kamb A. Graded mode of transcriptional induction in yeast pheromone signalling revealed by single-cell analysis. *Yeast* **2001**, 18(14):1331-1338.

[440] Bourbonnais Y, Bolin D, Shields D. Secretion of somatostatin by *Saccharomyces cerevisiae*. Correct proteolytic processing of pro-α-factor-somatostatin hybrids requires the products of the *KEX2* and *STE13* genes. *J Biol Chem* **1988**, 263(30):15342-15347.

[441] Fowler TJ, DeSimone SM, Mitton MF, Kurjan J, Raper CA. Multiple sex pheromones and receptors of a mushroom-producing fungus elicit mating in yeast. *Mol Biol Cell* **1999**, 10(8):2559-2572.

[442] Hennig S, Clemens A, Rödel G, Ostermann K. A yeast pheromone-based inter-species communication system. *Appl Microbiol Biotechnol* **2015**, 99(3):1299-1308.

[443] Mayrhofer S, Pöggeler S. Functional characterization of an α-factor-like *Sordaria macrospora* peptide pheromone and analysis of its interaction with its cognate receptor in *Saccharomyces cerevisiae*. *Eukaryot Cell* **2005**, 4(4):661-672.

[444] Olesnicky NS, Brown AJ, Dowell SJ, Casselton LA. A constitutively active G-protein-coupled receptor causes mating self-compatibility in the mushroom *Coprinus*. *EMBO J* **1999**, 18(10):2756-2763.

[445] Forsburg SL. Comparison of *Schizosaccharomyces pombe* expression systems. *Nucleic Acids Res* **1993**, 21(12):2955-2956.

[446] Davey J, Davis K, Imai Y, Yamamoto M, Matthews G. Isolation and characterization of krp, a dibasic endopeptidase required for cell viability in the fission yeast *Schizosaccharomyces pombe*. *EMBO J* **1994**, 13(24):5910-5921.

[447] Hegner J, Siebert-Bartholmei C, Kothe E. Ligand recognition in multiallelic pheromone receptors from the basidiomycete *Schizophyllum commune* studied in yeast. *Fungal Genet Biol* **1999**, 26(3):190-197.

[448] Bücking-Throm E, Duntze W, Hartwell LH, Manney TR. Reversible arrest of haploid yeast cells in the initiation of DNA synthesis by a diffusible sex factor. *Exp Cell Res* **1973**, 76(1):99-110.

[449] Chan RK. Recovery of *Saccharomyces cerevisiae* mating-type a cells from G1 arrest by α factor. *J Bacteriol* **1977**, 130(2):766-774.

[450] Schellenberger A. Sixty years of thiamin diphosphate biochemistry. *Biochim Biophys Acta* **1998**, 1385(2):177-786.

[451] Jain A, Mehta R, Al-Ani M, Hill JA, Winchester DE. Determining the role of thiamine deficiency in systolic heart failure: a meta-analysis and systematic review. *J Card Fail* **2015**, 21(12):1000-1007.

[452] Lu'o'ng KV, Nguyễn LT. The role of thiamine in cancer: possible genetic and cellular signaling mechanisms. *Cancer Genomics Proteomics* **2013**, 10(4):169-185.

[453] Gibson GE, Hirsch JA, Fonzetti P, Jordan BD, Cirio RT, Elder J. Vitamin B1 (thiamine) and dementia. *Ann N Y Acad Sci* **2016**, 1367(1):21-30.

[454] McQuire TA, Young PG. Joint regulation of the *nmt1* promoter and sporulation by Thi1 and Thi5 in *Schizosaccharomyces pombe*. *Curr Genet* **2006**, 50(4):269-279.

[455] Schweingruber AM, Fankhauser H, Dlugonski J, Steinmann-Loss C, Schweingruber ME. Isolation and characterization of regulatory mutants from *Schizosaccharomyces pombe* involved in thiamine-regulated gene expression. *Genetics* **1992**, 130(3):445-449.

[456] Schweingruber AM, Dlugonski J, Edenharter E, Schweingruber ME. Thiamine in *Schizosaccharomyces pombe*: dephosphorylation, intracellular pool, biosynthesis and transport. *Curr Genet* **1991**, 19(4):249-254.

[457] Javerzat JP, Cranston G, Allshire RC. Fission yeast genes which disrupt mitotic chromosome segregation when overexpressed. *Nucleic Acids Res* **1996**, 24(23):4676-4683.

[458] Nakamura Y, Arai A, Takebe Y, Masuda M. A chemical compound for controlled expression of *nmt1*-driven gene in the fission yeast *Schizosaccharomyces pombe*. *Anal Biochem* **2011**, 412(2):159-164.

[459] Maundrell K. *nmt1* of fission yeast. A highly transcribed gene completely repressed by thiamine. *J Biol Chem* **1990**, 265(19):10857-10864.

[460] Akyilmaz E, Yaşa I, Dinçkaya E. Whole cell immobilized amperometric biosensor based on *Saccharomyces cerevisiae* for selective determination of vitamin B1 (thiamine). *Anal Biochem* **2006**, 354(1):78-84.

[461] Akyilmaz E, Yorganci E. A novel biosensor based on activation effect of thiamine on the activity of pyruvate oxidase. *Biosens Bioelectron* **2008**, 23(12):1874-1877.

[462] von Vacano B, Xu R, Hirth S, Herzenstiel I, Rückel M, Subkowski T, Baus U. Hydrophobin can prevent secondary protein adsorption on hydrophobic substrates without exchange. *Anal Bioanal Chem* **2011**, 400(7):2031-2040.

[463] Danov KD, Radulova GM, Kralchevsky PA, Golemanov K, Stoyanov SD. Surface shear rheology of hydrophobin adsorption layers: laws of viscoelastic behaviour with applications to long-term foam stability. *Faraday Discuss* **2012**, 158:195-221.

[464] Danov KD, Kralchevsky PA, Radulova GM, Basheva ES, Stoyanov SD, Pelan EG. Shear rheology of mixed protein adsorption layers vs their structure studied by surface force measurements. *Adv Colloid Interface Sci* **2015**, 222:148-161.

[465] Radulova GM, Golemanov K, Danov KD, Kralchevsky PA, Stoyanov SD, Arnaudov LN, Blijdenstein TB, Pelan EG, Lips A. Surface shear rheology of adsorption layers from the protein HFBII hydrophobin: effect of added β-casein. *Langmuir* **2012**, 28(9):4168-4177.

[466] Bonazza K, Gaderer R, Neudl S, Przylucka A, Allmaier G, Druzhinina IS, Grothe H, Friedbacher G, Seidl-Seiboth V. The fungal cerato-platanin protein EPL1 forms highly ordered layers at hydrophobic/hydrophilic interfaces. *Soft Matter* **2015**, 11(9):1723-1732.

[467] Albuquerque P, Kyaw CM, Saldanha RR, Brigido MM, Felipe MS, Silva-Pereira I. Pbhyd1 and Pbhyd2: two mycelium-specific hydrophobin genes from the dimorphic fungus *Paracoccidioides brasiliensis*. *Fungal Genet Biol* **2004**, 41(5):510-520.

[468] Bolyard MG, Sticklen MB. Expression of a modified Dutch elm disease toxin in *Escherichia coli*. *Mol Plant Microbe Interact* **1992**, 5(6):520-524.

[469] Espino-Rammer L, Ribitsch D, Przylucka A, Marold A, Greimel KJ, Herrero Acero E, Guebitz GM, Kubicek CP, Druzhinina IS. Two novel class II hydrophobins from *Trichoderma* spp.

stimulate enzymatic hydrolysis of poly(ethylene terephthalate) when expressed as fusion proteins. *Appl Environ Microbiol* **2013**, 79(14):4230-4238.

[470] Kirkland BH, Keyhani NO. Expression and purification of a functionally active class I fungal hydrophobin from the entomopathogenic fungus *Beauveria bassiana* in *E. coli*. *J Ind Microbiol Biotechnol* **2011**, 38(2):327-335.

[471] Kudo T, Sato Y, Hara T, Joh T, Tasaki Y. Heterogeneous expression and emulsifying activity of class I hydrophobin from *Pholiota nameko. Mycoscience* **2011**, 52(4):283-287.

[472] Peñas MM, Asgeirsdóttir SA, Lasa I, Culiañez-Macià FA, Pisabarro AG, Wessels JG, Ramírez L. Identification, characterization, and In situ detection of a fruit-body-specific hydrophobin of *Pleurotus ostreatus*. *Appl Environ Microbiol* **1998**, 64(10):4028-4034.

[473] Rey AA, Hocher A, Kwan AH, Sunde M. Backbone and sidechain ^{1}H, ^{13}C and ^{15}N chemical shift assignments of the hydrophobin MPG1 from the rice blast fungus *Magnaporthe oryzae*. *Biomol NMR Assign* **2013**, 7(1):109-112.

[474] Tagu D, De Bellis R, Balestrini R, De Vries OM, Piccoli G, Stocchi V, Bonfante P, Martin F. Immunolocalization of hydrophobin HYDPt-1 from the ectomycorrhizal basidiomycete *Pisolithus tinctorius* during colonization of *Eucalyptus globulus* roots. *New Phytol* **2001**, 149(1):127-135.

[475] Wang Z, Feng S, Huang Y, Qiao M, Zhang B, Xu H. Prokaryotic expression, purification, and polyclonal antibody production of a hydrophobin from *Grifola frondosa*. *Acta Biochim Biophys Sin (Shanghai)* **2010**, 42(6):388-395.

[476] Lohrasbi-Nejad A, Torkzadeh-Mahani M, Hosseinkhani S. Heterologous expression of a hydrophobin HFB1 and evaluation of its contribution to producing stable foam. *Protein Expr Purif* **2016**, 118:25-30.

[477] Sarlin T, Kivioja T, Kalkkinen N, Linder MB, Nakari-Setälä T. Identification and characterization of gushing-active hydrophobins from *Fusarium graminearum* and related species. *J Basic Microbiol* **2012**, 52(2):184-194.

[478] Li W, Gong Y, Xu H, Qiao M, Niu B. Identification properties of a recombinant class I hydrophobin rHGFI. *Int J Biol Macromol* **2015**, 72:658-663.

[479] Niu B, Gong Y, Gao X, Xu H, Qiao M, Li W. The functional role of Cys3-Cys4 loop in hydrophobin HGFI. *Amino Acids* **2014**, 46(11):2615-2625.

[480] Wang P, He J, Sun Y, Reynolds M, Zhang L, Han S, Liang S, Sui H, Lin Y. Display of fungal hydrophobin on the *Pichia pastoris* cell surface and its influence on *Candida antarctica* lipase B. *Appl Microbiol Biotechnol* **2016**, 100(13):5883-5895.

[481] Linder M, Selber K, Nakari-Setälä T, Qiao M, Kula MR, Penttilä M. The hydrophobins HFBI and HFBII from *Trichoderma reesei* showing efficient interactions with nonionic surfactants in aqueous two-phase systems. *Biomacromolecules* **2001**, 2(2):511-517.

[482] Linder MB, Qiao M, Laumen F, Selber K, Hyytiä T, Nakari-Setälä T, Penttilä ME. Efficient purification of recombinant proteins using hydrophobins as tags in surfactant-based two-phase systems. *Biochemistry* **2004**, 43(37):11873-11882.

[483] Kivioja JM, Kurppa K, Kainlauri M, Linder MB, Ahopelto J. Electrical transport through ordered self-assembled protein monolayer measured by constant force conductive atomic force microscopy. *Appl Phys Lett* **2009**, 94:183901.

[484] Szilvay GR, Paananen A, Laurikainen K, Vuorimaa E, Lemmetyinen H, Peltonen J, Linder MB. Self-assembled hydrophobin protein films at the air-water interface: structural analysis and molecular engineering. *Biochemistry* **2007**, 46(9):2345-2354.

[485] Bhimji A, Zaragoza AA, Live LS, Kelley SO. Electrochemical enzyme-linked immunosorbent assay featuring proximal reagent generation: detection of human immunodeficiency virus antibodies in clinical samples. *Anal Chem* **2013**, 85(14):6813-6819.

[486] Wu J, Park JP, Dooley K, Cropek DM, West AC, Banta S. Rapid development of new protein biosensors utilizing peptides obtained *via* phage display. *PLoS One* **2011**, 6(10):e24948.

[487] Knichel M, Heiduschka P, Beck W, Jung G, Göpel W. Utilization of a self-assembled peptide monolayer for an impedimetric immunosensor. *Sensors Actuat B Chem* **1995**, 28(2):85-94.

[488] Rickert J, Göpel W, Beck W, Jung G, Heiduschka P. A 'mixed' self-assembled monolayer for an impedimetric immunosensor. *Biosens Bioelectron* **1996**, 11(8):757-768.

[489] Moraes ML, Lima LR, Silva RR, Cavicchioli M, Ribeiro SJ. Immunosensor based on immobilization of antigenic peptide NS5A-1 from HCV and silk fibroin in nanostructured films. *Langmuir* **2013**, 29(11):3829-3834.

[490] Li Y, Cai C. Click chemistry-based functionalization on non-oxidized silicon substrates. *Chem Asian J* **2011**, 6(10):2592-2605.

[491] Marechal A, El-Debs R, Dugas V, Demesmay C. Is click chemistry attractive for separation sciences? *J Sep Sci* **2013**, 36(13):2049-2062.

[492] Fan H, Wang X, Zhu J, Robillard GT, Mark AE. Molecular dynamics simulations of the hydrophobin SC3 at a hydrophobic/hydrophilic interface. *Proteins* **2006**, 64(4):863-873.

[493] Wang X, de Vocht ML, de Jonge J, Poolman B, Robillard GT. Structural changes and molecular interactions of hydrophobin SC3 in solution and on a hydrophobic surface. *Protein Sci* **2002**, 11(5):1172-1181.

[494] Wang X, Permentier HP, Rink R, Kruijtzer JA, Liskamp RM, Wösten HA, Poolman B, Robillard GT. Probing the self-assembly and the accompanying structural changes of hydrophobin SC3 on a hydrophobic surface by mass spectrometry. *Biophys J* **2004**, 87(3):1919-1928.

[495] Gazzera L, Corti C, Pirrie L, Paananen A, Monfredini A, Cavallo G, Bettini S, Giancane G, Valli L, Linder MB, Resnati G, Milani R, Metrangolo P. Hydrophobin as a nanolayer primer that enables the fluorinated coating of poorly reactive polymer surfaces. *Adv Mater Interfaces* **2015**, 2(14):1500170.

[496] Prin C, Bene MC, Gobert B, Montagne P, Faure GC. Isoelectric restriction of human immunoglobulin isotypes. *Biochim Biophys Acta* **1995**, 1243(2):287-289.

[497] Hinterdorfer P, Dufrêne YF. Detection and localization of single molecular recognition events using atomic force microscopy. *Nat Methods* **2006**, 3(5):347-355.

[498] Tang J, Ebner A, Badelt-Lichtblau H, Völlenkle C, Rankl C, Kraxberger B, Leitner M, Wildling L, Gruber HJ, Sleytr UB, Ilk N, Hinterdorfer P. Recognition imaging and highly ordered

molecular templating of bacterial S-layer nanoarrays containing affinity-tags. *Nano Lett* **2008**, 8(12):4312-4319.

[499] Marquart M, Deisenhofer J. The three-dimensional structure of antibodies. *Immunol Today* **1982**, 3(6):160-166.

[500] Data sheet for Anti-HA antibody (Roche Diagnostics GmbH, Germany). Available online: http://www.sigmaaldrich.com/content/dam/sigma-aldrich/docs/Roche/Bulletin/1/roahabul.pdf (last accessed: 17 October 2016)

[501] Fukuda N, Ishii J, Kaishima M, Kondo A. Amplification of agonist stimulation of human G-protein-coupled receptor signaling in yeast. *Anal Biochem* **2011**, 417(2):182-187.

[502] Gordon A, Colman-Lerner A, Chin TE, Benjamin KR, Yu RC, Brent R. Single-cell quantification of molecules and rates using open-source microscope-based cytometry. *Nat Methods* **2007**, 4(2):175-181.

[503] Ishii J, Matsumura S, Kimura S, Tatematsu K, Kuroda S, Fukuda H, Kondo A. Quantitative and dynamic analyses of G protein-coupled receptor signaling in yeast using Fus1, enhanced green fluorescence protein (EGFP), and His3 fusion protein. *Biotechnol Prog* **2006**, 22(4):954-960.

[504] Lee SS, Horvath P, Pelet S, Hegemann B, Lee LP, Peter M. Quantitative and dynamic assay of single cell chemotaxis. *Integr Biol (Camb)* **2012**, 4(4):381-390.

[505] Pincus D, Ryan CJ, Smith RD, Brent R, Resnekov O. Assigning quantitative function to post-translational modifications reveals multiple sites of phosphorylation that tune yeast pheromone signaling output. *PLoS One* **2013**, 8(3):e56544.

[506] Thomson TM, Benjamin KR, Bush A, Love T, Pincus D, Resnekov O, Yu RC, Gordon A, Colman-Lerner A, Endy D, Brent R. Scaffold number in yeast signaling system sets tradeoff between system output and dynamic range. *Proc Natl Acad Sci USA* **2011**, 108(50):20265-20270.

[507] Brown AJ, Dyos SL, Whiteway MS, White JH, Watson MA, Marzioch M, Clare JJ, Cousens DJ, Paddon C, Plumpton C, Romanos MA, Dowell SJ. Functional coupling of mammalian receptors to the yeast mating pathway using novel yeast/mammalian G protein alpha-subunit chimeras. *Yeast* **2000**, 16(1):11-22.

[508] Jackson CL, Hartwell LH. Courtship in *S. cerevisiae*: both cell types choose mating partners by responding to the strongest pheromone signal. *Cell* **1990**, 63(5):1039-1051.

[509] Apanovitch DM, Slep KC, Sigler PB, Dohlman HG. Sst2 is a GTPase-activating protein for Gpa1: purification and characterization of a cognate RGS-Gα protein pair in yeast. *Biochemistry* **1998**, 37(14):4815-4822.

[510] Konopka JB, Jenness DD, Hartwell LH. The C-terminus of the *S. cerevisiae* α-pheromone receptor mediates an adaptive response to pheromone. *Cell* **1988**, 54(5):609-620.

[511] Reneke JE, Blumer KJ, Courchesne WE, Thorner J. The carboxy-terminal segment of the yeast α-factor receptor is a regulatory domain. *Cell* **1988**, 55(2):221-234.

[512] Jenness DD, Burkholder AC, Hartwell LH. Binding of α-factor pheromone to *Saccharomyces cerevisiae* **a** cells: dissociation constant and number of binding sites. *Mol Cell Biol* **1986**, 6(1):318-320.

[513] Sen M, Marsh L. Noncontiguous domains of the α-factor receptor of yeasts confer ligand specificity. *J Biol Chem* **1994**, 269(2):968-973.

[514] Malleshaiah MK, Shahrezaei V, Swain PS, Michnick SW. The scaffold protein Ste5 directly controls a switch-like mating decision in yeast. *Nature* **2010**, 465(7294):101-105.

[515] Hartwell LH. Mutants of *Saccharomyces cerevisiae* unresponsive to cell division control by polypeptide mating hormone. *J Cell Biol* **1980**, 85(3):811-822.

[516] Moore SA. Comparison of dose-response curves for α factor-induced cell division arrest, agglutination, and projection formation of yeast cells. Implication for the mechanism of α factor action. *J Biol Chem* **1983**, 258(22):13849-13856.

[517] Yu RC, Pesce CG, Colman-Lerner A, Lok L, Pincus D, Serra E, Holl M, Benjamin K, Gordon A, Brent R. Negative feedback that improves information transmission in yeast signalling. *Nature* **2008**, 456(7223):755-761.

[518] Manney TR. Expression of the *BAR1* gene in *Saccharomyces cerevisiae*: induction by the α mating pheromone of an activity associated with a secreted protein. *J Bacteriol* **1983**, 155(1):291-301.

[519] Carmona-Gutierrez D, Eisenberg T, Büttner S, Meisinger C, Kroemer G, Madeo F. Apoptosis in yeast: triggers, pathways, subroutines. *Cell Death Differ* **2010**, 17(5):763-773.

[520] Severin FF, Hyman AA. Pheromone induces programmed cell death in *S. cerevisiae*. *Curr Biol* **2002**, 12(7):R233-235.

[521] Zhang NN, Dudgeon DD, Paliwal S, Levchenko A, Grote E, Cunningham KW. Multiple signaling pathways regulate yeast cell death during the response to mating pheromones. *Mol Biol Cell* **2006**, 17(8):3409-3422.

[522] Eriotou-Bargiota E, Xue CB, Naider F, Becker JM. Antagonistic and synergistic peptide analogues of the tridecapeptide mating pheromone of *Saccharomyces cerevisiae*. *Biochemistry* **1992**, 31(2):551-557.

[523] Singer B, Riezman H. Detection of an intermediate compartment involved in transport of α-factor from the plasma membrane to the vacuole in yeast. *J Cell Biol* **1990**, 110(6):1911-1922.

[524] Herrick D, Parker R, Jacobson A. Identification and comparison of stable and unstable mRNAs in *Saccharomyces cerevisiae*. *Mol Cell Biol* **1990**, 10(5):2269-2284.

[525] HomoloGene database. Available online: http://www.ncbi.nlm.nih.gov/homologene (last accessed: 5 July 2016).

[526] Immune Epitope Database Analysis Resource, Antibody Epitope Prediction tool. Available online: http://tools.immuneepitope.org/tools/bcell (last accessed: 5 July 2016).

[527] Hedges SB. The origin and evolution of model organisms. *Nat Rev Genet* **2002**, 3(11):838-849.

[528] Hedges SB, Blair JE, Venturi ML, Shoe JL. A molecular timescale of eukaryote evolution and the rise of complex multicellular life. *BMC Evol Biol* **2004**, 4:2.

[529] Böhm J, Hoff B, O'Gorman CM, Wolfers S, Klix V, Binger D, Zadra I, Kürnsteiner H, Pöggeler S, Dyer PS, Kück U. Sexual reproduction and mating-type-mediated strain development in the

penicillin-producing fungus *Penicillium chrysogenum*. *Proc Natl Acad Sci USA* **2013**, 110(4):1476-1481.

[530] Marsh L, Herskowitz I. STE2 protein of *Saccharomyces kluyveri* is a member of the rhodopsin/β-adrenergic receptor family and is responsible for recognition of the peptide ligand α factor. *Proc Natl Acad Sci USA* **1988**, 85(11):3855-3859.

[531] Hao N, Nayak S, Behar M, Shanks RH, Nagiec MJ, Errede B, Hasty J, Elston TC, Dohlman HG. Regulation of cell signaling dynamics by the protein kinase-scaffold Ste5. *Mol Cell* **2008**, 30(5):649-656.

[532] Yuan H, Zhang R, Shao B, Wang X, Ouyang Q, Hao N, Luo C. Protein expression patterns of the yeast mating response. *Integr Biol (Camb)* **2016**, 8(6):712-719.

[533] Leibowitz MJ, Wickner RB. A chromosomal gene required for killer plasmid expression, mating, and spore maturation in *Saccharomyces cerevisiae*. *Proc Natl Acad Sci USA* **1976**, 73(6):2061-2065.

[534] PomBase database. Available online: http://www.pombase.org/ (last accessed: 5 July 2016).

[535] Wood V, Gwilliam R, Rajandream MA, Lyne M, Lyne R, Stewart A, Sgouros J, Peat N, Hayles J, Baker S, Basham D, Bowman S, Brooks K, Brown D, Brown S, Chillingworth T, Churcher C, Collins M, Connor R, Cronin A, Davis P, Feltwell T, Fraser A, Gentles S, Goble A, Hamlin N, Harris D, Hidalgo J, Hodgson G, Holroyd S, Hornsby T, Howarth S, Huckle EJ, Hunt S, Jagels K, James K, Jones L, Jones M, Leather S, McDonald S, McLean J, Mooney P, Moule S, Mungall K, Murphy L, Niblett D, Odell C, Oliver K, O'Neil S, Pearson D, Quail MA, Rabbinowitsch E, Rutherford K, Rutter S, Saunders D, Seeger K, Sharp S, Skelton J, Simmonds M, Squares R, Squares S, Stevens K, Taylor K, Taylor RG, Tivey A, Walsh S, Warren T, Whitehead S, Woodward J, Volckaert G, Aert R, Robben J, Grymonprez B, Weltjens I, Vanstreels E, Rieger M, Schäfer M, Müller-Auer S, Gabel C, Fuchs M, Düsterhöft A, Fritzc C, Holzer E, Moestl D, Hilbert H, Borzym K, Langer I, Beck A, Lehrach H, Reinhardt R, Pohl TM, Eger P, Zimmermann W, Wedler H, Wambutt R, Purnelle B, Goffeau A, Cadieu E, Dréano S, Gloux S, Lelaure V, Mottier S, Galibert F, Aves SJ, Xiang Z, Hunt C, Moore K, Hurst SM, Lucas M, Rochet M, Gaillardin C, Tallada VA, Garzon A, Thode G, Daga RR, Cruzado L, Jimenez J, Sánchez M, del Rey F, Benito J, Domínguez A, Revuelta JL, Moreno S, Armstrong J, Forsburg SL, Cerutti L, Lowe T, McCombie WR, Paulsen I, Potashkin J, Shpakovski GV, Ussery D, Barrell BG, Nurse P. The genome sequence of *Schizosaccharomyces pombe*. *Nature* **2002**, 415(6874):871-880.

[536] Abel MG, Zhang YL, Lu HF, Naider F, Becker JM. Structure-function analysis of the *Saccharomyces cerevisiae* tridecapeptide pheromone using alanine-scanned analogs. *J Pept Res* **1998**, 52(2):95-106.

[537] Egel R. Physiological aspects of conjugation in fission yeast. *Planta* **1971**, 98(1):89-96.

[538] Mata J, Lyne R, Burns G, Bähler J. The transcriptional program of meiosis and sporulation in fission yeast. *Nat Genet* **2002**, 32(1):143-147.

[539] Brett ME, DeFlorio R, Stone DE, Eddington DT. A microfluidic device that forms and redirects pheromone gradients to study chemotropism in yeast. *Lab Chip* **2012**, 12(17):3127-3134.

[540] Conlon P, Gelin-Licht R, Ganesan A, Zhang J, Levchenko A. Single-cell dynamics and variability of MAPK activity in a yeast differentiation pathway. *Proc Natl Acad Sci USA* **2016**, 113(40):E5896-E5905.

[541] Hegemann B, Unger M, Lee SS, Stoffel-Studer I, van den Heuvel J, Pelet S, Koeppl H, Peter M. A cellular system for spatial signal decoding in chemical gradients. *Dev Cell* **2015**, 35(4):458-470.

[542] Ventura AC, Bush A, Vasen G, Goldín MA, Burkinshaw B, Bhattacharjee N, Folch A, Brent R, Chernomoretz A, Colman-Lerner A. Utilization of extracellular information before ligand-receptor binding reaches equilibrium expands and shifts the input dynamic range. *Proc Natl Acad Sci USA* **2014**, 111(37):E3860-E3869.

[543] Frykman S, Srienc F. Cell cycle-dependent protein secretion by *Saccharomyces cerevisiae*. *Biotechnol Bioeng* **2001**, 76(3):259-268.

[544] Tommasino M, Maundrell K. Uptake of thiamine by *Schizosaccharomyces pombe* and its effect as a transcriptional regulator of thiamine-sensitive genes. *Curr Genet* **1991**, 20(1-2):63-66.

[545] Purbia R, Paria S. A simple turn on fluorescent sensor for the selective detection of thiamine using coconut water derived luminescent carbon dots. *Biosens Bioelectron* **2016**, 79:467-475.

[546] Sun J, Liu L, Ren C, Chen X, Hu Z. A feasible method for the sensitive and selective determination of vitamin B1 with CdSe quantum dots. *Microchim Acta* **2008**, 163:271-276.

[547] Li Y, Wang P, Wang X, Cao M, Xia YS, Cao C, Liu MG, Zhu CQ. An immediate luminescence enhancement method for determination of vitamin B1 using long-wavelength emitting water-soluble CdTe nanorods. *Microchim Acta* **2010**, 169:65-71.

[548] Rao KJ, Paria S. Green synthesis of gold nanoparticles using aqueous *Aegle marmelos* leaf extract and their application for thiamine detection. *RSC Adv* **2014**, 4:28645-28652.

[549] Bohrer D, Cícero do Nascimento P, Ramirez AG, Mendonça JK, de Carvalho LM, Pomblum SC. Determination of thiamine in blood serum and urine by high-performance liquid chromatography with direct injection and post-column derivatization. *Microchem J* **2004**, 78(1):71-76.

[550] Pérez-Ruiz T, Martínez-Lozano C, García-Martínez MD. Simultaneous determination of thiamine and its phosphate esters by a liquid chromatographic method based on post-column photolysis and chemiluminescence detection. *J Pharm Biomed Anal* **2009**, 50(3):315-319.

[551] Milani R, Pirrie L, Gazzera L, Paananen A, Baldrighi M, Monogioudi E, Cavallo G, Linder M, Resnati G, Metrangolo P. A synthetically modified hydrophobin showing enhanced fluorous affinity. *J Colloid Interface Sci* **2015**, 448:140-147.

[552] Sarkar T, Gao Y, Mulchandani A. Carbon nanotubes-based label-free affinity sensors for environmental monitoring. *Appl Biochem Biotechnol* **2013**, 170(5):1011-1025.

[553] Balasubramanian K, Kern K. 25th anniversary article: label-free electrical biodetection using carbon nanostructures. *Adv Mater* **2014**, 26(8):1154-1175.

[554] Chartuprayoon N, Zhang M, Bosze W, Choa YH, Myung NV. One-dimensional nanostructures based bio-detection. *Biosens Bioelectron* **2015**, 63:432-443.

[555] Zhang GJ, Ning Y. Silicon nanowire biosensor and its applications in disease diagnostics: a review. *Anal Chim Acta* **2012**, 749:1-15.

[556] Özel RE, Hayat A, Andreescu S. Recent developments in electrochemical sensors for the detection of neurotransmitters for applications in biomedicine. *Anal Lett* **2015**, 48(7):1044-1069.

[557] Meisinger C, Sommer T, Pfanner N. Purification of *Saccharomyces cerevisiae* mitochondria devoid of microsomal and cytosolic contaminations. *Anal Biochem* **2000**, 287(2):339-342.

[558] Data sheet for lysozyme (Carl Roth GmbH + Co. KG, Germany). Available online: http://www.carlroth.com/downloads/spez/en/8/SPEZ_8259_EN.pdf (last accessed: 17 October 2016).

[559] GenScript Inc. protocol 81_20050505152013. Available online: http://www.genscript.com/peptide/RP01002-FactorMatingPheromoneyeast.html (last accessed: 27 June 2016).

Appendix A – Sequence information

A.1 Sequence of the recombinant hydrophobin EAS

```
  1    ATG GGC AGC AGC CAT CAT CAT CAT CAT CAC AGC AGC GGC CTG GTG
  1    M   G   S   S   H   H   H   H   H   H   S   S   G   L   V

 46    CCG CGC GGC AGC CAT ATG GCT AGC ATC GGC CCC AAC ACC TGC TCC
 16    P   R   G   S   H   M   A   S   I   G   P   N   T   C   S

 91    ATC GAC GAC TAC AAG CCT TAC TGC TGC CAG TCT ATG TCC GGC CCC
 31    I   D   D   Y   K   P   Y   C   C   Q   S   M   S   G   P

136    GCC GGC TCC CCT GGT CTC CTC AAC CTC ATC CCC GTC GAC CTC AGC
 46    A   G   S   P   G   L   L   N   L   I   P   V   D   L   S

181    GCC TCG CTC GGC TGC GTT GTC GGT GTC ATC GGC TCC CAA TGT GGT
 61    A   S   L   G   C   V   V   G   V   I   G   S   Q   C   G

226    GCC AGC GTC AAG TGC TGC AAG GAC GAT GTT ACC AAC ACC GGC AAC
 76    A   S   V   K   C   C   K   D   D   V   T   N   T   G   N

271    TCC TTC CTC ATC ATC AAC GCT GCC AAC TGC GTT GCC TAA
 91    S   F   L   I   I   N   A   A   N   C   V   A   *
```

Figure A1. Nucleotide and amino acid sequence of the recombinant hydrophobin EAS. Sequences corresponding to the $(His)_6$-tag and the mature EAS hydrophobin are highlighted in gray and orange, respectively. The recognition site of the *Nhe*I restriction endonuclease used for molecular cloning is underlined.

A.2 Sequence of the recombinant hydrophobin EAS-α

```
  1    ATG GGC AGC AGC CAT CAT CAT CAT CAT CAC AGC AGC GGC CTG GTG
  1    M   G   S   S   H   H   H   H   H   H   S   S   G   L   V

 46    CCG CGC GGC AGC CAT ATG GCT AGC ATC GGC CCC AAC ACC TGC TCC
 16    P   R   G   S   H   M   A   S   I   G   P   N   T   C   S

 91    ATC GAC GAC TAC AAG CCT TAC TGC TGC CAG TCT ATG TCC GGC CCC
 31    I   D   D   Y   K   P   Y   C   C   Q   S   M   S   G   P

136    GCC GGC TCC CCT GGT CTC CTC AAC CTC ATC CCC GTC GAC CTC AGC
 46    A   G   S   P   G   L   L   N   L   I   P   V   D   L   S

181    GCC TCG CTC GGC TGC GTT GTC GGT GTC ATC GGC TCC CAA TGT GGT
 61    A   S   L   G   C   V   V   G   V   I   G   S   Q   C   G

226    GCC AGC GTC AAG TGC TGC AAG GAC GAT GTT ACC AAC ACC GGC AAC
 76    A   S   V   K   C   C   K   D   D   V   T   N   T   G   N

271    TCC TTC CTC ATC ATC AAC GCT GCC AAC TGC GTT GCC GGA TCC GGC
 91    S   F   L   I   I   N   A   A   N   C   V   A   G   S   G

316    GGC GGC GGC AGC GGC GGC GGC GGC AGC GGC GGC GGC GGC AGC ACT
106    G   G   G   S   G   G   G   G   S   G   G   G   G   S   T

361    AGT TGG CAT TGG CTG CAG CTG AAA CCG GGC CAG CCG ATG TAT TAA
121    S   W   H   W   L   Q   L   K   P   G   Q   P   M   Y   *
```

Figure A2. Nucleotide and amino acid sequence of the recombinant hydrophobin EAS-α. Sequences corresponding to the $(His)_6$-tag and the mature EAS hydrophobin are highlighted in gray and orange, respectively. Sequences regarding the $(GGGGS)_3$ linker are printed in bold, whereas sequences corresponding to the α-factor pheromone are highlighted in blue. Recognition sites of the restriction endonucleases used for molecular cloning (*Nhe*I, *Bam*HI and *Spe*I) are underlined.

A.3 Sequence of the chimeric *map2/MFα1* gene

```
  1    ATG AAG ATC ACC GCT GTC ATT GCC CTT TTA TTC TCA CTT GCT GCT
  1    M   K   I   T   A   V   I   A   L   L   F   S   L   A   A

 46    GCC TCA CCT ATT CCA GTT GCC GAT CCT GGT GTG GTT TCA GTT AGC
 16    A   S   P   I   P   V   A   D   P   G   V   V   S   V   S

 91    AAG TCA TAT GCT GAT TTC CTT CGT GTT TAC CAA AGT TGG AAC ACT
 31    K   S   Y   A   D   F   L   R   V   Y   Q   S   W   N   T

136    TTT GCT AAT CCT GAT AGA CCC AAC TTG AAA AAG CGC GAA TTC GAA
 46    F   A   N   P   D   R   P   N   L   K   K   R   E   F   E

181    GCT GCT CCC GCA AAA ACT TAT GCT GAT TTC CTT CGT GCT TAT CAA
 61    A   A   P   A   K   T   Y   A   D   F   L   R   A   Y   Q

226    AGT TGG AAC ACT TTT GTT AAT CCT GAC AGA CCC AAT TTG AAA AAG
 76    S   W   N   T   F   V   N   P   D   R   P   N   L   K   K

271    CGT GAG TTT GAA GCT GCC CCA GAG AAG TGG CAT TGG TTG CAA CTA
 91    R   E   F   E   A   A   P   E   K   W   H   W   L   Q   L

316    AAA CCT GGC CAA CCA ATG TAC AAA AAG CGC GAA TTC GAA GCT GCT
106    K   P   G   Q   P   M   Y   K   K   R   E   F   E   A   A

361    CCC GCA AAA TGG CAT TGG TTG CAA CTA AAA CCT GGC CAA CCA ATG
121    P   A   K   W   H   W   L   Q   L   K   P   G   Q   P   M

406    TAC AAA AAG CGC ACT GAA GAA GAT GAA GAG AAT GAG GAA GAG GAT
136    Y   K   K   R   T   E   E   D   E   E   N   E   E   E   D

451    GAA GAA TAC TAT CGC TTT CTT CAG TTT TAT ATC ATG ACT GTC CCA
151    E   E   Y   Y   R   F   L   Q   F   Y   I   M   T   V   P

496    GAG AAT TCC ACT ATT ACA GAT GTC AAT ATT ACT GCC AAA TTT GAG
166    E   N   S   T   I   T   D   V   N   I   T   A   K   F   E

541    AGC TAA
181    S   *
```

Figure A3. DNA sequence of the chimeric *map2/MFα1* gene and amino acid sequence of the respective pheromone precursor protein. Sequences corresponding to the *S. pombe* P-factor pheromone and the *S. cerevisiae* α-factor pheromone are highlighted in red and blue, respectively. Sequences corresponding to putative N-linked glycosylation sites are printed in bold.

A.4 Sequence of the recombinant hydrophobin EAS-HA

```
  1    ATG GGC AGC AGC CAT CAT CAT CAT CAT CAC AGC AGC GGC CTG GTG
  1    M   G   S   S   H   H   H   H   H   H   S   S   G   L   V

 46    CCG CGC GGC AGC CAT ATG GCT AGC ATC GGC CCC AAC ACC TGC TCC
 16    P   R   G   S   H   M   A   S   I   G   P   N   T   C   S

 91    ATC GAC GAC TAC AAG CCT TAC TGC TGC CAG TCT ATG TCC GGC CCC
 31    I   D   D   Y   K   P   Y   C   C   Q   S   M   S   G   P

136    GCC GGC TCC CCT GGT CTC CTC AAC CTC ATC CCC GTC GAC CTC AGC
 46    A   G   S   P   G   L   L   N   L   I   P   V   D   L   S

181    GCC TCG CTC GGC TGC GTT GTC GGT GTC ATC GGC TCC CAA TGT GGT
 61    A   S   L   G   C   V   V   G   V   I   G   S   Q   C   G

226    GCC AGC GTC AAG TGC TGC AAG GAC GAT GTT ACC AAC ACC GGC AAC
 76    A   S   V   K   C   C   K   D   D   V   T   N   T   G   N

271    TCC TTC CTC ATC ATC AAC GCT GCC AAC TGC GTT GCC GGA TCC GGC
 91    S   F   L   I   I   N   A   A   N   C   V   A   G   S   G

316    GGC GGC GGC AGC GGC GGC GGC GGC AGC GGC GGC GGC GGC AGC ACT
106    G   G   G   S   G   G   G   G   S   G   G   G   G   S   T

361    AGT TAC CCA TAC GAT GTT CCT GAC TAT GCG TAA
121    S   Y   P   Y   D   V   P   D   Y   A   *
```

Figure A4. Nucleotide and amino acid sequence of the recombinant hydrophobin EAS-HA. Sequences corresponding to the $(His)_6$-tag and the mature EAS hydrophobin are highlighted in gray and orange, respectively. Sequences regarding the $(GGGGS)_3$ linker element are printed in bold, whereas sequences for the HA epitope are highlighted in green. Recognition sites of the *Nhe*I, *Bam*HI and *Spe*I restriction endonucleases used for molecular cloning are underlined.

A.5 Sequence of the recombinant HA-EGFP

```
  1    ATG TAC CCA TAC GAT GTT CCT GAC TAT GCG ATG GTG AGC AAG GGC
  1    M   Y   P   Y   D   V   P   D   Y   A   M   V   S   K   G

 46    GAG GAG CTG TTC ACC GGG GTG GTG CCC ATC CTG GTC GAG CTG GAC
 16    E   E   L   F   T   G   V   V   P   I   L   V   E   L   D

 91    GGC GAC GTA AAC GGC CAC AAG TTC AGC GTG TCC GGC GAG GGC GAG
 31    G   D   V   N   G   H   K   F   S   V   S   G   E   G   E

136    GGC GAT GCC ACC TAC GGC AAG CTG ACC CTG AAG TTC ATC TGC ACC
 46    G   D   A   T   Y   G   K   L   T   L   K   F   I   C   T

181    ACC GGC AAG CTG CCC GTG CCC TGG CCC ACC CTC GTG ACC ACC CTG
 61    T   G   K   L   P   V   P   W   P   T   L   V   T   T   L

226    ACC TAC GGC GTG CAG TGC TTC AGC CGC TAC CCC GAC CAC ATG AAG
 76    T   Y   G   V   Q   C   F   S   R   Y   P   D   H   M   K

271    CAG CAC GAC TTC TTC AAG TCC GCC ATG CCC GAA GGC TAC GTC CAG
 91    Q   H   D   F   F   K   S   A   M   P   E   G   Y   V   Q

316    GAG CGC ACC ATC TTC TTC AAG GAC GAC GGC AAC TAC AAG ACC CGC
106    E   R   T   I   F   F   K   D   D   G   N   Y   K   T   R

361    GCC GAG GTG AAG TTC GAG GGC GAC ACC CTG GTG AAC CGC ATC GAG
121    A   E   V   K   F   E   G   D   T   L   V   N   R   I   E

406    CTG AAG GGC ATC GAC TTC AAG GAG GAC GGC AAC ATC CTG GGG CAC
136    L   K   G   I   D   F   K   E   D   G   N   I   L   G   H

451    AAG CTG GAG TAC AAC TAC AAC AGC CAC AAC GTC TAT ATC ATG GCC
151    K   L   E   Y   N   Y   N   S   H   N   V   Y   I   M   A

496    GAC AAG CAG AAG AAC GGC ATC AAG GTG AAC TTC AAG ATC CGC CAC
166    D   K   Q   K   N   G   I   K   V   N   F   K   I   R   H

541    AAC ATC GAG GAC GGC AGC GTG CAG CTC GCC GAC CAC TAC CAG CAG
181    N   I   E   D   G   S   V   Q   L   A   D   H   Y   Q   Q

586    AAC ACC CCC ATC GGC GAC GGC CCC GTG CTG CTG CCC GAC AAC CAC
196    N   T   P   I   G   D   G   P   V   L   L   P   D   N   H

631    TAC CTG AGC ACC CAG TCC GCC CTG AGC AAA GAC CCC AAC GAG AAG
211    Y   L   S   T   Q   S   A   L   S   K   D   P   N   E   K

676    CGC GAT CAC ATG GTC CTG CTG GAG TTC GTG ACC GCC GCC GGG ATC
226    R   D   H   M   V   L   L   E   F   V   T   A   A   G   I

721    ACT CTC GGC ATG GAC GAG CTG TAC AAG CTC GAG CAC CAC CAC CAC
241    T   L   G   M   D   E   L   Y   K   L   E   H   H   H   H

766    CAC CAC TGA
256    H   H   *
```

Figure A5. Nucleotide and amino acid sequence of the recombinant HA-EGFP. Sequences corresponding to the HA epitope, EGFP and the $(His)_6$-tag are highlighted in red, green and gray, respectively. The recognition site of the *Xho*I restriction endonuclease used for molecular cloning is underlined.

A.6 Sequence of the recombinant hydrophobin EAS-α-KR

```
  1    ATG GGC AGC AGC CAT CAT CAT CAT CAT CAC AGC AGC GGC CTG GTG
  1    M   G   S   S   H   H   H   H   H   H   S   S   G   L   V

 46    CCG CGC GGC AGC CAT ATG GCT AGC ATC GGC CCC AAC ACC TGC TCC
 16    P   R   G   S   H   M   A   S   I   G   P   N   T   C   S

 91    ATC GAC GAC TAC AAG CCT TAC TGC TGC CAG TCT ATG TCC GGC CCC
 31    I   D   D   Y   K   P   Y   C   C   Q   S   M   S   G   P

136    GCC GGC TCC CCT GGT CTC CTC AAC CTC ATC CCC GTC GAC CTC AGC
 46    A   G   S   P   G   L   L   N   L   I   P   V   D   L   S

181    GCC TCG CTC GGC TGC GTT GTC GGT GTC ATC GGC TCC CAA TGT GGT
 61    A   S   L   G   C   V   V   G   V   I   G   S   Q   C   G

226    GCC AGC GTC AAG TGC TGC AAG GAC GAT GTT ACC AAC ACC GGC AAC
 76    A   S   V   K   C   C   K   D   D   V   T   N   T   G   N

271    TCC TTC CTC ATC ATC AAC GCT GCC AAC TGC GTT GCC GGA TCC GGC
 91    S   F   L   I   I   N   A   A   N   C   V   A   G   S   G

316    GGC GGC GGC AGC GGC GGC GGC GGC AGC GGC GGC GGC GGC AGC ACT
106    G   G   G   S   G   G   G   G   S   G   G   G   G   S   T

361    AGT TGG CAT TGG CTG CAG CTG AAA CCG GGC CAG CCG ATG TAT AAA
121    S   W   H   W   L   Q   L   K   P   G   Q   P   M   Y   K

406    CGT TAA
136    R   *
```

Figure A6. Nucleotide and amino acid sequence of the recombinant hydrophobin EAS-α-KR. Sequences corresponding to the $(His)_6$-tag and the mature EAS hydrophobin are highlighted in gray and orange, respectively. Sequences regarding the $(GGGGS)_3$ linker element are printed in bold and sequences for the α-factor pheromone are highlighted in blue. Sequences corresponding to the C-terminal lysine-arginine moiety are printed in red. Recognition sites of the *Nhe*I, *Bam*HI and *Spe*I restriction endonucleases used for molecular cloning are underlined.

Appendix B – Additional results

B.1 Pheromone activity of surfaces functionalized with EAS-α towards yeast reporter cells carrying or lacking the cell wall

Pheromone activity of hydrophobic surfaces functionalized with EAS-α was assessed by employing pheromone-responsive reporter cells of *S. cerevisiae*. The **a**-type strain BY4741 *Δbar1 FIG1-tRFP* was employed, carrying a deletion of the *BAR1* gene that rendered this strain 20-fold more sensitive to the α-factor pheromone than isogenic wild-type cells [418]. In addition, this strain harbored the *FIG1-tRFP* reporter gene cassette integrated into the genome to enable visualization of the pheromone response by analyzing *tRFP* expression.

Initial experiments suggested that surfaces functionalized with EAS-α did not elicit a pheromone response in the *S. cerevisiae* reporter cells (section 3.1.2.3). This might have resulted from limited accessibility of the Ste2p pheromone receptor (embedded in the plasma membrane) towards the α-factor immobilized at the surface, possibly due to steric hindrance by the yeast cell wall. In order to analyze the impact of the yeast cell wall, spheroblasts (lacking the cell wall due to *in vitro* enzymatic digestion) were also employed.

Spheroblasts were obtained by zymolyase treatment according to Meisinger *et al.* [557]. Both intact cells and spheroblasts were incubated in the presence or absence of synthetic α-factor or in polystyrene Petri dishes functionalized with EAS-α (section 2.8.4). Spheroblasts were cultivated in SD medium containing 1.2 M sorbitol to osmotically stabilize the cells lacking the cell wall. After incubation for 8 h at 30 °C without shaking, cells were recovered and cellular extracts were prepared (section 2.6.1). Finally, SDS-PAGE and immunological detection were carried out to analyze the expression of the *tRFP* reporter gene (Figure B1). Colloidal Coomassie staining revealed that comparable protein amounts were loaded in each lane (data not shown).

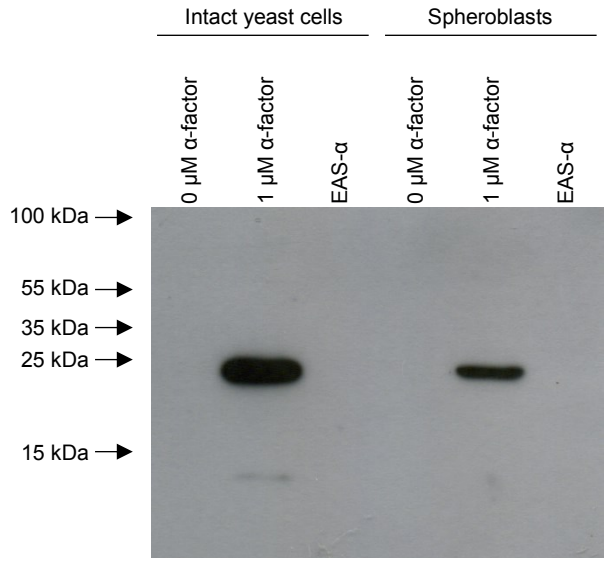

Figure B1. Analysis of the pheromone activity of polystyrene surfaces functionalized with EAS-α towards intact yeast cells and yeast spheroblasts. Pheromone-responsive intact cells or spheroblasts (BY4741 *Δbar1 FIG1-tRFP*) were grown in the absence or presence of synthetic α-factor or in polystyrene dishes functionalized with EAS-α. Cells were harvested after 8 h of incubation at 30 °C and cellular lysates (corresponding to 20 µg total protein) were separated *via* SDS-PAGE. Proteins were transferred to PVDF membranes and probed with tRFP antibodies.

Evidently, the *tRFP* reporter gene was expressed in both intact cells and spheroblasts upon treatment with synthetic α-factor, as indicated by the signal in the molecular weight range of 25 kDa corresponding to tRFP (calculated molecular weight of 26.1 kDa [405]). In contrast, *tRFP* expression could not be detected in reporter cells grown in the absence of the synthetic pheromone or cultivated on surfaces functionalized with EAS-α (Figure B1). Apparently, pheromone-induced *tRFP* expression was lower in spheroblasts compared to intact yeast cells. This might point at a reduced or delayed pheromone response of spheroblasts, potentially resulting from proteolytic degradation of the pheromone receptor by zymolyase treatment, given that zymolyase may contain trace amounts of proteases.

Nevertheless, the assays revealed that surfaces functionalized with EAS-α did not elicit a pheromone response in the reporter cells, independent on the presence of the cell wall. Thus, the absence of a detectable pheromone activity of surfaces functionalized with EAS-α was not exclusively caused by steric issues and additional factors need to be considered (section 4.1.4).

B.2 Influence of repeated antibody stripping on the signal intensity of the competitive ELISA

Class I hydrophobins self-assemble into highly robust monolayers that do not dissolve unless very harsh treatments such as 100 % TFA or formic acid are applied [129-135]. Therefore, the possibility to reuse hydrophobin-functionalized surfaces for multiple competitive ELISA measurements was assessed. Upon completion of a competitive ELISA measurement, the antibodies attached to the hydrophobin-functionalized surface were denatured by a combined treatment with reducing agents, detergents and heat (section 2.9.4) and the hydrophobin-functionalized surfaces were reused for competitive ELISA measurements.

In fact, the surfaces functionalized with the recombinant hydrophobins EAS and EAS-α could be reused for multiple measurements with comparable assay sensitivity (section 3.2.5). To further evaluate the behavior of the hydrophobin layers upon repeated antibody stripping cycles, putative losses in the signal intensity were analyzed by calculating the signal ratio according to the equation:

$$\text{Signal ratio} = \frac{\text{Absorbance value (reused surface)}}{\text{Absorbance value (freshly prepared surface)}}$$

Reused and freshly prepared hydrophobin-functionalized surfaces were treated with equal α-factor concentrations to calculate the signal ratio. The signal ratio, obtained for the set of data depicted in Figure 12, was plotted to investigate possible effects of repeated stripping on the competitive ELISA performance (Figure B2).

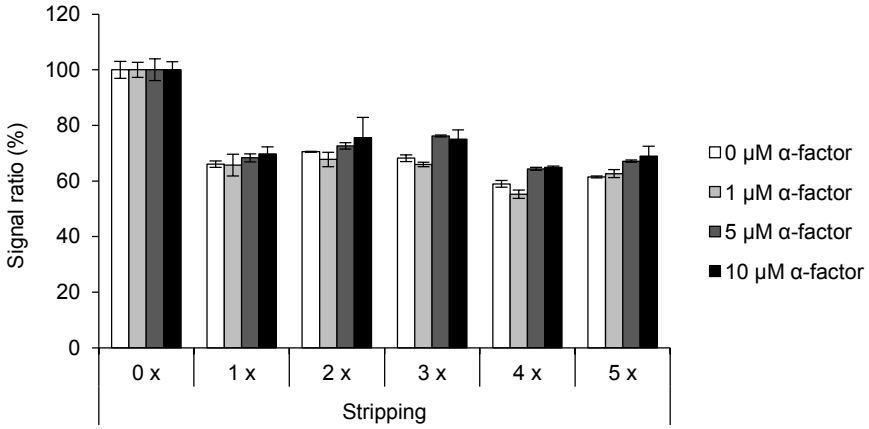

Figure B2. Analysis of the signal intensity upon repeated use of hydrophobin-functionalized surfaces. Polystyrene surfaces were functionalized with the recombinant hydrophobins (1.6 % EAS-α) and used repeatedly for competitive ELISA measurement by applying the antibody stripping procedure (section 2.9.4). To analyze the effect of repeated stripping cycles on the signal intensity, the signal ratio, calculated for the representative set of data depicted in Figure 12 (section 3.2.5), was plotted. Error bars indicate standard deviation.

A 30 – 40 % loss in signal intensity was evident after the first stripping cycle, whereas no further reduction in signal intensity upon subsequent stripping events was observed (Figure B2). These data suggested that a fraction of the recombinant hydrophobins was extracted by the hot SDS treatment used for antibody denaturation, consistent with the slight increase in the water contact angle upon hot SDS treatment of hydrophobin-functionalized substrates (section 3.1.2.1). Partial extraction of class I hydrophobins by hot SDS treatment has been observed in numerous studies [158, 213, 251, 257, 263, 280, 331, 396, 412-416]. However, further hydrophobin extraction upon subsequent stripping cycles was not evident, indicating that the remaining hydrophobins attached tightly to the polystyrene surfaces. In summary, hydrophobin-functionalized surfaces were sufficiently robust to allow for multiple competitive ELISA measurements (section 4.2.4).

B.3 Purification of recombinant HA-EGFP

To assess the versatility of the hydrophobin-based surface engineering technology, novel immunoassays for alternative analytes, focusing on the HA epitope instead of the yeast α-factor pheromone, were developed. Consequently, these immunoassays should allow for the detection and quantification of the HA peptide and of recombinant proteins fused to the HA epitope. To validate the latter possibility, a recombinant fluorescent protein carrying an N-terminal HA epitope (HA-EGFP) was utilized (see Appendix A.5 for DNA and amino acid sequence). The plasmid pET23b-HA-EGFP harboring the recombinant *HA-EGFP* gene was transformed into *E. coli* BL21 (DE3) pLysS and expression of the *HA-EGFP* gene was induced by IPTG addition (section 2.7.1.2). Recombinant proteins were purified by Ni^{2+} affinity chromatography under native conditions (section 2.7.2.3). Several fractions obtained during the purification process were separated *via* SDS-PAGE to evaluate the purification process and to analyze the purity and integrity of the purified recombinant protein (Figure B3).

Electrophoretic separation of these fractions revealed that the recombinant HA-EGFP (29.2 kDa calculated molecular weight [405]) was predominantly present in the whole-cell lysate, soluble and insoluble fractions as well as in the eluate of the Ni^{2+} affinity chromatography (Figure B3). Immunological detection using a GFP-specific antibody confirmed that the predominant signal in colloidal Coomassie staining corresponded to HA-EGFP. A second prominent signal in the molecular weight range slightly below 15 kDa observed in all fractions might be attributed to lysozyme (approximately 14 kDa [558]) added to lyse the cells as an initial step towards protein purification (section 2.7.2.3).

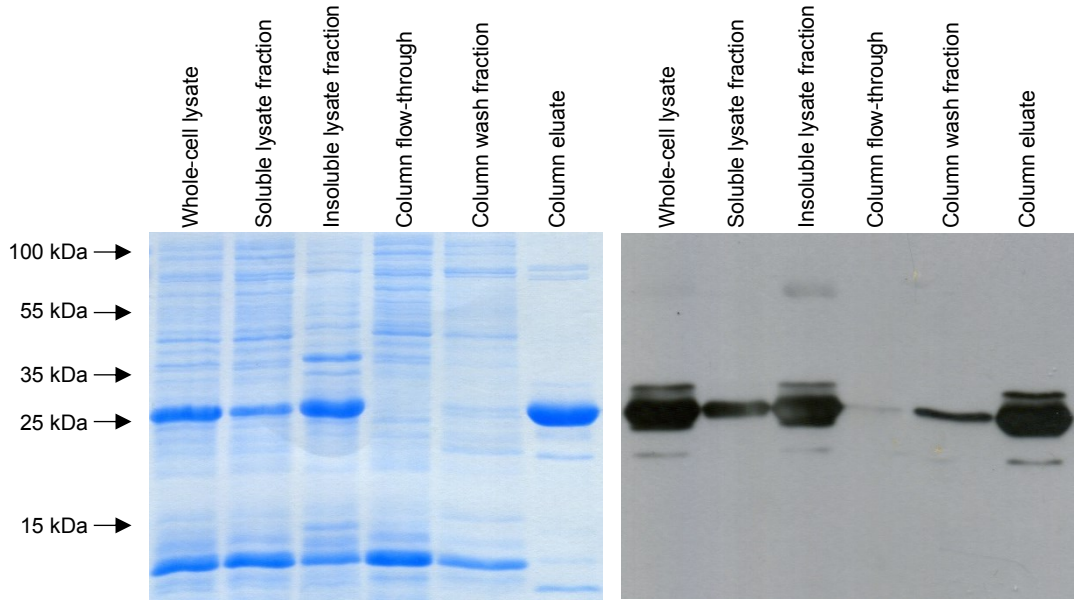

Figure B3. Evaluation of the purification process to obtain recombinant HA-EGFP. The vector pET23b-HA-EGFP was transformed into *E. coli* BL21 (DE3) pLysS, transformants were grown in LB medium and *HA-EGFP* expression was induced by IPTG addition (section 2.7.1.2). For protein purification (section 2.7.2.3), cells were lysed by sonication and lysozyme treatment (lane 1). The lysate was centrifuged to separate soluble compounds (lane 2) and insoluble compounds (lane 3). The soluble fraction was subjected to Ni^{2+} affinity chromatography and the column flow-through (lane 4), wash fractions (lane 5) and the column eluate (lane 6) were obtained. The purification process was analyzed by electrophoretic separation of the individual fractions (15 µg total protein in each fraction) *via* SDS-PAGE. Finally, proteins were visualized by colloidal Coomassie staining (left panel) or transferred to a PVDF membrane and probed with GFP-specific antibodies (right panel).

Importantly, the recombinant HA-EGFP was highly pure upon Ni^{2+} affinity chromatography, given that only few and faint additional signals were seen in the eluate fraction (Figure B3). Some of the contaminating proteins were also detected immunologically using the GFP-antibody, indicating that they most likely represented degradation products of the recombinant HA-EGFP. In summary, SDS-PAGE revealed that the recombinant fusion protein HA-EGFP could be obtained in high purity upon Ni^{2+} affinity chromatography. The purified protein was subsequently used for inverse ELISA measurements to analyze if the hydrophobin-based immunoassays could be applied to quantify recombinant proteins carrying the HA epitope (section 3.6.2.2).

B.4 Quantification of the yeast α-factor pheromone by HPLC

Several methods have been proposed to detect the *S. cerevisiae* α-factor pheromone, either based on its pheromone activity or on analytical chemistry methods such as mass spectrometry or HPLC (section 4.2.5). In this study, HPLC analysis was also carried out to quantify the α-factor pheromone, allowing for a comparison between the hydrophobin-based immunoassays and a commonly employed analytical chemistry method for peptide detection.

HPLC analysis was carried out using an Agilent 1200 series HPLC system (Agilent Technologies GmbH, Germany) equipped with a Kromasil 100-5C18 reversed phase column (Akzo Nobel Functional Chemicals B.V., The Netherlands) with a hydrophobic (C_{18}-modified) silica matrix. Detection of the α-factor was achieved by measuring the UV absorbance of the peptide pheromone at 280 nm using a diode array detector. Additionally, the intrinsic fluorescence of tryptophan residues was recorded by a fluorescence detector using excitation at 280 nm and recording the emitted light at 350 nm. To quantify the α-factor pheromone by means of liquid chromatography, the synthetic pheromone was diluted to a final concentration of 100 µM in EMM and passed through a 0.45 µm syringe filter. Serial dilutions of this stock solution in EMM were prepared and 5 µL of the pheromone-containing sample were finally injected into the HPLC column. HPLC analysis was carried out essentially as described previously [522, 559], employing acetonitrile as organic phase and TFA as an ion pairing agent. The solvent profile during the chromatographic separation is indicated in Table B1. The flow rate was adjusted to 1.0 mL/min.

Table B1. Solvent profile during HPLC separation of pheromone-containing samples.

Time	Solvent A	Solvent B	Remarks
0.01 min	95 %	5 %	Linear gradient
25.0 min	35 %	65 %	
25.1 min	5 %	95 %	Organic solvent wash (1)
35.0 min	5 %	95 %	
35.1 min	95 %	5 %	Column equilibration (2)
47.0 min	95 %	5 %	

(1) Upon chromatographic separation of the samples in a linear gradient, an organic solvent wash step was carried out to remove hydrophobic sample compounds from the column.

(2) After sample separation and removal of hydrophobic sample components, the column was equilibrated prior to injecting the next sample. Including a column equilibration step allowed for sequential injection of multiple samples in an automated manner.

Solvent A:	0.065 % (v/v) TFA
Solvent B:	0.05 % (v/v) TFA
	99.95 % (v/v) Acetonitrile

HPLC analysis allowed for the detection and quantification of the yeast α-factor pheromone. The α-factor could be separated from further compounds of the minimal medium (Figure B4 a), and the peak area obtained for the pheromone could be used to generate calibration plots based on the UV absorbance (Figure B4 b) or the intrinsic fluorescence of tryptophan residues (Figure B4 c) of the pheromone.

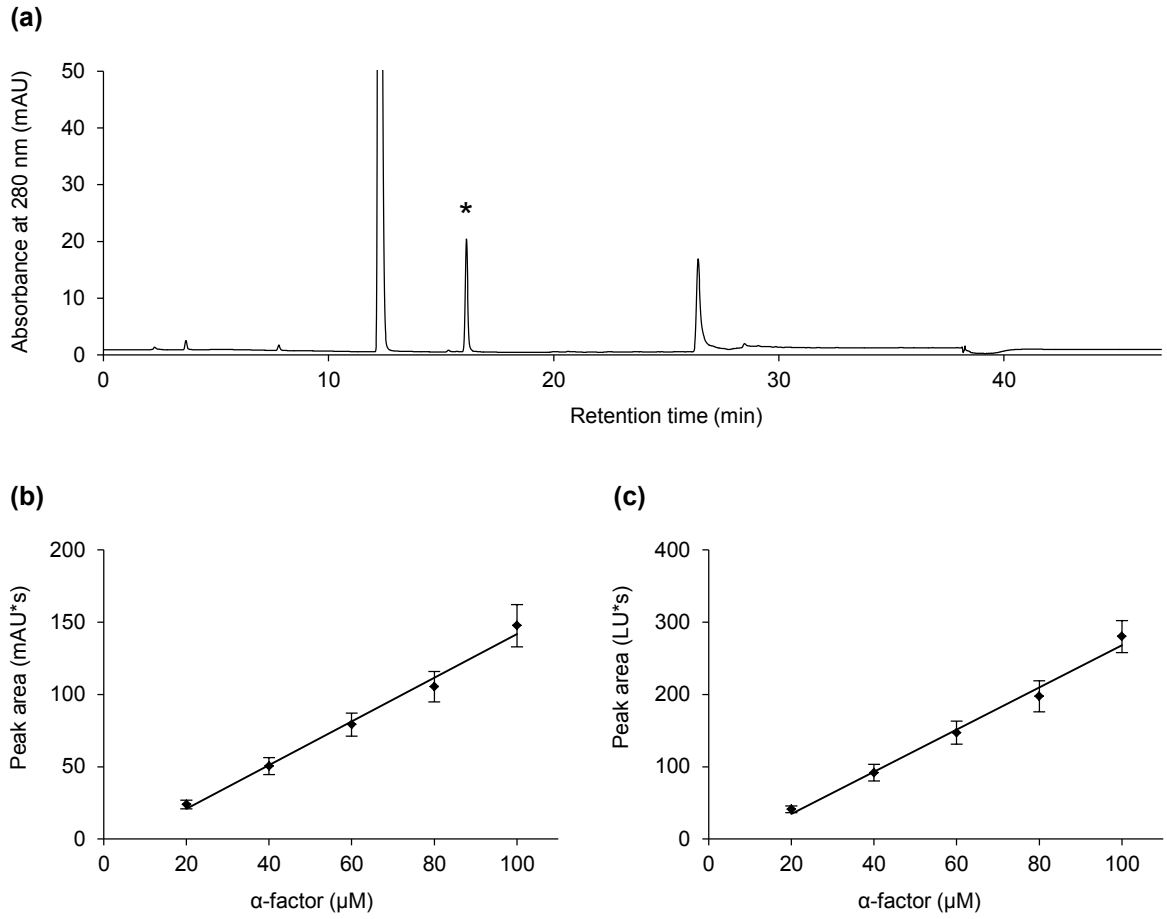

Figure B4. Detection and quantification of the α-factor pheromone by HPLC. (a) Representative chromatogram of a sample containing 100 µM α-factor in EMM based on monitoring of the UV absorbance at 280 nm. The marked peak corresponded to the α-factor. **(b)** Calibration of the peak area determined by UV absorbance measurements at 280 nm wavelength. **(c)** Calibration of the peak area obtained by detecting the intrinsic fluorescence of tryptophan residues. Excitation light source was adjusted to 280 nm and the light emission was recorded at 350 nm. Plotted values in (b) and (c) correspond to ten independent measurements for each α-factor concentrations. Error bars indicate standard deviation.

Three prominent peaks were detected upon chromatographic separation of EMM containing the α-factor pheromone (Figure B4 a). The predominant peak with a retention time of 12.1 min might be attributed to hydrogen phthalate used as a buffer component in EMM (section 2.4.3), whereas the peak with a retention time of 26.4 min might have resulted from a mixture of hydrophobic compounds eluted from the column during the organic solvent washing step. The α-factor pheromone (marked in Figure B4 a) eluted at a retention time of 16.2 min. The identity of this peak could be proven by employing pheromone-responsive *S. cerevisiae* reporter

cells. Upon collecting the peak fraction and addition to a reporter cell culture of *S. cerevisiae* BY4741 *Δbar1 FIG1-tRFP*, the yeast cells were found to form pronounced mating projections and to express the *tRFP* reporter gene, indicating that the cells underwent pheromone response (data not shown).

As the α-factor pheromone comprises two tryptophan residues and one tyrosine residue, the pheromone could be quantified by HPLC analysis based on its UV absorbance at 280 nm (Figure B4 b) and based on the intrinsic fluorescence of tryptophan residues (Figure B4 c). The peak area obtained in the chromatograms could be correlated with the α-factor concentrations, resulting in linear calibration plots that enabled pheromone quantification. Although the slope of the calibration curve obtained by fluorescence detection was higher than the slope of the calibration curve for UV absorbance (compare the y-axis in Figure B4 b and Figure B4 c), the limit of detection was in the range of 20 µM α-factor for both methods. Thus, HPLC-based pheromone quantification was 200,000-fold less sensitive than the inverse hydrophobin-based immunoassay (section 4.2.5).

B.5 Influence of C-terminal α-factor maturation on the interaction with the α-factor antibody

Studying the α-factor secretion of *S. cerevisiae* strains lacking the *KEX1* gene suggested that C-terminal pheromone maturation was essential for the interaction of the pheromone with its cognate antibody (section 4.3.3). To directly probe the influence of C-terminal pheromone maturation on the interaction with pheromone-specific antibodies, a fourth hydrophobin variant was generated (Figure B5 a). The recombinant EAS-α-KR hydrophobin was essentially similar to the EAS-α hydrophobin, but carried an additional lysine-arginine moiety at the C-terminal end (see Appendix A.6 for DNA and nucleic acid sequence), resembling the C-terminally immature α-factor pheromone secreted by *Δkex1* strains of *S. cerevisiae*.

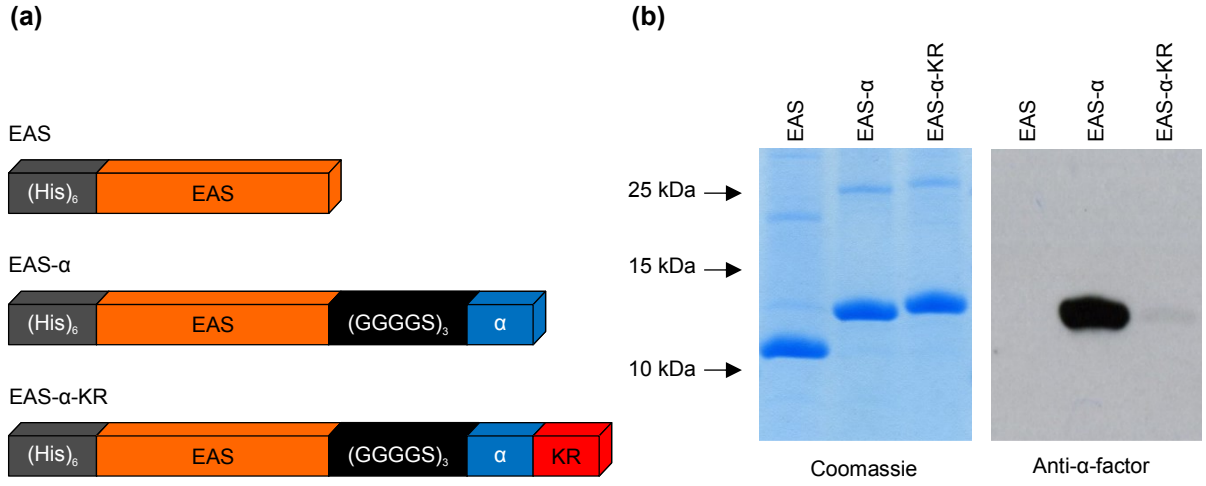

Figure B5. Analysis of the influence of C-terminal α-factor maturation on the interaction between the α-factor antibody and its cognate antigen. (a) Schematic illustration of the recombinant hydrophobins EAS, EAS-α and EAS-α-KR. All three hydrophobins carried the mature EAS hydrophobin with a $(His)_6$-tag at their N-terminus. Additionally, EAS-α carried a flexible $(GGGGS)_3$ linker element as well as the yeast α-factor pheromone at its C-terminus. The recombinant EAS-α-KR was identical to EAS-α but harbored an additional lysine-arginine moiety at its C-terminal end. **(b)** Electrophoretic separation of the recombinant hydrophobins. A fraction of each purified hydrophobin, corresponding to 3 µg of the recombinant hydrophobin, was subjected to Tricine SDS-PAGE and the proteins were visualized by colloidal Coomassie staining or transferred to PVDF membranes and probed immunologically by the α-factor antibody.

The recombinant hydrophobin EAS-α-KR was cloned into pET28b, expressed in *E. coli* T7 SHuffle® T7 Express *lysY* and purified by Ni^{2+} affinity chromatography as carried out for EAS and EAS-α (section 2.7). Upon electrophoretic separation by Tricine SDS-PAGE and visualization by colloidal Coomassie staining, a predominant signal corresponding to the monomeric hydrophobin was observed for all three recombinant hydrophobins (Figure B5 b). An additional faint signal, most likely representing the hydrophobin dimer, was also evident. The formation of stable dimers, even upon separation *via* SDS-PAGE, was previously reported for various hydrophobins [159, 214, 215, 227, 232, 307, 408-411]. Obvious differences in the affinity of the α-factor antibody towards EAS-α and EAS-α-KR were observed by immunological detection (Figure B5 b), indicating that the C-terminal lysine-arginine moiety present in EAS-α-KR severely affected the interaction of the recombinant hydrophobin with the pheromone-specific antibodies. These data suggested that C-terminal α-factor maturation was very essential for the interaction of the pheromone with the cognate antibody, implying that C-terminally immature pheromone molecules (secreted by *Δkex1* strains of *S. cerevisiae*) could not be measured by the hydrophobin-based immunoassays.

Acknowledgements

Without a doubt, this work has been one of the most challenging tasks I have been facing so far. Writing this thesis would not have been possible without the support and encouragement of several people, and I owe my deepest gratitude to them.

I would like to thank Professor Gerhard Rödel for providing the opportunity to learn and to work in his research group for more than seven years now. I am very thankful for his encouragement and guidance throughout the entire time period, and I am deeply grateful for his support that enabled to do my doctorate. I would also like to thank Professor Tilo Pompe for reviewing this thesis.

I am truly indebted to Dr. Kai Ostermann for his continuous support and encouragement, in the context of this work and far beyond. His imperturbable optimism was an unlimited source of motivation. I am also very thankful to him as well as to my colleague Falko Altenkirch for critically proofreading this thesis.

I am obliged to all present and former members of the research group for the pleasant atmosphere in the lab and in the office. In particular, I am deeply grateful to André Clemens for his valuable support throughout the entire time.

Professor Rainer Jordan and Maximilian Schneider are acknowledged for their support with water contact angle measurements. This work has been carried out within the research training group “Nano- and Biotechnologies for the Packaging of Electronic Systems” (DFG 1401). I would like to thank Professor Gerald Gerlach and Dr. Bärbel Knöfel for supervision and organization as well as all former members for the great atmosphere. The German Research Foundation is gratefully acknowledged for funding.

Finally, I owe my deepest gratitude to my family and friends for their continuous encouragement, motivation and invaluable support.

Authorship declaration

I, Stefan Hennig, hereby confirm that this dissertation and the experiments presented within are my own achievement. When the work published by others has been consulted, this has been clearly indicated. Quotes derived from the work of others have been clearly marked and the source is always given. Except for these quotations, this dissertation is entirely my own work. This thesis has not been submitted in this or similar form to any other authority.

Hiermit versichere ich, Stefan Hennig, dass ich diese Dissertation und die darin vorgestellten Arbeiten selbstständig verfasst und durchgeführt habe. Die vorliegende Arbeit wurde ohne zulässige Hilfe Dritter und ohne Benutzung anderer als der angegebenen Hilfsmittel angefertigt; die aus fremden Quellen direkt oder indirekt übernommenen Gedanken sind als solche kenntlich gemacht. Diese Dissertation wurde bisher weder im Inland noch im Ausland in gleicher oder ähnlicher Form einer anderen Prüfungsbehörde vorgelegt.

Die vorliegende Arbeit wurde von Oktober 2012 bis November 2016 am Institut für Genetik der Technischen Universität Dresden unter wissenschaftlicher Betreuung von Herrn Professor Gerhard Rödel angefertigt. Die Promotionsordnung der Fakultät Mathematik und Naturwissenschaften der Technischen Universität Dresden vom 23. Februar 2011 wird anerkannt.

Dresden, 3. November 2016 Stefan Hennig